



AFFIDAVIT

I declare that I have authored this thesis independently, that I have not used other than the declared sources/resources, and that I have explicitly indicated all material which has been quoted either literally or by content from the sources used. The text document uploaded to TUGRAZonline is identical to the present master's thesis dissertation.

Date

Signature

Acknowledgements

I would like to thank my advisor Daniel Scott Kieffer from the Institute of Applied Geosciences of TU Graz for his patience with my work, for taking the time to meet with him and discuss the progress or difficulties concerning the thesis, and for his enthusiasm for every idea or possible explanation concerning the present study.

I also wish to thank Gerhard Poscher from geo.zt for the possibility to work on this topic, for providing numerous records and existing data of the area of Landeck and of the present study area, for his willingness to share his knowledge and experience, to take the time to accompany Sabrina Kogler and me in the field for one day, and for the possibility to work on the thesis in the office of geo.zt.

My thanks also go to:

- Sandra Kuntner, Markus Ribis, Lukas Pergher and Markus Postl from geo.zt for providing records of previous projects, for their help with data acquisition and their processing in ArcGis®, for accompanying me in the field for one day and discussing my observations, and for the assistance with the sampling and the transportation of the drill cores obtained from the Perjen tunnel

- Manfred Blümel and Anton Kaufmann from the Institute of Rock Mechanics and Tunnelling of TU Graz for their help with the preparation of the samples for the triaxial compression and direct shear tests and the performance of the tests

- Gerhard Lauk and Markus Kaspar from the Institute of Applied Geosciences of TU Graz for their assistance in preparing the samples for the thin sections

- Daniela Engl for her time and incessant willingness to discuss any arising problem or idea concerning the investigated landslide, and for practical hints regarding the sampling and laboratory testing

- Sabrina Kogler for the joint approach to Landeck and our study areas and for her cooperation in sampling and in the laboratory work.

Contents

Abstract	IX
Kurzfassung	X
1. Introduction	1
1.1. Purpose and scope of work	1
1.2. Geographic setting	2
1.2.1. Site location	2
1.2.2. Climate	3
1.3. Regional geologic setting	5
1.3.1. Tectonometamorphic evolution	5
1.3.2. Quaternary evolution	9
1.4. Slope stability	10
1.4.1. Landslide processes	10
1.4.1.1. Failure mechanisms and landslide types	11
1.4.1.2. Landslide causes and triggering factors	14
1.4.1.3. Effects of landslides	15
1.4.2. Regional landslide activity	16
1.4.2.1. Zintlwald	16
1.4.2.2. Niedergallmigg	19
1.4.2.3. Other landslides (Perfuchsberg and Kopfwald/Glitt)	22
1.5. Previous geotechnical investigations	24
1.5.1. Geotechnical parameters of phyllitic and schistose rocks	24
1.5.2. Geotechnical studies in the area of Landeck	27
2. Methodology	32
2.1. Desk study	32
2.2. Field investigation	32
2.2.1. Mapping	32
2.2.2. Sampling	33
2.3. Laboratory investigation	34
2.3.1. Mineralogical and petrographic methods	34
2.3.2. Rock mechanics testing	34
2.3.2.1. Direct shear tests	34
2.3.2.1. Triaxial compression tests	36
2.4. Engineering geological analyses	36
2.4.1. Fabric analysis	36
2.4.2. Block theory and key block analysis	37
2.4.2. Slope stability analyses	39
3. Site conditions	41
3.1. Geological conditions in the study area	41
3.1.1. Lithological units	41
3.1.1.1. Quaternary deposits	41
3.1.1.2. Hard rocks	44
3.1.2. Geotechnical properties of the hard rock units	48
3.1.3. Structural geologic features	49
3.2. Geomorphology	51
3.2.1. Glacial morphology	51
3.2.2. Geomorphic characteristics of the lithological units	53
3.2.3. Other geomorphic features	54
3.3. Hydrology	57

3.4. Vegetation	59
3.5. Human settlements and infrastructure	60
4. Observations and Findings	61
4.1. Results from desk study.....	61
4.2. Observations and results from field work.....	65
4.3. Laboratory testing	69
4.3.1. Performed tests.....	69
4.3.2. Results of laboratory tests and comparison to previous investigations.....	70
4.4. Slope stability evaluation.....	72
4.4.1. Block Theory Analyses	72
4.4.2. First subsurface model of the landslide	75
4.4.3. Stability analyses using “Swedge”	78
4.4.4. Stability analyses using “Slide”	81
4.4.5. Analysis using “RocTopple”	85
4.5. Subsurface conditions.....	86
5. Discussion and Conclusions	89
6. References	93
7. Appendix	101

List of Figures

Figure 1: The area of Landeck with its most important geographic features that are mentioned in the present thesis (base map from BEV, 2014). The blue shaded areas represent the four largest landslides in this area.	2
Figure 2: Study area with its most important geographic features that are mentioned in the present thesis and the blue frame showing its exact location and extension (base map: Austrian Map 1:50000 (BEV, 2013)).....	3
Figure 3: Climate zones of Europe (base map after DIERCKE (2014)).....	4
Figure 4: Location of the meteorological stations (a) (BEV, 2014), and climate charts of Landeck (b), Galtür (c) and St. Anton am Arlberg (d) (TIROL ATLAS, 2013).	5
Figure 5: a) Schematic cross section showing the thrusting of the Austroalpine nappes over Penninic units and onto the European continent (modified after GEO DZ (2010)); b) Conception of the Austroalpine nappes according to TOLLMANN (1977); LAA...Lower Austroalpine, MAA..."Middle Austroalpine", UAA...Upper Austroalpine; light grey areas: basement nappes; dark grey areas: cover nappes; blue areas: position of the later Silvretta nappe; red arrows: direction of thrusting.....	6
Figure 6: Schematic cross section through the western part of the Eastern Alps (modified after GEO DZ (2010) using the map coloring of BOUSQUET et al. (2012)); UAA...Upper Austroalpine. The approximate location of the cross section is shown as black line in Figure 7.	6
Figure 7: Tectonic map of the Silvretta nappe and its surroundings (modified after BOUSQUET et al. (2012)); SI...Stanzertal line, EL...Engadine line, LN...Lechtal nappe, IN...Inntal nappe. The black line represents the approximate location of the cross section shown in Figure 6.....	7
Figure 8: The silvretta nappe with its division into Silvretta complex (orange), Venet complex (dashed area) and Landeck Phyllite (hatched area) according to GRUBER et al. (2010) (base map modified after BOUSQUET et al. (2012)). The extension of the Venet complex across the Arlberg down to the river Ill was drawn according to the geologic map of Vorarlberg 1:200000 by OBERHAUSER & RATAJ (1998). SI...Stanzertal line, EL...Engadine line; blue frame: approximate location of the study area.	8
Figure 9: Ice cover during the last glacial maximum (Würm) in the region of the study area (derived from http://earthscience.at/maps/). The contour lines of the Paznaun glacier for 2400 m and 2500 m a.s.l. are labeled.	10
Figure 10: Types of landslide movement: fall (a), topple (b), rotational slide (c), translational planar slide (d), wedge slide (e) and spread (f); Pictures a) and f) were taken from HIGHLAND & BOBROWSKY (2008), c) from USGS (2014) and b), d) and e) were modified after ROCSCIENCE (2014b).	13
Figure 11: Further types of landslide movement: rock slumping (a) with daylighting and non-daylighting discontinuities in red (modified after KIEFFER (1998)), column buckling (b) and block torsion (c) (GOODMAN & KIEFFER, 2000).....	14
Figure 12: Laserscan image (hillshade display from TIRIS (2013)) of the landslide Zintlwald with the two areas (re)activated in 2005 (red lines) and older currently inactive headscarps (green line) (after HENZINGER et al., 2009).....	17
Figure 13: Velocity field of the (re)activated landslide derived from refraction tomography (HENZINGER et al., 2009). From the different velocities the composition of the subsurface can be inferred. The black arrow marks a region with higher velocities, interpreted as a fragment of hard rock floating within more disintegrated and soil-like material.	18
Figure 14: Cross section through the deep-seated slope deformation Zintlwald and the western landslide (re)activated in 2005 (after B316 ARLBERGERSATZSTRASSE (2005)).	19
Figure 15: Laserscan image (hillshade display from TIRIS (2013)) of the landslide Niedergallmigg with the main scarps of its western and eastern sliding mass (red) as well as the secondary slides (orange) after ZANGERL et al. (2012).....	20
Figure 16: Cross section through the western sliding mass of the Niedergallmigg rockslide from the Matekopf in the south down to the river Inn in the north (ZANGERL et al., 2012).	22
Figure 17: Slope inclination display with dark colours representing steep areas and light colours representing flatter parts (from TIRIS (2013)) showing the landslides Perfuchsberg and Kopfwald/Glitt as well as the approximate boundaries of the landslide Gfäll of the present study (after KRAINER et al., 2004). The green line shows the location of the cross section of Figure 18.....	23
Figure 18: Cross section through the lowest part of the Perfuchsberg landslide – gained from refraction seismics and borings – showing that the sliding mass was thrust onto fluvio-glacial sediments of the overdeepened valley (after POSCHER (1993)). The location of the cross section is shown in Figure 17 as green line.	24

Figure 19: Orthophoto showing the B188 Paznaun valley road (orange) with the tunnel Gfäll, the gallery Gfäll and the new bridge across the river Trisanna, and the old road section with the old bridge in black (from TIRIS (2013)). The approximate borders of the landslide Gfäll (red) are drawn after KRAINER et al. (2004). The yellow circle frames the area where the geotechnical monitoring was performed from December 2004 on.....	30
Figure 20: Sampling positions (green points) and location of the three borings KB-ZL8-02, KB-ZL8-03 and KB-ZL8-04 (ASFINAG, 2012b), from which also samples were gained.....	33
Figure 21: Laboratory sample preparation and testing equipment: a) motor-driven grinding plate Planopol-3, b) PetroThin rock cutting machine, c) upper and lower shear box after grouting of the sample, d) direct shear test apparatus with mounted shear box, e) triaxial cell.	35
Figure 22: a) Block types VI-I for a tunnel excavation after GOODMAN (1989); b) Whole sphere projection of three discontinuity sets and one slope plane (dashed circle); blue: reference circle, red: one of the spherical polygons representing a joint pyramid. In this example the block with the JP code (001) would be removable, since it lies completely outside the slope circle (EP).....	38
Figure 23: a) SP and EP for a planar slope; b) SP and EP for a planar slope in stereographic projection of the lower hemisphere: EP lies inside the circle that represents the slope, SP outside; blue: reference circle (after GOODMAN (1989)).	38
Figure 24: Schematic sketch of toppling columns with the required input parameters for "RocTopple" (modified after ROCSCIENCE (2013)).	40
Figure 25: Geologic map of the study area (base map from BEV (2013)). The black and the blue line give the location of the transversal and longitudinal geologic cross section in chapter 4.5.	48
Figure 26: Lower hemisphere equal angle projection of the structural data of the study area: a) foliation planes (great circles and poles) with their average orientation (center of gravity) of $sf = 187/35$; b) fold axes with their average orientation of $FA = 256/32$; c) faults; d) slickensides.	50
Figure 27: Lower hemisphere equal angle projection of the structural data of the ten selected outcrops: a) poles of the joint sets j1 to j5 with density contour lines and their average orientations (centers of gravity); b) great circles and poles with density contour lines of the schistosity and its average orientation.	51
Figure 28: a) View toward northeast: glacial polish with glacial striation (blue line) east of the farmstead Vorgigggl; the strike of the schistosity (sf) is shown by the red line. b) View toward ESE: glacial polish with glacial striation (blue line) west of the farmstead Vorgigggl, where the polished surfaces are mostly overgrown with mosses.	52
Figure 29: Slope inclination display (obtained from ATLR (2013)) of the ridge in the north of the study area (dark areas mark steep slopes, light areas shallow parts). Glacial polishes occur on the southern side of the ridge, steep escarpments on the northern side. The approximate flow direction of the glacier is shown by the blue arrow.	52
Figure 30: Geomorphic map of the study area (blue frame) with a slope inclination display obtained from ATLR (2013) as base map.....	54
Figure 31: Obsequent breaks in slope: a) exposed uphill facing joint plane, b) trench leading toward ENE.	55
Figure 32: a) View from the western side of the Paznaun valley toward the Giggler Spitze showing the snow filled chutes leading down from the ridge and the obsequent breaks in slope along the entire mountain flank. b) Obsequent break in slope that can be traced all the way up to the north ridge of the Giggler Spitze.	55
Figure 33: a) Headscarp of the landslide Gfäll; b) Scarp at the toe of the landslide Gfäll down to the river Trisanna..	56
Figure 34: a) Northern one of the nearly vertical rock walls; b) Southern rock wall.	56
Figure 35: Examples of crevices in the adjacent areas behind the scarps of the landslide Gfäll.....	57
Figure 36: Hydrologic map (slope inclination display obtained from ATLR (2013) as base map) showing the observed springs s1 to s11 and the additional springs s12 to s17 according to WIS (2013).	59
Figure 37: Orthophoto (from TIRIS, 2013) showing the human settlements of the study area, the Giggler Alpe and the Giggler Spitze. The blue frame marks the border of the study area, the red line the area of the landslide Gfäll. The yellow arrows point at the temporary road built in 2005 and the following bridge.....	60
Figure 38: Slope inclination display with dark colours representing steep areas and light colours representing flatter parts (from TIRIS, 2013) showing the landslides Kopfwald/Glitt and Gfäll (blue frame: study area). The black contour lines were calculated from laserscan data (ATLR, 2013) using ArcMap® and represent today's contour lines. The green contour lines were drawn for an elevation of 1100, 1200 and 1300 m and result from the made assumptions concerning the course, depth and width of the Paznaun valley. The white line gives the location of the cross section of Figure 39.	63

Figure 39: Cross section through the study area showing today's surface as well as the constructed pre-failure surface (green). Area A features mass loss, area B mass increase. The overdeepening in the section of the landslide Gfäll is assumed to be approximately 50 m. The glacial shoulder on the western side of the valley is located at ~1300 m, which was transferred also to the eastern side. The location of the cross section is shown as white line in Figure 38. 63

Figure 40: Slope inclination display showing the lineaments outside the landslide Gfäll (red) and within the deposited mass (blue). The lineaments outside the landslide are also drawn to the south and the north in excess of the study area (blue frame)..... 64

Figure 41: Headscarp at its highest point in the east of the landslide with the joint sets j2 (red) and j3 (green) and the schistosity (brown). a) View toward southeast, b) view toward northeast. 65

Figure 42: a) Behind the headscarp in the northeast joint set j1 features open fractures; b) Open joint of joint set j1 at the northern border of the landslide; c) Open fracture approximately parallel to the schistosity, which at the northern border of the landslide is very steep due to folding..... 66

Figure 43: Examples of small escarpments (red lines) with stressed roots (a and b) and a ~30 cm wide fracture (yellow lines) in the ground surface (c) in the southwestern and western part of the study area within the deposited landslide mass. 66

Figure 44: a) Oblique trees inclined in different directions („drunken forest“); b) Tumbled trees at the scarp down to the river Trisanna in the west..... 67

Figure 45: a) Bulge with fractures in the asphalt road (temporary road into the Paznaun valley) in the southwest of the landslide Gfäll; b) Road to Schweißgut that is not asphalted at this section and features ~1 m of vertical displacement. 68

Figure 46: Stone wall on the eastern side of the road that leads from Schweißgut toward Hintergiggel in the south: a) Bulge from line A to line B with a horizontal displacement of ~1 m; b) Fractures in the stone wall along which the upper part was displaced downhill. 68

Figure 47: Displacement of the road at Schweißgut with the red lines showing the supposed location where the offset (approximately to the northwest) occurred or still occurs. The yellow lines represent a vertical fracture in the stone wall. The white lines A and B have the same positions as in Figure 46. 68

Figure 48: Whole sphere projection of the joint sets and the schistosity at outcrop 77. The blue circle is the reference circle; the black dotted circle represents the slope assumed with 290/45. The left plot shows the joint pyramids (JPs) and their codes with the six JPs of the removable blocks being labelled. The right plot gives the joint plane(s) along which the potential key blocks or key blocks would fail. In this example failure would occur along the intersection lines of j1 and j3 (13), j2 and j5 (25), j3 and j5 respectively with the schistosity (3sf and 5sf) and along the schistosity (sf) alone. 73

Figure 49: Contour plot of the friction angles for joint set j3 (= 1) and the schistosity (= 2) at outcrop 77. The blue circle is the reference circle. R marks the resultant force vector, which in this case lies in the field “12” at a friction contour line of ~18°, meaning that the block would slide down along the intersection line of plane 1 and plane 2 (here: j3 and schistosity) if the friction angle on the planes was lower than 18°..... 75

Figure 50: Schematic cross section through the study area showing the first attempt to produce the underground geometry of the landslide with the results from the block theory analyses. The green and yellow lines represent the directions of the lines of intersection of j3 and j5 respectively with the schistosity. The red line shows the required direction of a second plane or intersection line for failure to occur. 76

Figure 51: Intersection lines (blue points) of the joint sets j3 and j5 with the schistosity, j2 with j3 and j4 with j5 respectively resulting from all measurements at the ten selected outcrops. The average orientations (density maxima) are represented by the black points, the unfavourable orientations by the red points. ... 77

Figure 52: Adapted subsurface model with $\hat{I}_{3sf} = 285/27$ (green) as possible basis of the landslide. The red line represents $\hat{I}_{23} (= 259/51)$ which is supposed to form the headscarp..... 78

Figure 53: Wedge that was constructed according to the results of the block theory analyses and the afterwards made assumptions and inserted into “Swedge”. It shows the intersection line of j3 and the schistosity (sf) since they are supposed to produce the wedge as well as the assumed slope orientation and inclination according to the reconstruction of the pre-failure surface, the slope height, which was defined with 50 m resulting in a headscarp height of ~40 m, and the inserted tension crack that was used instead of a headscarp orientation. 79

Figure 54: Sensitivity plot showing the friction angle with respect to the percentage the tension crack (TC) is filled with water. 80

Figure 55: Sensitivity plot showing the friction angle with respect to the percentage of the slope height to which it is filled with water..... 80

Figure 56: Subsurface model showing a stepped failure surface formed by \hat{I}_{23} and \hat{I}_{3sf} 81

Figure 57: Discrete sliding surface (shear zone) in red after the initial steps (black) have been sheared off. 81

Figure 58: Cross section through the landslide that was evaluated in "Slide" showing the positions of the four different water tables (L1 and H1 for the situation of a hydrogeologic boundary along the boundary of paragneisses to phyllonitic micaschists, and L2 and H2 if the water table only depends on the level of the valley bottom).	83
Figure 59: Analysis result for the parameters given in Table 20 for the dry state showing the failure surface with the lowest factor of safety which is 1.037.	84
Figure 60: Sensitivity plot for the condition of no water and of low and high water tables (L1 and H1) that correspond to the boundary between paragneisses and phyllonitic micaschists. The grey points represent the analysis results for a cohesion of 500 kPa, the blue points for a cohesion of 300 kPa.	84
Figure 61: Sensitivity plot for the condition of no water and of low and high water tables (L2 and H2) that correspond to the level of the valley bottom. The grey points represent the analysis results for a cohesion of 500 kPa, the blue points for a cohesion of 300 kPa.	85
Figure 62: Result of the kinematic and stability analysis as well as the input parameters regarding toppling along joint set j1 using the software "RocTopple".	85
Figure 63: Longitudinal geologic cross section including the supposed subsurface of the landslide according to the conception of a discrete shear zone developing during movement. The location of the cross section can be taken from the geologic map in Figure 25 (chapter 3.1.1.2.)	87
Figure 64: Transversal geologic cross section including the supposed subsurface of the landslide according to the conception of a discrete shear zone developing during movement. The location of the cross section can be taken from the geologic map in Figure 25 (chapter 3.1.1.2.)	88

List of Tables

Table 1: Elevation, mean annual temperature and mean annual precipitation of the meteorological stations next to the study area (TIROL ATLAS, 2013) as well as annual sum of days with frost (daily temperature minimum <0.0 °C) (ZAMG, 2002).	4
Table 2: Testing results of uniaxial compressive strength (UCS), elastic modulus and splitting tensile strength of samples from the Innsbruck quartzphyllite with the loading direction parallel and perpendicular to the schistosity (SPAUN & THURO, 1994).	25
Table 3: Results of uniaxial and triaxial compression tests, and direct shear tests of quartzphyllites from the Lower Austroalpine (LAA) and the Greywacke zone (GWZ) (BUTTON, 2004).	26
Table 4: Average values of the maximum shear strength parameters along joints that are parallel to the foliation as well as the maximum and residual shear strength parameters of kakirites (ENGL et al., 2008).	26
Table 5: Uniaxial compressive strength (UCS), friction angle (φ) and cohesion (c) from triaxial compressive tests and direct shear tests on foliation surfaces, and indirect tensile strength perpendicular to the schistosity of the "Landeck quartzphyllite" (Venet complex) (BUTTON, 2004); β ...angle between loading direction and schistosity.	27
Table 6: Mean orientations of the schistosity (sf) and the seven joint sets at the Perjen tunnel (KÖHLER, 1983).	28
Table 7: Properties of rock mass types that correspond to the light phyllites (Landeck Phyllite) and the phyllonitic micaschists and schistose gneisses of the Venet complex for the construction of the second tube of the Perjen tunnel (ASFINAG, 2012a).	28
Table 8: Orientations of the schistosity (sf) and the joint sets (j1 to j4) with respect to the lithology and the geotechnical areas respectively (POSCHER, 2005).	30
Table 9: Rock mass parameters of the Venet complex applied for the construction of the tunnel Gfäll (POSCHER, 2005); UCS: uniaxial compressive strength, φ : friction angle.	31
Table 10: The geotechnical groups consisting of the lithological units of the study area which feature similar properties. Their characteristic parameters for rocks and joints were determined following ÖNORM EN ISO 14689-1 (n. s.: "not specified" in the course of field mapping).	49
Table 11: Average orientations (centers of gravity resulting from the density plot) of the joint sets j1 to j5 and the schistosity (sf) measured at the ten selected outcrops.	51

Table 12: Springs of the study area with their coordinates, local names, the information if they are tapped or not, the estimated discharges and the discharge amounts according to WIS (2013) if they were given. The springs s1 to s11 were observed in the field, the information about the springs s12 to s17 was taken from WIS (2013).	58
Table 13: Samples for direct shear tests with their lithology and the coordinates of the sampling position. Five samples were mounted as intact blocks, one was primarily split along the schistosity (sf) into two parts.	69
Table 14: Samples for triaxial compression tests with their lithology, the coordinates and the number of the boring from which they were taken as well as the corresponding depth, their diameter, length and weight.	70
Table 15: Results from direct shear tests: Properties of the developed shear plane (area, joint roughness coefficient and verbal roughness description) as well as friction angle φ and residual friction angle φ_{res} , cohesion c and residual cohesion c_{res} , dilation angle i , maximum shear stress τ_{max} and the shear path s at τ_{max} . The developed shear plane of sample 25/13s (red) was not entirely located within the 2 cm gap between the shear boxes and hence probably produced falsified values.	71
Table 16: Results from triaxial compression tests: Uniaxial compressive strength (UCS), the material constant m_i and the tensile strength σ_{tens} , cohesion c and friction angle φ , E- and V-modulus and the Poisson's ratio. ...	71
Table 17: Average orientation of the joint sets j1 to j5 and the schistosity (sf) at the ten selected outcrops (numbers 14 to 169) determined from density plots. At the outcrops 127 and 143 only the fold axes (FA) of the schistosity could be measured.	73
Table 18: Different combinations of discontinuities that could form removable blocks in a pre-failure slope of 290/45. Listed below them are the outcrop numbers in which these combinations occur producing removable blocks. At the outcrops 127 and 143 (blue) only the fold axes of the schistosity could be measured, which is why for the analysis an orientation of 180/35 was assumed for the schistosity since this is the average orientation in the study area. The combination of joint set j3 and j5 respectively with the schistosity occur most frequently (red frames). For outcrop 126 only safe removable blocks (type III blocks) were determined and therefore it is not contained in this table.	74
Table 19: Intersection lines resulting from all measured joint orientations of the ten selected outcrops that feature unfavourable orientations. Listed are their average orientations received from a density plot as well as the range of unfavourable orientations.	76
Table 20: Input parameters for the different rock types: unit weight, cohesion c and friction angle φ	82

Abstract

The area of Landeck in western Tyrol, Austria, shows a significant density of deep-seated landslides. In the course of the present thesis the geological conditions in the area of the landslide Gfäll, which is located at the entrance of the Paznaun valley, were investigated and the landslide processes (mechanisms, causes and triggers responsible for the slope movement) were evaluated. The scope of this work included geological and geomorphic mapping, documentation of the rock mass characteristics, rock mechanics testing of samples from the study area together with failure mode and slope stability analyses.

The headscarp of the landslide Gfäll is formed by two joint sets that strike approximately NE-SW and NW-SE. On the basis of engineering geological investigations performed, it is suggested that the landslide initiated as wedge-shaped blocks sliding along a stepped failure surface. With continued displacements these steps (or asperities) were subsequently sheared during progressive movement of the landslide. A basal shear zone consisting of sheared rock material (kakirites) is then suggested to have developed. Stability and sensitivity analyses give friction angles of the shear zone material for a limit equilibrium state of 20-25° depending on the hydraulic conditions within the slope. The reconstruction of the pre-failure topography based on a balanced cross section analysis led to an interpreted depth of the landslide of approximately 200 m. The landslide Gfäll is best classified as a deep-seated rockslide and features disintegration of the landslide debris increasing from the headscarp toward the toe resulting in secondary (soil-like) slides at the toe, which are currently active. The causes and triggers of the landslide Gfäll were likely influenced by Quaternary processes, such as the oversteepening of the toe or the liberation of a large amount of water during the melting of the glacier that facilitated weathering and erosion. The erosion of the river Trisanna at the toe of the landslide Gfäll and heavy rainfalls or snowmelts are assumed to have significant influence on the present movement of the landslide.

Kurzfassung

Der Großraum Landeck im Tiroler Oberland, Österreich, weist eine besondere Dichte an tiefgründigen Hangbewegungen auf. Im Zuge der vorliegenden Arbeit wurden die geologischen Bedingungen im Bereich der Massenbewegung Gfäll, welche sich am Eingang ins Paznauntal befindet, untersucht sowie Prozesse der Massenbewegung (Mechanismen, Ursachen und Auslöser der Hangbewegung) evaluiert. Die Aufgabenstellung der Arbeit enthielt eine geologische und geomorphologische Kartierung, die Dokumentation der Gebirgseigenschaften, die Durchführung felsmechanischer Laborversuche an Proben aus dem Untersuchungsgebiet sowie die Durchführung von Versagensmechanismus- und Stabilitätsanalysen.

Die Abrisskante der Massenbewegung Gfäll wird von zwei Trennflächenscharen gebildet, die in etwa NE-SW bzw. NW-SE streichen. Aufgrund der durchgeführten ingenieurgeologischen Untersuchungen wird davon ausgegangen, dass die Massenbewegung in Form eines Keilversagens einzelner Blöcke entlang einer gestuften Gleitfläche begann. Durch die fortlaufende Bewegung der Gesteinsmassen wurden diese Stufen (oder Unebenheiten) abgeschert und es wird daher angenommen, dass sich eine basale Scherzone bestehend aus zerschertem Gesteinsmaterial entwickelte. Stabilitäts- und Sensitivitätsanalysen ergaben für das Scherzonenmaterial im Grenzgleichgewichtszustand Reibungswinkel von 20-25° in Abhängigkeit von den hydraulischen Verhältnissen im Hang. Die Rekonstruktion der Topographie, wie sie vermutlich vor dem Auftreten der Massenbewegung aussah, wurde anhand einer balancierten Profilschnittauswertung durchgeführt und ermöglichte eine Ableitung der Tiefe der Massenbewegung von ungefähr 200 m. Die Massenbewegung Gfäll kann am besten als tiefgründige Felsgleitung klassifiziert werden, die mit der Entfernung von der Abrisskante eine zunehmende Auflösung des Gesteinsverbandes aufweist und im Hangfußbereich sekundäre (lockergesteinsartige) Rutschungen, welche zur Zeit aktiv sind, beinhaltet. Die Ursachen und Auslöser der Massenbewegung Gfäll waren vermutlich stark durch quartäre Prozesse, wie die Übersteilung des Hangfußes oder die Freisetzung großer Wassermengen während des Abschmelzens des Gletschers, was zusätzlich Verwitterung und Erosion begünstigte, geprägt. Die rezente Aktivität und Geschwindigkeit der Massenbewegung Gfäll wird vermutlich stark von der Erosion der Trisanna am Hangfuß sowie durch Starkniederschlagsereignisse und Schneeschmelzen beeinflusst.

1. Introduction

1.1. Purpose and scope of work

The area of Landeck in western Tyrol, Austria, shows a significant density of deep-seated landslides. Some of the landslides were investigated in course of civil engineering activity, including construction of power plants at the rivers Inn and Sanna or the construction of the tunnels Strengen and Perjen in the west and north of the town Landeck (Figure 1). Also a flood event in 2005 in this region and its consequences led to the necessity of more detailed investigations. Therefore a high state of knowledge exists for some of the slope movements, for instance *Zintwald* in the eastern Stanzer valley and *Niedergallmigg* in the upper Inn valley southeast of the town Landeck (Figure 1). Others, however, were only investigated at restricted selective points although they significantly influence technical infrastructure like railway tracks, streets or buildings. Examples for the latter are the landslides *Gfäll* at the entrance to the Paznaun valley and *Perfuchsberg* in the southwest of the town Landeck (Figure 1).

The purpose of the present study was to evaluate the geological conditions in the area of the landslide Gfäll, and to determine the occurring or preceded processes (mechanisms, causes and triggers responsible for the slope movement). Existing investigation and measurement data concerning the study area and existing laboratory testing data of similar rock types as well as testing results from the study area obtained in the course of the present thesis should thereby be included. Furthermore, the influence of the slope deformation on infrastructure and buildings was to be documented. The results from the landslide Gfäll should then be compared to the well documented examples (reference examples) of the above mentioned landslides Zintwald and Niedergallmigg.

To achieve the needed information the following steps of work were carried out:

- Desk study of existing literature and data, including orthophotos and laserscan data
- Geological, structural and geomorphic mapping plus rock sampling
- Rock mechanics testing to obtain comparative values from the site
- Engineering geological interpretation of the site features and the testing results
- Failure mode analyses and slope stability analyses to specify the landslide processes

1.2. Geographic setting

1.2.1. Site location

The study area is located in the Samnaun mountain range in the district Landeck in western Tyrol, Austria, and lies between the localities Tobadill in the north and See in the Paznaun valley in the south (Figure 1). It is about 3 km long and 1.5 km wide with the river Trisanna and the Giggel and Hintergiggel creek representing the western and the southern border respectively, and the north ridge of the Giggler Spitze forming the border to the east (Figure 2). In the north the study area reaches to the north of the farmstead Vorgiggel. The exact location and extension can be taken from Figure 2. Its elevation reaches from ~900 m above see level (a.s.l.) at the river Trisanna to nearly 2600 m a.s.l. north of the summit of the Giggler Spitze.

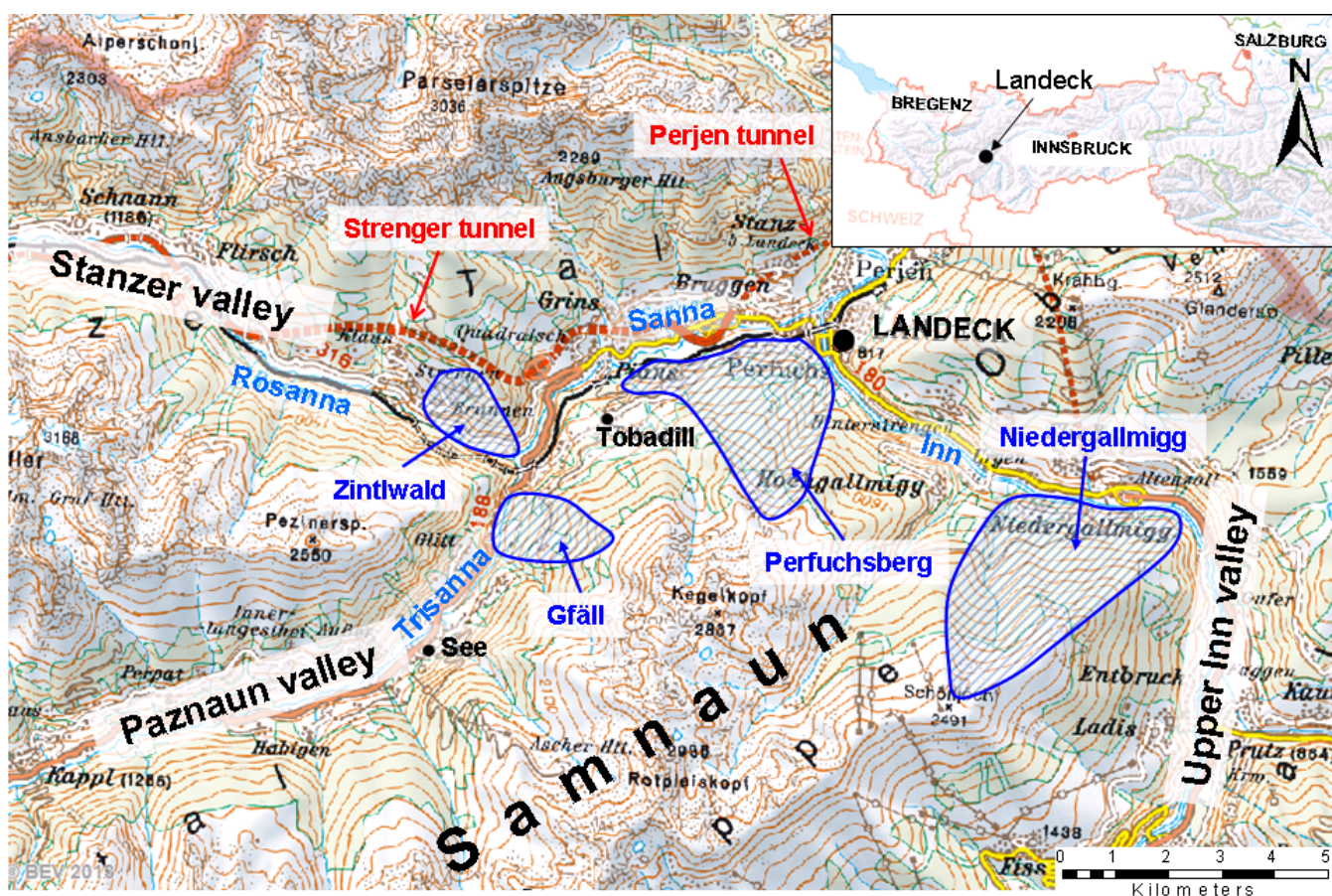


Figure 1: The area of Landeck with its most important geographic features that are mentioned in the present thesis (base map from BEV, 2014). The blue shaded areas represent the four largest landslides in this area.

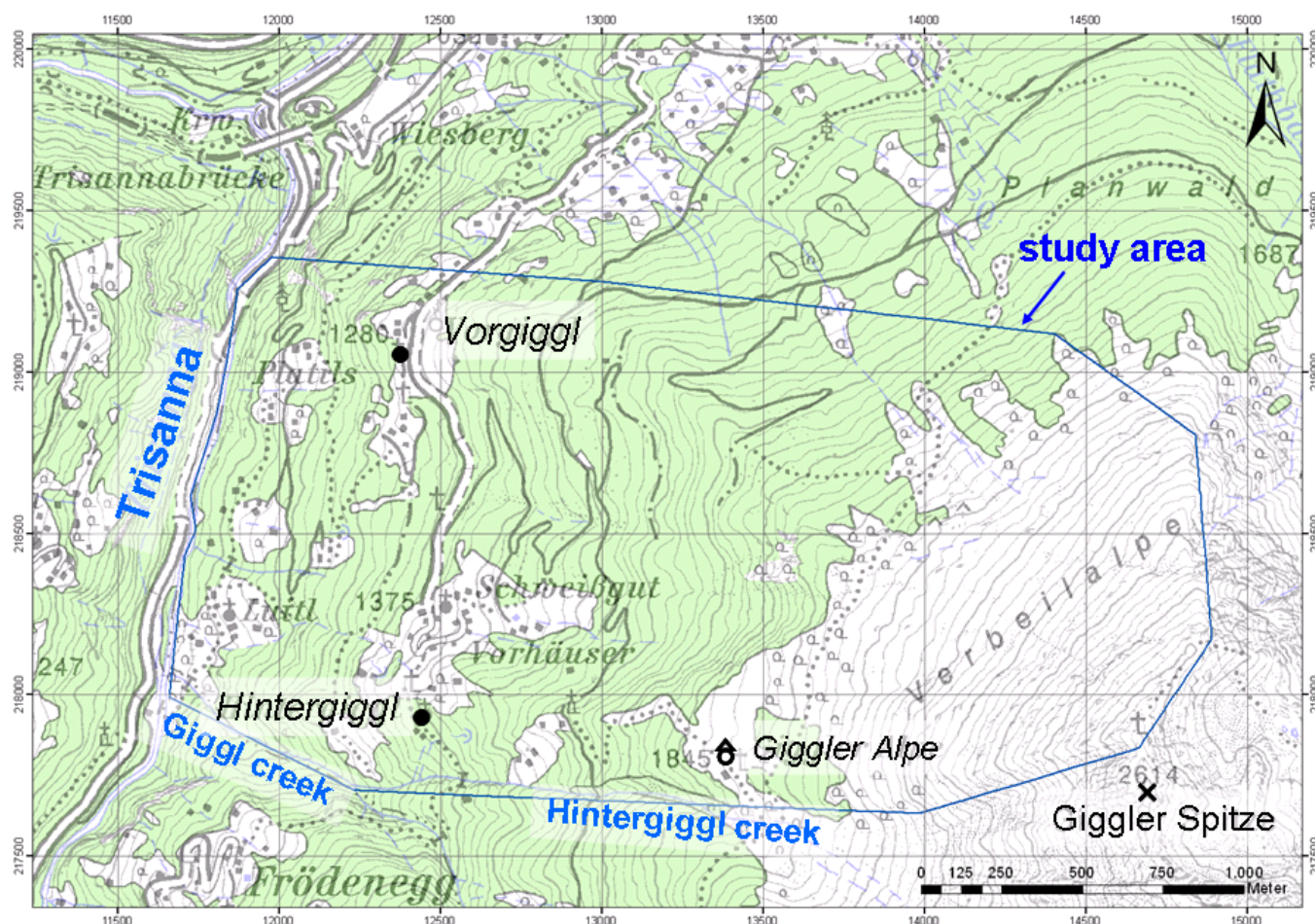


Figure 2: Study area with its most important geographic features that are mentioned in the present thesis and the blue frame showing its exact location and extension (base map: Austrian Map 1:50000 (BEV, 2013)).

1.2.2. Climate

Austria is located in the cold-temperate climate zone, more precisely in the transition zone between the oceanic climate in the west and the continental climate in the east (FORKEL, 2010; Figure 3). It is characterized by seasonal temperature variations with warm summers and cold winters and precipitation throughout the year, but with its maximum in summer (FORKEL, 2008). The study area though is situated in the Alpine region and therefore shows alpine climate character, i.e. generally lower temperatures and in many cases higher precipitation (in winter in the form of snow) than in other regions. The next meteorological stations to the study area are located at the town Landeck (785 m a.s.l.), at Galtür in the Paznaun valley (1587 m a.s.l.) and at St. Anton am Arlberg (1298 m a.s.l.) (Figure 4a). Figure 4b to 4d show the climate charts of these stations, giving the march of temperature and the amount of precipitation over the year as well as the mean annual temperature and the mean annual precipitation (TIROL ATLAS, 2013). The annual means are also summarized in

Table 1 together with the annual sum of days with frost (defined as days with a daily temperature minimum $<0.0\text{ }^{\circ}\text{C}$; ZAMG (2002)). Due to the situation and elevation (900-2600 m a.s.l.) of the study area, a mean annual temperature of approximately $6\text{ }^{\circ}\text{C}$ (at 900 m a.s.l.) to $-1\text{ }^{\circ}\text{C}$ (at 2600 m a.s.l.) and a mean annual precipitation of about 1000-1100 mm can be assumed.

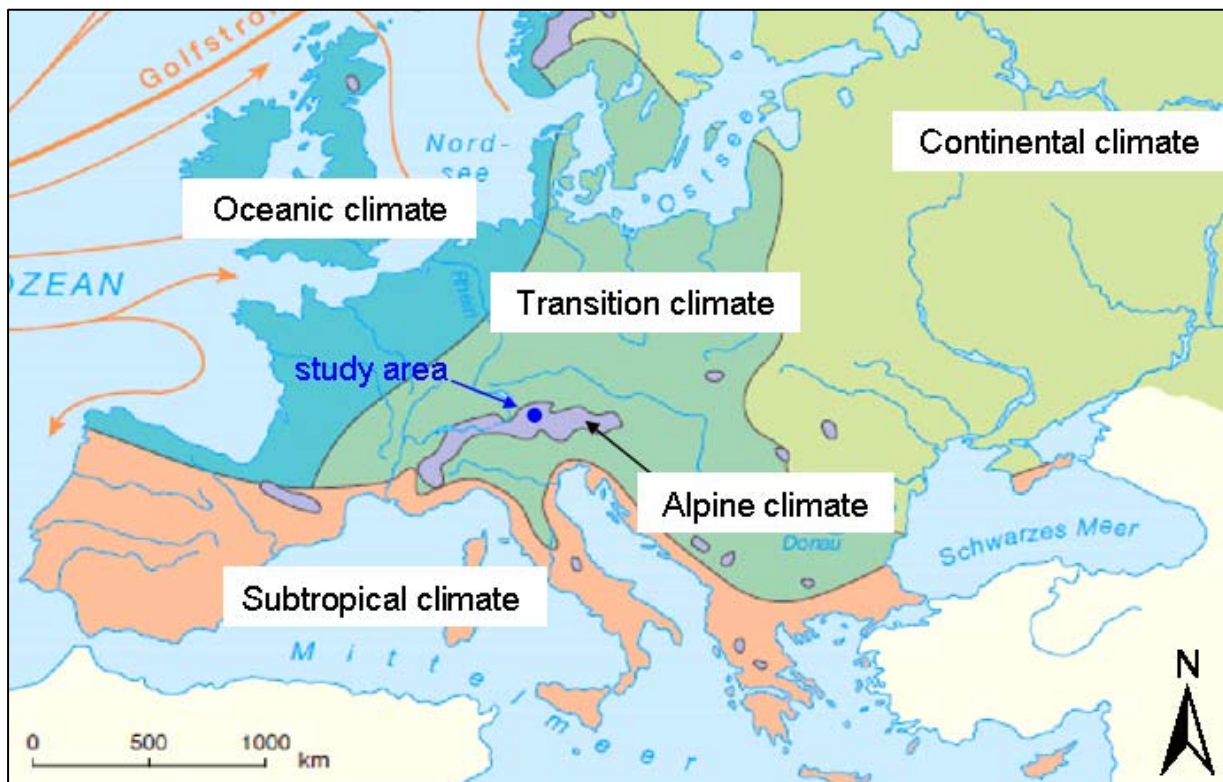


Figure 3: Climate zones of Europe (base map after DIERCKE (2014)).

Table 1: Elevation, mean annual temperature and mean annual precipitation of the meteorological stations next to the study area (TIROL ATLAS, 2013) as well as annual sum of days with frost (daily temperature minimum $<0.0\text{ }^{\circ}\text{C}$) (ZAMG, 2002).

Meteorological station	Elevation [m a.s.l.]	Mean annual temperature [$^{\circ}\text{C}$]	Mean annual precipitation [mm]	Annual sum of days with frost
Landeck	785	8.2	771	108.9
Galtür	1587	2.9	1123	193.9
St. Anton am Arlberg	1298	4.7	1304	169.5

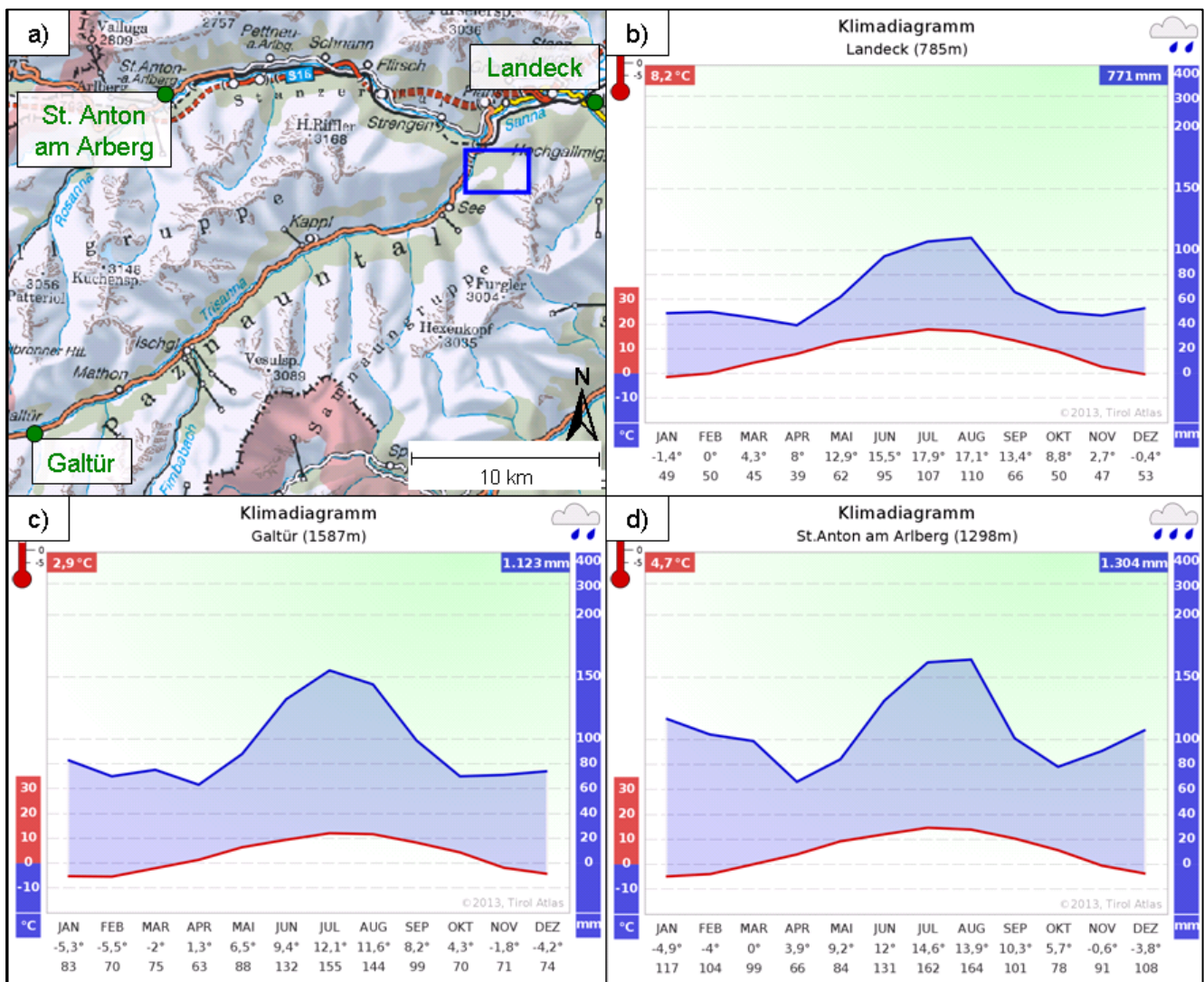


Figure 4: Location of the meteorological stations (a) (BEV, 2014), and climate charts of Landeck (b), Galtür (c) and St. Anton am Arlberg (d) (TIROL ATLAS, 2013).

1.3. Regional geologic setting

1.3.1. Tectonometamorphic evolution

The study area is composed of rocks of the Silvretta nappe (also called Silvretta-Seckau nappe system), which is part of the Austroalpine. According to TOLLMANN (1977) the Austroalpine nappe stack is divided into Upper, Middle and Lower Austroalpine and the Silvretta nappe belongs to the Middle Austroalpine (MAA) (Figure 5). Later authors like SCHMID et al. (2004) or SCHUSTER (2004) avoid the term “Middle Austroalpine”, since evidence was found that the former Upper Austroalpine is not structurally higher than the “Middle Austroalpine” but shows depositional contacts with it. Therefore, only Lower (LAA) and Upper Austroalpine (UAA) are distinguished and consequently the

Silvretta nappe is considered as part of the Upper Austroalpine basement nappes (Figure 5). The Silvretta nappe is the tectonically lowermost of the Upper Austroalpine nappes and lies above the Lower Austroalpine and Penninic units respectively (Figure 5 and Figure 6). It is confined by the Ötztal nappe in the northeast, the Penninic units of the Engadine window with the sinistral Engadine line in the east and southeast, the Err-Bernina nappe (Lower Austroalpine) in the southwest, Penninic units of Switzerland in the west as well as the Northern Calcareous Alps (NCA) and accordingly the Stanzertal fault zone, which separates the Silvretta nappe from the Bavarian nappes of the Northern Calcareous Alps, in the north (GRUBER et al., 2010; Figure 7).

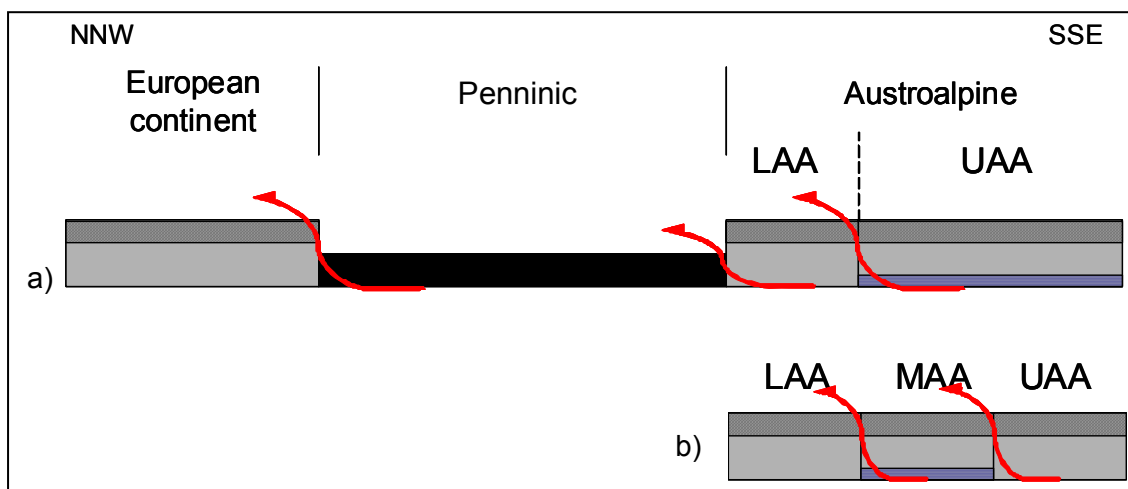


Figure 5: a) Schematic cross section showing the thrusting of the Austroalpine nappes over Penninic units and onto the European continent (modified after GEOZ (2010)); b) Conception of the Austroalpine nappes according to TOLLMANN (1977); LAA...Lower Austroalpine, MAA...“Middle Austroalpine”, UAA...Upper Austroalpine; light grey areas: basement nappes; dark grey areas: cover nappes; blue areas: position of the later Silvretta nappe; red arrows: direction of thrusting.

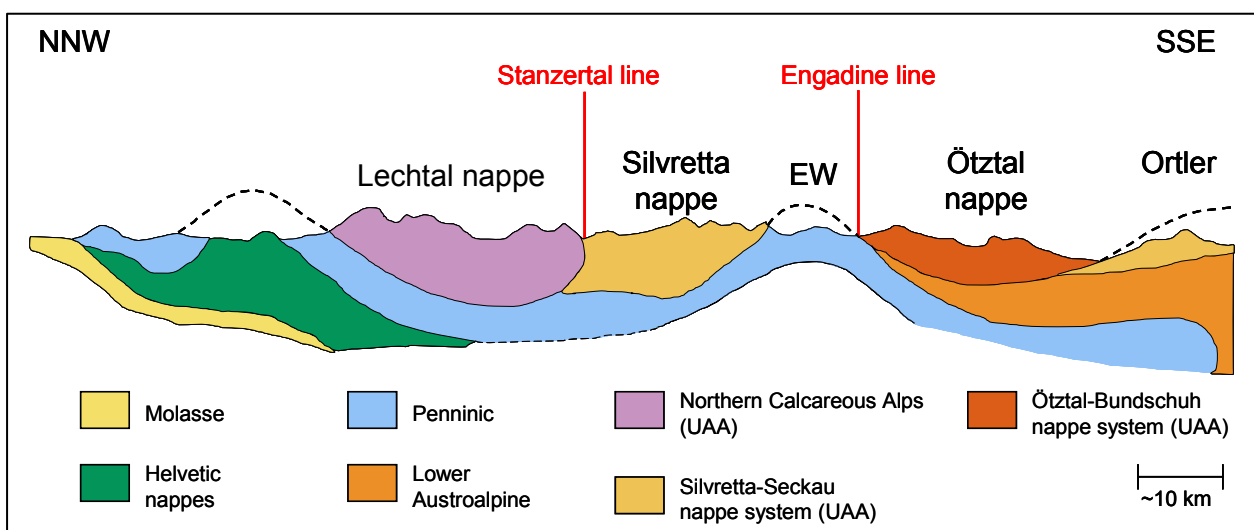


Figure 6: Schematic cross section through the western part of the Eastern Alps (modified after GEOZ (2010) using the map coloring of BOUSQUET et al. (2012)); UAA...Upper Austroalpine. The approximate location of the cross section is shown as black line in Figure 7.

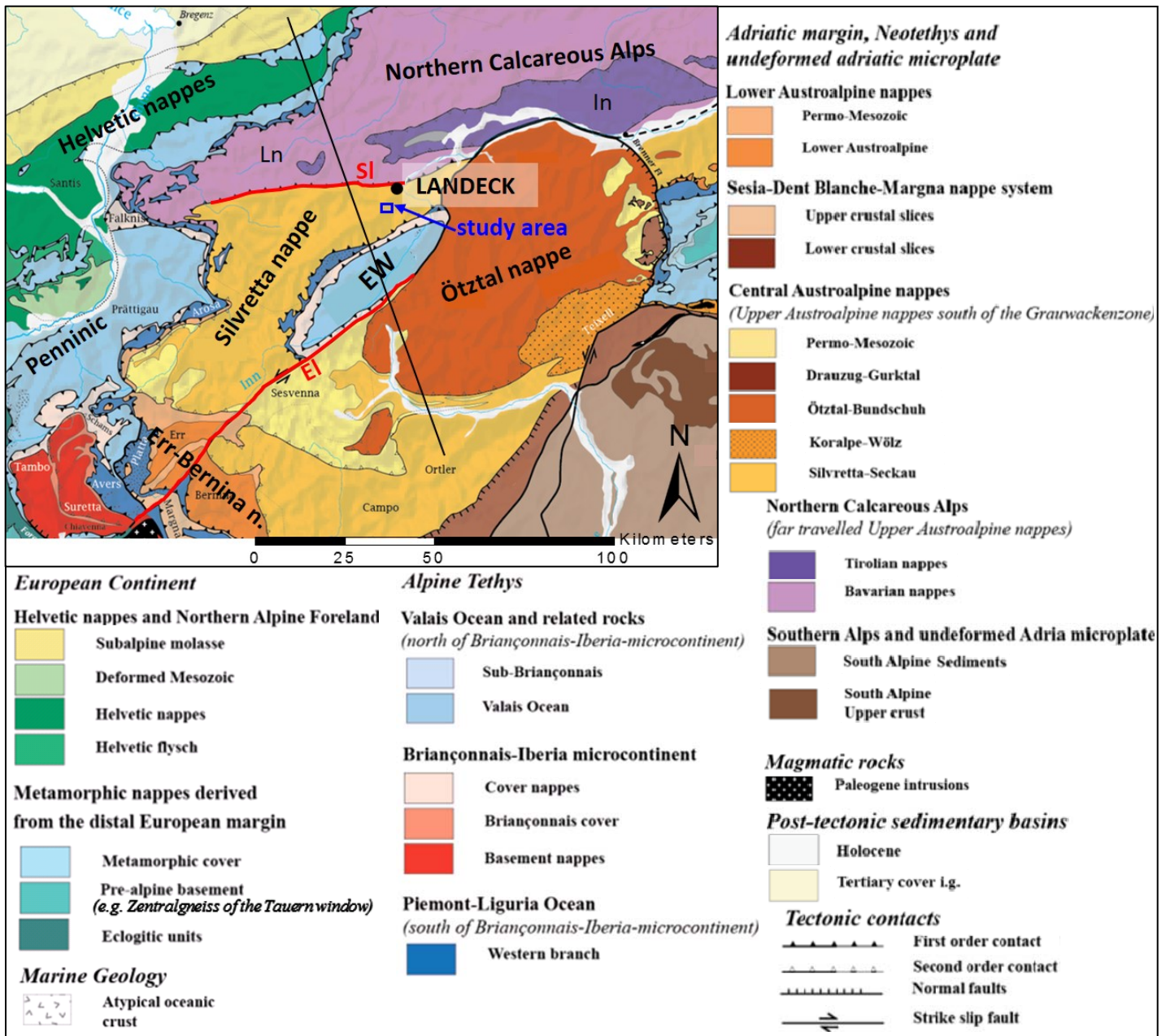


Figure 7: Tectonic map of the Silvretta nappe and its surroundings (modified after BOUSQUET et al. (2012)); SI...Stanzertal line, EI...Engadine line, Ln...Lechtal nappe, In...Inntal nappe. The black line represents the approximate location of the cross section shown in Figure 6.

According to its **tectonometamorphic evolution** GRUBER et al. (2010) divide the Silvretta nappe into three different complexes (Figure 8):

- The *Silvretta complex* in the central and southern part of the Silvretta nappe comprising the Silvretta crystalline sensu stricto which consists of amphibolites, ortho- and paragneisses, minor occurrences of migmatites and eclogites as well as Permian pegmatites near the border to the penninic Engadine window. It shows a mineral paragenesis and ductile deformation reflecting especially the Variscan metamorphic event that reached amphibolite to eclogite facies

conditions (metamorphic peak in the Devonian: 370 ± 17 Ma (MAGGETTI & FLISCH, 1993)) and was not affected by the Eoalpine and Alpine metamorphism.

- The *Venet complex* in the northern part of the Silvretta nappe, characterized by a retrograde overprint associated with the Alpine metamorphic event in the Cretaceous (110-90 Ma (MAGGETTI & FLISCH, 1993)), which also led to structural shortening in this area. The *Venet complex* was formerly known under the informal term “Landecker Quartzphyllite Zone” or “Landecker Phyllite-Gneiss Zone” and is composed of sometimes highly deformed micaschists and paragneisses that partly show phyllonitic structure. This structure also led to the name “quartzphyllonites” instead of quartzphyllites emphasizing their tectonic instead of a metamorphic evolution (cp. KÖHLER, 1983).
- The *Landeck Phyllite* at the border to the Northern Calcareous Alps in the north, which consists of light phyllites that only show prograde Alpine metamorphism (110-90 Ma (MAGGETTI & FLISCH, 1993)) reaching greenschist facies conditions.

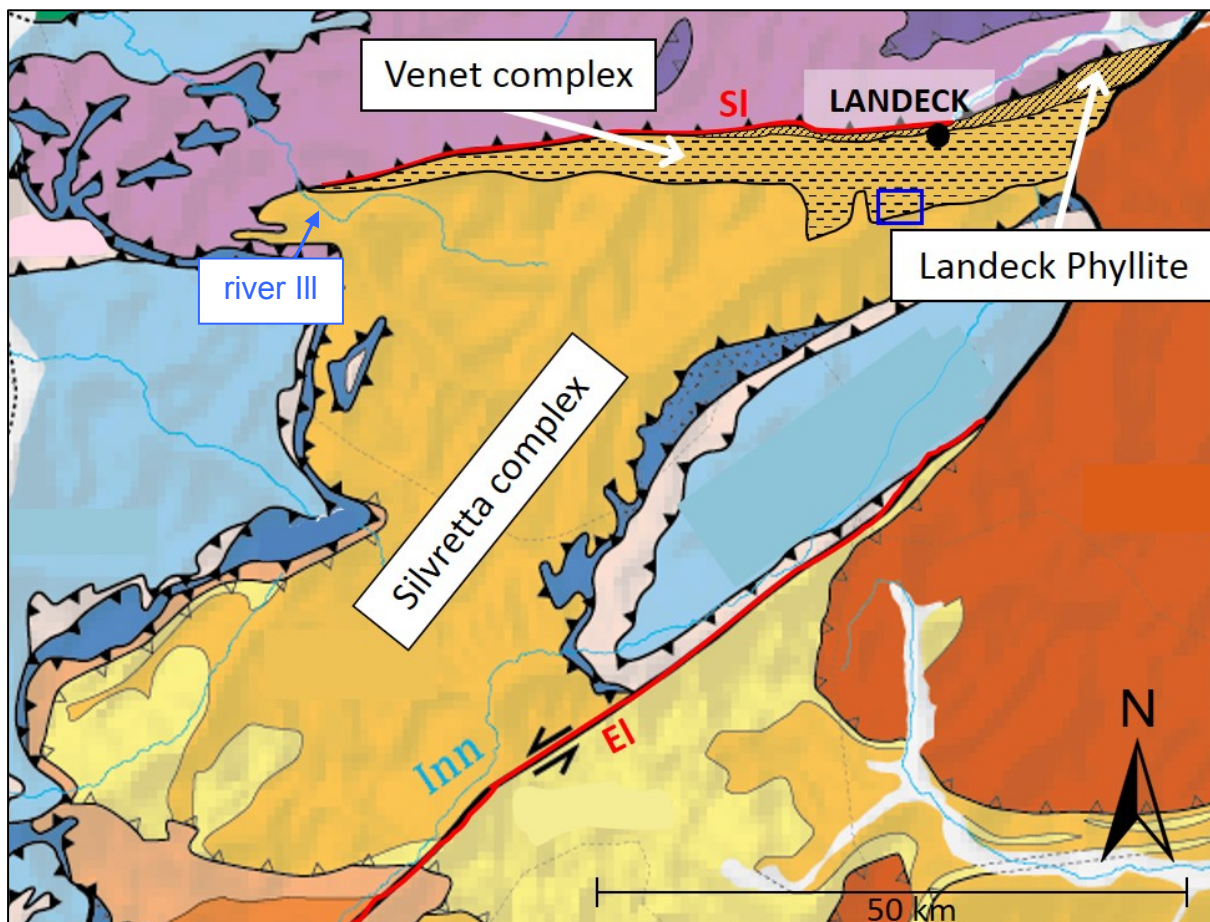


Figure 8: The silvretta nappe with its division into Silvretta complex (orange), Venet complex (dashed area) and Landeck Phyllite (hatched area) according to GRUBER et al. (2010) (base map modified after BOUSQUET et al. (2012)). The extension of the Venet complex across the Arlberg down to the river III was drawn according to the geologic map of Vorarlberg 1:200000 by OBERHAUSER & RATAJ (1998). SI...Stanzertal line, EI...Engadine line; blue frame: approximate location of the study area.

The **structural geologic evolution** of the Silvretta nappe is reflected by its joint set system, which originated from the Eocene (56-34 Ma) to Oligocene (34-23 Ma) phase of compression in NNE-SSW direction associated with the collision of the Adriatic with the European plate. This compression can especially be observed in the *Landeck Phyllite* near the Stanzertal line (Figure 8), a fault zone striking ENE-WSW to ESE-WNW and consisting of several steeply south or north dipping faults. The Stanzertal fault zone was also active during the thrusting of the Silvretta nappe onto the Northern Calcareous Alps in the Miocene (23-5.3 Ma) and is assumed to be related to the genesis and orientation of the Stanzer valley as well as the northeastern part of the Paznaun valley (GRUBER et al., 2010).

1.3.2. Quaternary evolution

In the Quaternary (2.58-0 Ma (GIBBARD et al., 2010)) the Alps were subject to several glacial episodes. Since the Middle Pleistocene (~800 ka) four periods of glaciation (Günz, Mindel, Riss and Würm) are known. During the Last Glacial Maximum (24-21 ka, Würmian glacial period) the Paznaun, Stanzer and Inn valley in the area of Landeck were covered with ice up to 2000-2300 m a.s.l. (Figure 9), resulting in a typical glacial morphology of the valleys and their adjacent slopes (GRUBER et al., 2010). Due to glacial dynamics and the weight of these thick ice masses many Alpine valleys evolved from V-shaped into U-shaped valleys, which often show a significant overdeepening, meaning that the top of the bedrock is located sometimes hundreds of meters below today's surface and was covered with fluvial or fluvio-glacial deposits in late-glacial to post-glacial times. The overdeepening of valleys is often related to pre-defined tectonic structures, the confluence of two or more glaciers, highly erodible lithologies and the strong erosional effect of the glaciers, which is much more efficient compared to fluvial erosion (PREUSSER et al., 2010). In addition to U-shaped valleys, characteristics of glacial overprints are cirques, glacial polishes and whale backs as well as moraine sediments or sediments at the ice margin, which consist of transported loose material (of moraine or talus deposits) that was re-deposited at the margin of collapsing dead ice especially in areas where creeks of secondary valleys flew into the main valley (GRUBER et al., 2010).

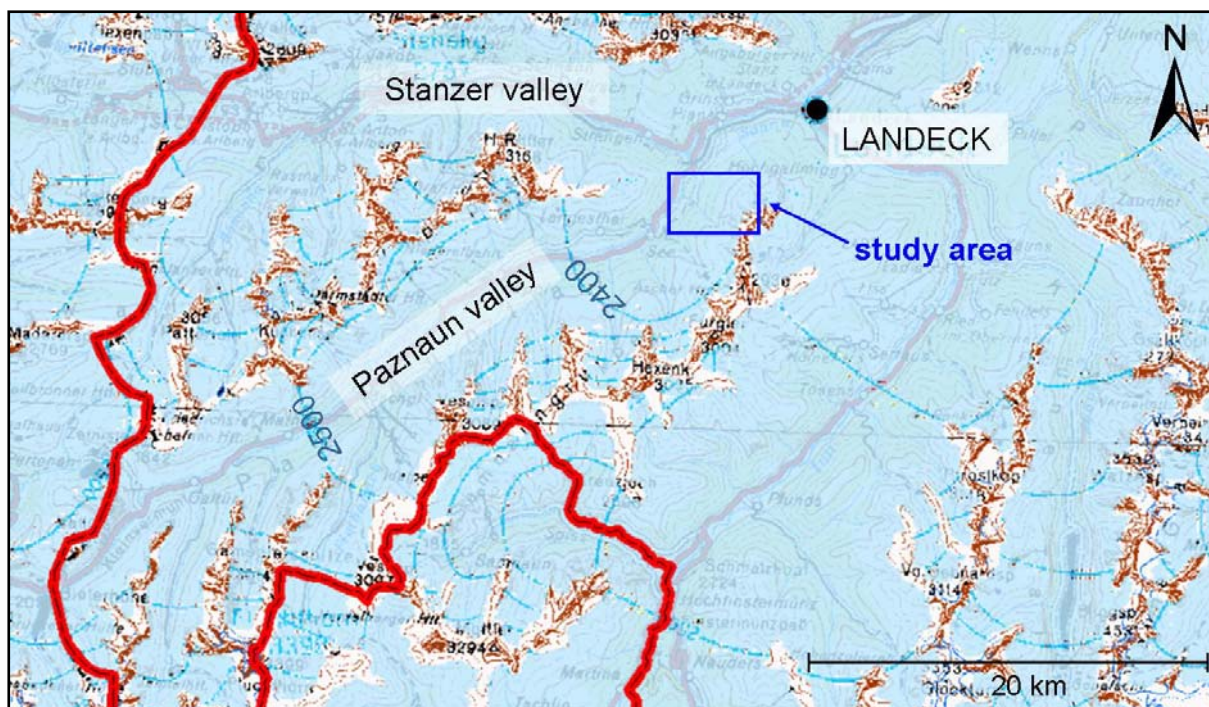


Figure 9: Ice cover during the last glacial maximum (Würm) in the region of the study area (derived from <http://earthscience.at/maps/>). The contour lines of the Paznaun glacier for 2400 m and 2500 m a.s.l. are labeled.

The formation of U-shaped valleys and their overdeepening also led to over-steepening of the adjacent slopes often resulting in gravitational slope deformations starting immediately after the melting of the glacier in late-glacial time. These slope movements caused changes in the course of valleys and sometimes also built natural dams leading to episodic retention of rivers (GRUBER et al., 2010).

1.4. Slope stability

1.4.1. Landslide processes

In the present thesis, similar to VARNES & IAEG (1984), any kind of gravitational mass movement on a slope (comprising rock or soil material) is termed “landslide”, although their mechanism may not meet the definition of a true “slide” (e.g. rockfalls, topples, flows, etc.). The process of a landslide comprises its failure mechanism, the involved material, the type and velocity of movement or deformation, the state of activity, and the causes and triggering factors responsible for the evolution of the landslide as well as the resulting effects. The knowledge of these parameters is important for the understanding of

the landslide and subsequently to be able to take reasonable actions to stabilize the affected slope or prevent further damage (CRUDEN & VARNES, 1996). In the following chapter an overview of landslide types as well as their causes, triggering factors and effects shall be given.

1.4.1.1. Failure mechanisms and landslide types

There have been numerous attempts and approaches to classify landslides. In the present thesis the classification concerning the **type of movement** following CRUDEN & VARNES (1996) shall be used. It distinguishes five different types of landslide kinematics:

- Fall: On steep slopes rock or soil material, which was previously separated from the intact rock or undisturbed soil mass by small sliding or toppling movements (except in case of undercutting), detaches along a surface without (or with only little) shear displacement (Figure 10a). The detached mass subsequently descends by (free) falling, bouncing and rolling depending on the slope inclination, with the movement being very rapid to extremely rapid (>3 m/min).
- Topple: A rock or cohesive soil mass rotates about a point or edge that is located below its center of gravity. The displacement of the mass can be extremely slow (<16 mm/year) to extremely rapid (<5 m/s), and can subsequently cause falls or slides of the loosened material (CRUDEN & VARNES, 1996). Furthermore, toppling failures can go quite deep and also affect large mountain slopes (e.g. REITNER & LINNER, 2009). The rock mass can consist of single or multiple blocks formed by joints dipping into the slope. The single layers or columns tend to overhang and form obsequent scarps (upslope facing exposures). Toppling can only occur, when sliding is kinematically inadmissible, meaning there is no possible sliding plane or it does not daylight into the slope or the excavation (GOODMAN & KIEFFER, 2000). For flexural toppling to be kinematically admissible, GOODMAN & BRAY (1976) stated the following condition (Figure 10b):

$$(90 - \delta + \varphi) < \alpha \quad (1)$$

(δ ...dip angle of the concerned discontinuity, φ ...friction angle of the discontinuity, α ...dip angle of the slope)

- **Slide:** A soil or rock mass moves downslope on one or more surfaces of rupture or on a relatively thin shear zone. Depending on the geometry of the sliding surface rotational slides (concave, curved sliding surface) and translational slides (planar or undulating sliding surface) can be distinguished (Figure 10c and 10d). For hard rocks translational slides can be further divided into planar slides, where sliding occurs along one plane which must daylight into the slope or excavation, and wedge slides, where sliding occurs along the line of intersection of two non-parallel discontinuities if the intersection line daylights (GOODMAN & SHI, 1985; Figure 10e). Failure planes can also be composed of two or more discontinuity sets (foliation and joint sets), resulting in a stepped rupture surface. The velocities of slides can reach from extremely slow to extremely rapid (CRUDEN & VARNES, 1996).
- **Spread:** A cohesive soil or rock mass extends and its separated fragments subside into the softer underlying material with the surface of rupture showing no considerable shear strain (Figure 10f). Types of spreads include block spreads and liquefaction spreads.
- **Flow:** A soil or rock material moves in a spatially continuous way with its velocity distribution similar to a viscous fluid. The shear surfaces are closely spaced and only develop temporarily (CRUDEN & VARNES, 1996). There are also cases where no shear zones develop at all. The velocities of flows range from extremely slow (flow processes in hard rock, which are also called rock creeps) to extremely rapid (debris flows) (ZANGERL et al., 2008).

Other types of movement, not mentioned in the classification above, are for example rock slumping (KIEFFER, 1998), column buckling or block torsion (GOODMAN & KIEFFER, 2000). Rock slumping is the rotation of blocks formed by a steep, non-daylighting discontinuity set, and a shallow dipping discontinuity, which daylights (Figure 11a). Buckling occurs when thin rock columns fail due to compression (Figure 11b), whereas block torsion describes the failure of a single block which rotates about an axis if sliding is blocked (Figure 11c).

In addition to the type of movement, landslides can be distinguished, for example, according to their **velocity** from *extremely slow* (<16 mm/year) to *extremely rapid* (>5 m/s) or according to the **material** they consist of. The material can either be described as rock (intact rock before the displacement) or

soil (loose material resulting from transport or weathering), which is divided into *earth* ($\geq 80\%$ of the particles < 2 mm) and *debris* (20-80% of the particles > 2 mm). Furthermore, the **state of activity** (*active* or *inactive*) can be taken into account. An inactive landslide where the causes are still present and the possibility of further movement remains existent is *dormant*, whereas inactive landslides that become active again are called *reactivated* (CRUDEN & VARNES, 1996).

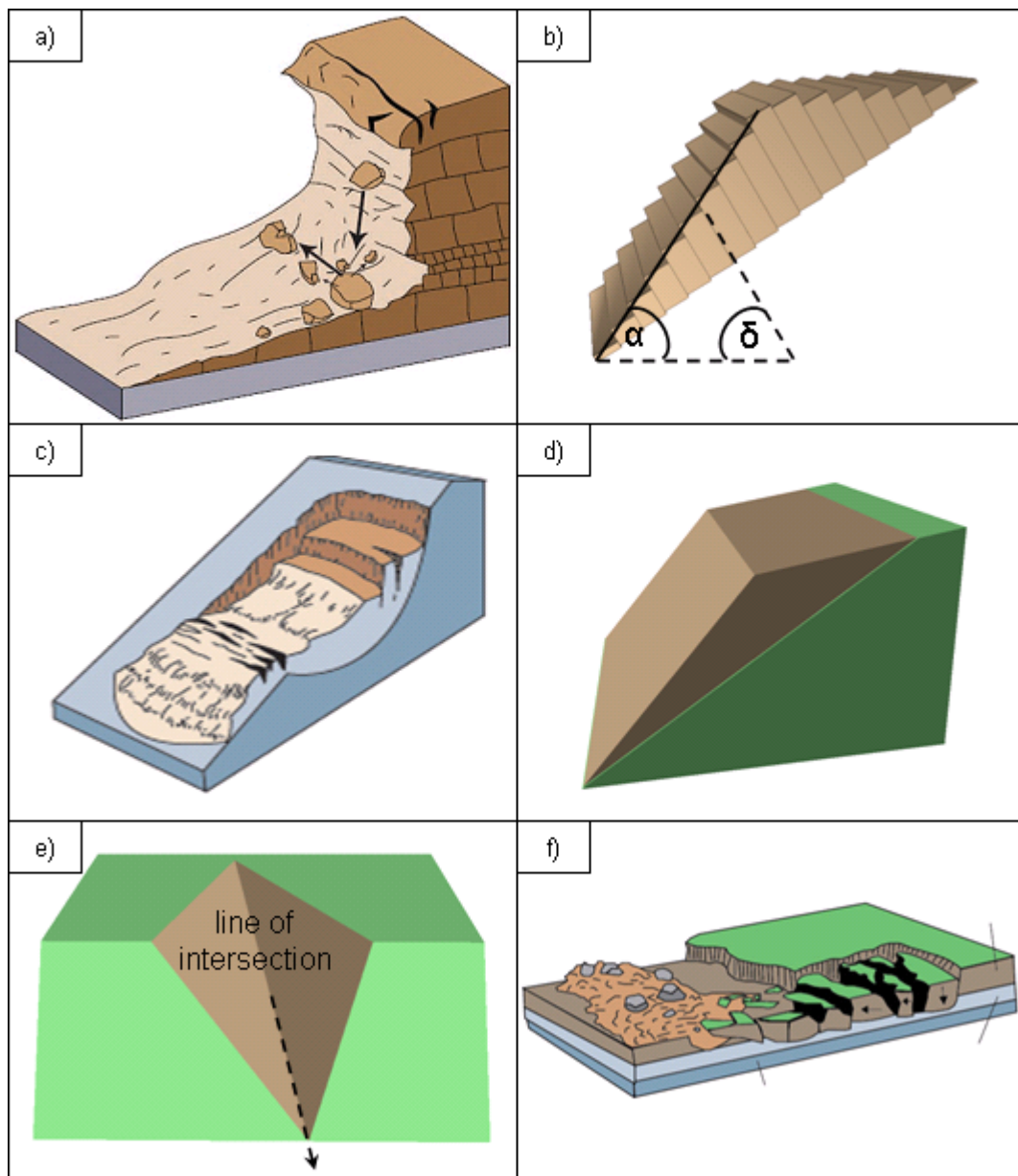


Figure 10: Types of landslide movement: fall (a), topple (b), rotational slide (c), translational planar slide (d), wedge slide (e) and spread (f); Pictures a) and f) were taken from HIGHLAND & BOBROWSKY (2008), c) from USGS (2014) and b), d) and e) were modified after RocSCIENCE (2014b).

If a rock slope consists of several rock or soil types with different geotechnical properties and different structural features, a landslide which affects the entire slope will very likely also comprise more than

one type of failure or movement (GOODMAN & KIEFFER, 2000). CRUDEN & VARNES (1996) proposed the term *composite slides* for this type of landslides.

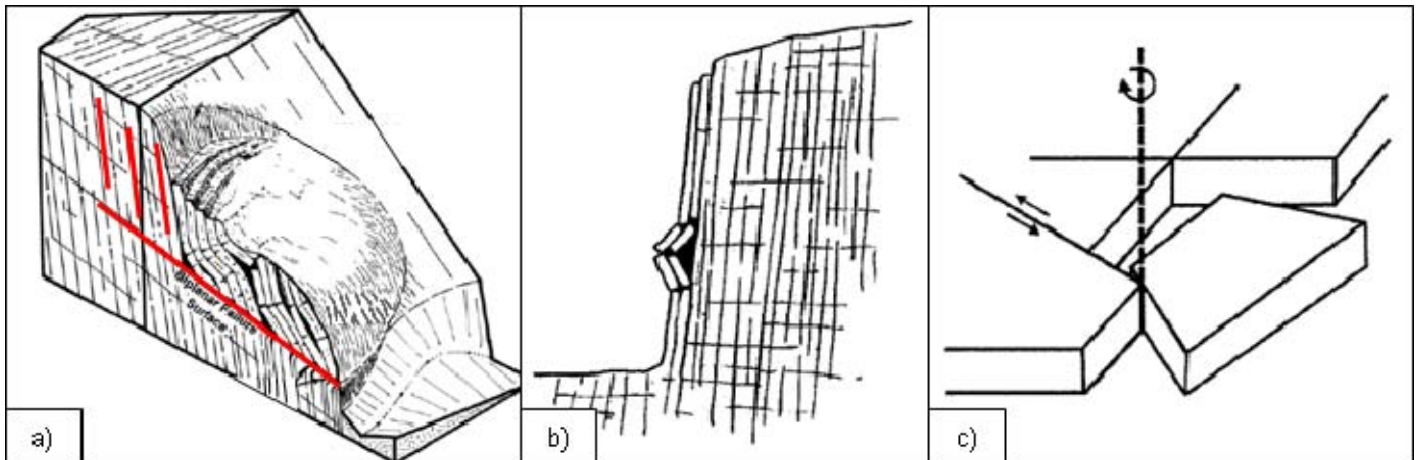


Figure 11: Further types of landslide movement: rock slumping (a) with daylighting and non-daylighting discontinuities in red (modified after KIEFFER (1998)), column buckling (b) and block torsion (c) (GOODMAN & KIEFFER, 2000).

In connection with glacial overprinted landscapes (oversteepened slopes and overdeepened valleys) several expressions are used for large and deep landslides or unstable mountain slopes. According to ZISCHINSKY (1968) the terms *Bergzerreißung* (“mountain splitting”) and *Talzus Schub* (“closing-up of valleys”) describe the morphologic phenomena at the mountain ridge and in the toe region of a slope respectively, which often result from the tendency of compensating oversteepened flanks. However, particularly “*Talzus Schub*” is used for whole landslides as well, generally indicating a relatively slow downslope movement (often without the formation of a distinct sliding or shear zone), and is sometimes also called *creeping slope* referring to its velocity in the range of cm/year (e.g. EDER et al. (2006)) or *sagging mountain slope* (e.g. MOSER, 2002a, b). The term *Sackung* (“sagging” – or “subsidence” after ZISCHINSKY (1969)) also became popular for slowly deforming mountain slopes, but was applied for different mechanisms and deformation processes, which led to confusions (POISEL et al., 2011). If the exact mode of failure or type of movement is known, e.g. the term rockslide (or also deep-seated rockslide) can be used, otherwise the general expressions *deep-seated (gravitational) slope deformations* or *deep-seated landslides* are suitable (e.g. ZANGERL et al. (2007), ZANGERL & PRAGER (2008)).

1.4.1.2. Landslide causes and triggering factors

To understand the processes involved in slope deformations, not only the failure mechanism or landslide type is important, but also the determination of the causes and triggering factors. The *causes*

of a landslide are the sum of factors that make a slope vulnerable to failure and form the condition so that a landslide could potentially occur. The *trigger*, however, is the factor that finally initiates the movement (WIECZOREK, 1996). Landslide causes are, for example, the geological or morphological conditions including the occurrence of weak, weathered or jointed material, contrasts in permeability or stiffness, or glacially steepened slopes (CRUDEN & VARNES, 1996).

A landslide finally occurs when the destabilizing (or driving) forces exceed the stabilizing (or resisting) forces. This is expressed by the Factor of Safety (FS):

$$FS = \frac{\sum R}{\sum D} \quad (R \dots \text{resisting forces, } D \dots \text{driving forces}) \quad (1)$$

If the factor of safety is >1 the slope is stable, if it is <1 the landslide can occur. If $FS=1$, the slope is in a limiting (or equilibrium) state. Resisting forces include the shear strength of the material, engineering constructions such as retaining walls or anchors, water control (drainages), and the protection of the ground surface against erosion. Driving forces, which therefore act as triggering factors, are changes in the hydrogeologic conditions (heavy rainfalls, snowmelt, rapid reservoir drawdown) or changes in the loading conditions (additional load on the crest, or excavation or erosion of the toe), earthquakes, volcanic activity, denudation and the factor of time (KIEFFER, 2012).

1.4.1.3. Effects of landslides

The effects of landslides can be numerous, like for instance the changes in the morphology of a mountain slope, the changes in the course of valleys and rivers, or the disposal of loose material (geotechnic soils). The motivation of studying landslides, however, results from the effects they can have on human life in the broadest sense, i.e. the fact that they can cause loss of life or property as well as environmental harm. The term **hazard** describes the probability that such a potentially damaging landslide occurs within a given time and area. **Risk** (or total risk), however, is defined as the expected economic impact, environmental impact, and social impact (number of lives lost, people injured, or damage to property) caused by a particular landslide. It can also be seen as the product of the *elements at risk* (people, properties, economic activities, and environment), the *vulnerability* (degree of loss to the elements at risk) and the hazard (VARNES & IAEG, 1984). Beside the risk to human lives and houses, engineering geology and civil engineering especially deal with the impact of

landslides on constructions, such as roads, tunnels, bridges, railway tracks, water pipes, sewage pipes and gas pipes, reservoir dams, etc. Some of the tasks in this context are: the recognition and evaluation of potential landslides, finding a way to avoid an already affected or potentially unstable slope, the monitoring of the slope if avoidance is not feasible, and taking actions to repair affected engineering structures or prevent further damage.

To minimize the risk so-called susceptibility maps (marking territories favouring slope failures) and hazard maps (showing the probability of landslide occurrences in specific areas) are prepared for many regions. These maps divide the territory into zones which subsequently are used as recommendations where to construct buildings, infrastructure, etc., and where not. The risk assessment, however, deals with the determination of the loss or damage to the elements at risk, that would be caused by a landslide (GUZZETTI, 2005).

1.4.2. Regional landslide activity

In the area of Landeck several mountain slopes are affected by deep-seated landslides. In the following chapter the selected reference examples for the present thesis (Zintlwald and Niedergallmigg) shall be described. Furthermore, some other landslides of this area are mentioned giving their state of investigation or knowledge.

1.4.2.1. Zintlwald

The landslide Zintlwald is located in the eastern Stanzer valley, south of the “Zintlkopf” and reaches down to the river Rosanna in the south (Figure 12). It is situated in the *Venet complex* of the Silvretta nappe south of the Northern Calcareous Alps (GRUBER et al., 2010; see chapter 1.3.1.). The area of the landslide Zintlwald mainly consists of quartzphyllonites and phyllonitic micaschists, and was subject to intense tectonic activity resulting in a distinct foliation (generally dipping to the south to southeast), and faults with partly heavily sheared rock materials. The landslide Zintlwald was known as deep-seated slope deformation for a long time, but was assumed to be inactive in great parts – except for some extremely slowly moving areas of the toe. It became subject to detailed investigations after two smaller subareas of it accelerated in August 2005 during a heavy rainfall and flood event (Figure 12). A section of the B316 Arlberg road with a maximum vertical displacement of 8 m and parts

of the power plant Wiesberg as well as the subsequent penstock were destroyed (HENZINGER et al., 2009).

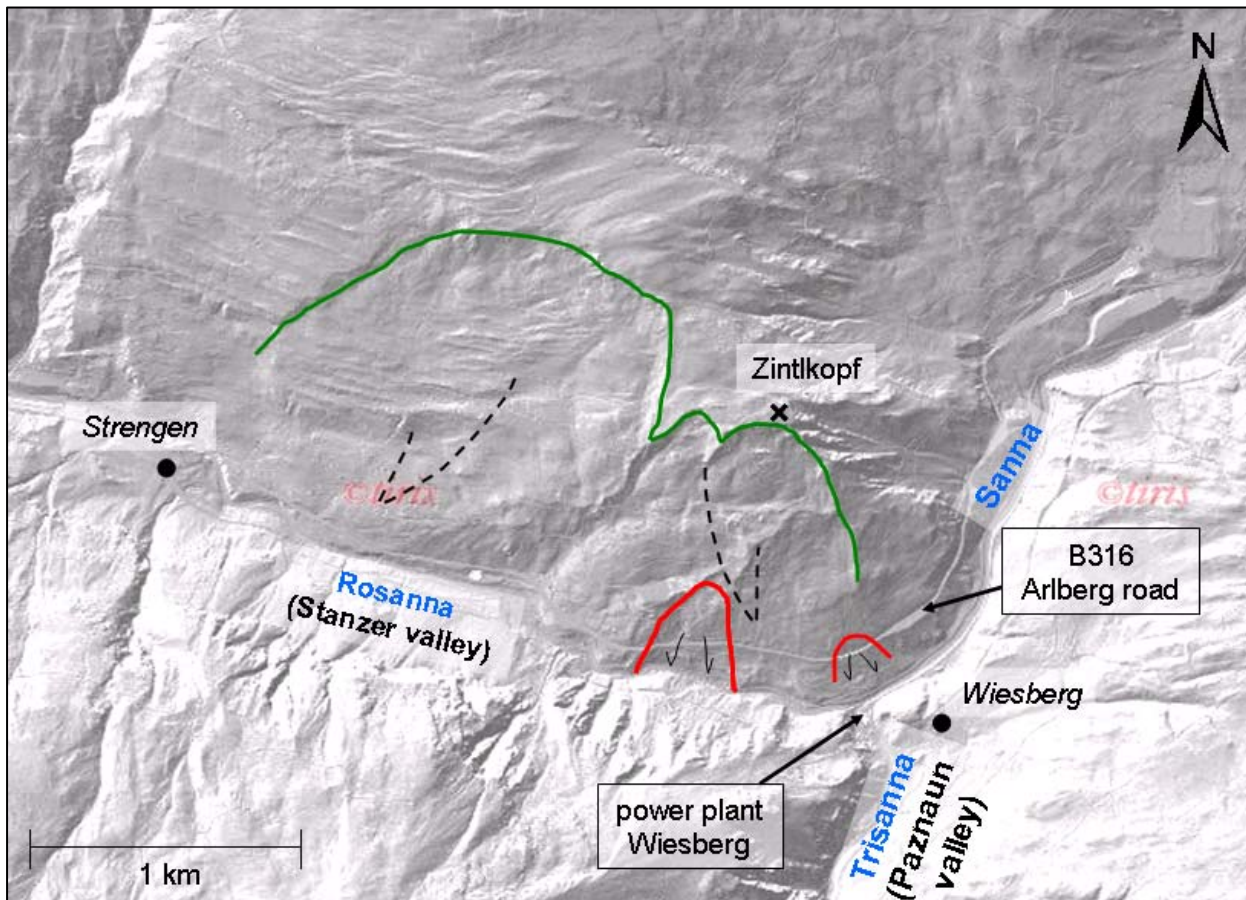


Figure 12: Laserscan image (hillshade display from TIRIS (2013)) of the landslide Zintlwald with the two areas (re)activated in 2005 (red lines) and older currently inactive headscarps (green line) (after HENZINGER et al., 2009).

Field investigations and a first geodetic monitoring via surface measurement points, followed by a long-time monitoring from November 2005 on, as well as further investigations later in 2005 and in 2006 (reflection and refraction seismics as well as core borings, which were afterwards installed as inclinometers and piezometers respectively) allowed the determination of the landslide kinematics and processes. It could be deduced that the areas showing the highest deformation rates are connected with those where the top of the bedrock descends and leaves a bearing of ~30-40 m (sometimes even more) of soil-like material. The transition to the intact rock, however, is diffuse, since it is broken to large fragments embedded within a more disintegrated, fine-grained matrix (Figure 13; HENZINGER et al., 2009). Furthermore, it could be seen that the valley of the Rosanna was once deeper and also broader, and that the landslide Zintlwald in its toe region has moved into this former valley and most likely over fluvial Rosanna sediments. The mechanisms and deformation velocities differ spatially and also in depth (POSCHER et al., 2006). EDER et al. (2006) and POSCHER et al. (2006) describe three different types of movement for the landslide Zintlwald:

- Large part of the slope reaching from the east of the Zintlkopf to Strengen shows very slow movements (of a few cm/year or less) or is currently even inactive. This is referred to as the *creeping slope deformation* represented by old headscarps (Figure 12). Its depth is not known and its movement doesn't affect the road or any other constructions. An activation of the entire deep-seated landslide in terms of a catastrophic failure is not expected.
- Smaller parts within the above mentioned creeping slope feature increased, but still very slow velocities (of a few cm/day or m/year respectively). The two areas (re)activated in 2005 are considered to be related to the formation of shallow sliding surfaces within the soil-like material or along older failure surfaces. The thickness of the sliding masses is assumed to reach a few tens of meters. HENZINGER et al. (2009) estimate the depth of the sliding zone with 25 to 30 m beneath the Arlberg road (Figure 14).
- Debris flows that sometimes evolve from the uppermost layers of the soil-like material travel with moderate velocities of up to 1.3 m/day. Their movement is clearly correlated to precipitation and phases of snowmelt.

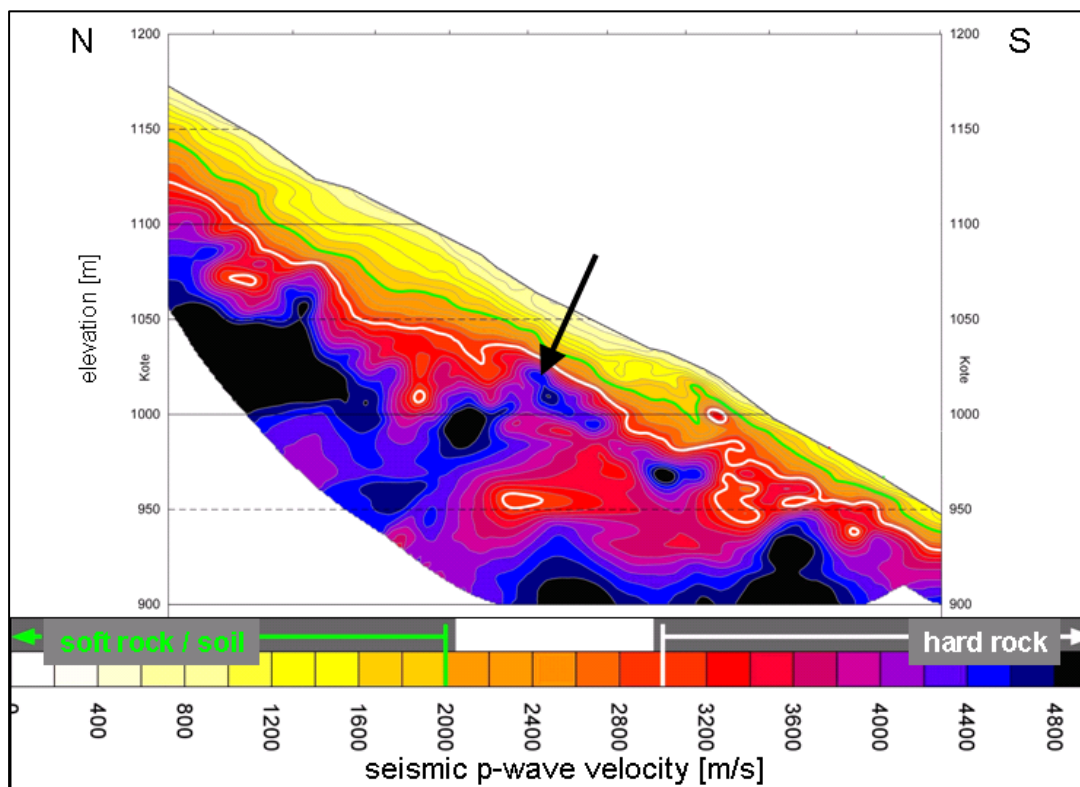


Figure 13: Velocity field of the (re)activated landslide derived from refraction tomography (HENZINGER et al., 2009). From the different velocities the composition of the subsurface can be inferred. The black arrow marks a region with higher velocities, interpreted as a fragment of hard rock floating within more disintegrated and soil-like material.

The triggering factors of the 2005 landslides were the erosion of the toe by the river Rosanna and the rising groundwater level within the slope. The varying subsurface conditions mentioned above result in a small-scale differing groundwater situation. The quartzphyllonite itself exhibits only low permeability and no persistent groundwater level, whereas the disintegrated and soil-like material allows a considerably higher conductivity. Open crevices in the upper (extensional) parts of the sliding masses additionally facilitated the infiltration of surface waters (POSCHER et al., 2006). Therefore, the taken actions to stabilize the slope or at least decelerate its movement included the support of the river bed of the river Rosanna to prevent further erosion, and the drainage of the steeper areas of the slope (HENZINGER et al., 2009).

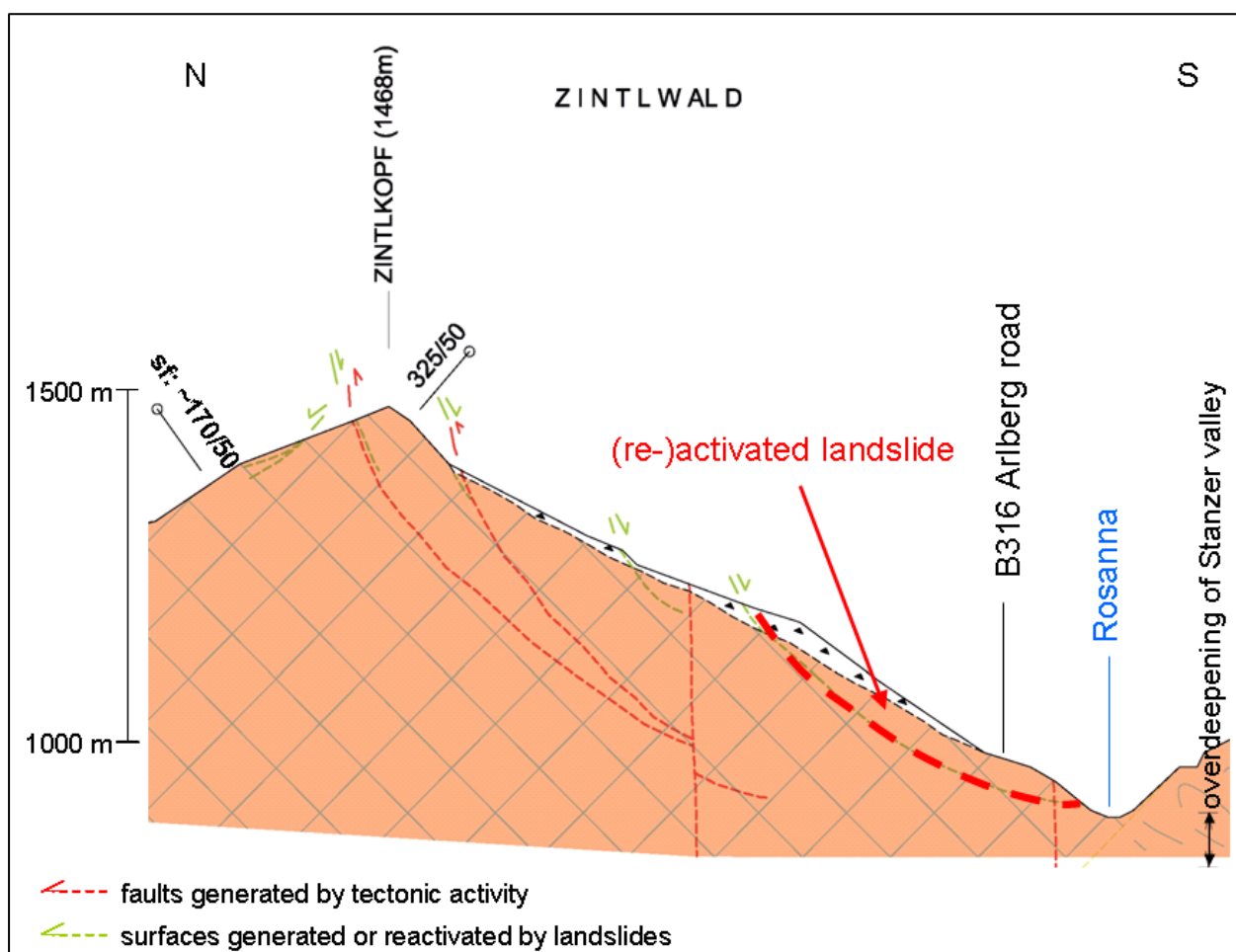


Figure 14: Cross section through the deep-seated slope deformation Zintlwald and the western landslide (re)activated in 2005 (after B316 ARLBERGERSATZSTRASSE (2005)).

1.4.2.2. Niedergallmigg

The landslide Niedergallmigg is located in the upper Inn valley southeast of the town Landeck and reaches from the Matekopf in the south down to the river Inn in the north (Figure 15). It is situated in

the Silvretta nappe with the middle and lower part belonging to the *Venet complex* (consisting of phyllonitic micaschists and paragneisses, and partly amphibolites) and the headscarp area built up by biotite-muscovite schists and paragneisses of the *Silvretta complex* (see chapter 1.3.1.). The foliation planes generally dip to the southeast (into the slope) with flat to medium inclined dip angles, sometimes due to folding also to the northwest. The area of the landslide also features steeply dipping brittle faults that strike E-W. The hard rock units are often covered by moraine deposits or rockfall blocks. The landslide affects the village Niedergallmigg, the weir of the power plant Inn/Runserau, and the river Inn that erodes at the toe of the landslide (KIRSCHNER, 2006).

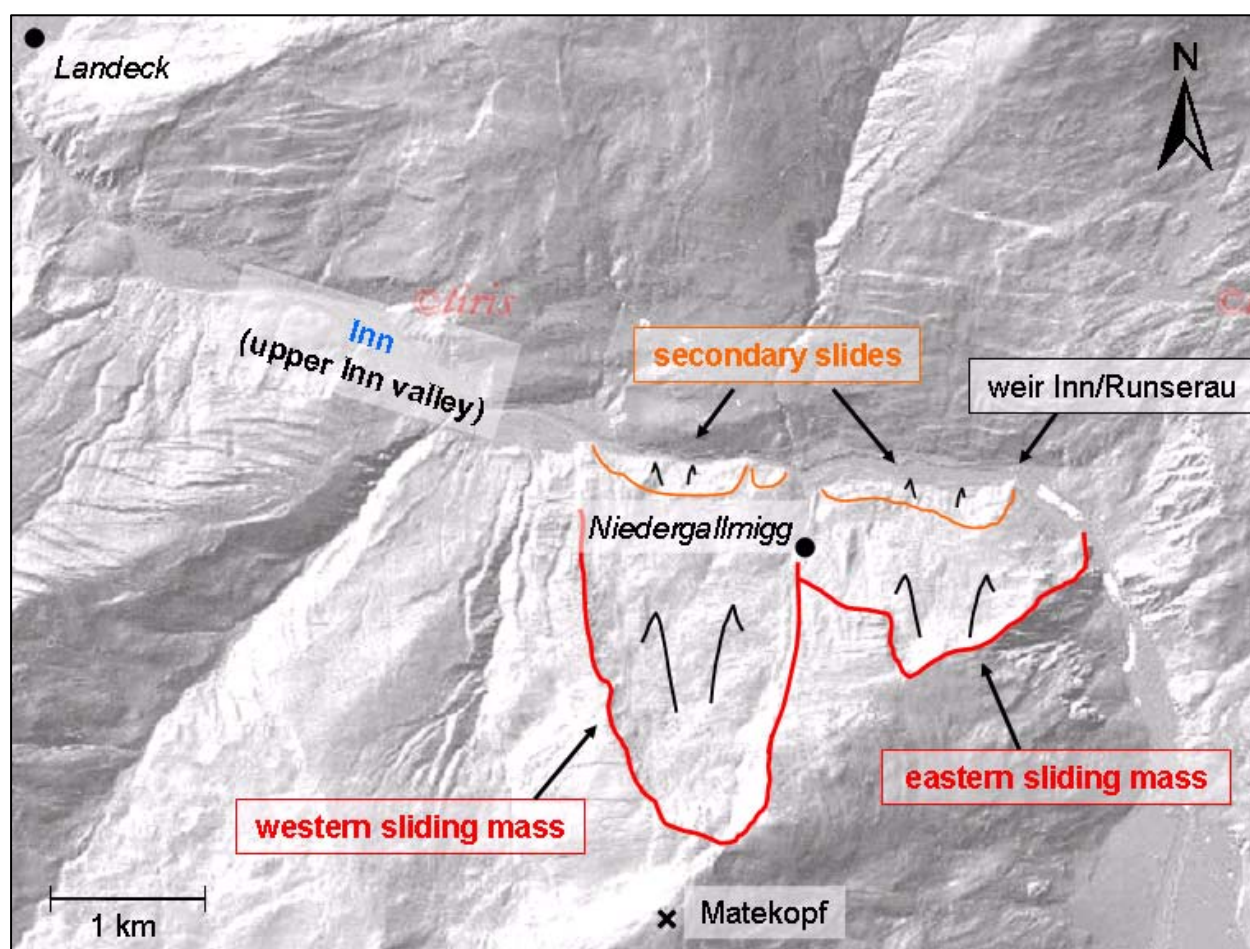


Figure 15: Laserscan image (hillshade display from TIRIS (2013)) of the landslide Niedergallmigg with the main scarps of its western and eastern sliding mass (red) as well as the secondary slides (orange) after ZANGERL et al. (2012).

The landslide Niedergallmigg can be divided into a western and an eastern sliding mass (Figure 15). According to ZANGERL et al. (2012) the eastern sliding mass is dormant or moving extremely slowly (with a few mm/year), whereas the western sliding mass shows movement rates of up to approximately 7 cm/year. Velocities received from geodetic monitoring between 1974 and 1996 were even given with up to 10 cm/year (KIRSCHNER, 2006). Already then it was assumed that the entire

slope from the Inn up to the Matekopf was moving. From 2003 to 2006 further monitoring and investigations were carried out, which confirmed the earlier results, and allowed the determination of further landslide characteristics:

- From reflection and refraction seismics a maximum depth of the landslide of 320 m could be deduced. The results also suggest that fragments of hard rock form isolated sliding bodies (KIRSCHNER, 2006).
- Field studies show that the headscarp of the landslide was formed by orthogonal joint sets that strike NE-SW and NW-SE. The formation of the sliding zone was favoured by folding and semi-ductile deformation resulting in intensely broken and sheared rocks at the border between *Venet complex* and *Silvretta complex* (KIRSCHNER, 2006). The existence of a discrete sliding zone is not proven but still assumed due to the difference in the seismic velocities between the intact rock and the deformed sliding mass, as well as the formation of a headscarp across the entire slope (ZANGERL et al., 2012).
- The plunge of the total displacement vectors decrease from 36° in the upper part of the landslide to 6° in the lower part, hypothesizing a rotational sliding behaviour of the above mentioned shear zone (Figure 16; ZANGERL et al., 2012).
- Due to the changes in the slope topography as well as the fracturing and fragmentation of the rock mass caused by the landslide, also the mechanical and hydrogeological conditions changed leading to secondary slides at the toe of the slope (Figure 15) that are more like soil-type slides in contrast to the entire landslide which is termed rockslide. These secondary slides were probably also favoured by the erosion of the river Inn and heavy rain fall or snowmelt (ZANGERL et al., 2012).
- It could also be deduced that the sliding mass was thrust on the fluvial or fluvio-glacial sediments of the overdeepened valley and deflected the course of the river Inn to the north (Figure 16). Area and volume balances show that a large volume of the landslide material at its toe is missing, supposing high fluvial erosion rates of the river Inn that lead to such mass losses (ZANGERL et al., 2012).

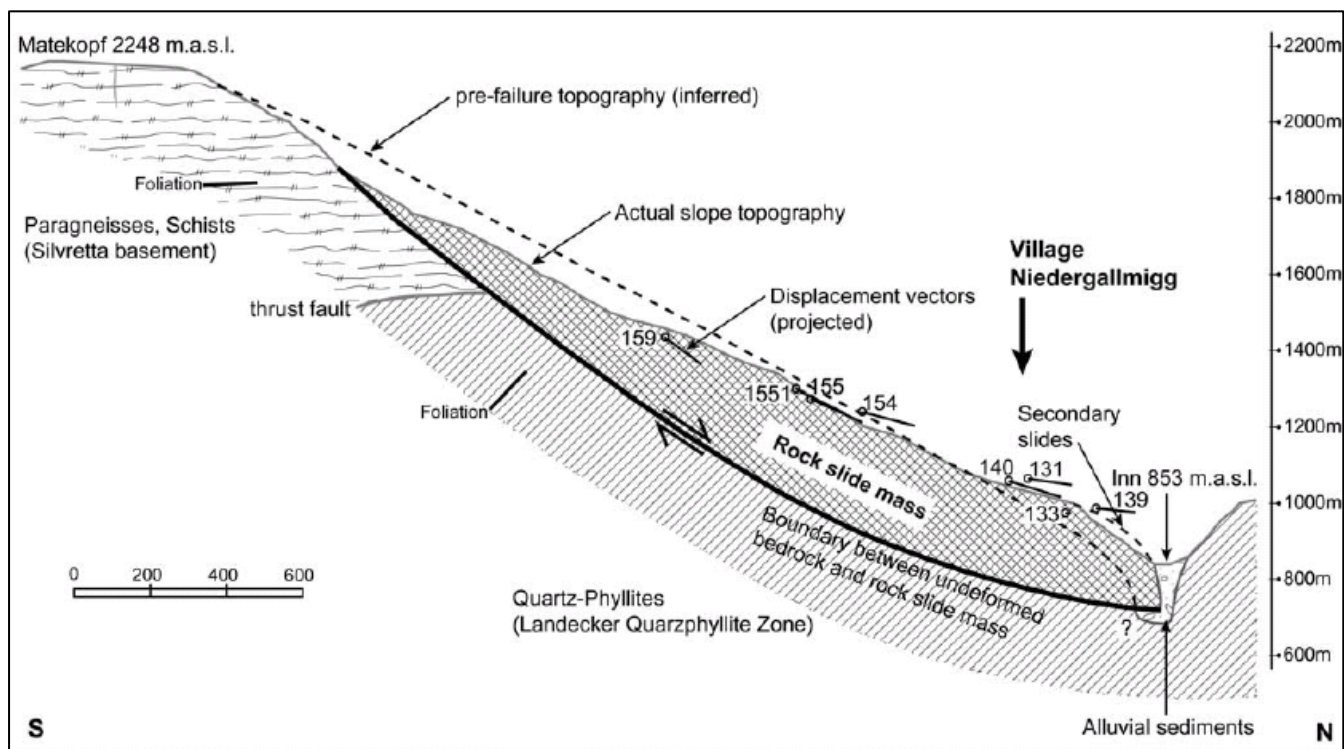


Figure 16: Cross section through the western sliding mass of the Niedergallmigg rockslide from the Matekopf in the south down to the river Inn in the north (ZANGERL et al., 2012).

1.4.2.3. Other landslides (Perfuchsberg and Kopfwald/Glitt)

The landslide **Perfuchsberg** is one of the largest deep-seated slope deformations in this area and is located southwest of the town Landeck. It reaches from the Thialkopf in the south down to the rivers Sanna and Inn in the north and northeast respectively (Figure 17). The area of the landslide is situated within the *Venet complex* of the Silvretta nappe (see chapter 1.3.1.) and mainly consists of phyllonitic micaschists generally dipping to the south. The landslide is characterized by a well defined concave headscarp area with mountain splitting phenomena (like tension cracks and trenches) behind it, and a convex shaped deposition area. Parts of the landslide are active or are moving as separate slides or creeping masses, which is shown by secondary scarps especially in the lower region of the landslide (GRUBER et al., 2010). From borings and refraction seismics at the toe of the landslide it could be inferred that the landslide was thrust onto fluvio-glacial valley infill sediments (Figure 18). They also allowed the determination of the glacially formed valley bottom approximately 100 m below today's surface (POSCHER, 1993). The movement and processes of the entire landslide, however, have not yet been investigated.

Another landslide, that has not been subject to detailed geological investigations so far, is the landslide **Kopfwald/Glitt** between the locality See and the entrance of the Paznaun valley. It is located on the western side of the valley and reaches from the point “Am Stein” in the west down to the river Trisanna in the east (Figure 17). It is situated in the *Silvretta complex* (see chapter 1.3.1.) and is built up by biotite-muscovite schists and paragneisses as well as lenses of amphibolites. The foliation planes in this area generally dip to the northwest. Similar to the landslide Perfuchsberg also the landslide Kopfwald/Glitt is characterized by a well defined headscarp and a convex shaped deposition area. Furthermore, it deflected the course of the river Trisanna to the southeast (Figure 17) and caused the (episodic) retention of the river Trisanna and the subsequent formation of a lake at the locality See. It was only in the Late Middle Ages that this lake finally fell dry (GRUBER et al., 2010).

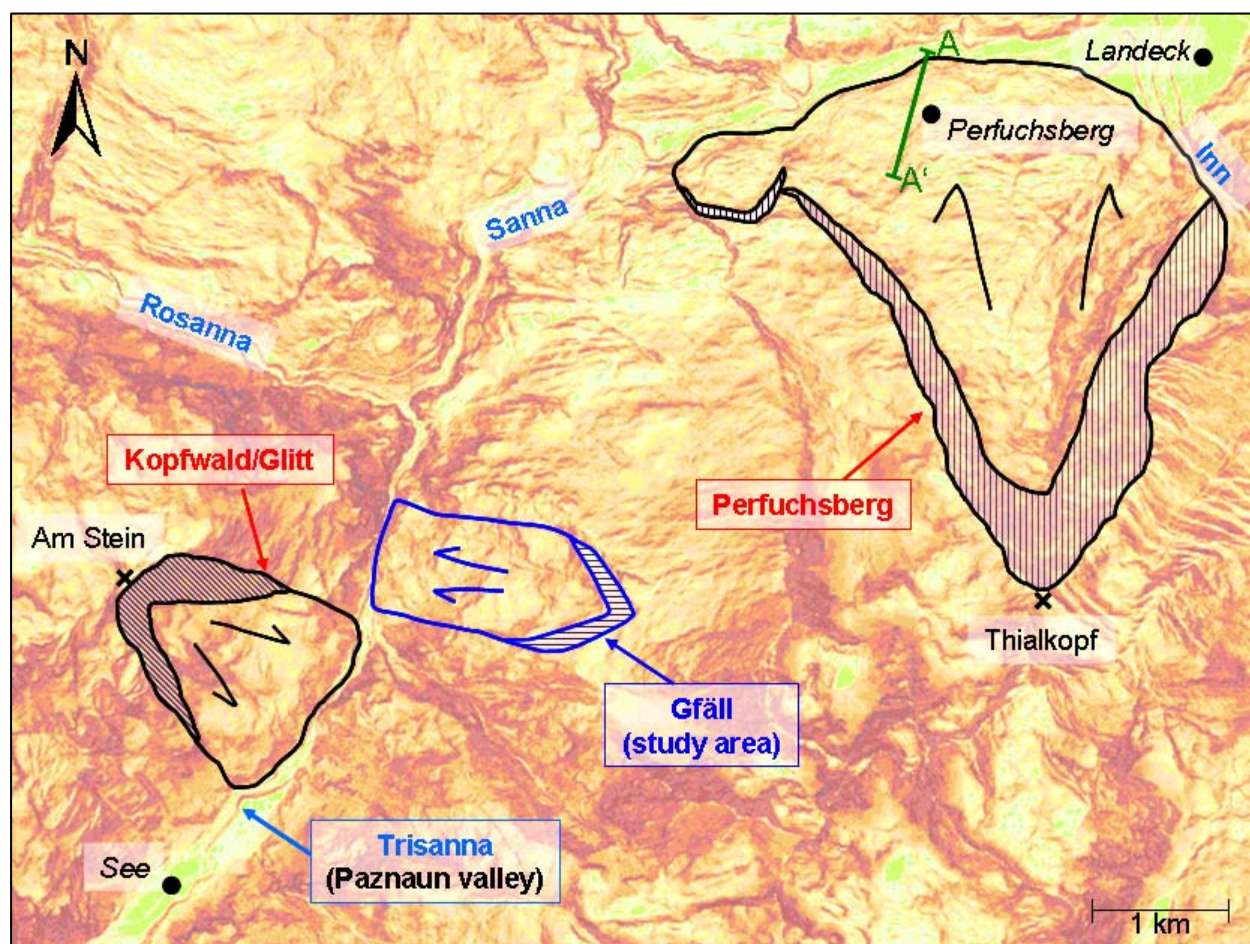


Figure 17: Slope inclination display with dark colours representing steep areas and light colours representing flatter parts (from TIRIS (2013)) showing the landslides Perfuchsberg and Kopfwald/Glitt as well as the approximate boundaries of the landslide Gfäll of the present study (after KRAINER et al., 2004). The green line shows the location of the cross section of Figure 18.

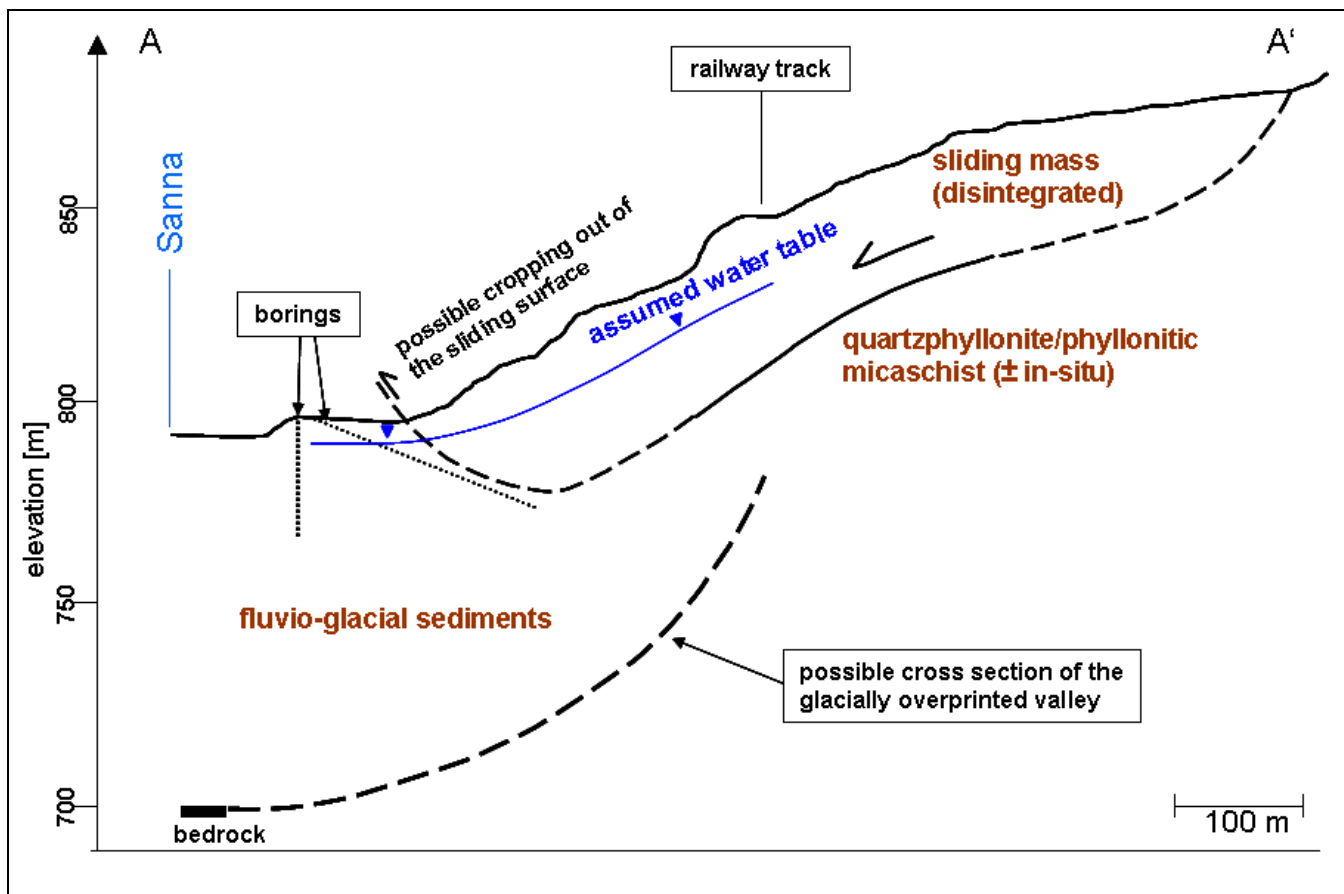


Figure 18: Cross section through the lowest part of the Perfuchsberg landslide – gained from refraction seismics and borings – showing that the sliding mass was thrust onto fluvio-glacial sediments of the overdeepened valley (after POSCHER (1993)). The location of the cross section is shown in Figure 17 as green line.

1.5. Previous geotechnical investigations

1.5.1. Geotechnical parameters of phyllitic and schistose rocks

A major characteristic of phyllitic and schistose rocks is their anisotropy, i.e. different behaviour or properties (such as strength parameters) in different orientations corresponding to a plane of weakness (schistosity). RAMAMURTHY et al. (1993) investigated the engineering behaviour of Himalayan phyllites with respect to their anisotropy. They found that the uniaxial compressive strength is highest, when β , the angle between the loading direction (σ_1) and the plane of weakness (schistosity), is 90° . The lowest values are found for $30^\circ \leq \beta \leq 40^\circ$ (dip angles of schistosity consequently are between 60° and 50°). The maximum tensile strength is reached at $\beta = 0^\circ$, the minimum tensile strength at $\beta = 90^\circ$. With increasing confining pressure also the compressive strength of the tested phyllites increases, although in a non-linear way. The same results concerning the

uniaxial compressive strength were attained by THURO (1998), who investigated the Innsbruck quartzphyllite (Tyrol, Austria). He also found that the uniaxial compressive strength is highest, when the loading direction is perpendicular to the schistosity ($\beta = 90^\circ$), whereas it reaches only 80 % to 90 % when the loading direction is parallel to the schistosity ($\beta = 0^\circ$). Table 2 gives the uniaxial compressive strength, elastic modulus and splitting tensile strength received from tests on the Innsbruck quartzphyllite that were run perpendicular and parallel to the orientation of the schistosity (SPAUN & THURO, 1994).

Table 2: Testing results of uniaxial compressive strength (UCS), elastic modulus and splitting tensile strength of samples from the Innsbruck quartzphyllite with the loading direction parallel and perpendicular to the schistosity (SPAUN & THURO, 1994).

	parallel			perpendicular		
	UCS [MPa]	Elastic modulus [GPa]	Splitting tensile strength [MPa]	UCS [MPa]	Elastic modulus [GPa]	Splitting tensile strength [MPa]
Average [MPa]	32	18.4	6.3	40	20.7	2.3
Minimum [MPa]	20	9.8	3.2	22	10.5	0.9
Maximum [MPa]	43	34.8	12	74	31.7	5.5

BUTTON (2004) gives geotechnical parameters for phyllitic and schistose rocks in alpine environments. The samples consisting of phyllites, quartzphyllites and carbonaceous phyllites were gained from tunnel projects in Lower Austroalpine units (LAA) and in the Greywacke zone (GWZ). Table 3 summarizes the results of uniaxial and triaxial compression tests as well as direct shear tests along the foliation planes for quartzphyllites. For different kinds of sheared phyllites (graphitic, chloritic, sericitic and micaceous phyllites) tested by a multiple stage, load controlled direct shear test BUTTON (2004) gives an average friction angle of 24.5° and a cohesion of 0-0.6 MPa as well as an average residual friction angle of 26° with a residual cohesion of 0.04 MPa.

ENGL et al. (2008) provide average values of shear strength parameters of shear products (i.e. kakirites) of schists, paragneisses and different phyllites, and of joints parallel to the schistosity. The results are compiled from published laboratory data of previous investigations and tests. The average values of the maximum and residual shear strength parameters of kakirites developed from phyllites, quartzphyllites, carbonaceous phyllites, schists and paragneisses, and the maximum shear strength parameters of different phyllites along joints that are parallel to the foliation are given in Table 4. ENGL et al. (2008) found the quartzphyllite to feature the highest shear strength along the foliation planes and also the highest residual shear strength as kakirite. The variance of the data that

is sometimes quite high results from the natural heterogeneities of the kakirites and from the varying testing conditions of different studies. ENGL et al. (2008) also emphasize that for questions concerning landslides and slope stability especially the residual shear strength is important.

Table 3: Results of uniaxial and triaxial compression tests, and direct shear tests of quartzphyllites from the Lower Austroalpine (LAA) and the Greywacke zone (GWZ) (BUTTON, 2004).

	Uniaxial test	Triaxial test		Direct shear test (multiple stage test, load controlled, along foliation)			
	UCS [MPa]	φ [°]	c [MPa]	φ [°]	c [MPa]	φ_{res} [°]	c_{res} [MPa]
LAA		3 samples		9 samples			
Minimum	-	30.1	8	28	0	16	0
Maximum	-	33.1	14.2	48	0.45	36	0.2
GWZ	72 samples	2 samples		5 samples			
Minimum	2.5	41	11.9	-	-	21	0.02
Maximum	180	46.3	14.15	-	-	31	0.66
Average	38.4						

Table 4: Average values of the maximum shear strength parameters along joints that are parallel to the foliation as well as the maximum and residual shear strength parameters of kakirites (ENGL et al., 2008).

	Maximum shear strength along joints parallel to the foliation		Maximum shear strength of kakirites		Residual shear strength of kakirites	
	φ [°]	c [MPa]	φ [°]	c [MPa]	φ_{res} [°]	c_{res} [MPa]
Phyllite	24.2	0.19			26.6	0.013
Quartzphyllite	30.5	0.38			27.7	0.167
Carbonaceous phyllite	29.9	0.14			24.4	0
Schist			23.7	0.739		
Paragneiss (Ötztal nappe)			33.9	0.023		

NICKMANN & THURO (2010) point out that, especially for engineering constructions, it is important to distinguish between rocks of decreasing strength (weak rocks) and rocks that show a constant strength over a long period of time (“true” hard rocks), and to use suitable methods and tests to consider this strength variability. Weak rocks are characterized by a loss of strength within days to a few years depending on the content of swellable minerals, the grain size distribution (voids), the fabric (e.g. micro-cracks) and the weathering. From a geotechnical point of view NICKMANN et al. (2006) grant weak rocks a position between cohesive soils and hard rocks. However, the transition between these three groups of rocks is variable.

1.5.2. Geotechnical studies in the area of Landeck

As basis for several geotechnical investigations in the area of Landeck the geologic map Landeck on a scale of 1:75000 published by AMPFERER & HAMMER (1922) and a more detailed geologic map on a scale of 1:50000 published by the Geologische Bundesanstalt in 2004 (KRAINER et al., 2004) are used. In the corresponding explanation reports (AMPFERER & HAMMER (1924) and GRUBER et al. (2010) respectively) general information about geotechnical characteristics is given. In the following paragraphs the results obtained from construction projects in the area of Landeck (the tunnels Strengen, Perjen and Gfäll) and from the flood event in August 2005 are summarized.

BUTTON (2004) provides testing results of samples of the so-called “Landeck quartzphyllite” (*Venet complex* after GRUBER et al. (2010)) that were gained in the course of the construction of the **Strenger tunnel** west of the town Landeck. Table 5 summarizes the geotechnical parameters uniaxial compressive strength (UCS), friction angle φ and cohesion c from both triaxial tests and direct shear tests as well as the indirect tensile strength. The direct shear tests were performed parallel to the foliation, the indirect tensile strength was determined perpendicular to the foliation planes.

Table 5: Uniaxial compressive strength (UCS), friction angle (φ) and cohesion (c) from triaxial compressive tests and direct shear tests on foliation surfaces, and indirect tensile strength perpendicular to the schistosity of the “Landeck quartzphyllite” (*Venet complex*) (BUTTON, 2004); β ...angle between loading direction and schistosity.

	UCS [MPa]	Triaxial test		Direct shear test		Indirect tensile strength ($\beta=90^\circ$)
		φ [°]	c [MPa]	φ [°]	c [MPa]	[MPa]
Minimum	12	32	3.5	25	0.4	2.7
Maximum	55	44	5.4	28	0.6	12.4
Average	16 ($\beta=20^\circ$), 38 ($\beta=10^\circ$)					

Further investigations of the geology and especially of the geotechnical parameters of the *Landeck Phyllite* and the phyllonitic micaschists of the *Venet complex* (see chapter 1.3.1.) were carried out in the course of the design and construction of the first and second tube of the **Perjen tunnel** north of the town Landeck. KÖHLER (1983) deals with the engineering geological situation at the first tube of the Perjen tunnel. He describes the phyllonites (including the *Landeck Phyllite*) as distinctly foliated rocks with lamellar cleavage that feature low stability. The foliation planes, which are covered with sericite, dip approximately to the south (Table 6) and do often act as planes of movement (shear planes).

Faults within the phyllonites are not clearly confined against the adjacent rock mass, but the material becomes more phyllonitic and can even turn into fine-grained (clayey) loose material near the fault core. The phyllonites are sensitive to water and, although their water capacity itself is low, even a low moisture content can lead to softening of joint fillings or fault breccia materials, which increases the possibility of rock mass movement. Joints in the phyllonites are of only minor importance, since they feature a more plastic behaviour. The quartzitic or gneissic intercalations, however, show several joint sets with often short spacing and feature a higher stability and lower sensitivity to water. The mean orientations of the seven different joint sets documented by KÖHLER (1983) are given in Table 6.

Table 6: Mean orientations of the schistosity (sf) and the seven joint sets at the Perjen tunnel (KÖHLER, 1983).

sf	j1	j2	j3	j4	j4'	j5	j6
168/62	200/77	174/83	59/60	156/80	131/73	89/73	109/74
195/85							

ASFINAG (2012a) operated with the design and construction of the second tube of the Perjen tunnel. Here, light phyllites, phyllonitic micaschists and schistose gneisses similar to KRÄINER et al. (2004) are distinguished. The properties of the corresponding rock mass types were evaluated primarily following ÖNORM EN ISO 14689-1 and are summarized in Table 7. The degree of weathering can reach from 0 (fresh) to 4 (completely weathered), the variability from 1 (not variable) to 5 (strongly variable). The roughness of joint planes is described by two properties depending on the scale: the adjectives “stepped”, “undulating” and “planar” are used for the range of cm to m, the adjectives “rough” and “smooth” for the range of mm.

Table 7: Properties of rock mass types that correspond to the light phyllites (Landeck Phyllite) and the phyllonitic micaschists and schistose gneisses of the Venet complex for the construction of the second tube of the Perjen tunnel (ASFINAG, 2012a).

	Rocks			Joints				
	UCS	Weathering	Variability	Spacing	Roughness	Weathering	Aperture	Filling
	[MPa]	(0 - 4)	(1 - 5)	[mm]		(0 - 4)	[mm]	
Light phyllite (Landeck Phyllite)	5 - 50	0	3	< 20	planar, smooth	0 - 1	< 0.1	partly plastic fillings
Phyllonitic micaschist (Venet complex)	5 - 50	0	2	20 - 60	planar, smooth	0 - 1	< 0.1	partly plastic fillings
Schistose gneiss (Venet complex)	5 - 50	0	1	< 20	planar, smooth	0 - 1	< 0.1	-

The landslide Gfäll has been known for a long time. Already in the explanation report corresponding to the geologic map Landeck on a scale of 1:75000 by AMPFERER & HAMMER (1924) it is mentioned as rockfall blocks covering the orographic right slope to the Trisanna at the entrance of the Paznaun valley. On the geologic map of Landeck on a scale of 1:50000 (KRAINER et al., 2004) the landslide Gfäll is mapped as an area of “deeply loosened and moved rock”. In the explanation report by GRUBER et al. (2010) it is called active slope deformation of “Schweißgut/Hintergiggel/Vordergiggel” (after farmsteads and small localities respectively) and for its headscarp area an elevation of 1900 m a.s.l. at the Giggler Alpe is stated (Figure 19). Since the hazard which the landslide Gfäll caused to the road into the Paznaun valley (B188 Paznaun valley road) and also to the corresponding bridge across the river Trisanna (bridge “Gfäll”) was recognized, a project to relocate the road onto the opposite side of the valley was started in 2004. In the course of this project the **tunnel Gfäll** on the western side of the valley had to be designed following immediately after a new bridge across the Trisanna. The tunnel should then lead directly into the existing gallery Gfäll (Figure 19). In the course of the preliminary investigations morphologic features as well as lithological and structural parameters of the rocks and rock masses (all belonging to the *Venet complex*) were evaluated. Table 8 gives the obtained fabric data for the defined geotechnical areas with respect to the lithology. It can be seen that the schistosity generally dips to the south to southeast, but due to folding sometimes also to the north or northeast respectively. The rock mechanics parameters like compressive or shear strength were not tested in the course of this project but were determined according to reference projects. The applied values for the rock mass types as well as the properties of the joint planes are summarized in Table 9. There, in addition to “rough” and “smooth” also “slickensided” is used as description of the joint roughness (POSCHER, 2005). In March 2005 four vertical core borings were drilled at the abutments of the new bridge Gfäll, two on the western side of the Trisanna and two on the eastern side. The borings on the western side (KB1 and KB2) cut through the phyllonitic bedrock, whereas the borings on the eastern side (KB3 and KB4) were drilled to a depth of 30 m and 22.5 m respectively, but only cut through fluvial sediments, intercalating with cobbles and boulders that possibly originate from the landslide Gfäll, and did not reach the bedrock (HENZINGER, 2005).

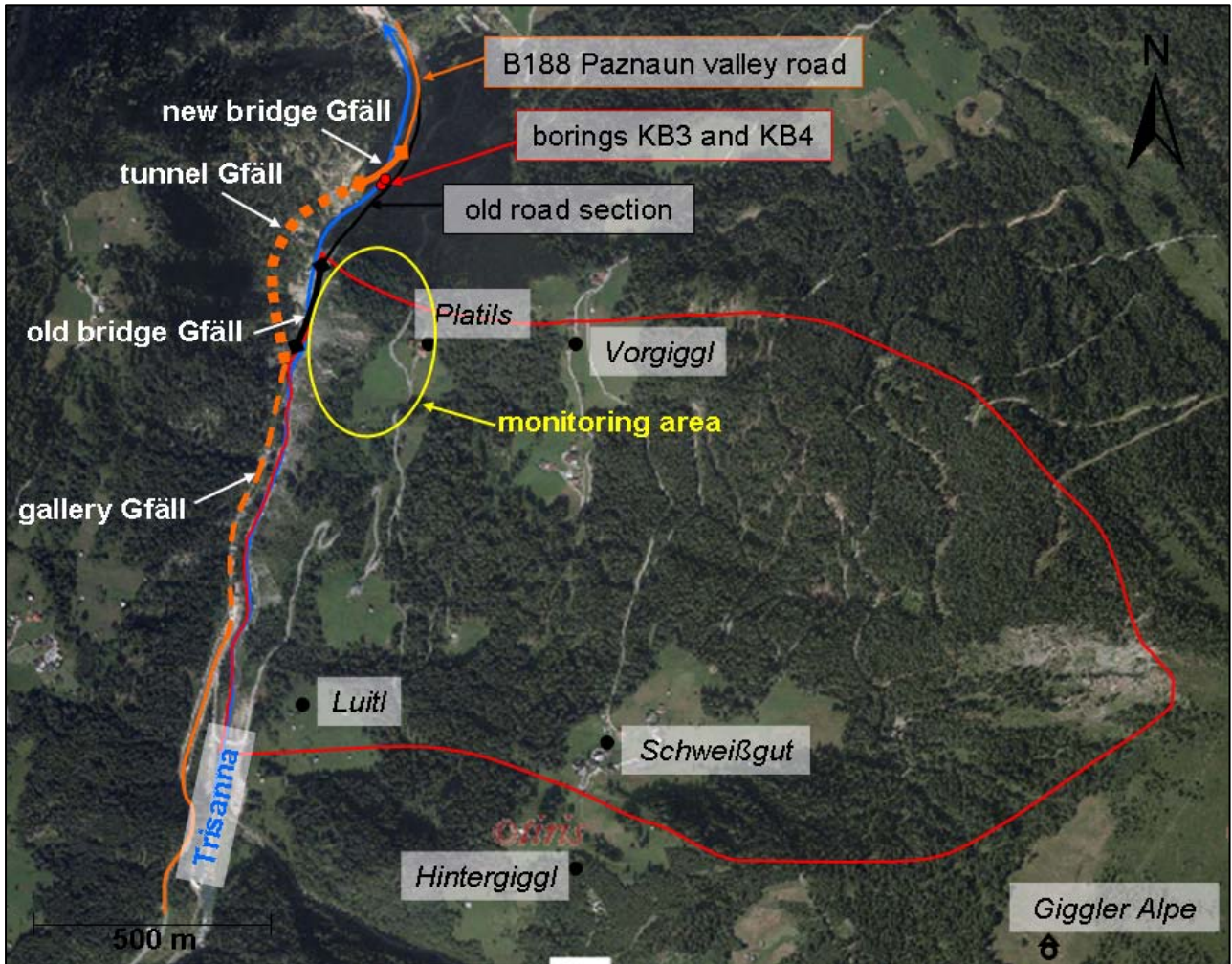


Figure 19: Orthophoto showing the B188 Paznaun valley road (orange) with the tunnel Gfäll, the gallery Gfäll and the new bridge across the river Trisanna, and the old road section with the old bridge in black (from TIRIS (2013)). The approximate borders of the landslide Gfäll (red) are drawn after KRAINER et al. (2004). The yellow circle frames the area where the geotechnical monitoring was performed from December 2004 on.

Table 8: Orientations of the schistosity (sf) and the joint sets (j1 to j4) with respect to the lithology and the geotechnical areas respectively (POSCHER, 2005).

	sf	j1	j2	j3	j4
Phyllonites	190/50 - 190/60	190/40	250/80	90/10	40/60
	10/70 - 30/30		250/90		
Phyllonitic micaschists	140/70 - 140/80	130/90	240/80		90/70
	40/30 - 40/40				
Phyllonitic micaschists (quartz lenses, gneissic)	160/60	120/40 - 160/90	250/80		90/70 - 90/80
Micaschists to gneisses	160/45 - 160/60	110/80 - 130/50	240/30		

Table 9: Rock mass parameters of the Venet complex applied for the construction of the tunnel Gfäll (POSCHER, 2005); UCS: uniaxial compressive strength, ϕ : friction angle.

	UCS	Cohesion	ϕ	Block size dimensions	Joint roughness	Joint aperture, filling	Interlayers
	[MPa]	[MPa]	[°]	[m]			
Phyllonites	0.75	0.3	25	0.06 - 0.1	planar - undulating, smooth - slickensided	closed	-
Phyllonitic micaschists to gneisses	4.0	0.6	30	0.1 - 0.3	planar - undulating, smooth	partly open, none	-
Micaschists and gneisses	12.5	1.7	45	0.1 - 1	planar - undulating, rough - smooth	partly open, none	cataclasites up to several cm thick

Above the northern end of the old bridge Gfäll a geotechnical monitoring program was installed for the concerned slope in Dezember 2004. During the snowmelt in spring 2005 displacements of 1-5 cm were detected. In August 2005 heavy rainfalls caused the river Trisanna to flood parts of the Paznaun valley. In the section of the **landslide Gfäll** this led to undercutting and erosion of the right river bank along with accelerated movements of the lowermost parts of the landslide from the farmstead Luitl in the south to the north of the old bridge Gfäll (Figure 19). Due to the landslide Gfäll, which is called "Platils-Luitl-Schweißgut" and described as active creeping slope by HEIBEL et al. (2005), the rock mass in this section is disintegrated and loosened up to a depth of several tens of meters, leaving a soil-like material (cobbles to large boulders). The precipitation waters of the rainfall event could easily infiltrate into crevices and pores of the rock mass reducing its friction and consequently also the strength. Therefore, the Paznaun valley road and the old bridge were endangered by rock falls originating from the oversteepened flanks of the landslide toe. From August 29 to September 8, 2005, settlements of up to approximately 4 m were stated and a regress of the scarp of sometimes several meters per day was observed during daily inspections after the heavy rainfalls on August 22 and August 23. The highest movement rates were detected in the south and not at the northern slope above the bridge Gfäll, where the geodetic monitoring had been installed (HEIBEL et al., 2005). From September 6, 2005, to November 24, 2005, total displacements of ten surface measurement points near the farmstead Platils ranged from 1 mm to 8 mm toward WSW to NNW. This range, however, lies within the measurement accuracy (OPH, 2005). HEIBEL et al. (2005) suppose that the erosion of the river bank resulting from the flood event activated or accelerated at least the toe area of the whole landslide Gfäll, and that the future behaviour of the slope will be governed by the infiltration of precipitation waters and further erosion of the river bank.

2. Methodology

2.1. Desk study

Prior to the field work existing literature concerning the landslide Gfäll and the geology of the study area were compiled. Laserscan pictures (so-called hillshade display) as well as orthophotos (TIRIS, 2013) were then used to obtain an overview of the major geomorphic and structural features of the present study area. Both can already serve to define possible structural geologic lineaments and parts of the landslide. For a further morphological inspection laserscanning data (DTM – Digital Terrain Model) with a resolution of 1 m (ATLR, 2013) were used with the geographic information system program ArcMap[®]. With it hillshade displays lighted from different directions as well as a so-called slope display (based on the inclination angle of the slope) were generated. Especially the slope display together with contour lines helps to determine structures such as trenches, chutes, rock faces or concave-convex shapes since it only shows the ground surface without vegetation.

2.2. Field investigation

2.2.1. Mapping

Geologic and geomorphologic mapping was carried out between June and August 2013 on a map scale of 1:5000. As base maps the topographic map of Austria (BEV, 2013) and the hillshade display (TIRIS, 2013) were used in the field. The geologic mapping was based on the map sheet 144 Landeck of the Geologische Bundesanstalt (KRAINER et al., 2004) and its legend which, however, was modified for the present thesis.

For selected hard rock units thin sections were made and therefore the mineralogical descriptions are based on macroscopic and microscopic observations. For a few lithological units the descriptions were only done during fieldwork by determination of the containing minerals at fresh surfaces of hand rock samples using a loupe. The further equipment for field mapping consisted of rock hammer, geologic compass, topographic map and hillshade display of laserscanning data on a scale of 1:5000, camera, GPS device (with altimeter) and barometric altimeter.

2.2.2. Sampling

During the field mapping fourteen rock samples were collected from outcrops for determining the rock type and mineralogy from macroscopic point of view and for the later fabrication of thin sections. The dimensions of the samples were approximately 10 cm long, 7 cm wide and 5 cm high.

In October 2013 additional thirteen samples for direct shear tests on the schistosity were taken. Therefore two outcrops were selected in the present study area and two additional outcrops located somewhat more to the north between the localities Tobadill and Perfuchsberg (Figure 20). The samples were gained from the in-situ outcrops using hammer and chisel and had to have a size of approximately 15x15 cm (min. 10x10 cm) and a height of at least 12-16 cm. For the triaxial compression tests fourteen more samples were selected from drill cores with 10 cm diameter of the borings KB-ZL8-02, KB-ZL8-03 and KB-ZL8-04, that were drilled in the course of the preliminary investigation of the second tube of the Perjen tunnel (ASFINAG, 2012b). The location of the three borings can also be taken from Figure 20.

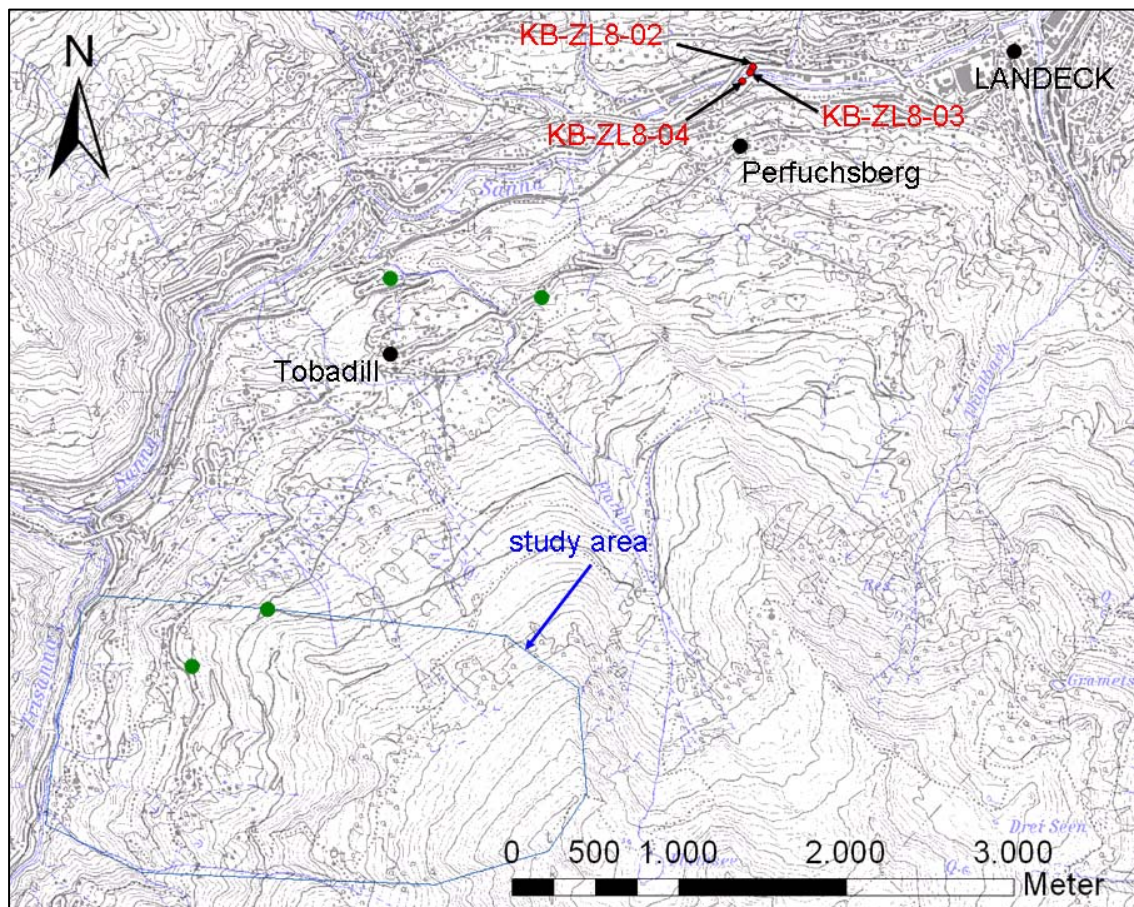


Figure 20: Sampling positions (green points) and location of the three borings KB-ZL8-02, KB-ZL8-03 and KB-ZL8-04 (ASFINAG, 2012b), from which also samples were gained.

2.3. Laboratory investigation

2.3.1. Mineralogical and petrographic methods

To be able to describe the mineralogy and microscopic fabric of the rock samples (see chapter 2.2.2.) a total of fifteen thin sections were prepared. Ten thin sections were made from the fourteen hand rock samples taken during field mapping, the other five derive from samples gained for the direct shear tests. In a first preparation step the samples were cut with the stone saw to pieces of approximately 2x4 cm. Then they were polished with a 120 µm motor-driven grinding plate (Planopol-3; Figure 21a) and after that with 600 µm silicon carbide powder on a metal plate by hand. Next, the pieces were stuck on glass pads with the dimensions of 4.6x2.7 cm (also polished with 600 µm silicon carbide powder) with epoxy resin and put into the drying oven for hardening. When dried the samples were cut and polished with the PetroThin rock cutting machine to a thickness of ~50 µm (Figure 21b). The residual 20 µm were again polished by hand on the metal plate with silicon carbide powder, so that the final thin section had a thickness of approximately 30 µm. The thin sections were then investigated on their mineralogy under a transmitting light microscope following TRÖGER (1982) and photomicrographs of them are attached in Appendix 5.

2.3.2. Rock mechanics testing

The values received in rock mechanics testing were used as reference values to be compared with testing results of other investigations and as guiding values for the input parameters needed for the engineering geological analyses.

2.3.2.1. Direct shear tests

Stiffness controlled direct shear tests were performed at the rock mechanics laboratory of TU Graz following ISRM (2013). Six samples were selected and cut with the stone saw to pieces of about 15x15 cm, if they were larger than that. Five samples were mounted as intact specimens, one was primarily split with hammer and chisel along a foliation plane, giving the chance to measure its roughness before testing. All samples were then set in grout in one half of the quadratic (20x20 cm) shear boxes and after hardening into the second half, in such a way that a 2 cm gap was left between the upper and lower shear box (Figure 21c). After hardening of the grout the shear box could be

mounted into the shearing apparatus (Figure 21d). At the beginning of the test the specimen was loaded (with a normal stress of 15 kN) and unloaded twice. Only after that the shear force was applied and no more vertical displacement of the specimen is allowed. This leads to increasing normal and shear stress, which are recorded during the test together with the shear path. Usually the test is proceeded until a shear path of 20 mm is covered. The apparatus allows a maximum travel of 25 mm. After testing, the failure plane was documented by photographs and also the exact area and the roughness (joint roughness coefficient (JRC) plus verbal description) were determined. From the measurements during the test the friction angle φ [°], the residual friction angle φ_{res} [°], the cohesion c [MPa], the dilation angle i [°], the maximum shear stress τ_{max} [MPa] and the shear path at the maximum shear stress $s(\tau_{max})$ [mm] were determined.

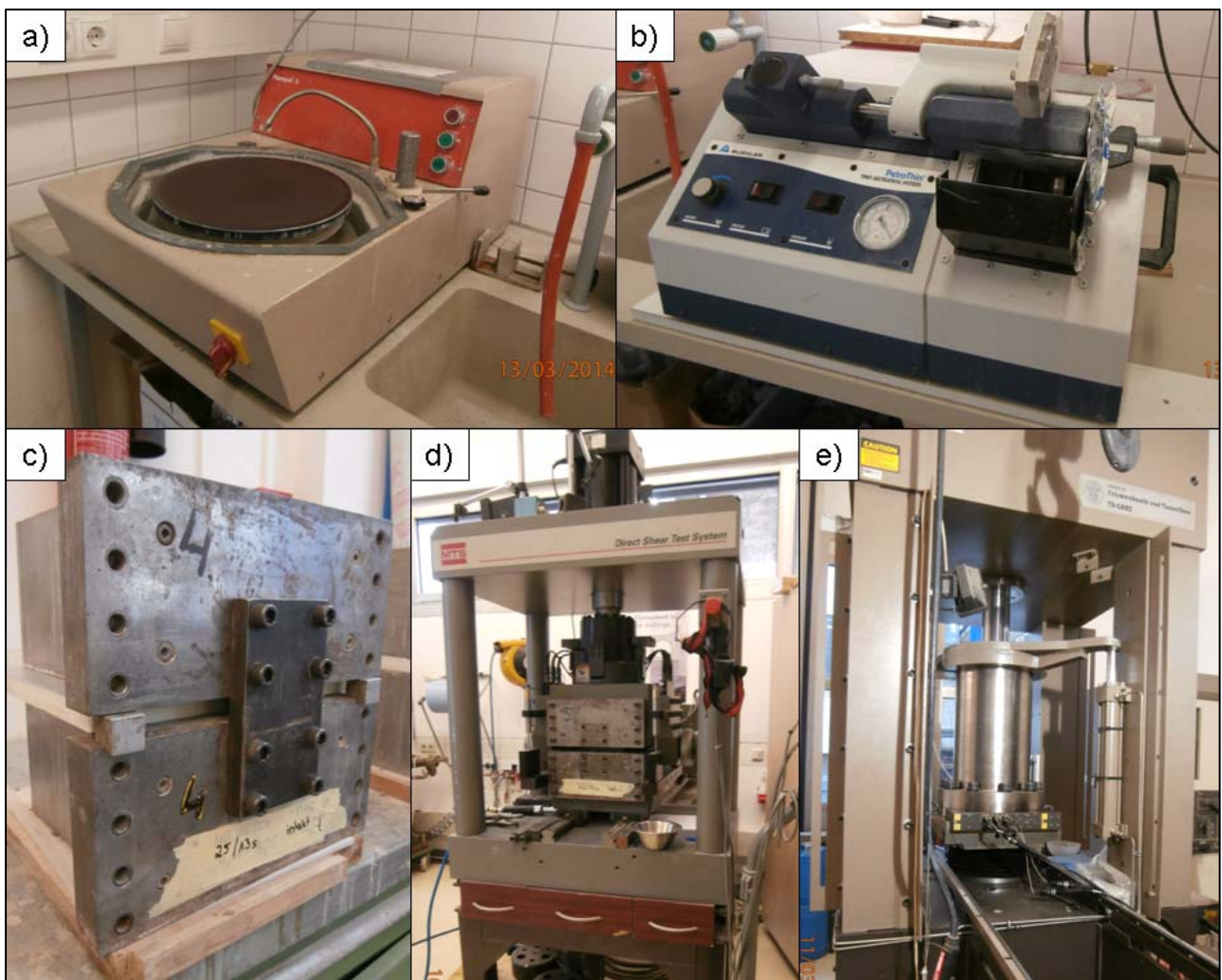


Figure 21: Laboratory sample preparation and testing equipment: a) motor-driven grinding plate Planopol-3, b) PetroThin rock cutting machine, c) upper and lower shear box after grouting of the sample, d) direct shear test apparatus with mounted shear box, e) triaxial cell.

2.3.2.1. Triaxial compression tests

Triaxial compression tests were also carried out at the rock mechanics laboratory of TU Graz generally following ISRM (1983). Two drill core samples were selected, out of which smaller cores with an approximate length of 10 cm and diameter of 5 cm were drilled. Before testing, the mass and the exact length and diameter of the specimens as well as the travelling time of sonic waves (p-waves) were measured. Then the specimens were shrink-wrapped into a Teflon membrane, which is used to prevent the confining fluid from entering the specimen. After that, transducers for measuring the circumferential deformation of the specimen were attached and then it was put into the triaxial cell (Figure 21e). After filling the cell with the confining fluid (in this case oil), which is responsible for the confining pressure, the loading device could start applying the axial load. During triaxial compression tests the axial load and the confining pressure as well as the circumferential deformation of the specimen are measured. From them the parameters of the Hoek-Brown criterion (uniaxial compressive strength UCS [MPa], the material constant m_i and the tensile stress σ_{tens} [MPa]) and of the Mohr-Coulomb criterion (friction angle φ [°] and cohesion c [MPa]) as well as the elastic parameters (E-Modulus [GPa], V-Modulus [GPa] and Poisson's ratio) can be calculated.

2.4. Engineering geological analyses

2.4.1. Fabric analysis

The analysis of the structural data (schistosity and joint sets) was carried out using the software package "Dips 6.0" (ROCSOURCE, 2012). All data are plotted as equal angle projections on the lower hemisphere. The mean orientations of the schistosity and joint set data are obtained from a density plot using the Fisher contour distribution. A density plot gives the concentration of poles, displayed using contour lines, where the central value of the highest density can be taken as mean orientation (center of gravity) of the discontinuity set (ISRM, 2007). The joint sets were defined by cluster analyses and in some cases by adding set windows by hand respectively. The schistosity data are plotted as great circles and poles; joints are displayed as poles.

2.4.2. Block theory and key block analysis

To verify the assumptions that were made due to field observations concerning the failure initiation, the failure mode and kinematics of the investigated landslide key block analyses based on block theory were performed. Block theory usually is used to determine structurally controlled failure especially for outcrops or tunnels. For a block to be able to form at least four surfaces, which can be any combination of joint planes and free surfaces (slope or excavation surface), are required (GOODMAN & SHI, 1985). In a fractured rock mass different types of blocks can be found. The three **non-removable blocks** (types VI-IV) and the three **removable blocks** (types III-I) are defined by GOODMAN (1989) and GOODMAN & SHI (1985) respectively as follows (Figure 22a):

- Type VI blocks are *joint blocks*. They do not intersect the slope or excavation surface.
- Type V blocks are *infinite blocks*. They have an intersection with the excavation plane but are not finite unless new fractures develop.
- Type IV blocks are *tapered blocks*. They cannot move toward the free space because due to their shape they are stopped by their adjacent blocks.
- Type III blocks are *safe removable blocks*. They lack a sliding mode (cannot fall or slide even without friction) and therefore are stable.
- Type II blocks are *potential key blocks*. They are safe due to the available friction on their potential sliding plane(s). They have a sliding mode, but with a negative sliding force.
- Type I blocks are *key blocks*. They have a positive sliding force and, unless support is provided, they will fail if they are exposed.

For a block to be removable two conditions have to be fulfilled: First, the joint pyramid (JP) of the block is not empty, and second, the joint pyramid (JP) has no intersection with the excavation pyramid (EP), i.e. it lies completely within the space pyramid (SP). A **joint pyramid (JP)** is formed by joint surfaces and represents block shapes in the rock mass. In a stereographic whole sphere projection JPs plot as spherical polygons resulting from the intersection of the great circles that represent the discontinuity planes (Figure 22b; GOODMAN & SHI, 1985). For a planar slope or excavation plane the **excavation pyramid (EP)** is the area below the excavation plane, whereas the **space pyramid (SP)** is the area above it (Figure 23a; GOODMAN, 1989). In a stereographic lower hemisphere projection of a convex slope EP lies inside the circle that represents the slope, and SP outside (Figure 23b). Therefore, a

block of a convex slope is removable, if JP lies outside the circle which represents the slope (or excavation plane) (Figure 22b; GOODMAN & SHI, 1985).

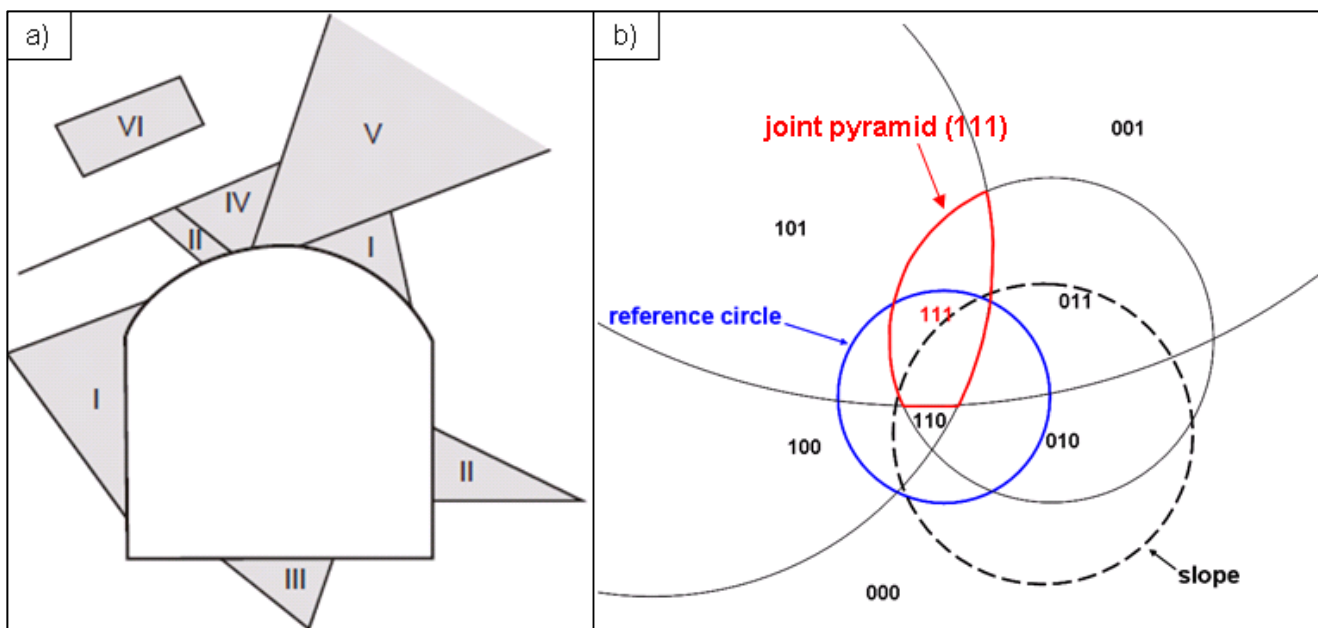


Figure 22: a) Block types VI-I for a tunnel excavation after GOODMAN (1989); b) Whole sphere projection of three discontinuity sets and one slope plane (dashed circle); blue: reference circle, red: one of the spherical polygons representing a joint pyramid. In this example the block with the JP code (001) would be removable, since it lies completely outside the slope circle (EP).

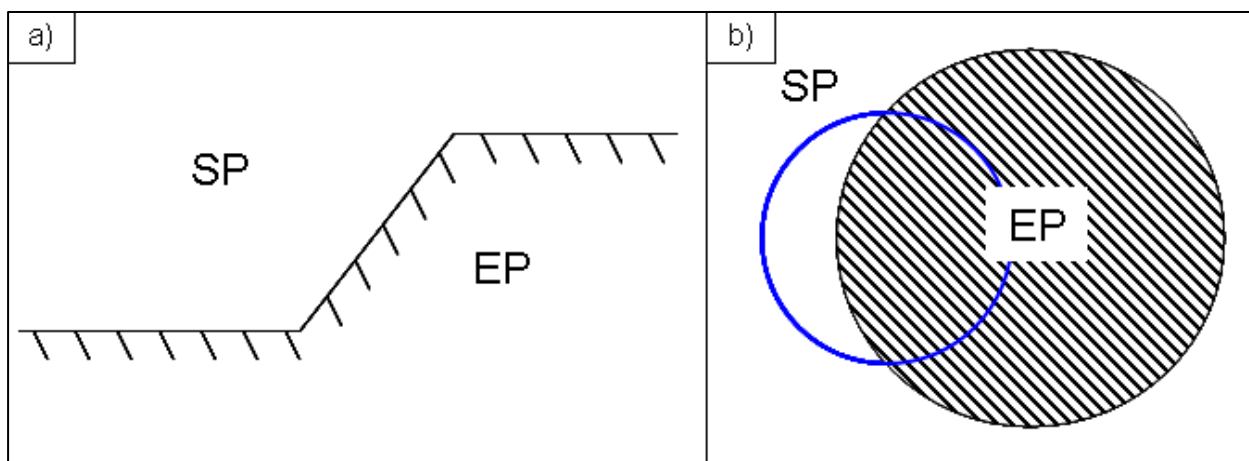


Figure 23: a) SP and EP for a planar slope; b) SP and EP for a planar slope in stereographic projection of the lower hemisphere: EP lies inside the circle that represents the slope, SP outside; blue: reference circle (after GOODMAN (1989)).

For the present study a block theory software after GOODMAN & SHI (1985), which was modified by LIU (2004) and LIU & KIEFFER (2008) respectively, was used for the key block analyses. In this thesis the stereographic projection is always a lower hemisphere projection. The discontinuity data were first plotted in whole sphere projection to identify blocks that are kinematically admissible to fail (removable blocks) and to get their JP codes (program B02HPGL by LIU (2004)). Then, a mode analysis

(program B10HPGL by LIU (2004)) was performed to distinguish safe removable blocks (type III) from potential key blocks and key blocks (type II and type I), and to get the mode of failure (falling, sliding on one plane or sliding along the line of intersection of two planes) for the type I and II blocks. Finally, a sliding equilibrium stability analysis was performed (program B04HPGL by LIU & KIEFFER (2008)) to get the required friction angle φ_R at which failure would occur. Therefore, a resultant force vector $R = (0/0/-1)$, i.e. only the weight, was assumed.

2.4.2. Slope stability analyses

Stability analyses serve to find out if a slope under certain presuppositions is stable or not. Moreover, they can be used to determine how single parameters can be modified without having an influence on the overall stability of the concerned slope, or how they can be modified to put the slope into a limit equilibrium state. An important measure therefore is the factor of safety (see chapter 1.4.1.2.). For the present thesis the stability analyses were carried out using the software packages “Swedge 6.0” (ROCSCIENCE, 2014a) and “Slide 6.0” (ROCSCIENCE, 2010). Furthermore, a toppling analysis was performed using the software package “RocTopple 1.0” (ROCSCIENCE, 2013). In the following paragraphs the needed input parameters as well as the obtained information for the particular software packages are summarized.

The program “**Swedge 6.0**” deals with the 3-D analyses of wedge-shaped blocks that slide along the intersection line of two discontinuity planes. In the course of the present thesis it was used to check the results obtained from the key block analyses and to get the sliding direction as well as the factor of safety for dry and water filled joints. The required input parameters were the geometry of the slope (orientation, height and bench width), the orientation of the discontinuity planes that form the wedge as well as their properties (cohesion and friction angle), and the unit weight of the rock. Optional, a tension crack with user-defined orientation and length could be inserted. In a second analysis step a water pressure was added to see the influence of water that acts in a jointed rock mass.

The program “**Slide 6.0**” is originally applied for the two-dimensional analysis of soils. In this case, it was used to analyse the failure along a distinct basal shear zone, since sheared rock material rather behaves like a soil. Similar to “Swedge” it served to get the factor of safety in wet and dry state of the

slope. As input data a geologic cross section through the landslide parallel to the sliding direction was needed and the location of the sliding surface had to be (roughly) defined. The further input parameters were the unit weight, cohesion and friction angle of the rock and soil materials and the location of the water table within the slope. The analysis was performed without water and for four different water tables.

The program “**RocTopple 1.0**” provides a two-dimensional analysis and was used to check if toppling was kinematically admissible. The input parameters were the height and inclination of the slope (or rock face), the width of the toppling columns, the upper slope angle, the block base angle and the overall base inclination (Figure 24).

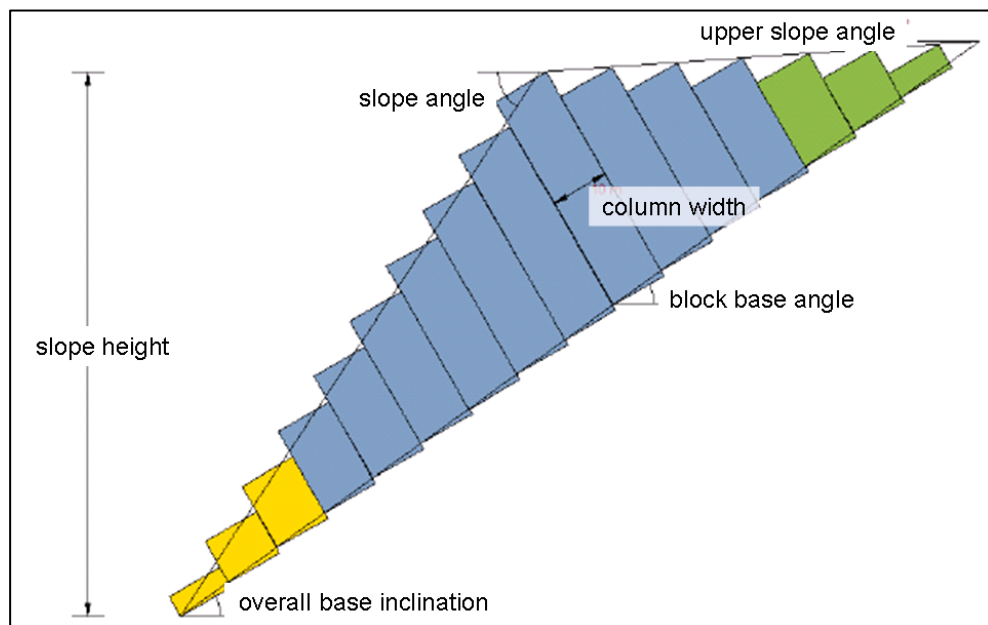


Figure 24: Schematic sketch of toppling columns with the required input parameters for "RocTopple" (modified after RocSCIENCE (2013)).

3. Site conditions

3.1. Geological conditions in the study area

3.1.1. Lithological units

The lithological units of the study area were numbered from 1 to 16 and are documented on the geologic map (Figure 25 and Appendix 1). In the following chapter the units are described separating the hard rocks of the crystalline Silvretta nappe from the different sediment deposits of the Quaternary.

3.1.1.1. Quaternary deposits

In this chapter the occurrences of Quaternary deposits in the study area and their characteristics are described. Their engineering geological classification was done for seven selected outcrops (Appendix 3) using field estimation methods primarily following ÖNORM EN ISO 14688-1 and -2.

1 Alluvium

Alluvial deposits in the study area are restricted to the southwest margin, where the Hintergiggel creek flows into the Giggel creek and both together into the river Trisanna. The sediments transported by the Hintergiggel and the Giggel creek mainly are gravels with cobbles and boulders (*co bo Gr*) with a maximum grain size of approximately 30 cm in diameter. The particles are subangular to subrounded and occur in a loose state. They intercalate with angular material that was episodically deposited in the course of heavy rainfalls. The components are of different rock types occurring upstream, such as different micaschists, paragneisses, orthogneisses and amphibolites. Typically fluvial sandy gravels (*sa Gr*) only occur at the riverbank of the river Trisanna, but also there they are mixed with cobbles, boulders and large boulders (up to 80 cm in diameter), which however are rounded.

2 Talus

Talus deposits occur beneath rock walls from which they originate. Therefore they are angular to subangular and only consist of the certain rock type(s) building up the said rock wall. Such deposits can be found all over the investigation area. Greater areas are covered by them in the east. There, several chutes leading from the north ridge of the Giggler Spitze approximately to the northwest serve

as transport ways for loose rock material and are partly filled with talus deposits themselves. In adjacent areas of these chutes (especially in the lower parts) talus deposits are found too, but they are mostly covered with vegetation. The talus deposits occur in loose state and show varying grain sizes depending on the distance to the parent rock wall, but mainly are sandy gravels with cobbles (*sa co Gr*) sometimes containing boulders of up to ~50 cm in diameter.

3 Rockfall blocks

Rockfall blocks were only recorded in a few places of mappable extent at the bottom of rock faces. Other smaller occurrences coincide with talus deposits. Like talus the rockfall blocks are angular to subangular and are deposited beneath rock walls, but consist of boulders and large boulders (up to ~3 m in diameter) resulting from just a few rock fall events. They are also characterized by gravitational processes, causing the largest boulders to move furthest away from the rock wall.

4 Landslide Debris

The deposits of the landslide Gfäll occur from the scarp northwest of the Giggler Alpe down to the river Trisanna in the west. They are characterized by angular to subangular, unsorted boulders mixed with cobbles and large boulders (with a maximum diameter of about 5 m). Sometimes larger coherent slabs with e.g. 15 m in length can be seen. The landslide material is strongly fragmented and disintegrated with the degree of disintegration generally increasing with the distance from the headscarp. The components consist mainly of the dark grey to green paragneisses (9) and the phyllonitic micaschists (8). In the westernmost part of the landslide Gfäll the river Trisanna cuts its toe leading to relatively steep flanks. They consist of coherent slabs of intensely fractured rock mass that form scarps as well as restricted parts with sandy gravels (*sa Gr*) beneath them. These gravels contain cobbles and boulders of 10-40 cm as well as a few large boulders of up to 1 m in diameter in the southern region, whereas in the northern part boulders and large boulders of approximately 0.5 to 4 m in diameter were observed. The boulders and large boulders can be angular to subrounded. In the northern part the original landslide deposit is interrupted by talus sediments (*sa co bo Gr*) deriving from the scarp rock faces and forming fans toward the river Trisanna.

The deposits of the other landslides in the south toward the Hintergiggel and Giggel creek are generally finer-grained (mainly silty, sandy gravels (*si sa Gr*) with minor cobbles) than those of the landslide

Gfäll, because they occur within moraine sediments. Since they were not subject of the present thesis they were not investigated further.

5 Moraine Deposits mixed with Talus

In some parts talus is mixed with rounded components of moraine sediments which often were not accumulated there in the first place but transported and redeposited (like in the south or northwest of the study area) and therefore do not represent primary deposits of side or ground moraines. Furthermore, talus and moraine sediments often intercalate on a small scale (e.g. on the west and northwest flank of the Giggler Spitze) so that they were not differentiated during the mapping. Thus, following KRAINER et al. (2004) and GRUBER et al. (2010) who used the term “Moränenstreu vermischt mit Hangschutt” (meaning re-deposited moraine sediments mixed with talus), they were combined to one unit. The moraine deposits mixed with talus are silty, sandy gravels (*si sa Gr*) with minor cobbles and boulders up to a maximum of ~30 cm in diameter. The particles can be angular as well as subrounded to rounded. They are naturally packed and can feature layers without cobbles, but generally are unsorted and ungraded. In dry state they show a light brown to grey colour, which changes to middle brown or ochre in moist state.

6 Moraine Deposit

Moraine deposits are silty, sandy gravels (*si sa Gr*) with minor cobbles and seldom boulders (up to 50 cm in diameter). Only very rarely large boulders (up to 2 m in diameter) were observed. The components generally are rounded to subrounded, but glacial striation could only be detected scarcely. The moraine deposits in the study area are not compacted, but packed in a natural to dense state. The colour is light brown if the deposits are dry and middle brown in a moist state. The components can be of different rock types, e.g. micaschists, paragneisses and orthogneisses, but also of such not occurring in the present area, e.g. augengneisses, garnet amphibolites, diabases or carbonates. Moraine deposits occur at the Giggler Alpe and from there on to the west. The deposits in the southwestern part of the study area where the Giggel creek flows into the river Trisanna were also mapped as moraine deposits, but are probably no accumulations in terms of ground or side moraines. They rather are sediments that were transported by the Giggel creek (or its ancestor) and were deposited in late-glacial times during the collapse of the great ice masses at the margin of dead ice bodies (see chapter 1.3.2.).

3.1.1.2. Hard rocks

In the following chapter the characteristics of the hard rock units of the study area, which were gained during field mapping as well as from transmitting light microscopy of thin sections, are described. The geotechnical properties of the hard rocks are summarized in chapter 3.1.2.

7 Quartzite

Quartzites occur as butte ridges like in the southernmost part of the study area and as intercalating sequences especially within the phyllonitic micaschists, e.g. in the northeast. They are of light, nearly white to grey or greenish colour, sometimes brownish weathered, and are well foliated. Along with quartz they also contain macroscopically visible muscovite.

8 Phyllonitic Micaschist

The north and northwest of the study area is composed of fine-grained, light to dark grey, sometimes greenish micaschists. Due to weathering they often show yellow to brown or reddish surfaces. Since they were strongly affected and sheared by tectonic activities giving them a structure similar to phyllites (“phyllonitization”) they were named phyllonitic micaschists in the present thesis. In addition to their tectonic weakening these micaschists often are remarkably weathered near the surface making them a weak and often unstable rock type. They show a strong foliation within millimeters, which in most cases is puckered at cm- to dm-range. Besides, they are folded along larger east-west striking fold axes (chapter 3.1.3.). Quartz lumps, layers and lenses up to a thickness of 10 cm occur within them and they also intercalate with quartzites (7). Mineralogically (determined via transmitting light microscope) they consist of quartz, fine muscovite, sericite, plagioclase and kalifeldspar as well as zoisite and oxides as accessories (thin section 1 in Appendix 5). In hand rock samples sometimes also garnet is recognizable. In GRUBER et al. (2010) and KRAINER et al. (2004) respectively this unit is mapped as “light phyllitic garnet micaschists or garnet phyllites”, in AMPFERER & HAMMER (1922 and 1924) it is summarized as “phyllites”.

9 Paragneiss, dark grey, green

Great part of the central region of the study area is built up of paragneisses that show a light to dark grey or green colour on fresh surfaces and are brownish where they are weathered. These rocks are well foliated at the range of mm, but are relatively strong. Sometimes quartz lenses or veins occur

within them. They are fine- to middle-grained and contain quartz, feldspar (plagioclase and kalifeldspar), muscovite, sericite, minor biotite as well as rutile and ore minerals as accessories (thin sections 5, 12 and 14 in Appendix 5). In many cases there are only little amounts of micas and sometimes muscovite is altered to sericite. As another alteration product chlorite is found in some cases.

10 Micaschist, grey

The grey micaschists occur in the northeast as smooth transitions from the paragneisses (9), and in the south to southwest in the hanging wall of them. They are middle-grained and vary from grey to dark grey or green and show a brownish to reddish weathering colour. They are strongly foliated with the schistosity planes often being slightly puckered and contain quartz lenses up to 10 cm thickness. They differ from the paragneisses (9) in their increased mica content and minor amount of feldspar and also quartz. Generally they consist of muscovite, quartz, feldspar, minor biotite and chlorite and sometimes (especially in the northeastern part) garnet and also staurolite. In AMPFERER & HAMMER (1922 and 1924), KRAINER et al. (2004) and GRUBER et al. (2010) the paragneisses (9) and micaschists (10) are combined to one unit (“phyllitegneiss and micaschist” and “micaschist to paragneiss” respectively).

11 Paragneiss, grey, brown

The grey-brown paragneisses together with the biotite-muscovite schists (12), to which in some areas diffuse transitions can be found, build up the southeastern part of the study area. These paragneisses are of light to dark grey and brown colour, showing a more intensive brown where they are weathered. They are medium-grained and well foliated but massive, since they are rich in quartz and feldspar. Furthermore they contain biotite and (in most cases less) muscovite, sericite as alteration product of feldspars, zoisite and pyrite (thin sections 7 and 13 in Appendix 5). Quartz lenses and layers with a thickness of 1-10 cm, seldom up to 30 cm can be found.

12 Biotite-Muscovite Schist

The biotite-muscovite schists are similar to the grey-brown paragneisses (11) described above. They are grey to light brown and also weather brownish. They are medium-grained and well foliated but without puckering of the schistosity planes (in contrast to the grey micaschists (10)).

The biotite-muscovite schists mineralogically consist of quartz, muscovite and biotite in nearly equal amounts (sometimes also more biotite than muscovite) and feldspars (especially plagioclase). At the north ridge of the Giggler Spitze sometimes garnet can be seen. In GRUBER et al. (2010) and KRAINER et al. (2004) they are known as two-micaschists and are subsumed with the paragneisses (11).

13 Amphibolite

The amphibolites in the study area occur as relatively small lenses within the grey micaschists (10), grey-brown paragneisses (11) and the biotite-muscovite schists (12). Sometimes transitions to hornblende-plagioclasegneisses are possible (cp. GRUBER et al., 2010). They are of dark grey to dark green colour with light layers of plagioclase and get reddish to brownish where they are weathered. Although the amphibolites in the investigation area are often altered, they are strong, dense and massive rocks. They are fine-grained (seldom medium-grained) and show a moderately developed foliation making them break into slab-like bodies. Sometimes slickensides that are typical of amphibolites can be seen. They consist of the minerals amphibole (hornblende), plagioclase, clinozoisite, quartz and sometimes also kalifeldspar. In many cases secondary minerals like sericite and chlorite as alteration products of feldspars and hornblendes can be seen. Fractures are commonly healed by calcite and also quartz (thin section 15 in Appendix 5).

14 Albite-Blast Schist

The albite-blast schists ("Feldspatknottengneis" in AMPFERER & HAMMER (1924)) are well recognizable in the field due to their albite blasts with up to 5 mm in diameter. They are grey to brown and relatively light because of the feldspars. If weathered, they are rather brown. Generally they are compact (gneissic habitus), but are distinctly foliated and rich in micas (cp. GRUBER et al., 2010). Along with albite they also contain quartz, muscovite and little biotite. They show a smooth transition to the grey micaschists (10) by a slow decrease of the Ab-blasts.

15 Garnet Micaschist

Light garnet micaschists only were found in the southwestern part of the area. They are middle-grained and well foliated, showing a light grey to light brown (especially if weathered) colour. They are rich in quartz and therefore often quite massive and strong. Pure quartz layers with up to 10 cm

thickness could be found. Beside quartz the garnet micaschists consist of muscovite, biotite, little feldspar and garnets of 2-5 mm in diameter (thin section 9 in Appendix 5). According to GRUBER et al. (2010) sometimes also staurolite is contained, but could not be found in the course of mapping or in the thin section.

16 Orthogneis

Only two small occurrences of orthogneisses in the north and northeast of the study area could be mapped. They are light grey to yellowish or greenish, sometimes nearly white. They are medium-grained and distinctly foliated and are relatively strong and massive rocks. The mineral paragenesis consists of small grains of quartz, larger grains of plagioclase and kalifeldspar, and muscovite that is sometimes bended around the feldspar grains forming an augen (lense) texture. The feldspars are partly altered to sericite (thin sections 2, 3, 4 and 10 in Appendix 5). In AMPFERER & HAMMER (1922 and 1924), KRAINER et al. (2004) and GRUBER et al. (2010) the orthogneisses are specified as muscovite-granitegneisses.

Cataclasite

Cataclasites are strongly deformed hard rocks that evolved from different parent rocks. They feature an unoriented, chaotic texture (GRUBER et al., 2010). In the study area they were found especially on the northwest flank of the Giggler Spitze. Their parent rock types were the grey micaschists (10), grey-brown paragneisses (11) and biotite-muscovite schists (12). Therefore, the symbol for cataclasites on the geologic map is used additionally to the colours representing the rock types from which they originated. As a consequence of the different parent rocks, the cataclasites also consist of different minerals, such as quartz, feldspars, muscovite, biotite, sericite, zoisite, zircon, tourmaline, ore minerals, apatite and pyrite (thin sections 6, 8 and 11 in Appendix 5).

According to the subdivision of the Silvretta nappe stated by GRUBER et al. (2010) and KRAINER et al. (2004) respectively, most of the lithological units of the study area belong to the *Venet complex* (chapter 1.3.1.). Only the grey-brown paragneisses (11) and the biotite-muscovite schists (12) are considered as part of the *Silvretta complex*. Since this differentiation is not relevant for the problem of the present thesis, it is renounced going into details.

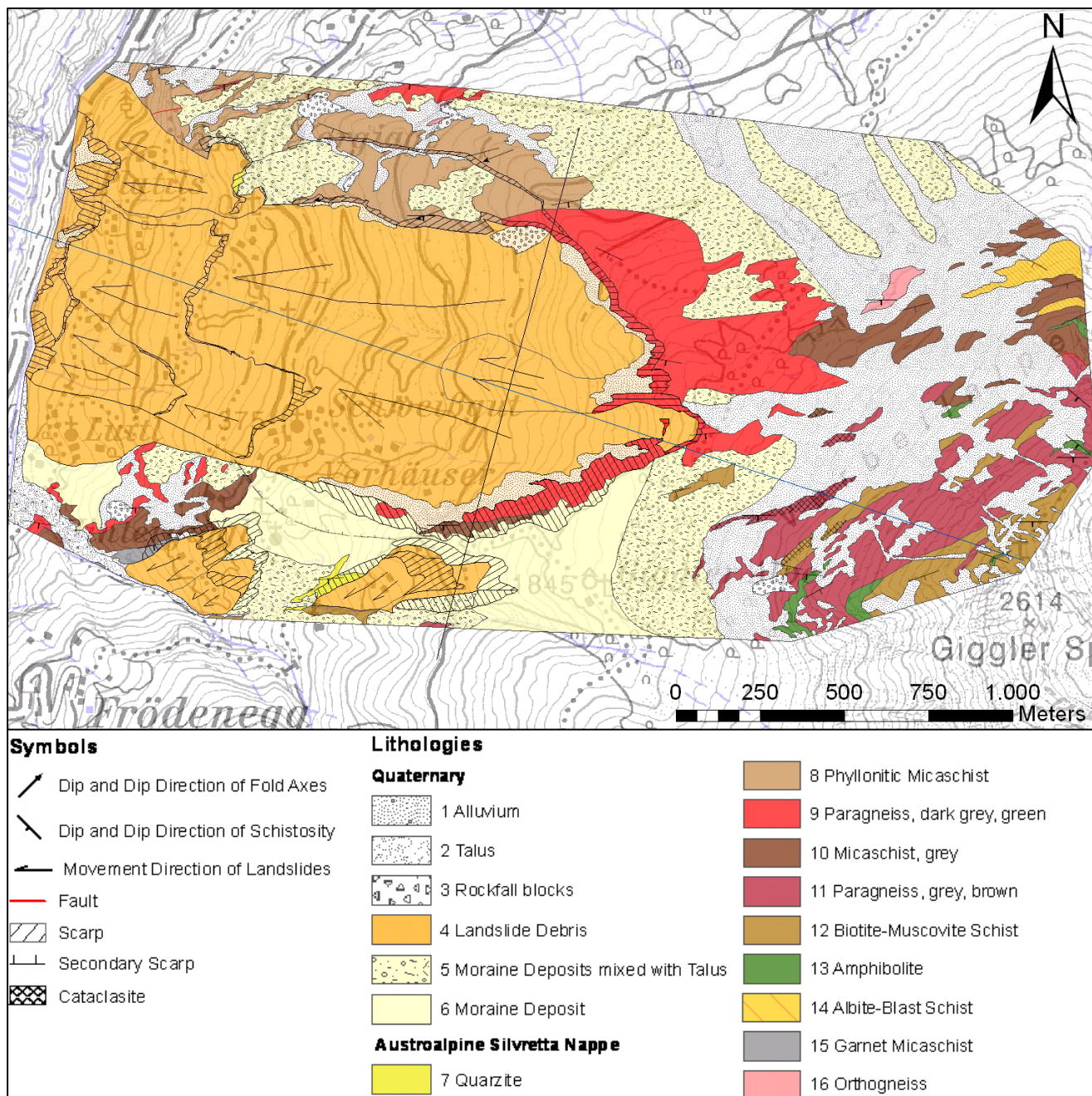


Figure 25: Geologic map of the study area (base map from BEV (2013)). The black and the blue line give the location of the transversal and longitudinal geologic cross section in chapter 4.5.

3.1.2. Geotechnical properties of the hard rock units

The geotechnical characteristics of the hard rock units in which the landslide Gfäll is located were determined for ten outcrops using field estimation methods following ÖNORM EN ISO 14689-1 (Appendix 3). The degree of weathering can reach from 0 (fresh) to 4 (completely weathered). The spacing of the joint planes is given as average intervals in mm. Their roughness is described by two properties depending on the scale: the adjectives “stepped”, “undulating” and “planar” are used for the range of cm to m, the adjectives “rough” and “smooth” for the range of mm. The observed apertures of

joint planes are given in mm, the persistence can reach from very low (< 1 m) to very high (> 20 m). The geometry of the block bodies formed by the joint sets can be polyhedral, tabular, prismatic, equidimensional, rhombic or columnar. Data for the other lithological units, for which no detailed outcrop documentation was done, were gained in the course of field mapping, but here not all of the parameters were specified. The lithological units which feature similar properties were then combined to geotechnical groups (Table 10). **Group 1** comprises the phyllonitic micaschists (8), the dark grey to green paragneisses (9) and the grey micaschists (10), **group 2** the quartzites (7), the grey to brown paragneisses (11), the biotite-muscovite schists (12), the garnet micaschists (15) and the orthogneisses (16), and **group 3** the amphibolites (13) and the albite-blast schists (14).

Table 10: The geotechnical groups consisting of the lithological units of the study area which feature similar properties. Their characteristic parameters for rocks and joints were determined following ÖNORM EN ISO 14689-1 (n. s.: "not specified" in the course of field mapping).

	Rocks		Joints						Block bodies
	UCS	Weathering	Spacing	Roughness	Aperture	Persistence	Water	Filling	
	[MPa]	(0 - 4)	[mm]		[mm]	[m]			
Group 1	5 - 25	1 - 2	20 - 200	undulating, smooth	0 - 50	medium (3 - 10)	-	partly plastic fillings	rhombic
Group 2	25 - 100	0 - 1	200 - 600	planar, rough	n. s.	n. s.	-	-	tabular to equidimensional
Group 3	50 - 100	0 - 1	60 - 600	planar - stepped, smooth	n. s.	n. s.	-	-	tabular to rhombic

3.1.3. Structural geologic features

The **schistosity** data of the study area including the corresponding **fold axes** were determined for numerous locations in the course of field mapping. A total of 162 foliation measurements and 16 fold axis measurements were collected. The schistosity generally strikes E-W to ESE-WNW and dips to the south. Due to folding sometimes deviant measurements (with dip directions to the northeast for example) can occur. The foliation planes feature an average dip direction and dip (center of gravity) of 187/35 (Figure 26a). The fold axes usually plunge flatly to the W to WSW, seldom to the E to ENE, with an average orientation of 256/32 (Figure 26b). Three **faults** could be recorded in the study area that strike approximately E-W (Figure 26c). For the measured **slickensides**, however, no preferred orientation could be found (Figure 26d). The total measurements are listed in Appendix 4.

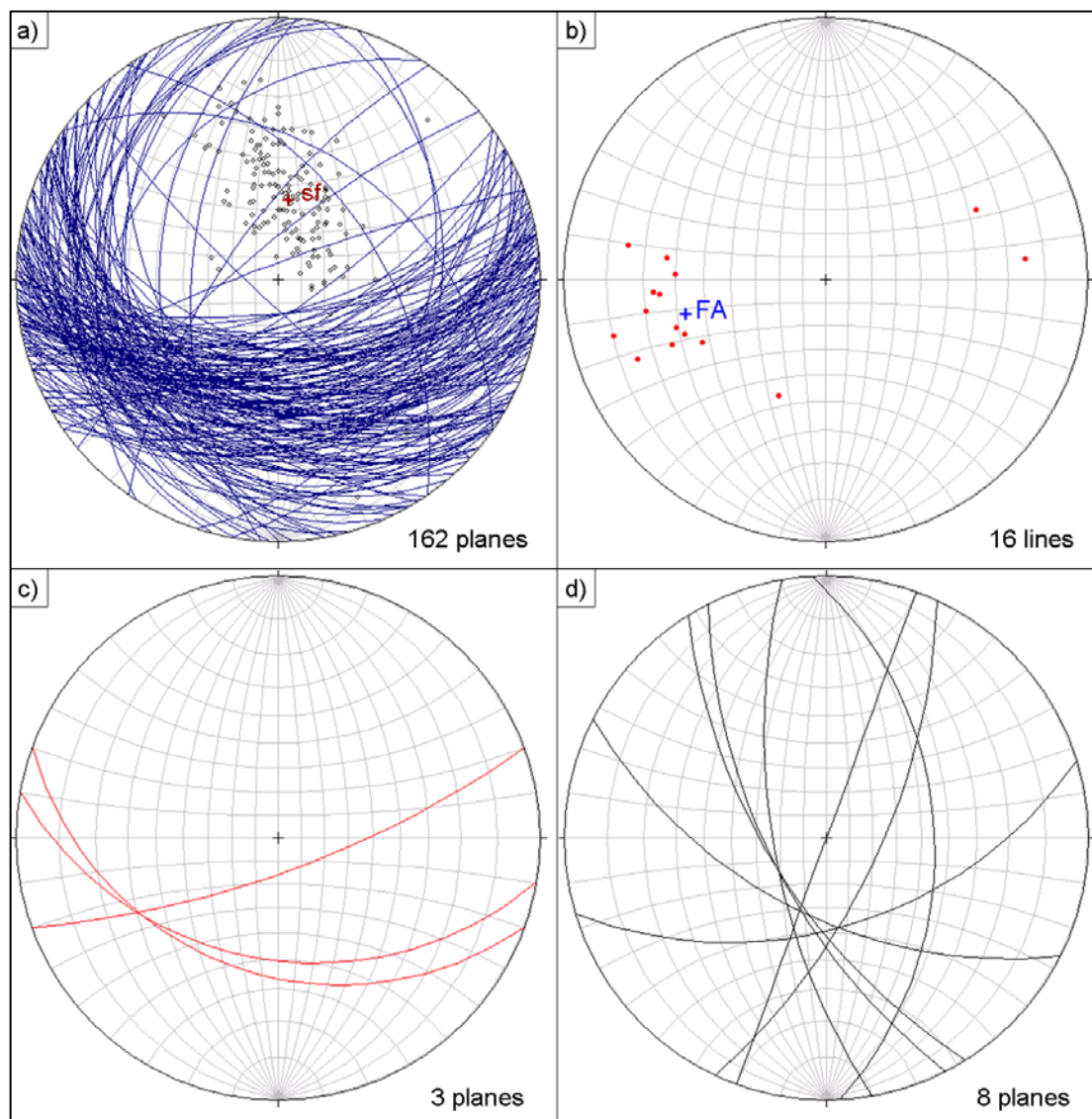


Figure 26: Lower hemisphere equal angle projection of the structural data of the study area: a) foliation planes (great circles and poles) with their average orientation (center of gravity) of $sf = 187/35$; b) fold axes with their average orientation of $FA = 256/32$; c) faults; d) slickensides.

The joint orientations were measured at ten selected outcrops (Appendix 3) resulting in five different joint sets in addition to the schistosity. Figure 27a shows the poles of the joint planes in a lower hemisphere equal angle projection. The contour lines mark the highest density in red giving the centers of gravity for the joint sets j1 to j5. Figure 27b shows the great circles and the corresponding poles of the schistosity with the contour lines and the center of gravity for the ten selected outcrops. The dip direction and dip of these centers of gravity are given in Table 11. The joint sets j1 and j2 were found at every of the ten selected outcrops except for one, whereas joint sets j4 and j5 could only be measured at a few outcrops. Joint set j3 is also very common (eight out of ten outcrops), but is overturned at three outcrops resulting in SSW to SSE dipping joint planes.

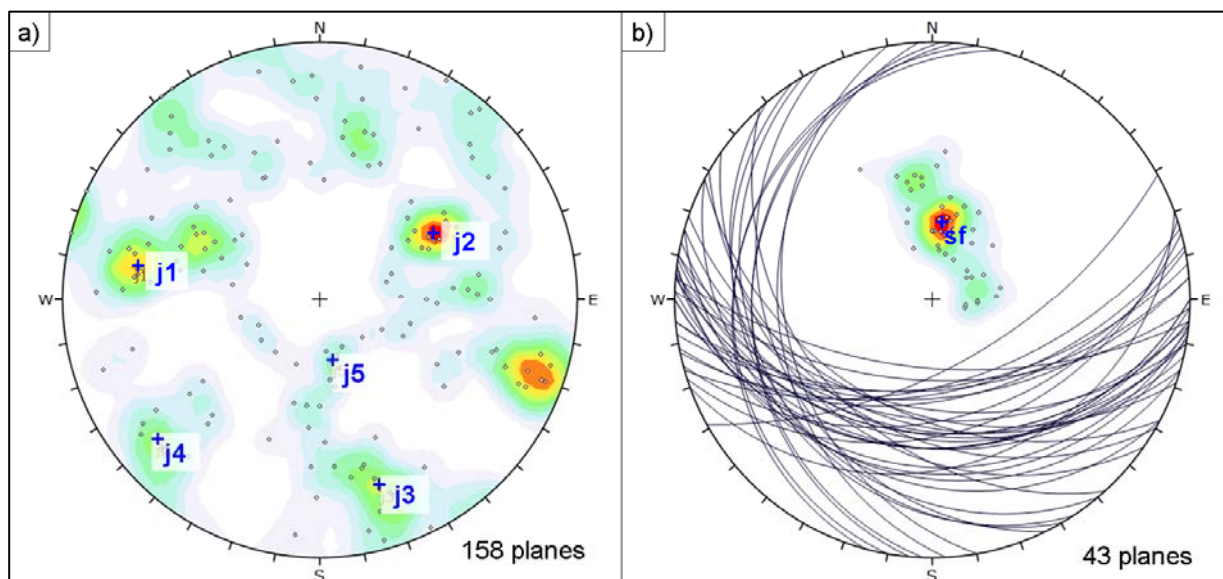


Figure 27: Lower hemisphere equal angle projection of the structural data of the ten selected outcrops: a) poles of the joint sets *j1* to *j5* with density contour lines and their average orientations (centers of gravity); b) great circles and poles with density contour lines of the schistosity and its average orientation.

Table 11: Average orientations (centers of gravity resulting from the density plot) of the joint sets *j1* to *j5* and the schistosity (*sf*) measured at the ten selected outcrops.

	<i>j1</i>	<i>j2</i>	<i>j3</i>	<i>j4</i>	<i>j5</i>	<i>sf</i>
Average orientation (Centers of gravity)	100/72	238/55	342/75	49/80	348/28	188/33

3.2. Geomorphology

3.2.1. Glacial morphology

In addition to the glacial sediments also morphologic features are evidences of the glacial overprint of the study area. Especially in the north near the farmstead Vorgiggl glacial polishes could be observed (Figure 28 and Figure 29). Sometimes also glacial striations (toward NNW to NNE) could be found, but in many cases the polished surfaces are overgrown with mosses making the recognition of striations difficult (Figure 28b). The glacial polishes occur on the southern side of a ridge which on its northern side features steep escarpments, resulting in a whale back morphology: flat and polished on the side that faced the glacier, and abrupt rock faces on the opposite side of the ridge (Figure 29).

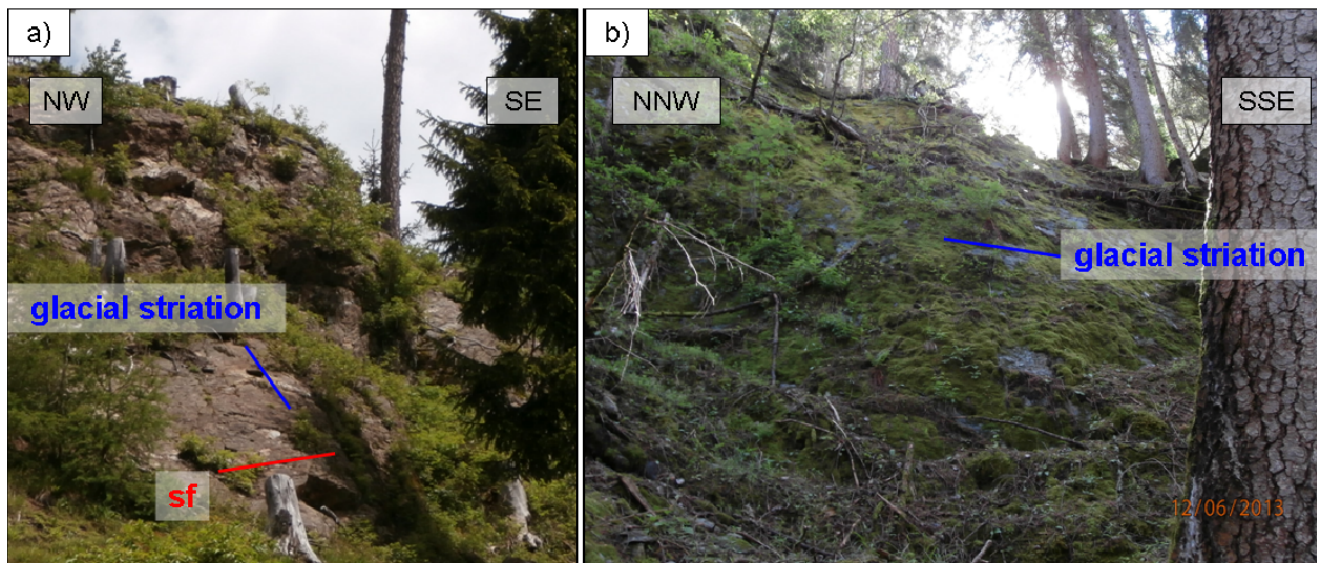


Figure 28: a) View toward northeast: glacial polish with glacial striation (blue line) east of the farmstead Vorgiggel; the strike of the schistosity (sf) is shown by the red line. b) View toward ESE: glacial polish with glacial striation (blue line) west of the farmstead Vorgiggel, where the polished surfaces are mostly overgrown with mosses.

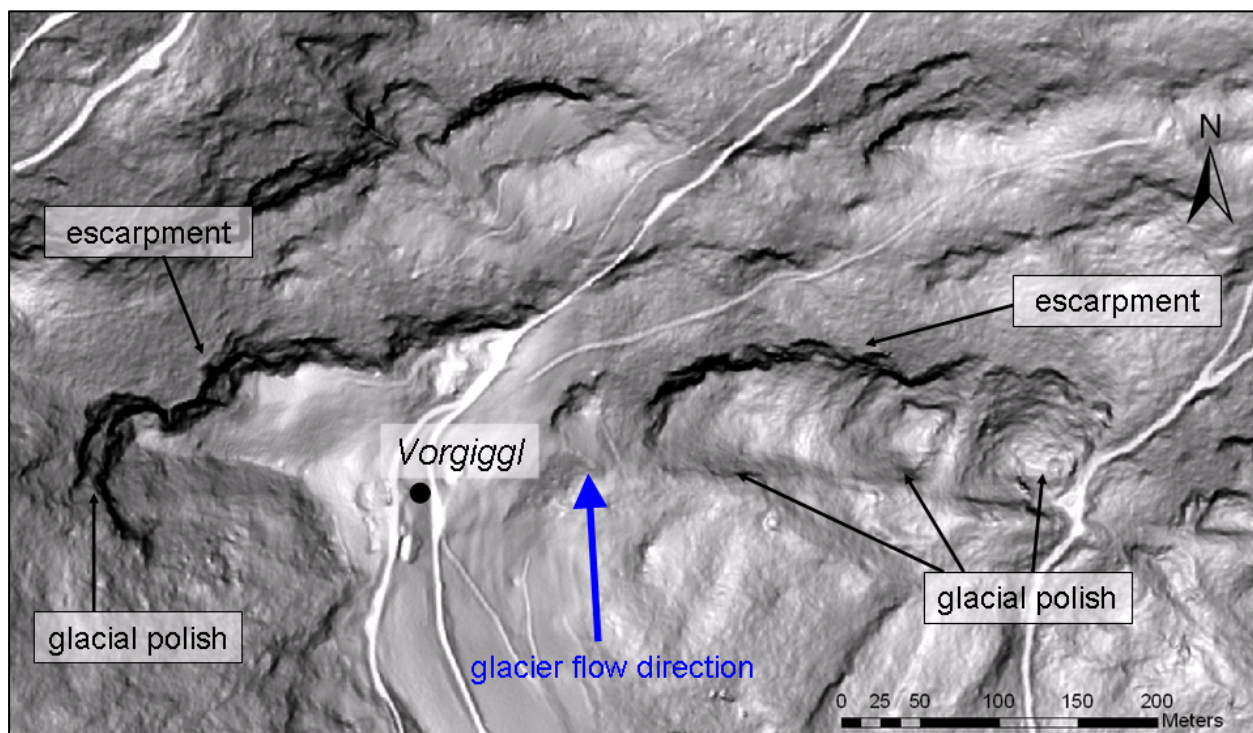


Figure 29: Slope inclination display (obtained from ATLR (2013)) of the ridge in the north of the study area (dark areas mark steep slopes, light areas shallow parts). Glacial polishes occur on the southern side of the ridge, steep escarpments on the northern side. The approximate flow direction of the glacier is shown by the blue arrow.

3.2.2. Geomorphic characteristics of the lithological units

The lithological units specified in chapter 3.1.1. (especially the Quaternary deposits) feature different morphologies that shall be described in the following paragraphs. The hard rock units often show similar geomorphic features and therefore were summarized for their characterization.

The alluvium (1) shows a smooth and uniform surface with an inclination decreasing from $\sim 25^\circ$ in the channel of the Giggler creek to $\sim 5^\circ$ at the river Trisanna. Talus deposits (2) also feature rather smooth surfaces and uniform slope inclinations (mostly $25-30^\circ$) that decrease with the distance to the parent rock wall. Deposits of rockfall blocks (3) are characterized by a more uneven morphology than a talus due to the larger grain sizes (usually boulders to large boulders). The slope inclinations where rockfall blocks were observed in the study area are very variable ($15-45^\circ$). Moraine deposits (6) and moraine deposits mixed with talus (5) have very smooth and uniform surfaces with slope inclinations that usually do not exceed 30° , except in the south where the Hintergiggler creek incised them. At the Giggler Alpe they form even flatter areas with inclinations of $10-20^\circ$. The landslide debris (4) is generally rather steep ($30-40^\circ$) and its surface morphology in large part is irregular and hummocky. Only flatter areas in between ($10-20^\circ$) feature a smoother surface. The reason therefor can either be that these areas belong to coherent slabs (instead of disintegrated boulders), or – as in some cases – that they were cleaned from greater blocks by men to serve as meadows. Several escarpments (up to an inclination of $\sim 55^\circ$) dipping approximately to the west can be found all over the landslide.

The grey to brown paragneisses (11), the biotite-muscovite schists (12) and the amphibolites (13) form steeper areas ($35-45^\circ$) interrupted by escarpments ($50-80^\circ$ and about 2-5 m in height) in the east of the study area toward the Giggler Spitze. The grey micaschists (10) and the garnet micaschists (15) in the southwest of the study area as well as the quartzites (7) in the south toward the Hintergiggler creek build up rock walls and ridges respectively featuring inclinations of 40° up to 80° . The phyllonitic micaschists (8) and the dark grey to green paragneisses (9) are generally characterized by soft and rounded morphologies. Only at the scarps of the landslide Gfäll and in the northwest toward the river Trisanna they form steep rock faces ($50-80^\circ$). The occurrences of albite-blast schists (14) and orthogneisses (16) are too small to feature particular morphologies.

3.2.3. Other geomorphic features

In this chapter the geomorphic features of the study area that are not restricted to a certain lithology are specified. The mapped features, which are chutes, obsequent and normal breaks in slope, scarps and secondary scarps, crevices and concave as well as convex slope shapes, are documented on the geomorphic map (Figure 30 and Appendix 2). **Concave morphologies** are generally found more frequently and in higher areas than the **convex morphologies**, which are less common and occur in the lower areas, often corresponding to a concave shape above it. Concave slope areas in many cases coincide with scarps. It can also be observed in some places that beneath one convex shape the next concave one is situated (Figure 30).

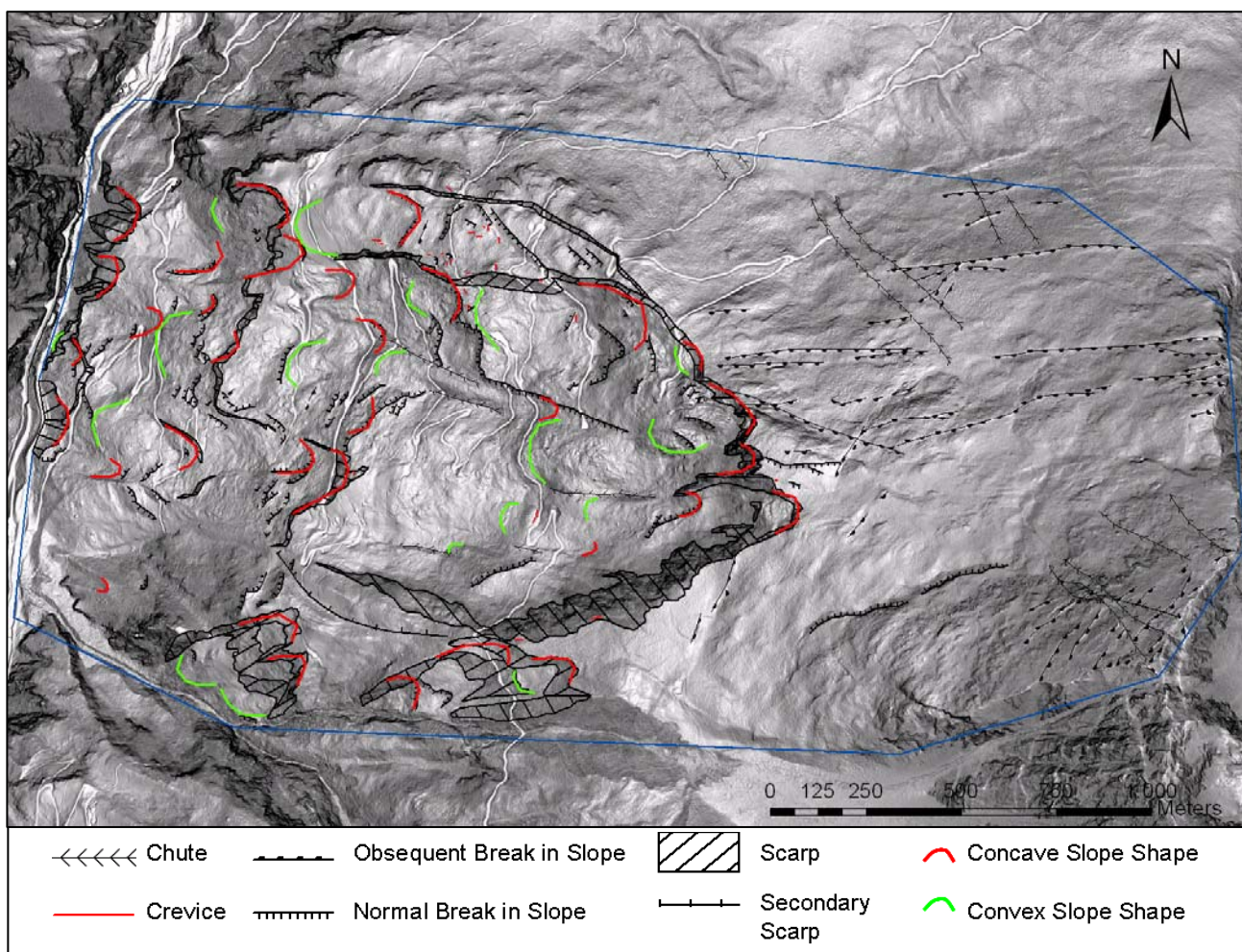


Figure 30: Geomorphic map of the study area (blue frame) with a slope inclination display obtained from ATR (2013) as base map.

From the north ridge of the Giggler Spitze three major **chutes** lead toward the northwest (Figure 32a) and are continued within the Quaternary deposits in the northeast of the study area. Another feature especially occurring in the east of the study area are approximately E-W and NE-SW striking

obsequent breaks in slope. Some of them are uphill facing scarps where the joint plane can be seen (Figure 31a), some of them form trenches of 1-2 m depth and 2-4 m width that can be traced at least over tens of meters, in most cases even along the entire slope (Figure 31b and Figure 32). **Normal breaks in slope** are downhill facing escarpments of varying height, which occur especially within the deposited mass of the landslide Gfäll and its adjacent areas.

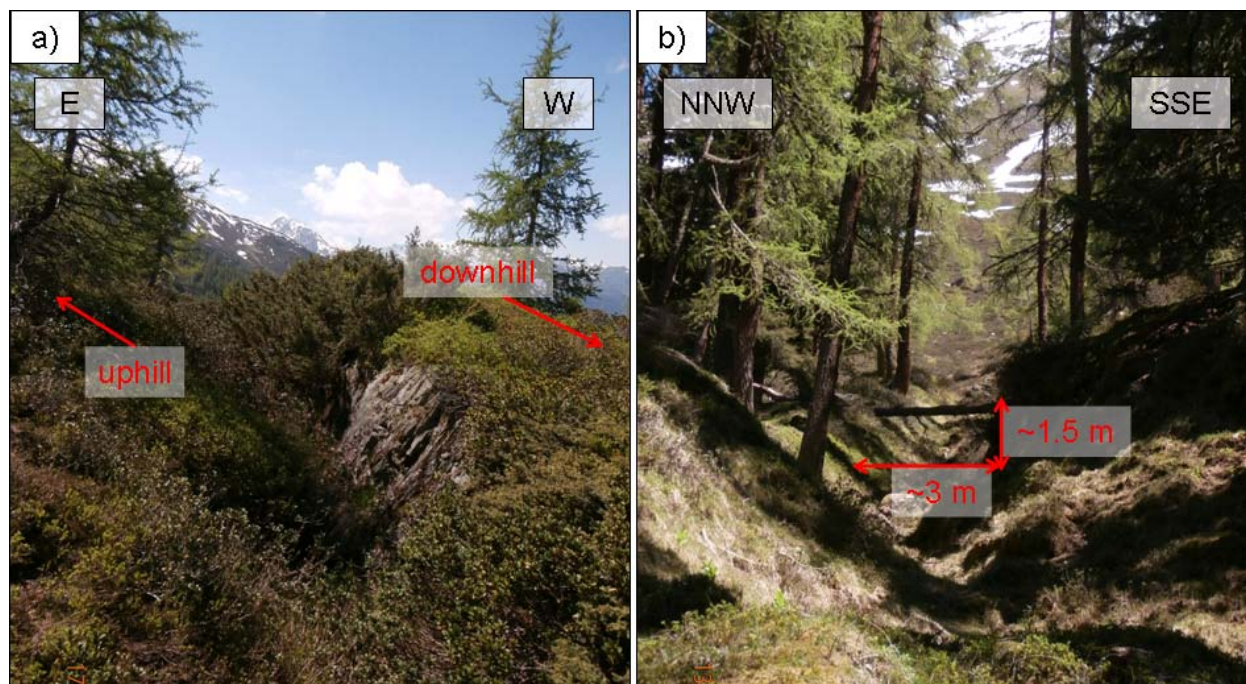


Figure 31: Obsequent breaks in slope: a) exposed uphill facing joint plane, b) trench leading toward ENE.

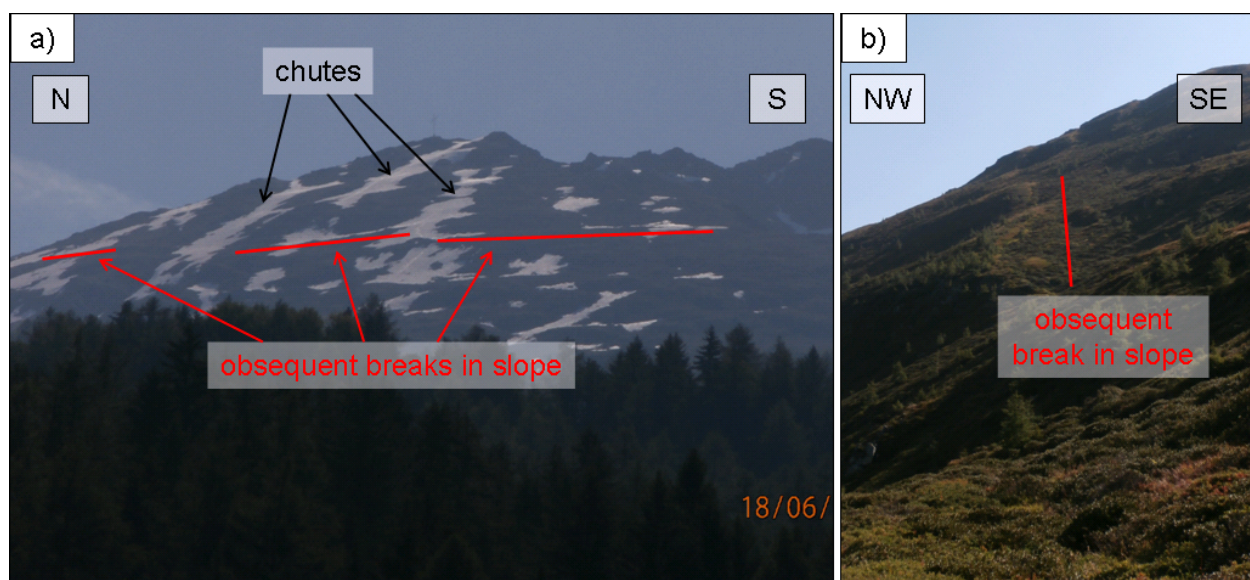


Figure 32: a) View from the western side of the Paznaun valley toward the Giggler Spitze showing the snow filled chutes leading down from the ridge and the obsequent breaks in slope along the entire mountain flank. b) Obsequent break in slope that can be traced all the way up to the north ridge of the Giggler Spitze.

Scarps mark the headscarp areas of the landslide Gfäll at approximately 1800-1900 m a.s.l. (Figure 33a) and of the landslides in the south toward the Hintergiggel and Giggel creek. Scarps also

occur within the deposited mass of the landslide Gfäll and at its toe down to the river Trisanna (Figure 33b). In the north of the study area two nearly vertical, E-W striking rock walls were observed that were also mapped as scarps. The northern one of these rock walls has a height of 1-3 m (Figure 34a), whereas the one ~200 m to the south features a height of approximately 15 m (Figure 34b). One **secondary scarp** was mapped in the south of the landslide Gfäll meaning a minor scarp where no outcrop is formed but not stating a chronological occurrence with regard to the other scarps.

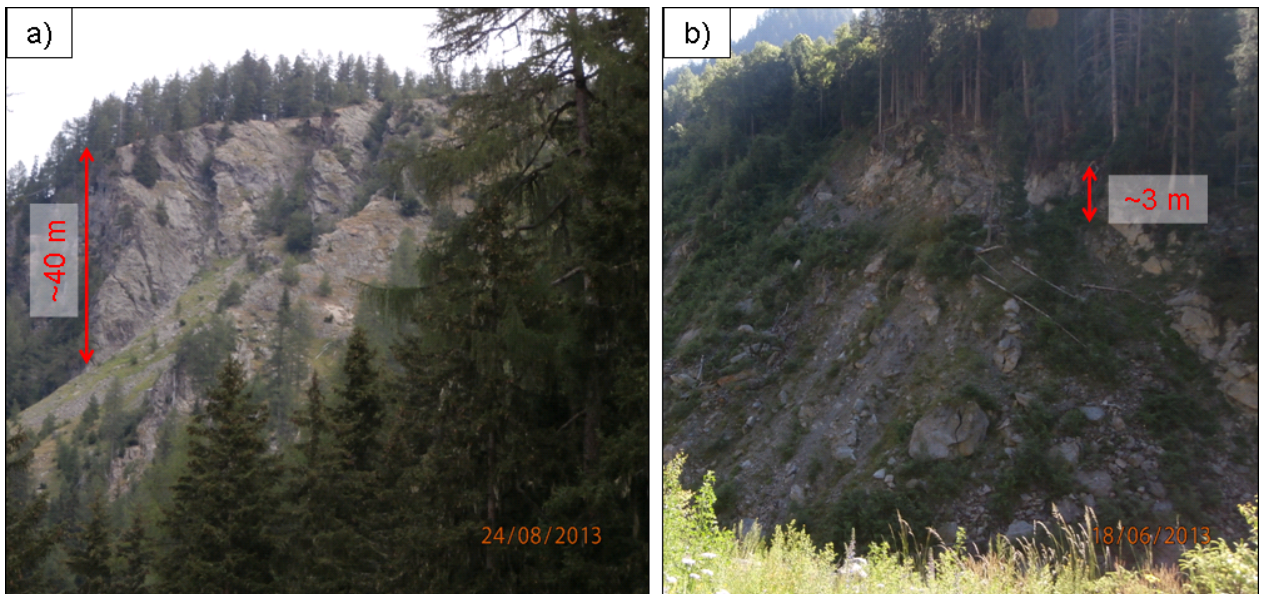


Figure 33: a) Headscarp of the landslide Gfäll; b) Scarp at the toe of the landslide Gfäll down to the river Trisanna.

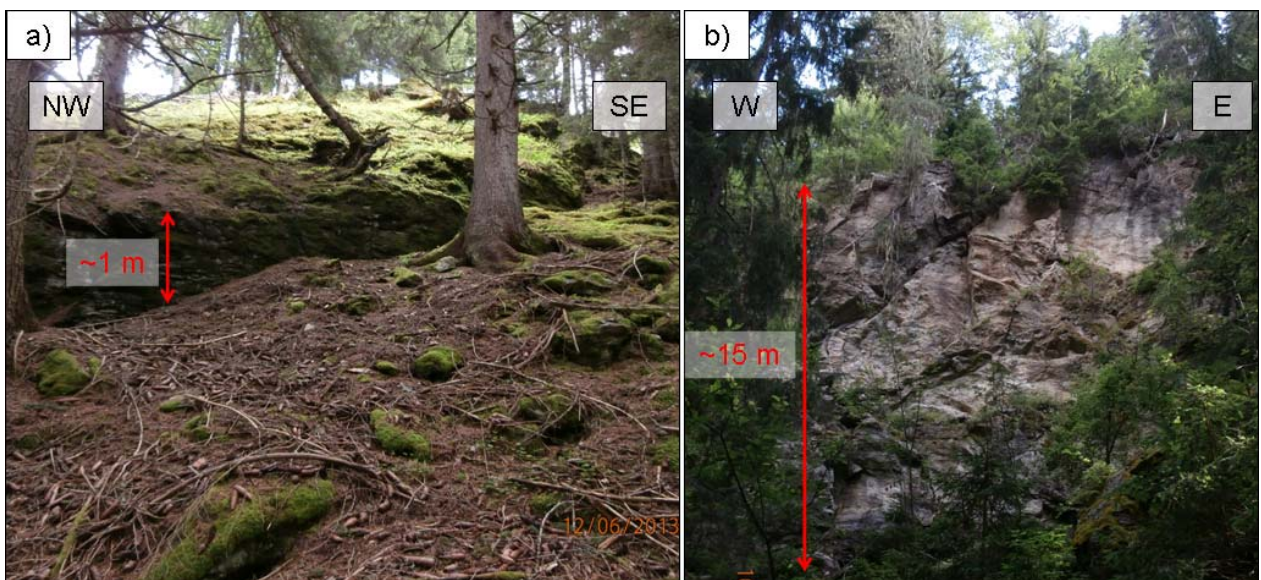


Figure 34: a) Northern one of the nearly vertical rock walls; b) Southern rock wall.

In the hard rocks behind the scarps of the landslide Gfäll **crevices** occur in ~E-W striking as well as ~N-S striking manner. They were observed with increased density in the north between the two nearly

vertical rock walls described above that were mapped as scarps. The crevices are of several meters in depth (up to 5 m were observed, but they probably go deeper) with an aperture normal to the fracture planes of 0.2 to ~3 m (Figure 35).



Figure 35: Examples of crevices in the adjacent areas behind the scarps of the landslide Gfäll.

3.3. Hydrology

In the study area eleven springs (numbered s1 to s11) were mapped during field work between June and August 2013 and – where it was possible – the discharge of the springs was estimated (Figure 36 and Table 12). For tapped springs only the discharge at the overflow pipe could be determined. In the water information system of Tyrol (WIS, 2013) some of these springs and also additional springs that were not recorded in the field are documented with their local names and were added to the hydrologic map (Figure 36) and Table 12 (springs s12 to s17). The springs in the study area generally feature low discharge amounts: A maximum of 1 l/s was observed at the Giggli spring (s1) but the discharge of most of the other springs did not exceed 0.05 l/s.

The hydrogeologic conditions of the study area change from east to west due to the different properties of the rock materials. The fractured gneisses, micaschists and amphibolites from the Giggler Alpe toward the Giggler Spitze only feature surface runoff (concentrated along the chutes) during heavy rainfalls. The rest of the water infiltrates into open fractures or into the Quaternary deposits. During field mapping no water could be observed there at all and only one spring (s17) is

located within the Quaternary sediments in the northeast of the study area. The phyllonitic micaschists generally feature a low hydraulic conductivity, but also here the crevices provide an opportunity for precipitation and surface waters to infiltrate. The springs of the study area are primarily located within the disintegrated landslide debris; only five of the 17 springs are located outside. In many cases the water of the springs drains away only a few meters after the outlet (for example at the springs s5 to s7) reflecting the high permeability of the (in large part) blocky material. The springs occur preferentially in niches at the toe of steeper slope parts (Figure 36). On the hydrologic map also the river Trisanna and the Hintergiggel and Giggel creek as well as little brooks are shown. The brooks, however, were not traced from their springs to their ends, but were only mapped where they were run across. It can be seen that the occurrence of brooks and therefore surface water increases toward the west to the areas of lower elevation.

Table 12: Springs of the study area with their coordinates, local names, the information if they are tapped or not, the estimated discharges and the discharge amounts according to WIS (2013) if they were given. The springs s1 to s11 were observed in the field, the information about the springs s12 to s17 was taken from WIS (2013).

Spring number	Coordinates		Spring name	State (tapping)	Estimated Discharge [l/s]	Comment	Discharge [l/s] according to WIS (2013)
	x	y					
s1	12968	218319	Giggel spring	tapped	0.75 - 1	at overflow pipe	minimum: 0.3
s2	11899	218165		not tapped	0.05		
s3	12598	217881	Mantl spring	tapped	0.25	at overflow pipe	
s4	12470	218652	Schad spring	tapped			
s5	12225	218490		not tapped			
s6	12209	218502	Eastern Wiesle spring	tapped			
s7	12963	218167	Wasserloch spring	not tapped	0.25	multiple outlet	~ 2
s8	12670	219245		not tapped	< 0.01	diffuse outlet	
s9	12692	219299	Wiesen spring	tapped	< 0.01	at overflow pipe	~ 0.02
s10	12880	219320	Vorgiggel spring	tapped	0.02	at overflow pipe	
s11	12303	218394	Lower Wiesle spring	not tapped	0.05		
s12	12050	218495	Luitl spring	tapped		from WIS (2013)	
s13	12134	218997	spring Platils	tapped		from WIS (2013)	
s14	12890	218542	Junkbrunnen spring	not tapped		from WIS (2013)	
s15	12808	218206	Stadles spring	tapped		from WIS (2013)	
s16	13212	218181	Lahngang springs	not tapped		from WIS (2013)	
s17	13485	219000	Schwarzbartlahnstrich springs	tapped		from WIS (2013)	

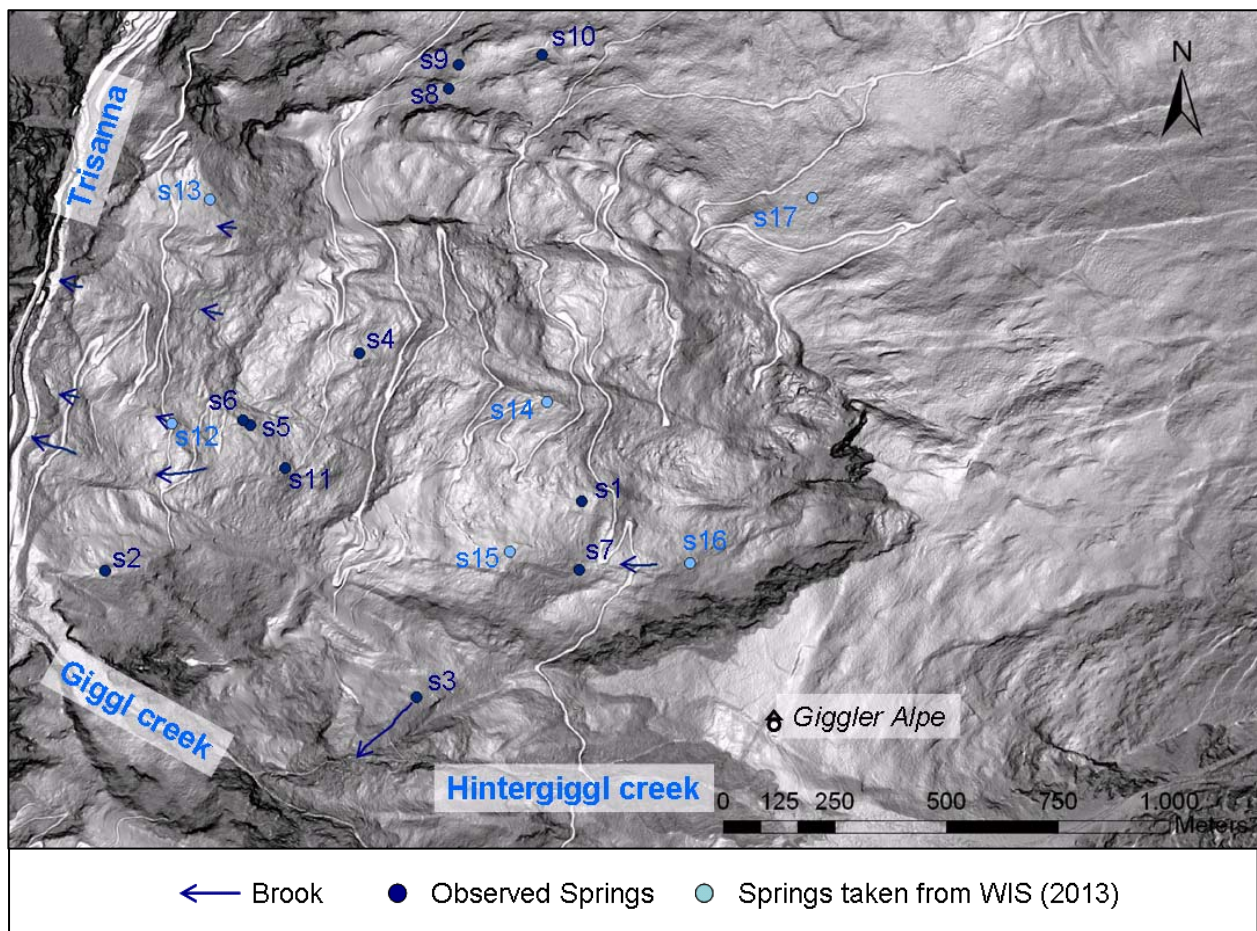


Figure 36: Hydrologic map (slope inclination display obtained from ATLR (2013) as base map) showing the observed springs s1 to s11 and the additional springs s12 to s17 according to WIS (2013).

3.4. Vegetation

To large part the study area is forested up to the timber line at approximately 1800-1900 m below the Giggler Alpe (Figure 37). Especially the steep slopes of the landslide deposit are covered with coniferous forest consisting mainly of spruces, pines and some larches. Only on the flatter areas in between some meadows occur. The boulders of the landslide debris are overgrown with mosses and lichens, in contrast to the younger rockfall blocks which in most cases are not yet covered with vegetation. In the lower areas and down to the river Trisanna hazel bushes, alders and birches can be found. An alpine pasture occurs at the Giggler Alpe and to its north. At its border to the headscarp of the landslide Gfäll also some alders grow. From the Giggler Alpe to the northeast and to the east toward the Giggler Spitze only some dwarf pines and shrubbery (e.g. alpine roses, juniper bushes, blueberry and mountain cranberry bushes) as well as mosses, herbage, lichens and some isolated small larches can be found.

3.5. Human settlements and infrastructure

In the study area smaller settlements are located, each consisting of only a few houses. The largest settlement is Schweißgut near the southern border of the landslide Gfäll (Figure 37). The others are called Platils and Vorgiggel in the northwest of the study area, Luitl in the southwest and Hintergiggel which is situated south of Schweißgut. All together they comprise about 30 to 40 houses of which only approximately five are located outside the area of the landslide Gfäll. The streets which are needed as access to the settlements are usually asphalt streets. Also the road which was built after the flood event in 2005 as temporary road into the Paznaun valley, when the old bridge Gfäll was closed for reasons of safety (chapter 1.5.2.), is an asphalt street and leads into the bridge across the river Trisanna (Figure 37). Further infrastructural facilities are driveways to meadows and forest roads that lead up to ~1600 m, in the north even higher.

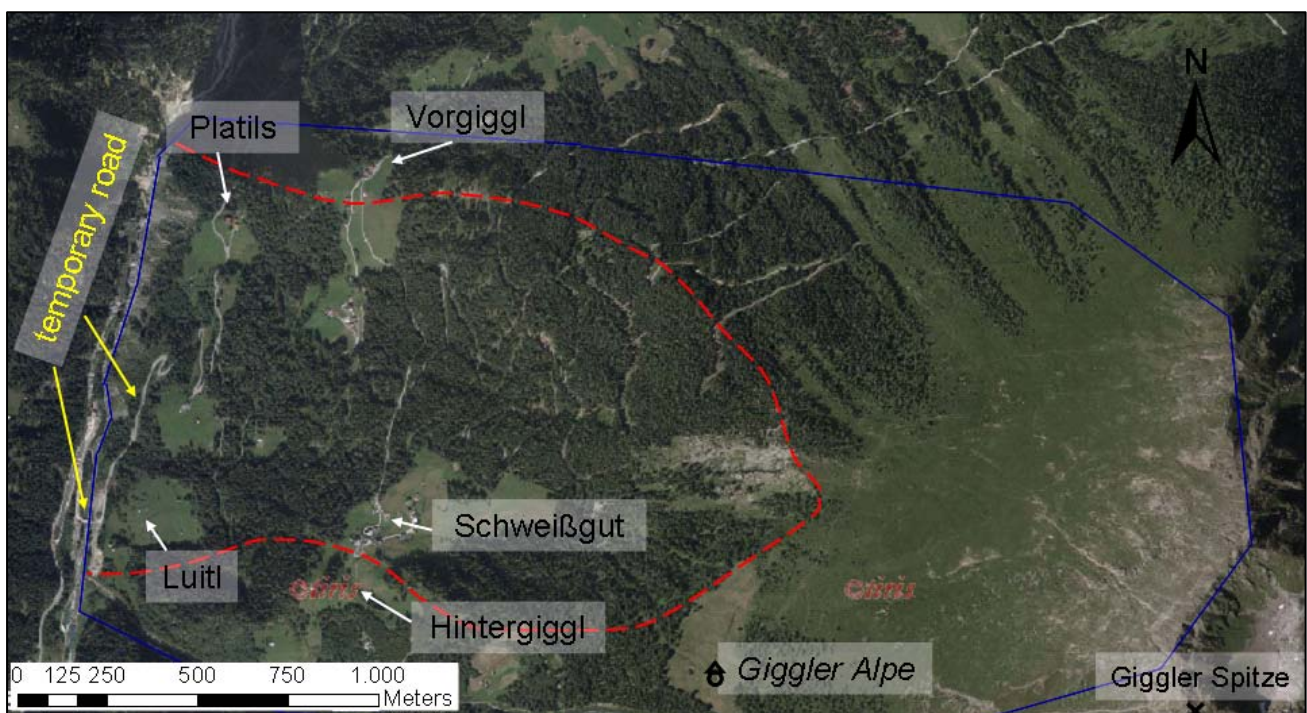


Figure 37: Orthophoto (from TIRIS, 2013) showing the human settlements of the study area, the Giggler Alpe and the Giggler Spitze. The blue frame marks the border of the study area, the red line the area of the landslide Gfäll. The yellow arrows point at the temporary road built in 2005 and the following bridge.

4. Observations and Findings

4.1. Results from desk study

As a first step during desk study existing literature of the landslide Gfäll was compiled and studied and remote sensing data were used to get an overview of the study area. In a later stage then, it was attempted to reconstruct the **pre-failure topography** of the area of the landslide Gfäll according to mass balance, meaning the loss of rock mass volume in the upper area of the landslide (area A in Figure 39) and the volume increase in the lower regions (area B in Figure 39). In the ideal case area A equals area B or is somewhat smaller due to the disintegration of the moved rock mass. Different information was consulted and assumptions were made to derive the pre-failure landscape surface:

- The pre-failure surface depends on the course of the Paznaun valley which in turn was influenced by the landslide Kopfwald/Glitt (chapter 1.4.2.3.) located on the western side of the valley between the locality See and the southern border of the landslide Gfäll (Figure 38). It was assumed that the landslide Kopfwald/Glitt deflected the river Trisanna to the southeast, whereas the landslide Gfäll deflected it approximately to the west and from this the contour lines (for 1100, 1200 and 1300 m on both sides of the valley) were drawn for the pre-failure stage of the two landslides (green lines in Figure 38).
- The width of the Paznaun valley at the locality See (1056 m a.s.l.) is approximately 300 m. From See to the southwest the valley gets somewhat narrower again, but still features a width of ~200 m at the valley bottom. Therefore, also for the section of the landslide Gfäll the pre-failure width of the Paznaun valley at its bottom was supposed to be 200 m.
- For the estimation of the depth and overdeepening of the Paznaun valley respectively, results from the borings on the northwestern edge of the study area, which were drilled during the preliminary investigations for the construction of the new bridge Gfäll (chapter 1.5.2.), and from geophysical measurements west of the town Landeck could be consulted. The borings indicate that the intact rock is situated at least more than 30 m deeper than today's surface and that also the river bed of the river Trisanna was deeper than today (HENZINGER, 2005). The geophysical

measurements give an overdeepening of the Stanzer valley west of Landeck of approximately 100 m related to today's surface (POSCHER, 1993). From these two values it can be derived that the pre-failure valley bottom of the Paznaun valley in the section of the landslide Gfäll must have been 30 m to max. 100 m deeper than today. Since the overdeepening west of Landeck results from the confluence of the Paznaun valley glacier with the Stanzer valley glacier, it is supposed that the overdeepening in the Paznaun valley, which was only caused by one glacier, is significantly lower and was therefore assumed with ~50 m (Figure 39).

- The location of a glacial shoulder in the study area is hard to determine, since most of the old landscape surface was changed by the landslide. According to GRUBER et al. (2010) the Paznaun valley was covered with ice up to 2000-2300 m a.s.l. during the Würmian maximum (Figure 39), but they don't state elevations of glacial shoulders either. On the opposite (western) side of the Paznaun valley, though, a glacial shoulder can be seen at ~1300 m and southwest of the locality See glacial shoulders can be seen at ~1400 m (Figure 38). These shoulders probably belong to a later glacial advance than the Würmian, but seem suitable for the area of the landslide Gfäll since they are located at an elevation between its headscarp (at ~1900 m) and its toe (at ~900 m).

From the above mentioned assumptions a pre-failure slope orientation of 290° (WNW) was received from the drawn contour lines. The inclination of the slope in its lower, oversteepened part was assumed with 45° (Figure 39). If the valley was assumed to have been steeper, it must have been broader than 200 m (which seems unlikely) or there would have been a flatter area in the upper slope region which, however, could not be observed on any side of the valley.

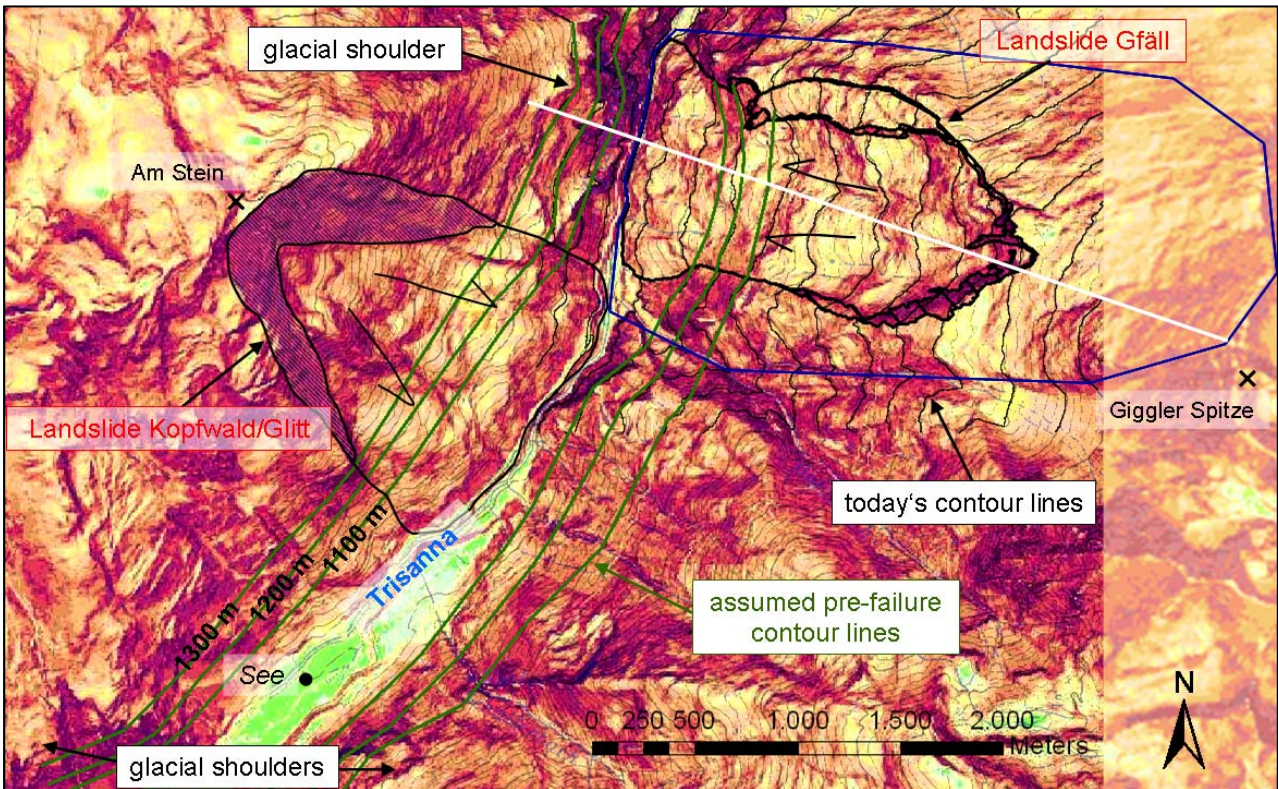


Figure 38: Slope inclination display with dark colours representing steep areas and light colours representing flatter parts (from TIRIS, 2013) showing the landslides Kopfwald/Glitt and Gfäll (blue frame: study area). The black contour lines were calculated from laserscan data (ATLR, 2013) using ArcMap® and represent today's contour lines. The green contour lines were drawn for an elevation of 1100, 1200 and 1300 m and result from the made assumptions concerning the course, depth and width of the Paznaun valley. The white line gives the location of the cross section of Figure 39.

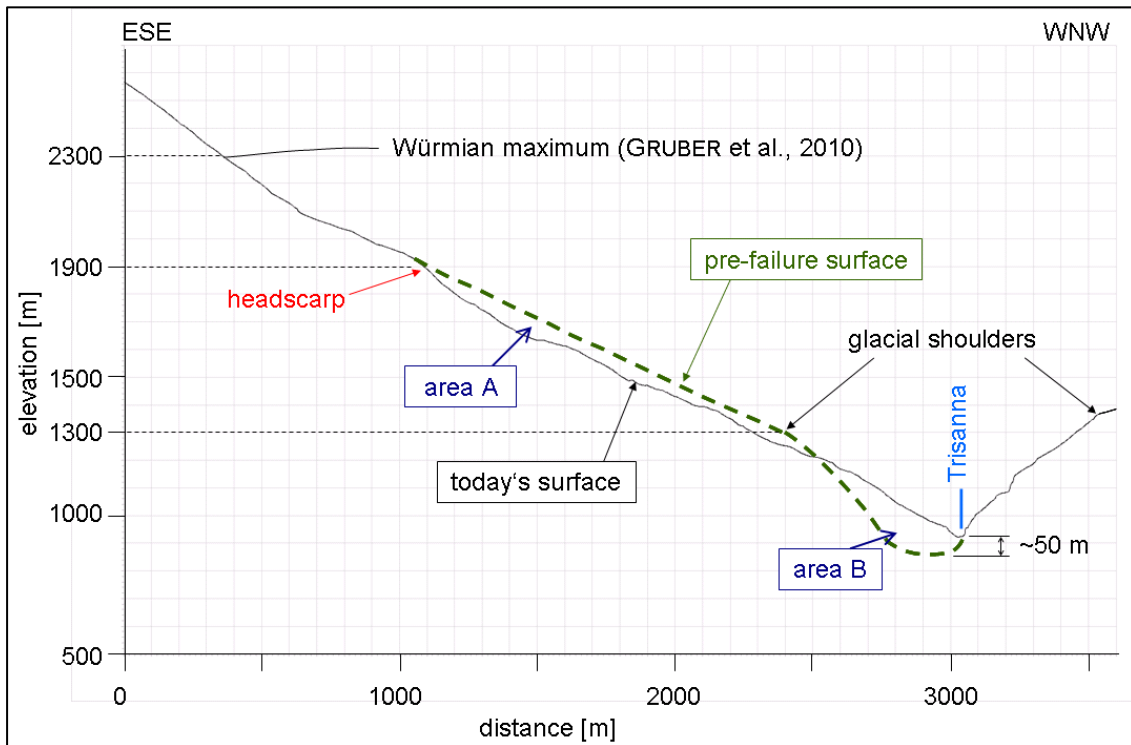


Figure 39: Cross section through the study area showing today's surface as well as the constructed pre-failure surface (green). Area A features mass loss, area B mass increase. The overdeepening in the section of the landslide Gfäll is assumed to be approximately 50 m. The glacial shoulder on the western side of the valley is located at ~1300 m, which was transferred also to the eastern side. The location of the cross section is shown as white line in Figure 38.

A further step of desk study was the **evaluation of lineaments**. A distinction between lineaments outside the landslide (red in Figure 40) and lineaments within the deposited mass (blue in Figure 40) was made. The lineaments outside the landslide Gfäll were determined in the south and the north in excess of the study area. The lineaments outside the landslide in large part represent the geomorphic features described in chapter 3.2.3. (chutes, obsequent and normal breaks in slope and scarps) and also correlate with the structural data (chapter 3.1.3.). Three main directions of lineaments occur:

- Approximately E-W bearing lineaments that seem to represent the schistosity and possibly joint set j5.
- NNE-SSW to NE-SW bearing lineaments that may represent the joint sets j1 and j3.
- NNW-SSE to WNW-ESE bearing lineaments that may represent the joint sets j2 and j4.

The lineaments within the deposited mass of the landslide mainly feature WNW-ESE and NE-SW to ENE-WSW bearing. Only some of them may represent the original rock structure, e.g. near the headscarp in the northeast of the landslide, but also in the lower region of the landslide in the west.

The others probably depict the direction of movement.

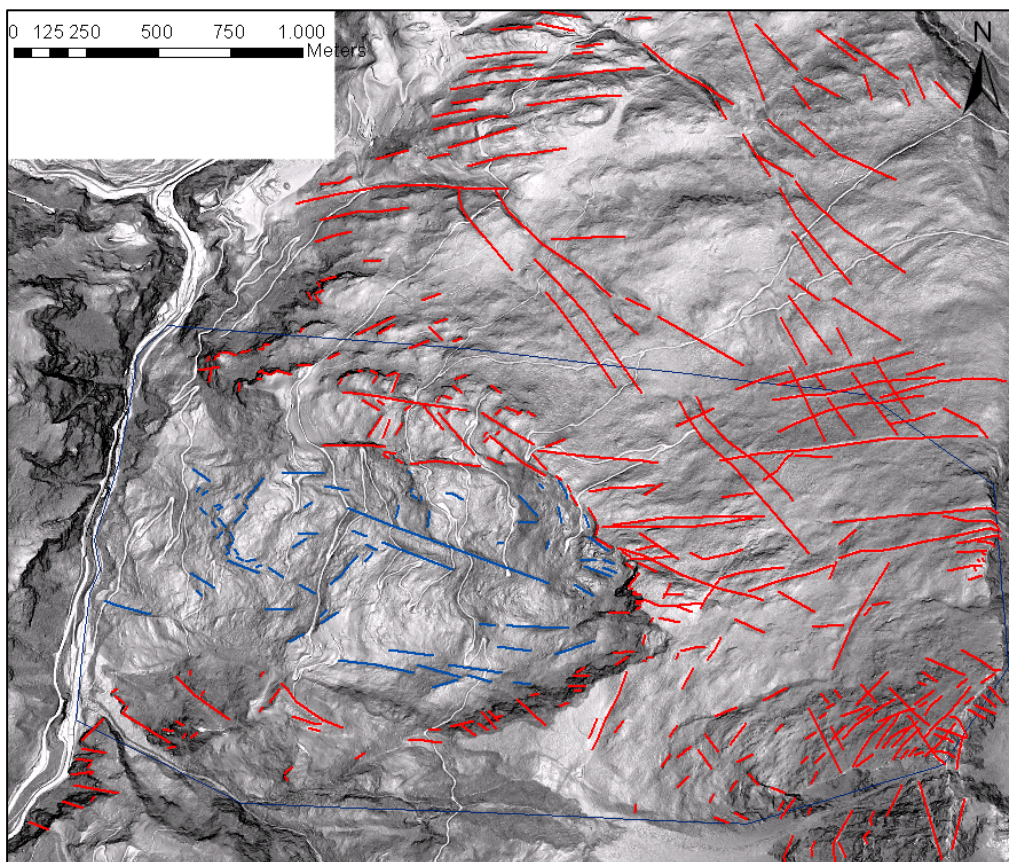


Figure 40: Slope inclination display showing the lineaments outside the landslide Gfäll (red) and within the deposited mass (blue). The lineaments outside the landslide are also drawn to the south and the north in excess of the study area (blue frame).

4.2. Observations and results from field work

Besides the already described site conditions (chapter 3.) like the different lithologies, structural data including the joint sets and their properties as well as geomorphic features, further observations regarding the landslide Gfäll were made in the field. They concern especially the location of the borders of the landslide and possible subdivisions of the deposited mass and shall be specified in this chapter.

The **headscarp** of the landslide Gfäll is not formed by a single plane that dips toward the west, but consists of at least two repeating planes. At the highest point of the headscarp in the east of the landslide the joint sets j2 (dipping to the southwest) and j3 (dipping to the northwest) together with the south dipping schistosity are involved (Figure 41). Behind the headscarp in the northeast open fractures were observed parallel to joint set j1 (Figure 42a). In the north of the landslide two nearly vertical rock walls were mapped as scarps (chapter 3.2.3.). At the southern one of them also open fractures along joint set j1 and along the schistosity, which in this region is nearly vertical due to folding, were observed with apertures normal to the joint planes of 5 to 20 cm (Figure 42b and c).

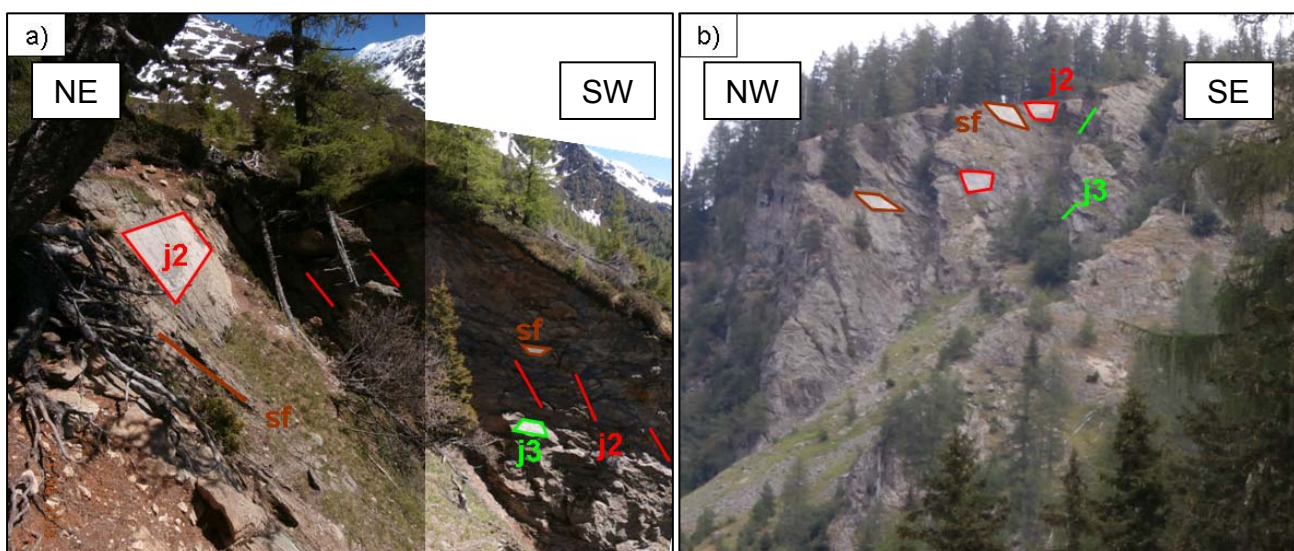


Figure 41: Headscarp at its highest point in the east of the landslide with the joint sets j2 (red) and j3 (green) and the schistosity (brown). a) View toward southeast, b) view toward northeast.

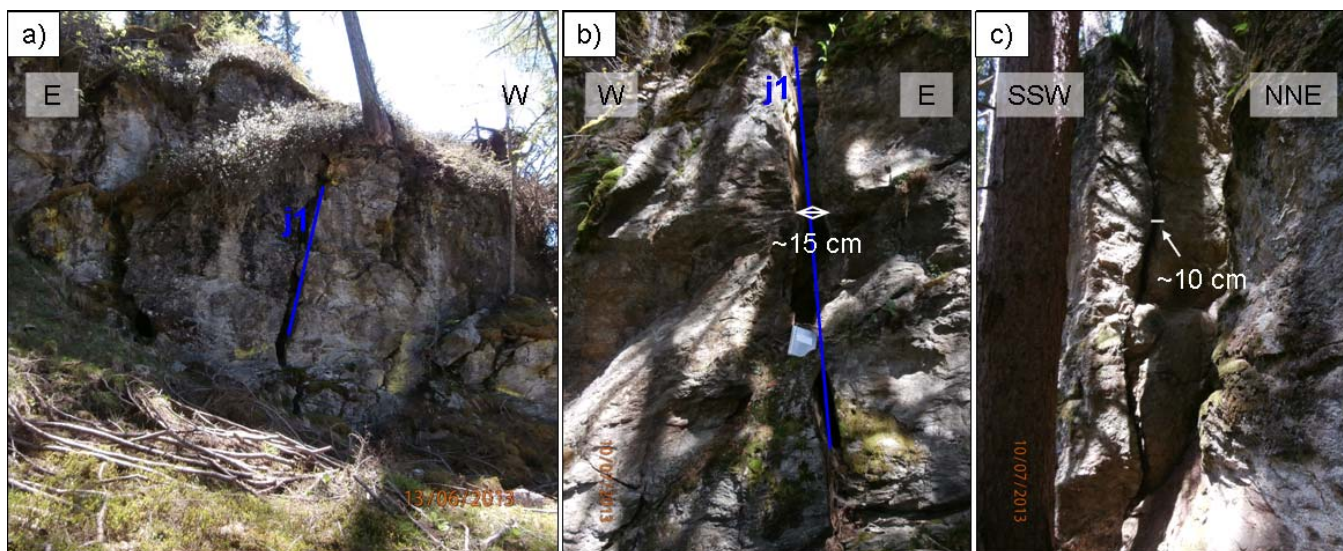


Figure 42: a) Behind the headscarp in the northeast joint set j1 features open fractures; b) Open joint of joint set j1 at the northern border of the landslide; c) Open fracture approximately parallel to the schistosity, which at the northern border of the landslide is very steep due to folding.

Indicators for movements or relative movements are stressed roots and fractures in ground. They could be found in the southwestern and western part of the study area within the landslide mass and in some cases they were not yet covered with a lot of leaves or needles indicating an age of less than one or two years (Figure 43). In this area the trees don't grow vertically but stand inclined in different directions ("drunken forest"; Figure 44a). At the scarps down to the river Trisanna, which are located at the toe of the landslide Gfäll in the west, tumbled trees can be found and further trees growing directly above the scarp are in danger to tumble (Figure 44b).

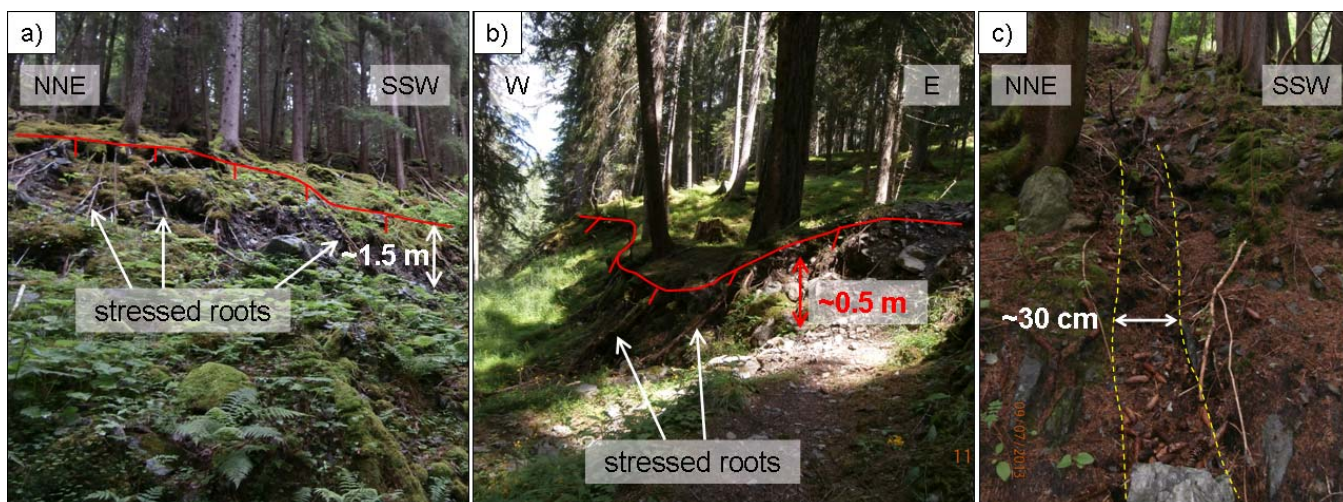


Figure 43: Examples of small escarpments (red lines) with stressed roots (a and b) and a ~30 cm wide fracture (yellow lines) in the ground surface (c) in the southwestern and western part of the study area within the deposited landslide mass.

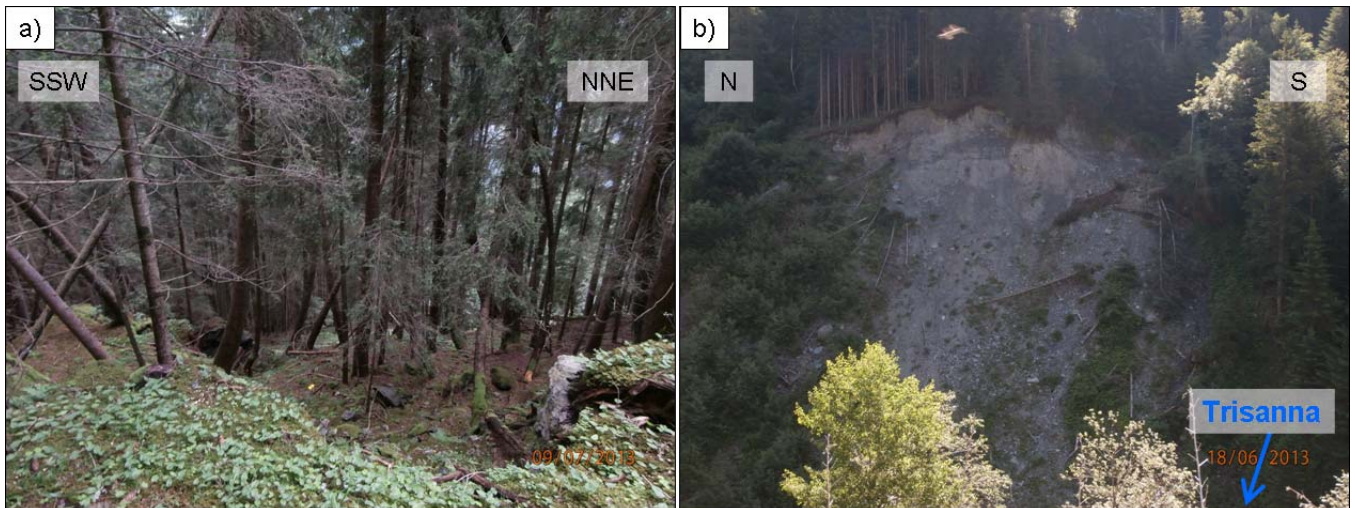


Figure 44: a) Oblique trees inclined in different directions („drunken forest“); b) Tumbled trees at the scarp down to the river Trisanna in the west.

The streets in the area of the landslide and stone walls beside them also feature signs of movements and have to be regularly renewed. In the road that was built as temporary road into the Paznaun valley in 2005 fractures and also bulges were observed in the asphalt at restricted points indicating differential movements (Figure 45a). The road to Schweißgut is not asphalted in a section of approximately 100 m in the north of the settling and shows a vertical displacement of ~1 m (Figure 45b). At Schweißgut in the area of the southern landslide boundary the stone wall beside the road was deformed on a length of approximately 15 m showing ~1 m of horizontal displacement (Figure 46a) and features open fractures along which the upper half was displaced ~2-3 cm downhill (Figure 46b). The asphalt road there shows a displacement approximately toward northwest with a vertical offset of ~0.5 m and the stone wall beside it also features a fracture but in vertical manner (Figure 47). However, at the houses of the human settlements that are located in the area of the landslide no fissures in the plaster or fractures in the walls could be observed.

The locations of the described fractures and settlements and of the escarpments with stressed roots were consulted to define areas with differential movements, i.e. smaller landslides within the landslide Gfäll that probably are still active (cp. geologic map in Appendix 1). Three of such slides were distinguished in the lower parts of the study area, west of the settling Schweißgut. The escarpments down to the river Trisanna were not considered as slides themselves, but as scarps resulting from the river erosion at the toe of the deposited landslide mass.

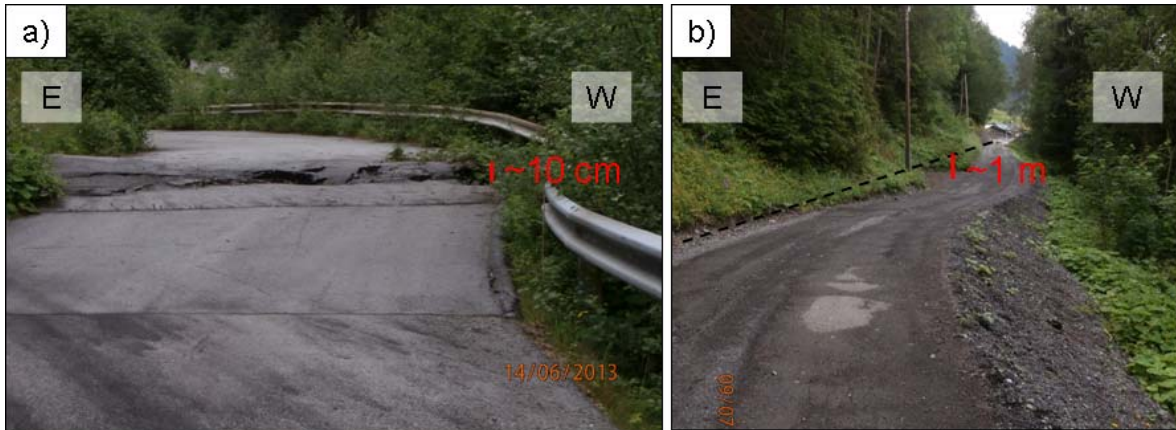


Figure 45: a) Bulge with fractures in the asphalt road (temporary road into the Paznaun valley) in the southwest of the landslide Gfäll; b) Road to Schweißgut that is not asphalted at this section and features ~1 m of vertical displacement.

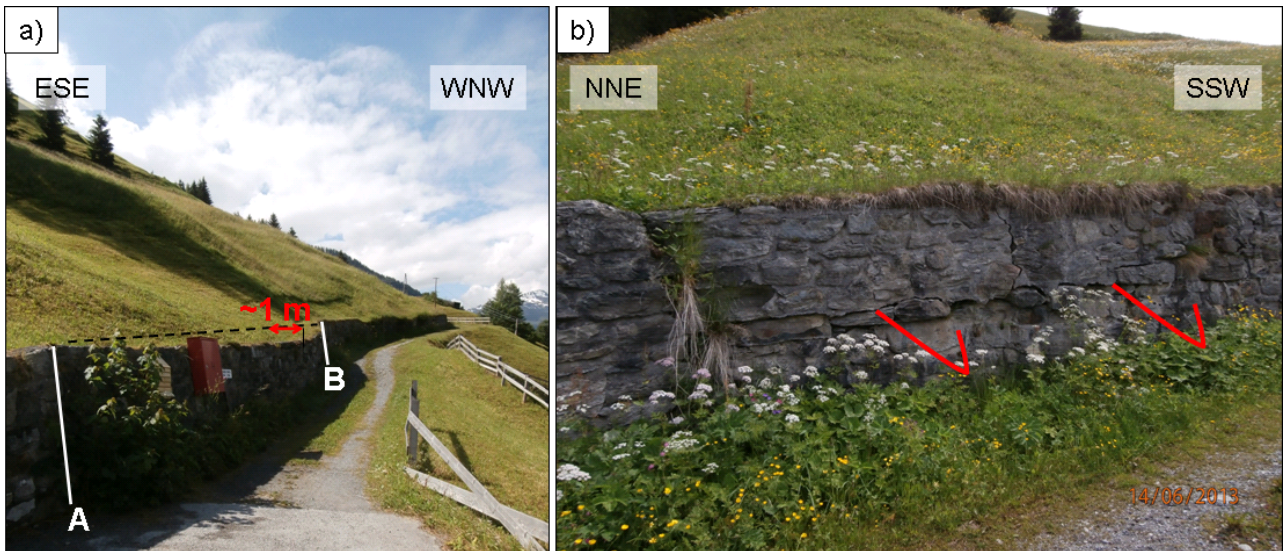


Figure 46: Stone wall on the eastern side of the road that leads from Schweißgut toward Hintergiggel in the south: a) Bulge from line A to line B with a horizontal displacement of ~1 m; b) Fractures in the stone wall along which the upper part was displaced downhill.

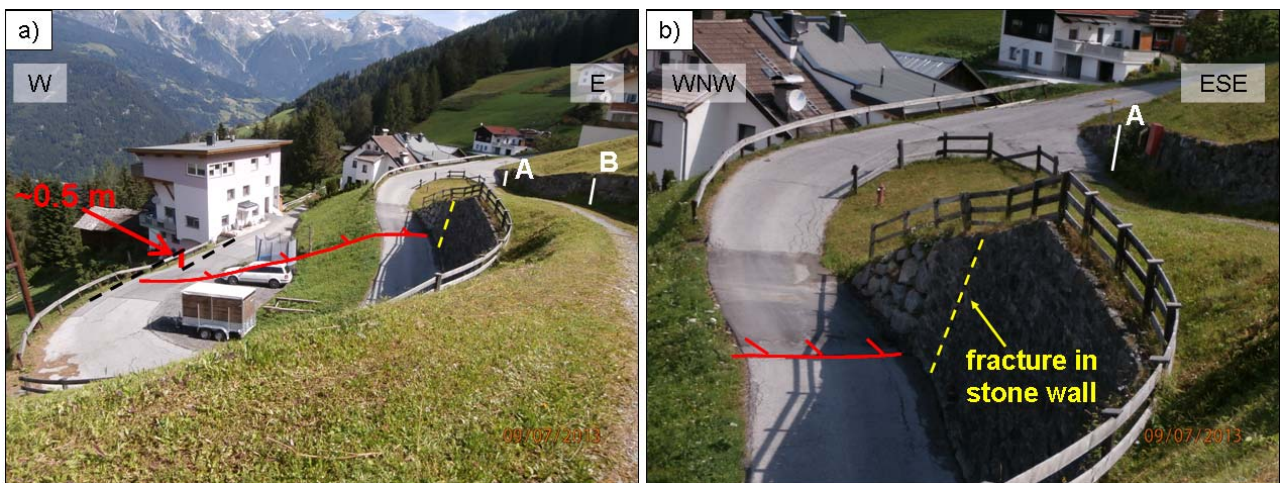


Figure 47: Displacement of the road at Schweißgut with the red lines showing the supposed location where the offset (approximately to the northwest) occurred or still occurs. The yellow lines represent a vertical fracture in the stone wall. The white lines A and B have the same positions as in Figure 46.

4.3. Laboratory testing

4.3.1. Performed tests

The field observations allow the suggestion that the failure of the landslide Gfäll involves the schistosity and one or more joint sets. The sampling of blocks, however, where the joint planes could be tested requires a lot of effort and was additionally expected to be complicated to nearly infeasible without the appropriate machines in the phyllonitic micaschists and also the dark grey to green paragneisses, which built up most of the landslide area. Therefore, it was decided to perform **direct shear tests** along foliation planes to get at least some reference values for the shear strength from the study area that can then be compared to testing results of previous investigations or similar rock types respectively. Table 13 gives the six tested samples, the lithologic unit to which they belong, the exact locations where they were taken, and if they were mounted as intact samples (in one piece) or split along a foliation plane prior to mounting. The sample 12/13 was selected from the drill core of boring KB-ZL8-03 (ASFINAG, 2012b) reaching from 17.35 m to 17.47 m depth. The other samples where collected from outcrops (chapter 2.2.2.).

Table 13: Samples for direct shear tests with their lithology and the coordinates of the sampling position. Five samples were mounted as intact blocks, one was primarily split along the schistosity (sf) into two parts.

Sample number	Lithology	Coordinates		Sample mounting
		x	y	
12/13	Phyllonitic micaschist (8)	15868	222475	intact
18/13k	Phyllonitic micaschist (8)	14625	221149	intact
22/13k	Phyllonitic micaschist (8)	13710	221265	intact
25/13s	Phyllonitic micaschist (8)	12555	218940	intact
32/13s	Paragneiss, dark grey, green (9)	12984	219274	intact
36/13s	Paragneiss, dark grey, green (9)	12984	219274	fracture along sf

On two drill core samples from the borings KB-ZL8-02 and KB-ZL8-04 (ASFINAG, 2012b) **triaxial compression tests** were performed to get reference values for the rock too, because they are often needed as input parameters in slope stability software. Table 14 shows the information about the borings and the depth from which the samples were gained, and gives the dimensions and the weight of the samples.

Table 14: Samples for triaxial compression tests with their lithology, the coordinates and the number of the boring from which they were taken as well as the corresponding depth, their diameter, length and weight.

Sample number	Lithology	Coordinates		Boring	Depth of sample [m]	Sample dimensions		Weight [g]
		x	y			Diameter [mm]	Length [mm]	
02/13	Phyllonitic micaschist (8)	15820	222423	KB-ZL8-04	39.8 - 39.97	51.51	98.21	567.1
08/13	Phyllonitic micaschist (8)	15886	222508	KB-ZL8-02	18.4 - 18.5	51.49	103.72	584.0

4.3.2. Results of laboratory tests and comparison to previous investigations

The results of the **direct shear tests** are summarized in Table 15. The friction angles (φ) vary between 24.1° and 29.1°, the residual friction angles (φ_{res}) between 22.9° and 24.5° for the phyllonitic micaschists. The dark grey to green paragneisses feature friction angles of 34° and 49.5° and residual friction angles of 24.6° and 29°. The cohesion (c) ranges for both lithologic units from 0.1 MPa to 0.81 MPa; residual cohesion c_{res} did not occur. The results from sample 25/13s (red in Table 15) were not considered, because the developed shear surface was not entirely located within the 2 cm gap between the shear boxes and hence probably produced falsified values. The joint roughness coefficient (JRC) of the shear surfaces ranges from 4 to 10 (12 only for sample 25/13s), but it can be said that the sheared surfaces are generally smooth and in most cases undulating. Pictures of the samples as well as the stress diagrams of the tests are attached in Appendix 6.

Compared to testing results in the literature the obtained shear strength parameters of the present study don't show major differences. BUTTON (2004) gives friction angles of 25° to 28° and cohesion values of 0.4 to 0.6 for direct shear tests along foliation planes of the "Landeck quartzphyllite" (*Venet complex*). ENGL et al. (2008) provide results of direct shear tests along joints parallel to the foliation of different phyllites, giving friction angles of 24.2° to 29.9° and cohesion values of 0.14 to 0.38 MPa.

Table 15: Results from direct shear tests: Properties of the developed shear plane (area, joint roughness coefficient and verbal roughness description) as well as friction angle φ and residual friction angle φ_{res} , cohesion c and residual cohesion c_{res} , dilation angle i , maximum shear stress τ_{max} and the shear path s at τ_{max} . The developed shear plane of sample 25/13s (red) was not entirely located within the 2 cm gap between the shear boxes and hence probably produced falsified values.

Sample number	Cross section area	JRC	Description of joint roughness	φ	φ_{res}	c	c_{res}	i	τ_{max}	$s(\tau_{max})$
	[cm ²]			[°]	[°]	[MPa]	[MPa]	[°]	[MPa]	[mm]
12/13	84.1	8	stepped - smooth	24.6	22.9	0.16	0	12.4	1.17	3.27
18/13k	250.4	4	planar - smooth	29.1	24.5	0.68	0	22.9	1.98	2.57
22/13k	193.5	6	undulating - smooth	24.1	23.7	0.23	0	15.4	0.73	0.93
25/13s	237.9	12	undulating - rough	39.7	26.2	2	0	36.3	3.84	0.35
32/13s	265.7	8	undulating - smooth	34	29	0.1	0	16	0.59	4.21
36/13s	206.3	10	undulating - rough	49.5	24.6	0.81	0	21.5	2.14	4.71

The results of the **triaxial compression tests** are shown in Table 16. The uniaxial compressive strength (UCS) reached 25.52 MPa and 31.15 MPa respectively. The Mohr-Coulomb criterion is given with friction angles of the rock of 36.31° and 41.62° and cohesion values of 7.08 MPa and 7.92 MPa. Pictures of the samples as well as the stress diagrams of the tests are also attached in Appendix 6.

The friction angles obtained from triaxial tests on samples of the “Landeck quartzphyllite” given by BUTTON (2004) are in the same range (32° to 44°), the cohesion values are somewhat lower (3.5 to 5.4 MPa). ASFINAG (2012a) only give a range for the uniaxial compressive strength of 5-50 MPa for both phyllonitic micaschists and schistose gneisses of the *Venet complex*. Thus, also the results of the triaxial compression tests are similar to them of previous investigations.

Table 16: Results from triaxial compression tests: Uniaxial compressive strength (UCS), the material constant m_i and the tensile strength σ_{tens} , cohesion c and friction angle φ , E- and V-modulus and the Poisson's ratio.

Sample number	Hoek-Brown			Mohr-Coulomb		Elastic parameters		
	UCS	m_i	σ_{tens}	c	φ	E-Modulus	V-Modulus	Poisson's ratio
	[MPa]		[MPa]	[MPa]	[°]	[GPa]	[GPa]	
02/13	25.52	10.22	-2.47	7.08	36.31	20.17	13.98	0.01
08/13	31.15	14.5	-2.14	7.92	41.62	29.43	17.73	0

4.4. Slope stability evaluation

To evaluate the mode of failure of the landslide Gfäll and the involved landslide processes and to support the theories that were made based on field observations and structural measurements, kinematic analyses and stability analyses were performed. From the desk study of the laserscan data and from field investigation it is known that the headscarp of the landslide Gfäll is not formed by one single plane, but involves at least two repeating discontinuity sets (chapter 4.2.). The structural measurements at ten selected outcrops (Appendix 3) revealed five different joint sets occurring in the study area in addition to the schistosity (chapter 3.1.3.). The orientation of the joint sets and the schistosity would seem to allow wedge sliding, which is why in a first step analyses involving these discontinuities were performed to see if wedge sliding was kinematically admissible. Only after that, the mode and stability analyses were carried out developing a model of the landslide's subsurface that was progressively adapted with the gain of knowledge.

4.4.1. Block Theory Analyses

For the **kinematic analysis** the problem of a deep-seated landslide was simplified using a block theory software (LIU, 2004) that usually is applied for key block analyses of outcrops or tunnel excavations. Nevertheless, the analysis was carried out for the data of every of the ten selected outcrops (Appendix 3) with respect to an assumed slope of 290/45 (according to the reconstruction of the pre-failure surface in chapter 4.1.), because due to in some cases significant differences it didn't seem reasonable to put all the structural data together and analyse them as if it was one single excavation. Therefore, the average orientation of every discontinuity set was determined from a density plot for every outcrop (Table 17). The data were then tested on plane and wedge sliding, searching for planes that within the pre-failure slope might have formed removable blocks. The joint planes were plotted in a stereographic whole sphere projection from which the joint pyramids that form removable blocks could be determined. A second plot then gave the joint plane(s) along which the key blocks (type I blocks) or potential key blocks (type II blocks) would fail. Figure 48 shows the results for outcrop number 77 as an example. The plots for every of the ten outcrops are attached in Appendix 7. It could be seen that wedge sliding is kinematically admissible along several combinations of discontinuity sets, but most frequently the joint sets j3 and j5 and the schistosity are involved (Table 18). Plane sliding in most cases is kinematically not admissible. Only for a few measurement

values also plane sliding was given to be possible but usually the orientation of the joint plane then deviates from the general orientation (for example the schistosity in outcrop 34).

Table 17: Average orientation of the joint sets j1 to j5 and the schistosity (sf) at the ten selected outcrops (numbers 14 to 169) determined from density plots. At the outcrops 127 and 143 only the fold axes (FA) of the schistosity could be measured.

Outcrop number	j1	j2	j3	j4	j5	sf	FA
14	112/54	266/58	197/72	54/64		172/49	
23	107/56	290/40	344/88			200/37	
28			349/67	47/62		269/25	
34	139/84	223/83		50/78		256/19	
77	158/60	258/65	330/89		349/34	236/20	
121	116/50	253/53		49/82	3/50	188/38	
126	102/86	229/56	198/64			178/27	
127	108/59	289/65	191/74	66/32	342/24	-	270/18
143	119/73	250/46	177/80			-	266/224
169	292/85	241/59	345/71			184/32	

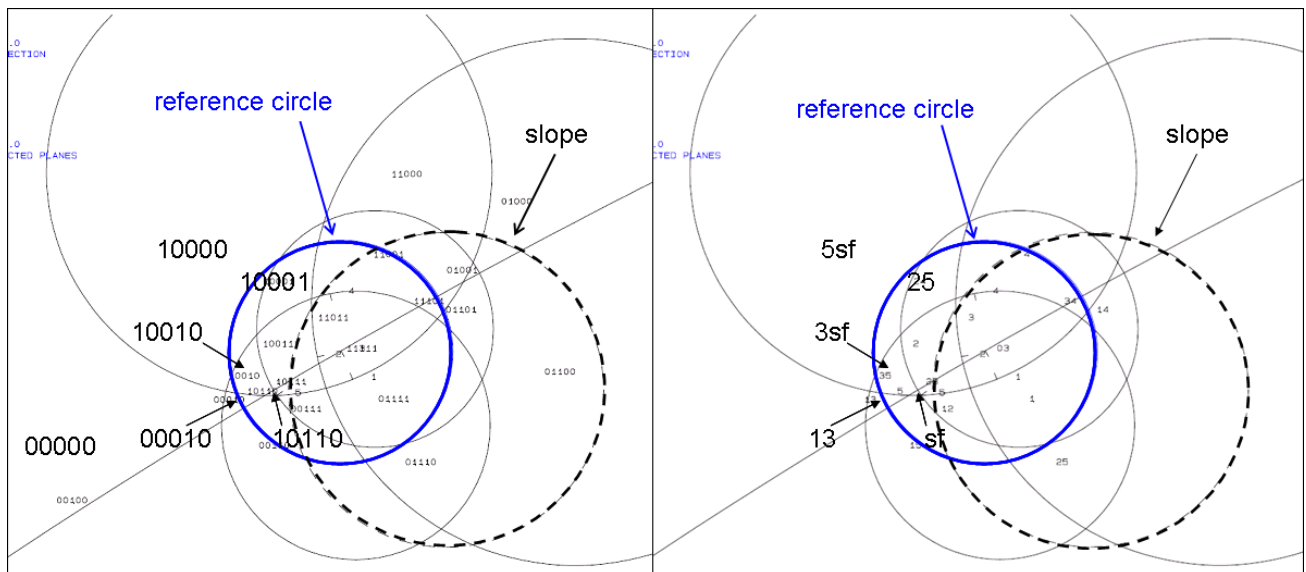


Figure 48: Whole sphere projection of the joint sets and the schistosity at outcrop 77. The blue circle is the reference circle; the black dotted circle represents the slope assumed with 290/45. The left plot shows the joint pyramids (JPs) and their codes with the six JPs of the removable blocks being labelled. The right plot gives the joint plane(s) along which the potential key blocks or key blocks would fail. In this example failure would occur along the intersection lines of j1 and j3 (13), j2 and j5 (25), j3 and j5 respectively with the schistosity (3sf and 5sf) and along the schistosity (sf) alone.

Table 18: Different combinations of discontinuities that could form removable blocks in a pre-failure slope of 290/45. Listed below them are the outcrop numbers in which these combinations occur producing removable blocks. At the outcrops 127 and 143 (blue) only the fold axes of the schistosity could be measured, which is why for the analysis an orientation of 180/35 was assumed for the schistosity since this is the average orientation in the study area. The combination of joint set j3 and j5 respectively with the schistosity occur most frequently (red frames). For outcrop 126 only safe removable blocks (type III blocks) were determined and therefore it is not contained in this table.

Disontinuites forming removable blocks	j1+j2	j1+j3	j2	j2+j3	j2+j4	j2+j5	j2+sf	j3+sf	j3+j5	j5+sf	sf
Outcrop numbers	127	77	23	23	14	77	34	23	127	77	34
					121	121		28		121	77
								77		127	
								143			
								169			

After wedge sliding was shown to be kinematically admissible a **mode analysis** was done to distinguish between type I blocks (featuring a positive sliding force) and type II blocks (featuring a negative sliding force). For an inserted friction angle of 30° most of the blocks turned out to be type II blocks (potential key blocks). The tables resulting from the mode analysis are given in Appendix 7.

As last step of the block theory analyses a **stability analysis** was done (using a block theory software modified by LIU & KIEFFER (2008)), which plots the contour lines of the friction angles corresponding to the joint plane(s) along which failure would occur. From the location of the resulting force vector R, which was assumed to be vertical, the friction angle (ϕ_M) that is required for failure to occur can be taken. This was done for every possible key block and potential key block of all ten outcrops showing that the required friction angle is generally very low (mostly between 0° and 15°). As an example the contour plot of the friction angle on the joint plane j3 and on the schistosity from outcrop 77 are shown in Figure 49. The other plots are attached in Appendix 7.

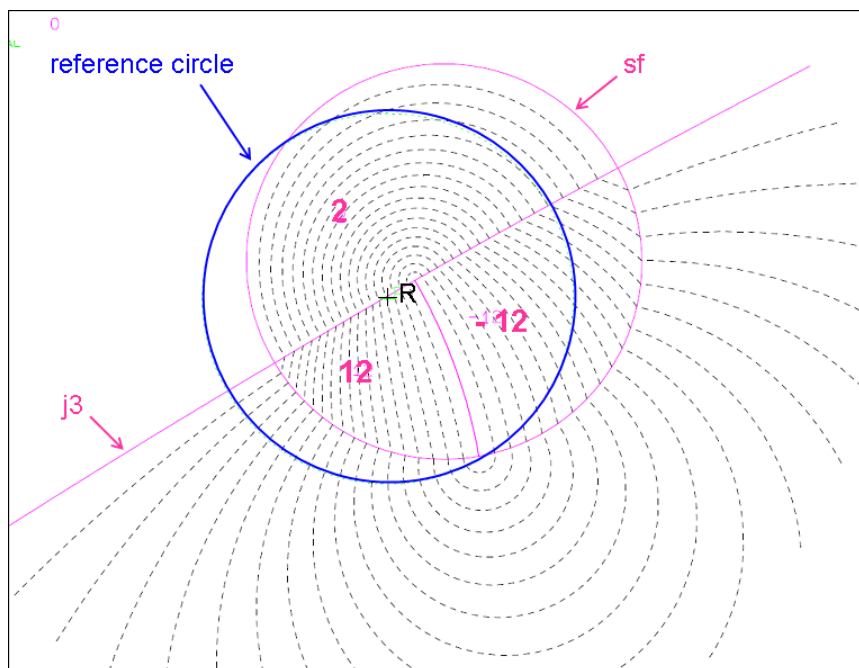


Figure 49: Contour plot of the friction angles for joint set j_3 ($= 1$) and the schistosity ($= 2$) at outcrop 77. The blue circle is the reference circle. R marks the resultant force vector, which in this case lies in the field “12” at a friction contour line of $\sim 18^\circ$, meaning that the block would slide down along the intersection line of plane 1 and plane 2 (here: j_3 and schistosity) if the friction angle on the planes was lower than 18° .

4.4.2. First subsurface model of the landslide

For stability analyses based on the geometry of the landslide a first model of the subsurface conditions of the landslide was needed, which was afterwards adapted corresponding to the progress of the analyses. Figure 50 shows the schematic cross section according to the reconstruction of the pre-failure surface and, since the joint sets j_3 and j_5 in combination with the schistosity form removable blocks according to the results of the mode analyses, the intersection lines of their average orientations were drawn as possible sliding directions in the cross section. The average orientations, however, produce very flatly plunging lines of intersection ($\hat{I}_{3sf} = 257/14$ and $\hat{I}_{5sf} = 269/6$). If the failure surface of the landslide was parallel to \hat{I}_{3sf} or \hat{I}_{5sf} like it is drawn in Figure 50, the landslide would feature a depth of 600-800 m in its upper part, which was supposed to be unlikely, and still would need a steeper second joint or line of intersection (red in Figure 50) that would lead from the headscarp to the sliding plane (green and yellow in Figure 50). Besides, very low friction angles of the material or very high water pressures within the slope would be required for failure to occur. Since this first subsurface model seems improbably to occur like this in nature it was not analysed further, but it was attempted to determine a more reasonable orientation and location of the failure plane. Therefore, not

only the intersection lines of the average joint orientations but all intersection lines of the ten outcrops were consulted to obtain the most unfavourable orientations (Figure 51, Table 19).

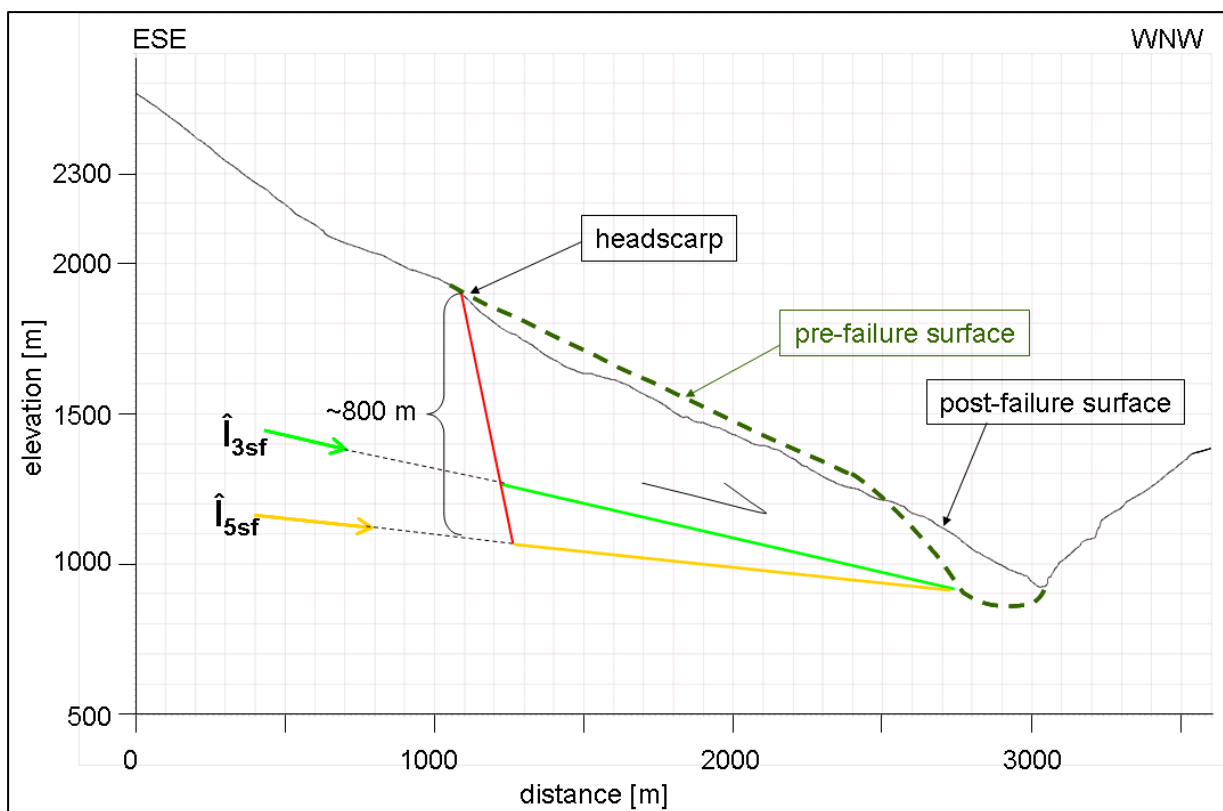


Figure 50: Schematic cross section through the study area showing the first attempt to produce the underground geometry of the landslide with the results from the block theory analyses. The green and yellow lines represent the directions of the lines of intersection of j_3 and j_5 respectively with the schistosity. The red line shows the required direction of a second plane or intersection line for failure to occur.

Table 19: Intersection lines resulting from all measured joint orientations of the ten selected outcrops that feature unfavourable orientations. Listed are their average orientations received from a density plot as well as the range of unfavourable orientations.

Intersections	Average orientation (density maximum)	Unfavourable orientations	
		from	to
\hat{i}_{3sf}	257/15	256/31	285/27
\hat{i}_{5sf}	270/15	270/19	322/17
\hat{i}_{23}	259/51		
\hat{i}_{45}	320/26	319/38	

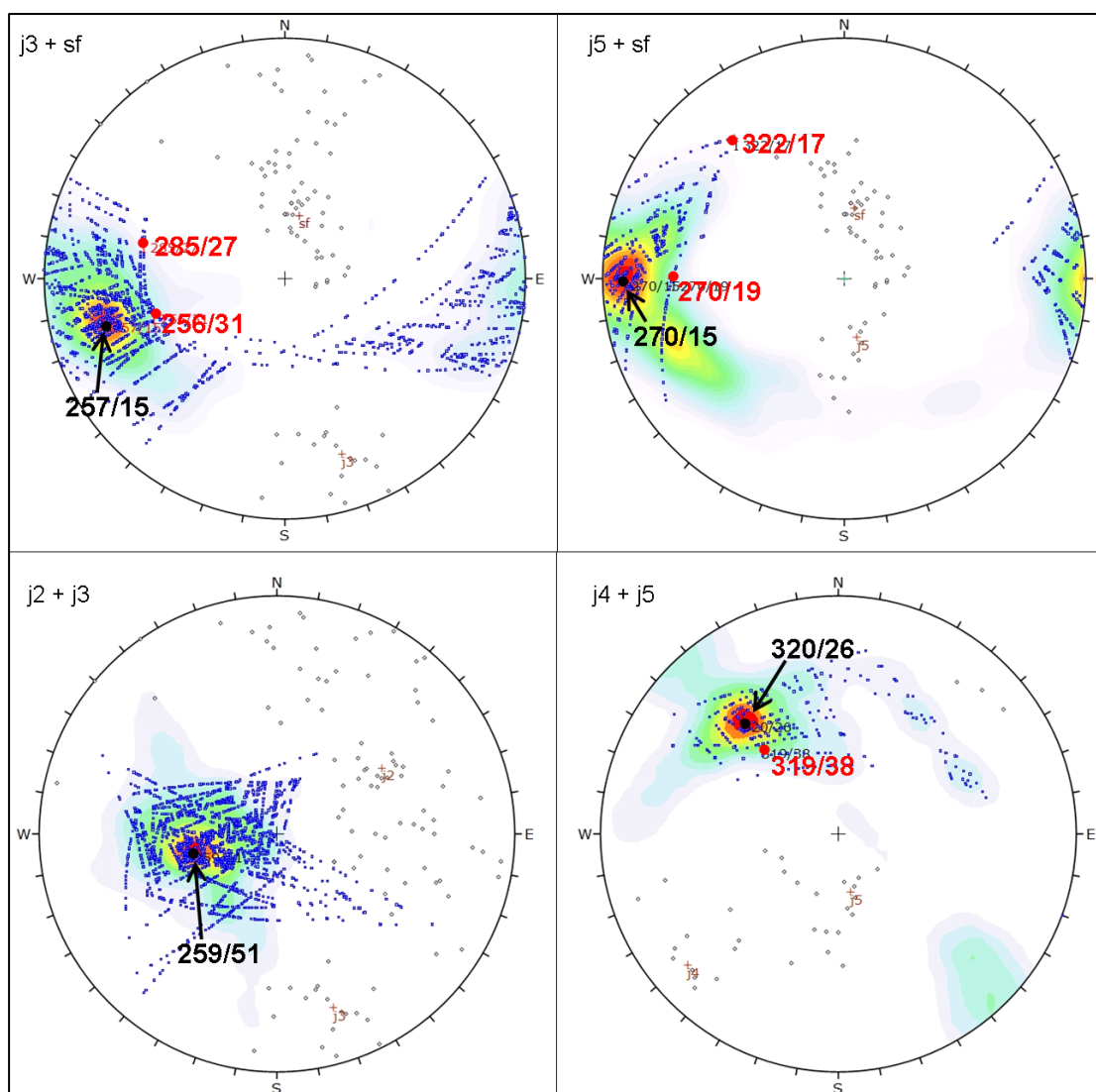


Figure 51: Intersection lines (blue points) of the joint sets j_3 and j_5 with the schistosity, j_2 with j_3 and j_4 with j_5 respectively resulting from all measurements at the ten selected outcrops. The average orientations (density maxima) are represented by the black points, the unfavourable orientations by the red points.

The unfavourable orientations of \hat{I}_{5sf} still plunge at low angles (up to 19°), which is why they were not considered in the further analyses. The intersection of j_3 with the schistosity produces steeper unfavourable plunges ($\sim 30^\circ$). \hat{I}_{45} is also inclined quite steeply ($26-38^\circ$) plunging to the northwest, but the joint sets j_4 and j_5 occur much less frequently than the others and therefore were assumed to be of minor importance. \hat{I}_{23} , which was not received from the block theory analyses because it does not daylight, features an orientation that would match the red line in Figure 50, just plunging at a lower angle of $\sim 50^\circ$. Since the joint sets j_2 and j_3 were also observed at the headscarp during field mapping this would seem reasonable. Figure 52 shows the adapted subsurface model with the unfavourable oriented intersection line \hat{I}_{3sf} (green) as possible basis of the landslide. \hat{I}_{3sf} was assumed with 285/27 because this is approximately the same dip direction as the pre-failure slope (290/45). The intersection

line $\hat{l}_{23} = 259/51$ is drawn as red line and is supposed to form the headscarp. The resulting depth of the landslide decreases to ~ 150 m if the unfavourable oriented \hat{l}_{3sf} is consulted.

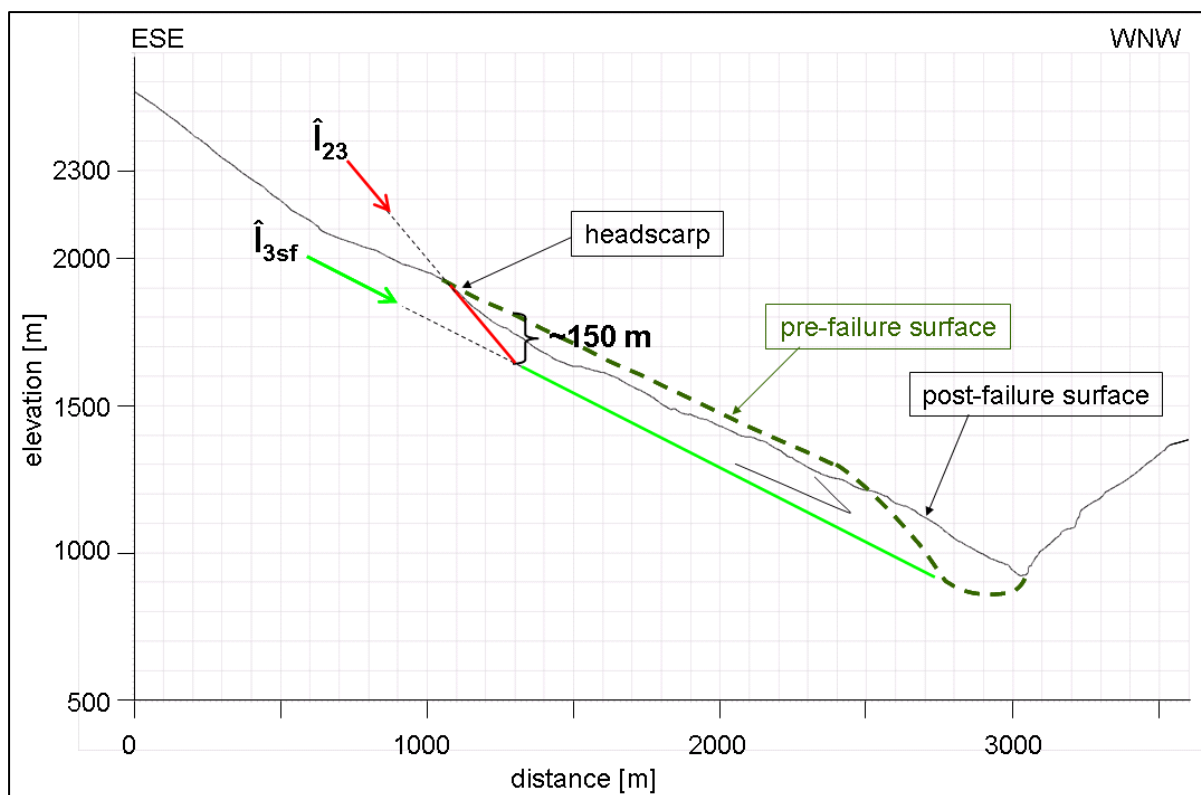


Figure 52: Adapted subsurface model with $\hat{l}_{3sf} = 285/27$ (green) as possible basis of the landslide. The red line represents $\hat{l}_{23} (= 259/51)$ which is supposed to form the headscarp.

4.4.3. Stability analyses using “Swedge”

The subsurface model shown in Figure 52 should be analysed with the software “Swedge 6.0” (ROCSOURCE, 2014a). The program gives the factor of safety for the defined wedge and facilitates a sensitivity analysis which shows the interaction and correlation of certain parameters. First of all, the unfavourable orientation of the line of intersection of joint set j3 and the schistosity had to be converted to the orientations of the corresponding joint planes because they are needed as input parameters. This was done with the program “Dips 6.0” (ROCSOURCE, 2012) by picking great circles that produce the required intersection lines. For $\hat{l}_{3sf} = 285/27$ the so obtained discontinuity orientations are 224/45 for the schistosity and 2/66 for j3. Since only two joint planes can be inserted, a tension crack was used instead of the joint sets j2 and j3, which are supposed to form the headscarp. The orientation of the tension crack was not inserted with the orientation of \hat{l}_{23} but was assumed with

~290/65 as the medium orientation of j_2 and j_3 . As orientation of the lower slope region 290/45 and for the upper slope face (above the bench) 290/25 was inserted according to the reconstruction of the pre-failure surface (cp. Figure 52). The slope height in "Swedge" is defined as vertical distance from the toe of the wedge to the bench. For the analyses of the present landslide the slope was not chosen as high as in Figure 52 where it is more than 400 m, but in such a way that the headscarp features a height of approximately 40 m because that matches the field observations. The wedge formed by j_3 combined with the schistosity was then analysed regarding its stability (Figure 53). In dry state (without water acting on the planes) the wedge is at its limit equilibrium state ($FS = 1$) if the friction angle is 17.7° ($\approx 18^\circ$) and the cohesion is 0.

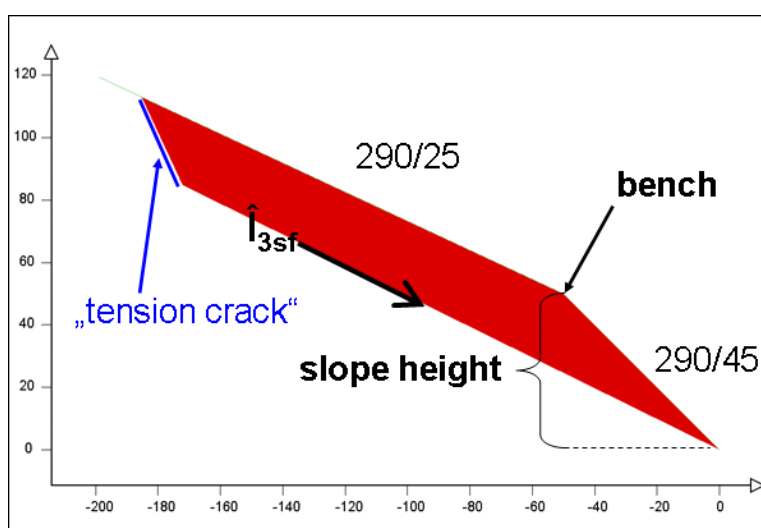


Figure 53: Wedge that was constructed according to the results of the block theory analyses and the afterwards made assumptions and inserted into "Swedge". It shows the intersection line of j_3 and the schistosity (sf) since they are supposed to produce the wedge as well as the assumed slope orientation and inclination according to the reconstruction of the pre-failure surface, the slope height, which was defined with 50 m resulting in a headscarp height of ~40 m, and the inserted tension crack that was used instead of a headscarp orientation.

The sensitivity analysis was performed to determine the correlation between the friction angle of the joint planes and the water pressure acting on them, i.e. to see how much water would be needed for failure, if the friction angle was higher than 18° . Two different models for inserting the water pressure were applied. One produces the highest water pressure at the bottom of the tension crack (*tension crack model*) and gives the water pressure as the percentage to which the tension crack is filled with water (% filled tension crack). The second model produces the highest water pressure at the toe of the slope (*toe peak model*) and gives it as percentage to which the slope height is filled with water (% filled slope height). For the sensitivity analyses the cohesion was assumed to be 0. The friction angle and the water pressure were changed in such a way that the factor of safety stayed equal to 1 (limit

equilibrium state). Figure 54 shows the sensitivity plot for the *tension crack model*. Figure 55 shows the sensitivity plot where the friction angle is plotted against the percentage of the slope height to which it is filled with water (*toe peak model*). The differences between the two models result especially from the different heights of slope and tension crack. It can be seen that the water pressures can't be increased to cause failure for very high friction angles of the joint planes, because for friction angles greater than $\sim 25^\circ$ (with the *tension crack model*) and probably greater than 35° (with the *toe peak model*) the slope would be completely filled with water. Reasonable friction angles of the joint planes resulting from the sensitivity analysis using "Swedge" are interpreted to range from 18° to 20° . For a friction angle of 20° average water pressures on the joint planes are given with 0.03 MPa (0.3 bar) and on the tension crack with 0.002 MPa (0.02 bar) for the *toe peak model*.

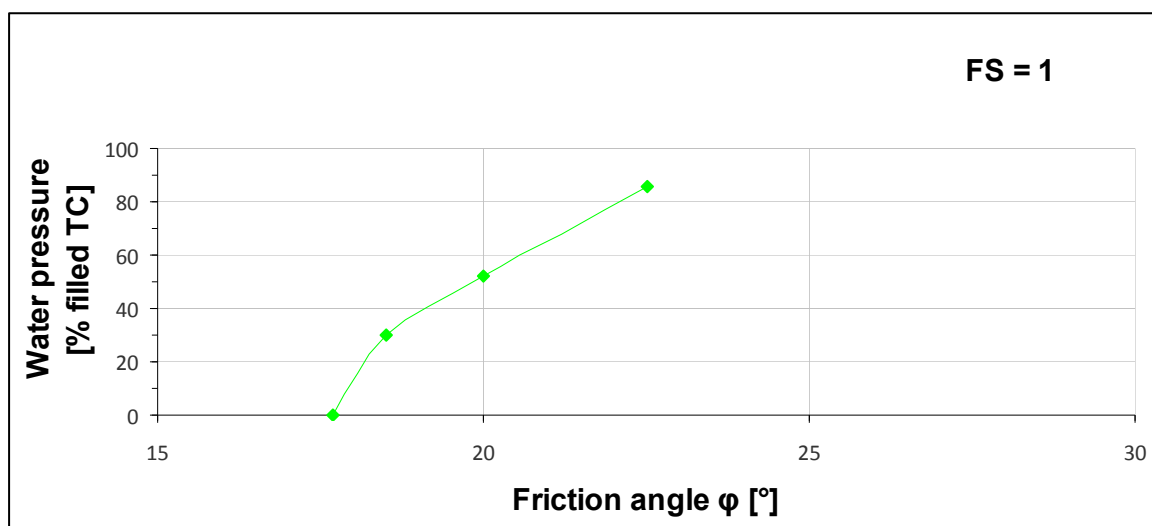


Figure 54: Sensitivity plot showing the friction angle with respect to the percentage the tension crack (TC) is filled with water.

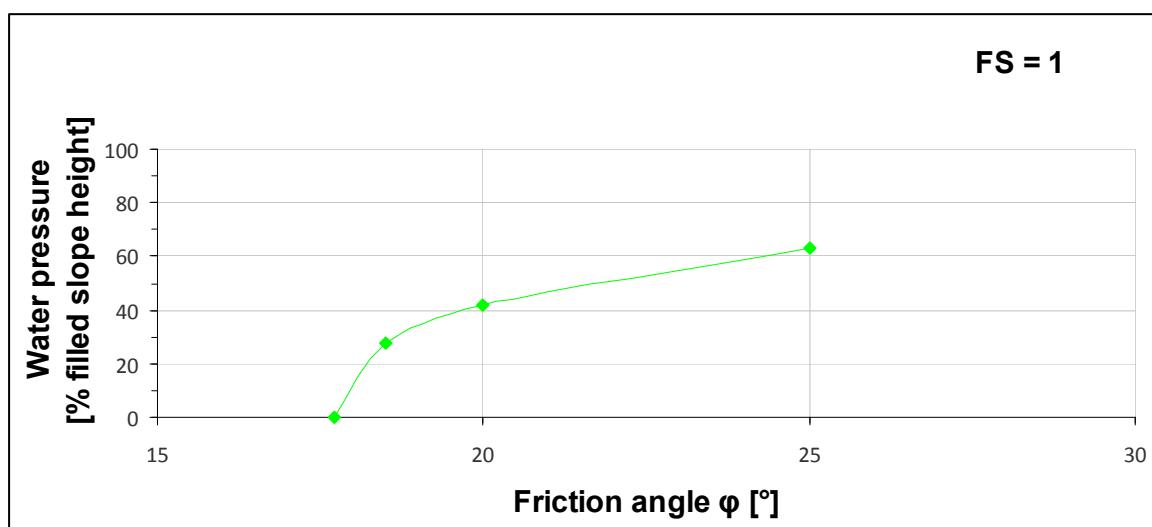


Figure 55: Sensitivity plot showing the friction angle with respect to the percentage of the slope height to which it is filled with water.

4.4.4. Stability analyses using “Slide”

In “Swedge” the entire landslide was analysed as one wedge, which however seems unlikely for a landslide of the dimensions like Gfäll because that would require two major discontinuity planes that persist over hundreds of meters. Therefore, the subsurface model was again changed, assuming the failure of blocks along a stepped failure surface that is formed by \hat{I}_{23} and \hat{I}_{3sf} (Figure 56). These steps, however, are supposed to get sheared off during the movement of the landslide and to develop a discrete shear zone (Figure 57). The landslide mass is assumed to disintegrate due to increased fracture development behaving more like a soil-type material.

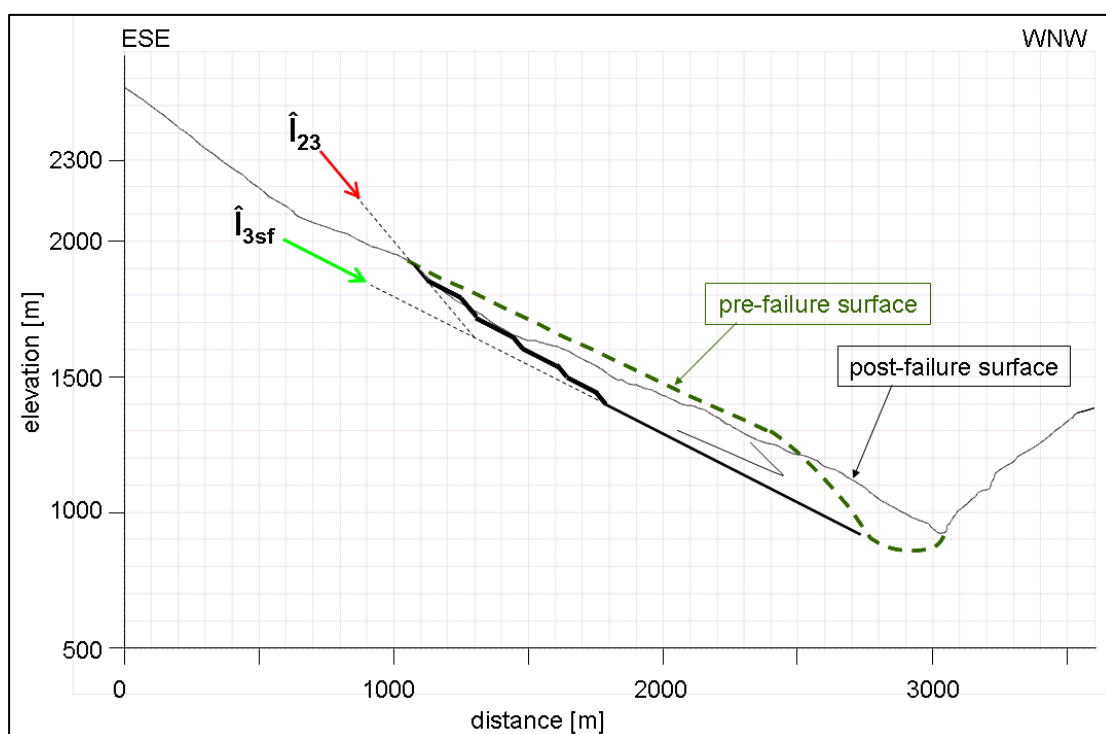


Figure 56: Subsurface model showing a stepped failure surface formed by \hat{I}_{23} and \hat{I}_{3sf} .

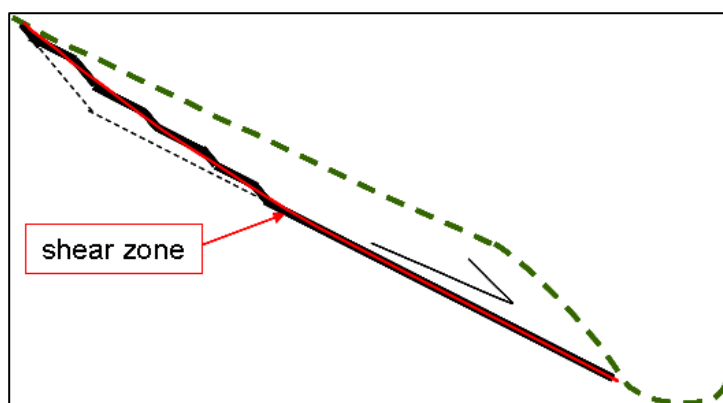


Figure 57: Discrete sliding surface (shear zone) in red after the initial steps (black) have been sheared off.

The software “Slide 6.0” (ROSCIENCE, 2010), which is usually applied for soils, was used to analyse the above shown shear zone, since sheared rock material behaves more like a soil. As input data the geologic cross section was needed and the parameters of the three different rock types (phyllonitic micaschists, dark grey to green paragneisses and shear zone material) had to be specified (Table 20). Cohesion and friction angle of the shear zone material were afterwards changed for the sensitivity analyses.

Table 20: Input parameters for the different rock types: unit weight, cohesion c and friction angle φ .

	Unit weight [kN/m ³]	c [kPa]	φ [°]
Paragneisses	27	1500	35
Phyllonitic micaschists	27	1000	25
Shear zone material	26	500	20

The stability analyses using “Slide” were performed for dry state, i.e. for the case of no water (or that the water table is located lower than the shear zone), and for four different locations of water tables within the slope (Figure 58) because the water table in the study area is not known and could not be derived from spring horizons. The water tables L1 and L2 in Figure 58 are lower water tables, the water tables H1 and H2 represent higher water tables. If the boundary of the paragneisses to the phyllonitic micaschists is supposed to be also an important hydrogeologic boundary the water tables L1 or H1 are conducted. They would result in springs along this boundary that was supposed to be located at an elevation of ~1200 m of the pre-failure slope. The water tables L2 and H2 only depend on the level of the valley bottom and would lead to effusion of water there, either in the form of springs or by infiltration into valley sediments or into the river Trisanna respectively. For the different water tables stability and sensitivity analyses were carried out to get the factor of safety for the defined properties and to show the correlation of friction angle and water within the slope.

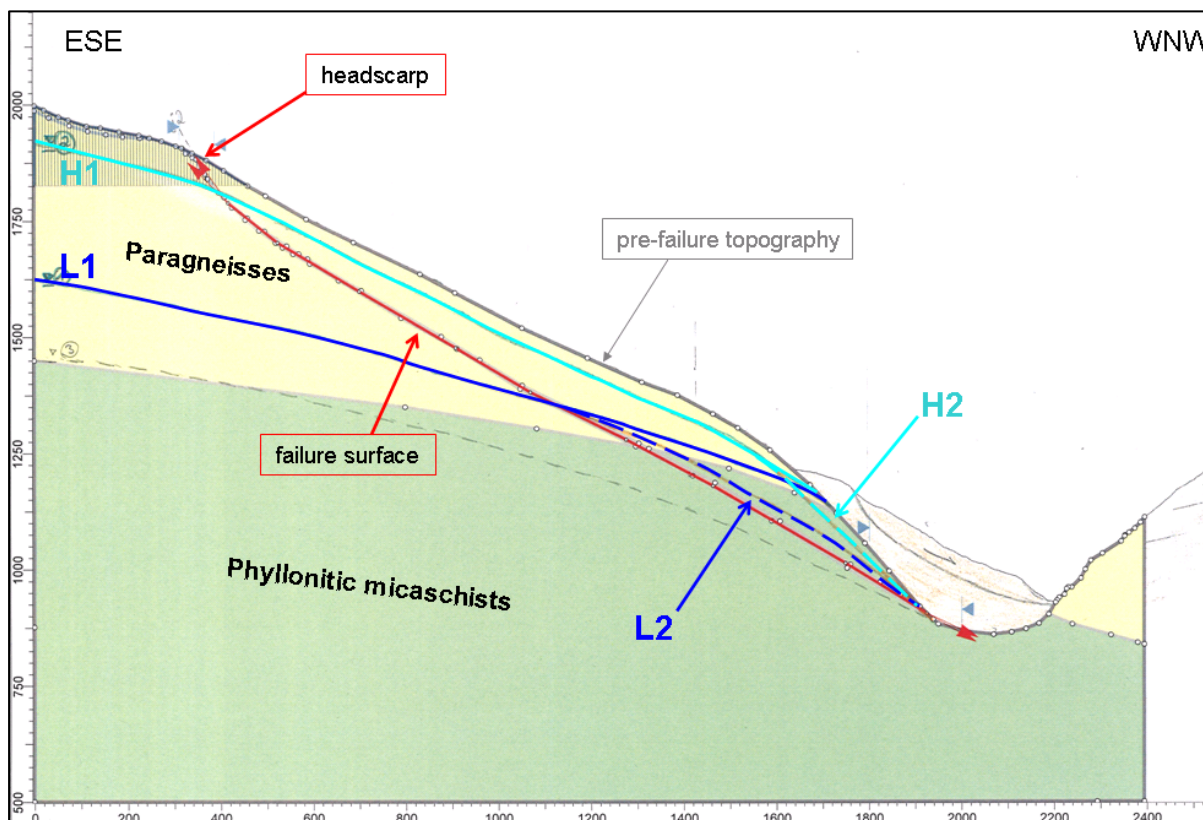


Figure 58: Cross section through the landslide that was evaluated in "Slide" showing the positions of the four different water tables (L1 and H1 for the situation of a hydrogeologic boundary along the boundary of paragneisses to phyllonitic micaschists, and L2 and H2 if the water table only depends on the level of the valley bottom).

For the input parameters given in Table 20 a factor of safety of 1.037 was received for the dry state. The corresponding failure surface is shown in Figure 59. For the sensitivity analyses the cohesion of the shear zone material was once assumed with 300 kPa and once with 500 kPa since investigations of shear zone materials by ENGL et al. (2008) state values ranging from 0 to ~700 kPa. Figure 60 shows the sensitivity plot for the water tables L1 and H1. For a cohesion of 500 kPa generally lower friction angles are needed for failure than for a cohesion of 300 kPa. The lower water table L1 results in required friction angles of 22° (for c = 500 kPa) and 27° (for c = 300 kPa). If the high water table H1 is consulted the friction angle can increase to 25.5° (for c = 500 kPa) and 31° (for c = 300 kPa) respectively. Figure 61 shows the sensitivity plot for the water tables L2 and H2 showing that in these cases generally lower friction angles are required for failure than for the water tables L1 and H1. The lower water table L2 results in required friction angles of 20° (for c = 500 kPa) and 24.8° (for c = 300 kPa) respectively, the higher water table H2 in required friction angles of 25° (for c = 500 kPa) and 31.5° (for c = 300 kPa). Reasonable friction angles of the shear zone material resulting from the

sensitivity analysis using “Slide” are interpreted to range from 19° to a maximum of 27° depending on the height and location of the water table within the slope.

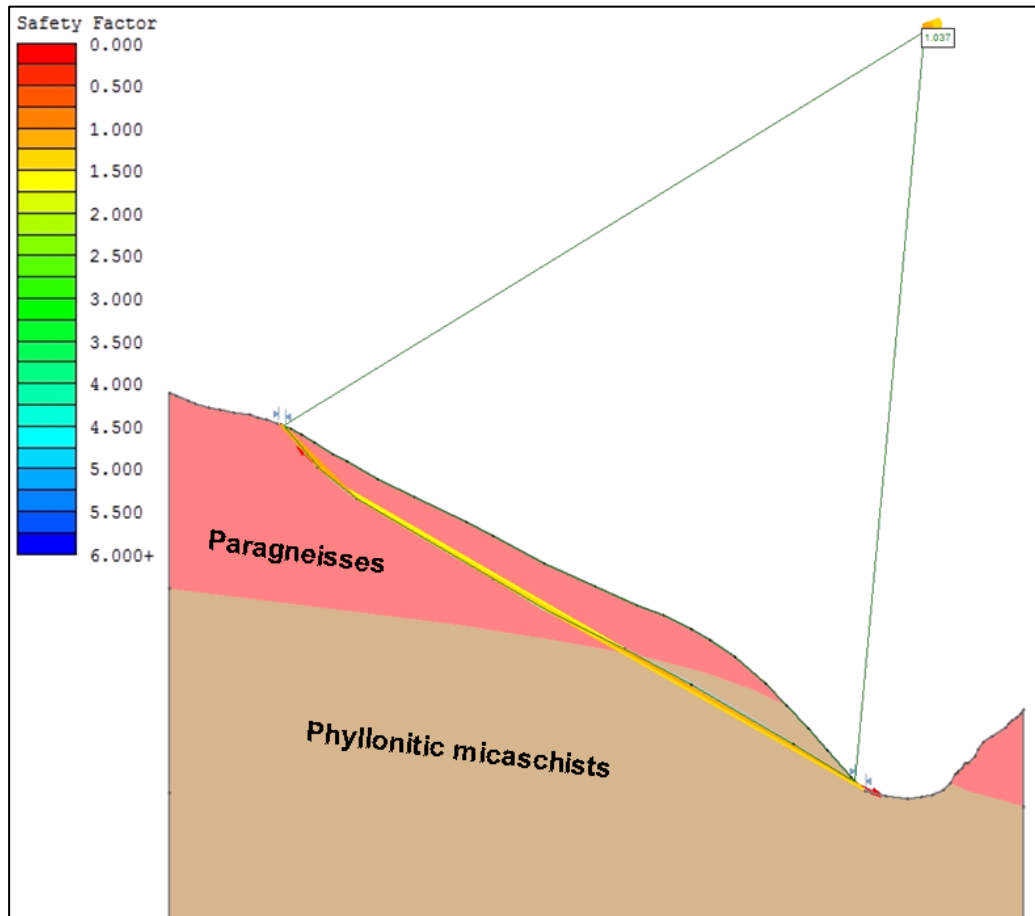


Figure 59: Analysis result for the parameters given in Table 20 for the dry state showing the failure surface with the lowest factor of safety which is 1.037.

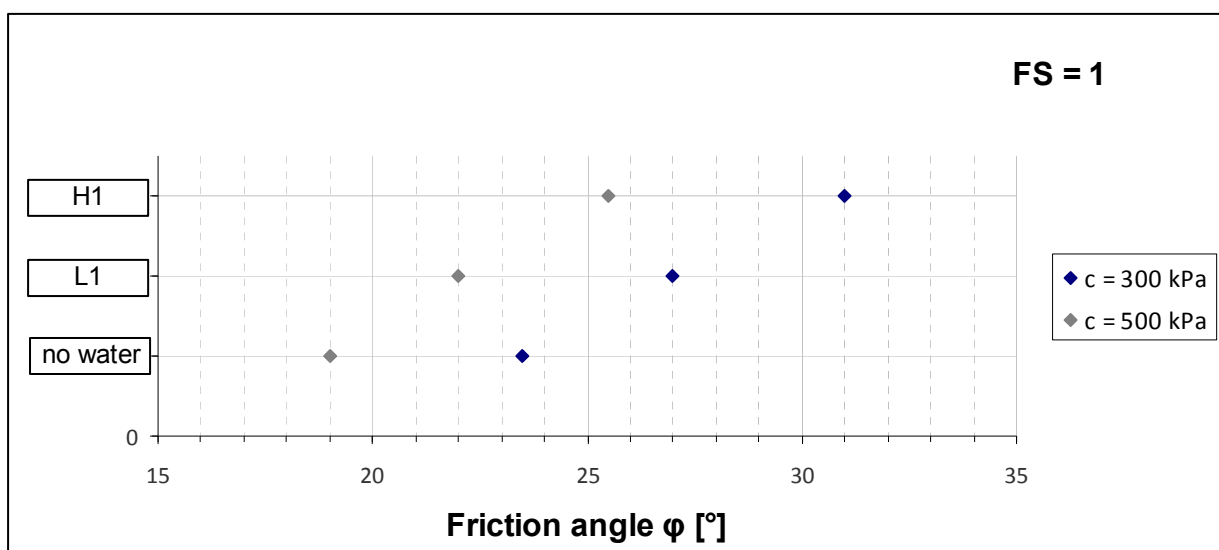


Figure 60: Sensitivity plot for the condition of no water and of low and high water tables (L1 and H1) that correspond to the boundary between paragneisses and phyllonitic micaschists. The grey points represent the analysis results for a cohesion of 500 kPa, the blue points for a cohesion of 300 kPa.

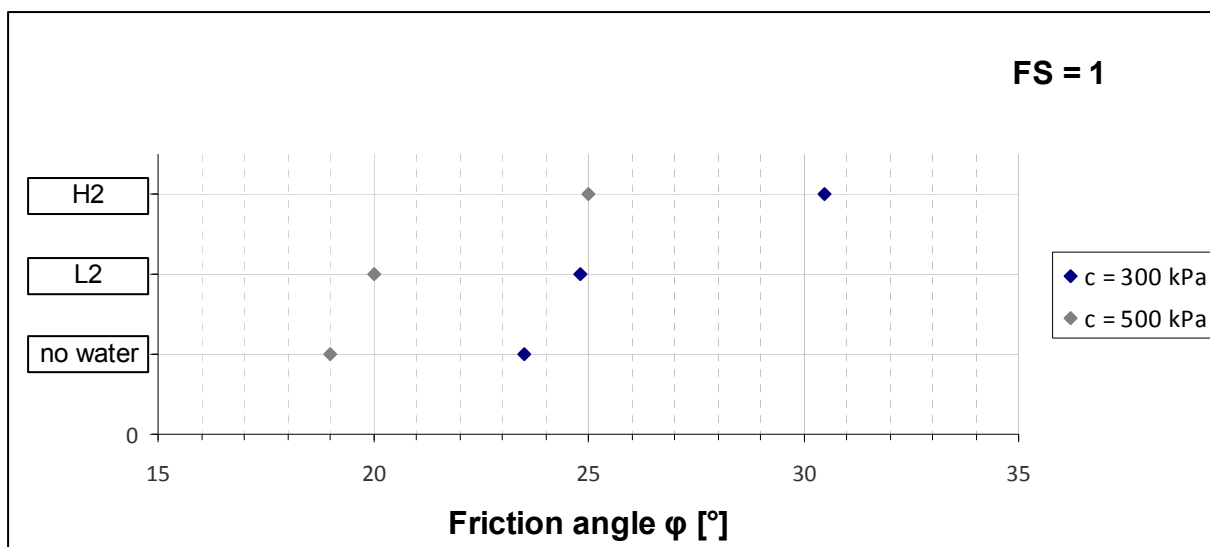


Figure 61: Sensitivity plot for the condition of no water and of low and high water tables (L2 and H2) that correspond to the level of the valley bottom. The grey points represent the analysis results for a cohesion of 500 kPa, the blue points for a cohesion of 300 kPa.

4.4.5. Analysis using “RocTopple”

In the upper region of the study area (behind the headscarp) obsequent breaks in slope were observed that strike approximately parallel to joint set j1 (~100/72). To find out if these breaks in slope could be caused by (deep-seated) toppling a kinematic and stability analysis using the software “RocTopple 1.0” (ROCSCIENCE, 2013) was carried out. For the input parameters concerning the slope given in Figure 62 toppling was shown to be kinematically admissible and a factor of safety of ~0.9 was received.

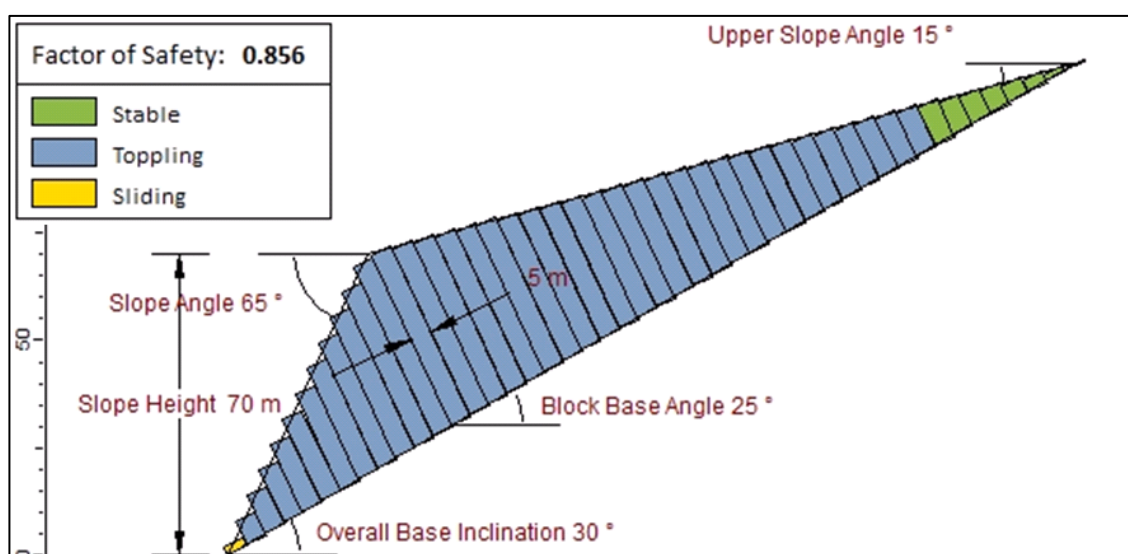


Figure 62: Result of the kinematic and stability analysis as well as the input parameters regarding toppling along joint set j1 using the software “RocTopple”.

4.5. Subsurface conditions

From the field investigations and slope stability analyses a model of the underground morphology and the depth of the landslide were derived. Figure 63 and Figure 64 show the longitudinal and transversal geologic cross sections including the supposed subsurface of the landslide, which is drawn according to the conception of a shear zone developing during movement. The maximum depth of the landslide is assumed with ~200 m and the overdeepening at the location of the river Trisanna with ~50 m according to the reconstruction of the pre-failure surface (chapter 4.1.). The boundaries of the smaller slides in the toe region of the landslide Gfäll were defined due to cracks in the streets or fractures in the walls beside them as well as fissures in the ground (sometimes spanned by roots) and due to the evaluation of laserscan data (slope inclination display). The smaller slide drawn in the upper part of the landslide Gfäll is assumed to be the debris of a secondary failure at the headscarp, since the headscarp in this area is not weathered as much as south or north of it. Due to the results obtained from the borings in the northwest of the landslide Gfäll (chapter 1.5.2.), it is supposed that the landslide Gfäll was thrust over fluvio-glacial sediments of the valley and that the landslide debris in its lowermost part is mixed with them. These fluvio-glacial sediments, however, are not drawn as an extra unit in the cross section, because they are assumed to feature a maximum thickness of ~10 m which is nearly not visible on the scale of the cross section. On the western side of the river Trisanna no mapping was done in the course of the present thesis, which is why the rock types drawn there in the cross sections are based on the geologic map 1:50.000 of Landeck (KRAINER et al., 2004).

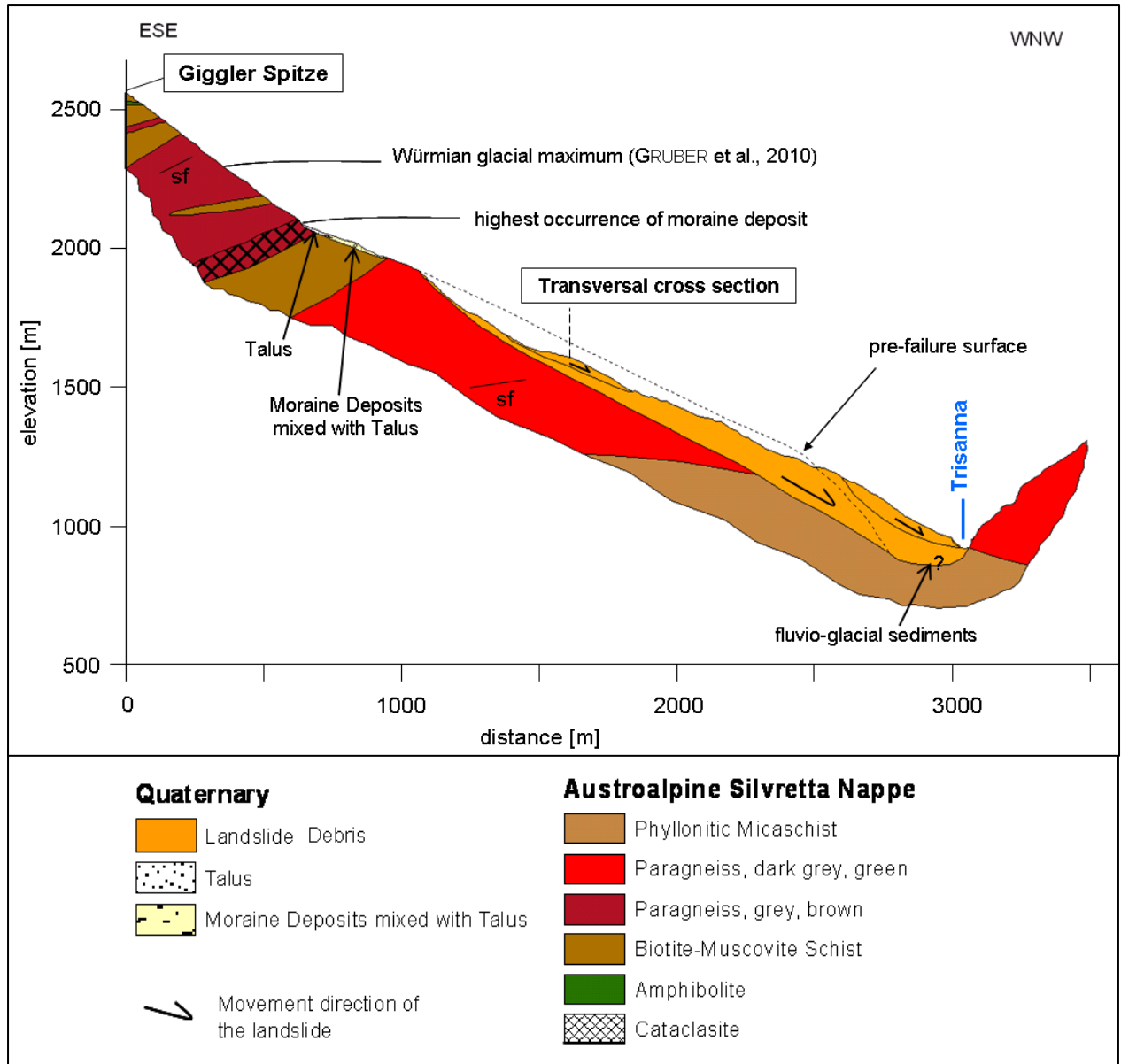


Figure 63: Longitudinal geologic cross section including the supposed subsurface of the landslide according to the conception of a discrete shear zone developing during movement. The location of the cross section can be taken from the geologic map in Figure 25 (chapter 3.1.1.2).

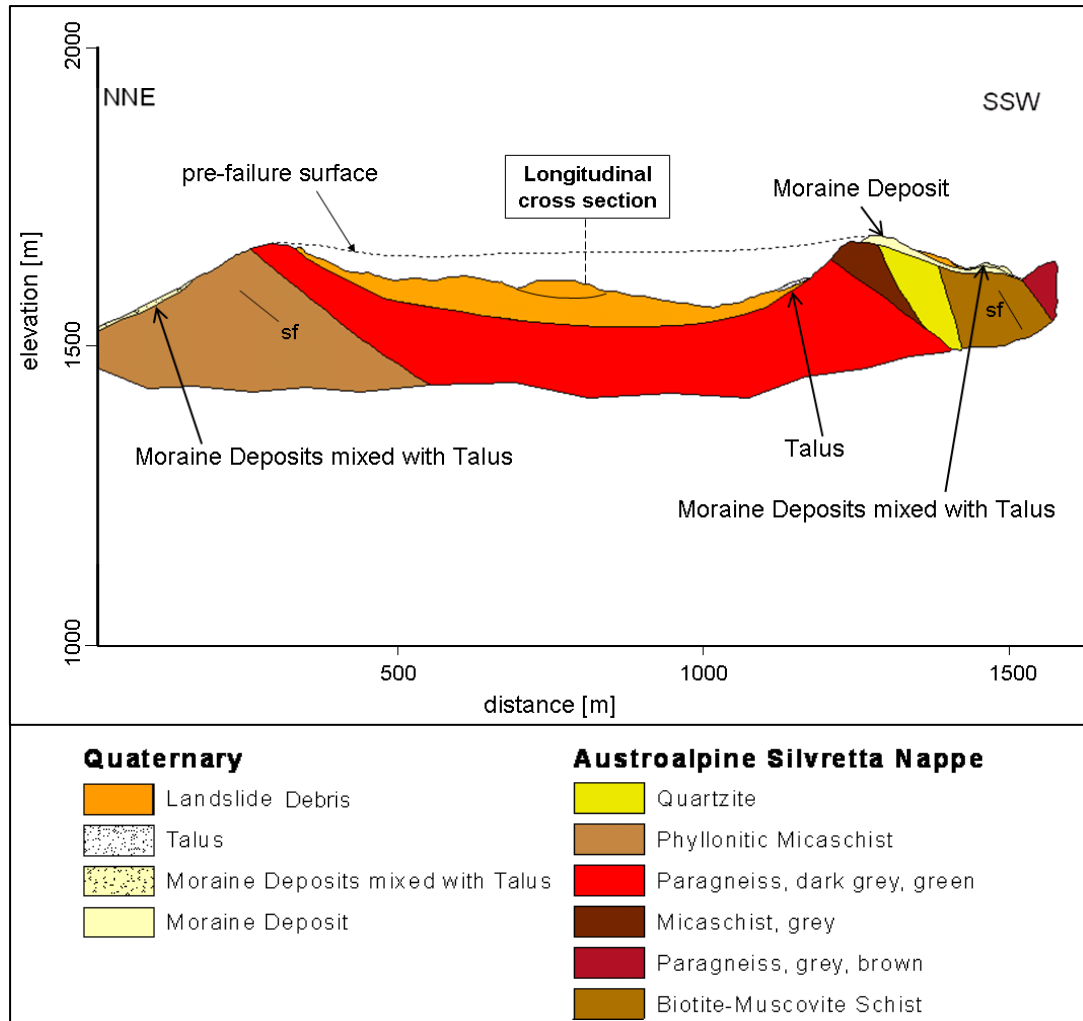


Figure 64: Transversal geologic cross section including the supposed subsurface of the landslide according to the conception of a discrete shear zone developing during movement. The location of the cross section can be taken from the geologic map in Figure 25 (chapter 3.1.1.2.).

5. Discussion and Conclusions

Engineering geological evaluation of the landslide Gfäll was made on the basis of detailed field mapping, structural geologic measurements and analyses, together with kinematic and stability analyses. Field observations and structural measurements revealed that the headscarp is formed by two joint sets (j2 and j3) that strike approximately NE-SW and NW-SE. Kinematic analyses show that wedge sliding is kinematically admissible along unfavourable oriented intersection lines of the joint set j3 and the schistosity, plunging toward the west at about 30°. However, based on the limited persistence of the rock mass discontinuities as compared to the scale of the landslide, it is considered unlikely that the entire landslide consists of a single discrete wedge. On the basis of engineering geologic investigations performed, it is suggested that the landslide initiated as blocks sliding along a stepped failure surface. With continued displacements these steps (or asperities) were subsequently sheared during progressive movement of the landslide. A basal shear zone consisting of sheared rock material (kakirites) is then suggested to have developed. Stability analyses using the software "Slide" produced a factor of safety >1 if the friction angle of the shear zone material is 20° and the cohesion 500 kPa. For lower friction angles (<19°) failure could occur without water pressure within the slope, i.e. the water table would be located beneath the failure surface. If water acting in the slope is invoked, unstable conditions (FS<1) were obtained for friction angles up to ~30°. However, the friction angles (and the corresponding water pressures) are supposed to be reasonable only up to ~25°, because higher friction angles require higher water tables to reach a limiting equilibrium condition, which result in excessively steep hydraulic gradients. The depth of the landslide was interpreted to be ~200 m resulting from the reconstruction of the pre-failure topography based on a balanced cross section analysis (chapter 4.1.) and from the inclination of the unfavourable oriented intersection line of joint set j3 and the schistosity. The internal structure of the landslide debris features longitudinal (WNW-ESE striking) as well as transversal (NE-SW to ENE-WSW striking) lineaments. The longitudinal lineaments are interpreted to represent differential movements within the overall slide mass, the transversal ones to represent areas of tensile stress that result in scarps within the landslide debris. The disintegration of the landslide mass increases from the headscarp toward the toe, resulting in secondary (soil-like) slides at the toe, which are active according to the geotechnical monitoring data from 2005 and also due to field observations (e.g. damaged streets and stone walls beside them, fissures in the ground, spanned roots). At the houses of the human settlements located on the landslide Gfäll no signs or

influences of the landslide movement could be observed. Due to the observations and engineering geological analyses, the landslide Gfäll is best classified as a deep-seated rockslide resulting from a wedge failure. The secondary slides within the disintegrated material in the toe region are judged as soil-type slides. Rock fall events are as well secondary failures originating from the scarps. Deep-seated toppling as failure mode of the landslide Gfäll is considered unlikely, since a prominent headscarp is formed across the entire slope and sliding is kinematically admissible. Only in the upper parts (behind the headscarp) features that could be caused by toppling (obsequent scarps) were identified.

Differences and similarities to the reference landslides Zintwald (EDER et al. (2006), POSCHER et al. (2006), HENZINGER et al. (2009)) and Niedergallmigg (KIRSCHNER (2006), ZANGERL et al. (2012); see also chapter 1.4.2.) are summarized below:

- In contrast to the interpreted failure mechanism of the landslide Gfäll, which is a rockslide featuring a wedge failure geometry, the landslide **Zintwald** is characterized by the mobilization of soil-like material (especially along small shear zones or old failure surfaces). Similar to Gfäll, however, the landslide Zintwald shows areas of varying activity and velocity. The large deep-seated slope deformation of Zintwald shows very slow movements or is currently even inactive. Only smaller and shallower parts within the landslide feature increased velocities. At Gfäll the signs of movement can also be found especially in the lower region of the landslide, where smaller slides are interpreted to occur within the overall slide mass. The activity of the whole landslide Gfäll, though, is not known. The landslide debris of both landslides consists of fragments of hard rock embedded within a more disintegrated, soil-like mass. River erosion at the toe and water infiltration into the disintegrated mass are supposed to have an important influence on the movement of both landslides.
- The development of the sliding zone of the landslide **Niedergallmigg** was favoured by folding and semi-ductile deformation resulting in intensely broken and sheared rocks at the border between *Venet complex* and *Silvretta complex*, whereas at Gfäll the basal sliding zone can only result from fracturing and from the shearing of the rocks during the movement of the landslide since it is completely located within the *Venet complex*. At Niedergallmigg the entire

slope from the headscarp down to the river Inn is moving, which for the landslide Gfäll is not known but interpreted to be unlikely based on the field observations that revealed signs of activity (like oblique trees, stressed roots, fissures in the ground, damaged streets) only in the lower half of the landslide debris. The similarities of the landslides Niedergallmigg and Gfäll are that the headscarp is formed by approximately orthogonal joint sets and that a discrete sliding zone is assumed. Furthermore, both landslides as a whole are judged to be rock slides, whereas secondary slides in the disintegrated material at the toes (that are triggered by river erosion or heavy rainfalls and snowmelts respectively) are soil-type slides.

Landscape evolution in the area of the landslide Gfäll was strongly influenced by Quaternary processes, since glacial sediment deposits and morphologic features such as whale backs or glacial polishes can be found. It is concluded that a glacier of varying thickness covered much of the study area. Its retreat led to relief favouring fracture formation and to the loss of the support (especially at the toe). Additionally, a large amount of water was liberated during the melting of the glacier facilitating weathering and erosion. The landslide most likely occurred in response to the oversteepened toe and was thrust onto fluvio-glacial sediments in the valley. The deposits of moraine material also render possible the assumption that the landslide occurred not in post-glacial but in late-glacial times and that the landslide debris was once more thrust by a glacier during a later advance. The erosion of the river Trisanna at the toe of the landslide Gfäll and heavy rainfalls or snowmelts are assumed to have significant influence on the present movement of the landslide.

To obtain detailed information regarding the depth of the landslide as well as the lithologic units beneath the landslide and about the composition and thickness of the proposed basal shear zone, further investigations would be required. Reflection and refraction seismic surveys in longitudinal and transversal directions (referring to the movement direction of the landslide) could show the depth of the disintegrated landslide mass and its contact to the intact rock. Subsequent core borings down to a depth corresponding to the results of the geophysical investigations would also show the depth of the landslide debris and would allow the investigation and testing of landslide and shear zone material. Drilling in the disintegrated mass, however, is supposed to be difficult due to the intercalation of boulders and finer-grained material. A geodetic monitoring (e.g. via surface measurement points) over

at least one year would serve to obtain the movement rates of the landslide, the total displacement vectors and to distinguish between areas of higher and lower velocities.

6. References

- AMPFERER, O. & HAMMER, W., 1922: Geologische Spezialkarte der Republik Österreich Blatt Landeck (5145), 1:75.000, herausgegeben von der Geologischen Bundesanstalt, Wien.
- AMPFERER, O. & HAMMER, W., 1924: Erläuterungen zur Geologischen Spezialkarte der Republik Österreich Blatt Landeck (5145).- herausgegeben von der Geologischen Bundesanstalt, 88 S., Wien.
- ASFINAG, 2012a: S16 Arlberg Schnellstraße, Perjontunnel 2. Röhre, Gebirgsarten und Gebirgsverhaltenstypen.- Technischer Bericht vom 27. April 2012, Planungsgemeinschaft Bernard – IBK, 55 S.
- ASFINAG, 2012b: S16 Arlberg Schnellstraße, Perjontunnel 2. Röhre, Bohrprotokolle.- Geologische Aufnahme durch Bernard Ing.
- ATLR, 2013: Laserscandaten Bereich Gfäll, Laserscanning – DGM/DOM 1 m Auflösung, Höhenschichtlinien 1 m, Schummerung.- Amt der Tiroler Landesregierung, Innsbruck.- received on August 20, 2013.
- B316 ARLBERGERSATZSTRASSE, 2005: Talzusub Zintwald, Profilschnitt 5.- received from: HEISEL, G., MATTLE, B. & POSCHER, G., 2005: Massenbewegung Zintwald: Geologische Erkenntnisse, Gefahrenkarte und Maßnahmenplanung.- Vortrag, 7. Geoforum Umhausen, November 2005.
- BEV, 2013: Bundesamt für Eich- und Vermessungswesen: KM50-R select, digital topographic map of Austria, mapping scale 1:50.000.- received on June 11, 2013.
- BEV, 2014: Bundesamt für Eich- und Vermessungswesen: Austrian Map online: www.austrianmap.at, accessed June 2014.
- BOUSQUET, R., SCHMID, S. M., ZEILINGER, G., OBERHÄNSLI, R., ROSENBERG, C., MOLLI, G., ROBERT, C., WIEDERKEHR, M. & ROSSI, P., 2012: Tectonic framework of the Alps. Map 1:1000000.- CCGM/CGMW.- https://earth.unibas.ch/tecto/research/Alps_tecto.png, accessed July 2014.
- BUTTON, E. A., 2004: A contribution to the characterization of phyllitic and schistose rock masses for tunnelling.- Gruppe Geotechnik Graz, Heft 22, 134 S.

CRUDEN, D. M. & VARNES, D. J., 1996: Landslide types and processes.- In: TURNER, A. K. & SCHUSTER, R. L.: Special Report 247: Landslides: Investigation and mitigation, TRB, National Research Council, Washington, D.C., p. 36-75.

DIERCKE, 2014: Diercke Weltatlas.- Klimate der Erde nach Neef/Flohn.- www.diercke.de/kartenansicht.xtp?artId=978-3-14-100751-0&stichwort=Passatklima&fs=1, accessed August 2014.

EDER, S., POSCHER, G. & PRAGER, C., 2006: Risk analyses and risk management – Slope instabilities in Alpine environments.- ECI Geohazards – Technical, Economical and Social Risk Evaluation, 7 p., June 2006, Lillehammer, Norway.

ENGL, D., FELLIN, W. & ZANGERL, C., 2008: Scherfestigkeiten von Scherzonen-Gesteinen – ein Beitrag zur geotechnischen Bewertung von tektonischen Störungen und Gleitzonen von Massenbewegungen.- Bull. Angew. Geol., Vol. 13/2, S. 63-81.

FORKEL, M., 2008: Die gemäßigte Klimazone – Das Übergangsklima.- www.m-forkel.de/klima/uebergang.html, accessed August 2014.

FORKEL, M., 2010: Die gemäßigte Klimazone.- www.m-forkel.de/klima/gemaesigt.html, accessed August 2014.

FROITZHEIM, N., 2011: Geology of the Alps Part 1: General remarks and Austroalpine nappes.- lecture notes by Nikolaus Froitzheim.- www.steinmann.uni-bonn.de/arbeitsgruppen/strukturgeologie/lehre/wissen-gratis/geologie-der-alpen, accessed on May 16, 2014.

GEODZ, 2010: Alpen.- GeoDZ, Das Lexikon der Erde.- www.geodz.com/deu/d/Alpen, downloaded on July 16, 2014.

GIBBARD, P. L., HEAD, M. J., WALKER, M. J. C. & THE SUBCOMMISSION ON QUATERNARY STRATIGRAPHY, 2010: Formal ratification of the Quaternary system/period and the Pleistocene series/epoch with a base at 2.58 Ma.- Journal of Quaternary Science, 25 (2), p. 96-102.

GOODMAN, R. E., 1989: Introduction to rock mechanics, 2nd edition.- 562 p., Wiley, New York.

- GOODMAN, R. E. & BRAY, J. W., 1976: Toppling of rock slopes.- Proc. Specialty conference on rock engineering for foundations and slopes, Boulder, Colorado.- American Society of Civil Engineers, Vol. 2, p. 201-234.
- GOODMAN, R. E. & KIEFFER, D. S., 2000: Behaviour of rock in slopes.- Journal of Geotechnical and Geoenvironmental Engineering, Vol. 126, No. 8, p. 675-684.
- GOODMAN, R. E. & SHI, G., 1985: Block theory and its application to rock engineering.- Prentice-Hall, Inc., Englewood Cliff, New Jersey, 338 p.
- GRUBER, A., PESTAL, G., NOWOTNY, A. & SCHUSTER, R., 2010: Erläuterungen zu Blatt 144 Landeck, Geologische Karte der Republik Österreich 1:50.000.- herausgegeben von der Geologischen Bundesanstalt, 206 S., Wien.
- GUZZETTI, F., 2005: Landslide hazard and risk assessment.- Dissertation, 373 p., Rheinische Friedrich-Wilhelms-Universität Bonn.
- HEIßEL, G., FIGL, T., GSTREIN, P., HENZINGER, J. & POSCHER, G., 2005: Gfällbrücke – Beurteilung der geologischen Situation.- Ingenieurgeologisches Gutachten vom 10. September 2005, 11 S.
- HENZINGER, J., 2005: Neue Gfällbrücke – Baugrunduntersuchungen.- Geotechnisches Gutachten vom 11. April 2005, 6 S., 4 Anlagen.
- HENZINGER, J., POSCHER, G., HEIßEL, G. & MATTLE, B., 2009: Hangbewegungen Zintlwald, 3 Jahre nach dem Anbruch.- Tagungsbeiträge 7. Österreichische Geotechniktagung, S. 145-156, Jänner 2009, Wien.
- HIGHLAND, L. M. & BOBROWSKY, P., 2008: The landslide handbook – A guide to understanding landslides.- U.S. Geological Survey, Circular 1325, 129 p., Reston, Virginia.
- ISRM, 1983: Suggested method for determining the strength of rock materials in triaxial compression.- International Journal of Rock Mechanics and Mining Sciences & Geomechanics Abstracts, Vol. 20, No. 6, p. 285-290.

- ISRM, 2007: Suggested methods for the quantitative description of discontinuities in rock masses.- In: ULUSAY, R. & HUDSON, J. A. (Eds.), 2007: The complete ISRM suggested methods for rock characterization, testing and monitoring: 1974-2006, p. 3-55, Ankara, Turkey.
- ISRM, 2013: Suggested method for laboratory determination of the shear strength of rock joints: revised version.- Rock Mechanics and Rock Engineering, Springer 2013.
- KIEFFER, D. S., 1998: Rock slumping: A compound failure mode of jointed hard rock slopes.- Dissertation, 183 p., University of California, Berkeley.
- KIEFFER, D. S., 2012: Lecture notes GEO.922 Mass movements, TU Graz.
- KIRSCHNER, H., 2006: Endbericht zur Untersuchung von Massenbewegungen im oberen Inntal.- Projekt A2.3, alpS-GmbH Zentrum für Naturgefahren Management, 74 S., Innsbruck.
- KÖHLER, M., 1983: Perjuntunnel (Landeck, Tirol): Baugeologische Verhältnisse, Prognose und tektonische Schlussfolgerungen.- Geol. Paläont. Mitt. Innsbruck, 12, S. 249-267.
- KRAINER, K., HAUSER, C., PAVLIK, W., PESTAL, G., NOWOTNY, A., ROCKENSCHAUB, M. & UCIK, F. H., 2004: Geologische Karte der Republik Österreich 1:50.000, Blatt 144 Landeck, herausgegeben von der Geologischen Bundesanstalt, Wien.
- MAGGETTI, M. & FLISCH, M., 1993: Evolution of the Silvretta Nappe.- In: VON RAUMER, J. F. & NEUBAUER, F. (Eds.), 1993: Pre-Mesozoic Geology in the Alps, Part III, p. 469-484, Springer-Verlag, Berlin Heidelberg.
- MOSER, M., 2002a: The effects of deep-seated mass movements on the alpine environment.- International Congress INTERPREAVENT 2002 in the Pacific Rim – Matsumoto, Japan.- Congress publication, Vol. 2, p. 641-653.
- MOSER, M., 2002b: Geotechnical aspects of landslides in the Alps.- In: 1st European Conference on landslides (2002), p. 23-43.
- NICKMANN, M., SPAUN, G. & THURO, K., 2006: Engineering geological classification of weak rocks.- Proc. 10th international IAEG Congress 2006, Geological Society of London, paper number 492, 9 p., Nottingham.

- NICKMANN, M. & THURO, K., 2010: Ingenieurgeologische Untersuchungen zur Charakterisierung veränderlich fester Gesteine.- Geotechnik, 33, S. 320-325.
- OBERHAUSER, R. & RATAJ, W., 1998: Geologisch-tektonische Übersichtskarte von Vorarlberg 1:200000, herausgegeben von der Geologischen Bundesanstalt, Wien.
- ÖNORM EN ISO 14688-1 and -2: Geotechnische Erkundung und Untersuchung – Benennung, Beschreibung und Klassifizierung von Boden, Teil 1: Benennung und Beschreibung (ISO: 14689-1:2002) und Teil 2: Grundlagen von Bodenklassifizierungen (ISO: 14688-2:2004).
- ÖNORM EN ISO 14689-1: Geotechnische Erkundung und Untersuchung – Benennung, Beschreibung und Klassifizierung von Fels, Teil 1: Benennung und Beschreibung (ISO: 14689-1:2003).
- OPH, 2005: Monitoring Oberhang Gfäll/Platils vom 6.9.2005 bis 24.11.2005.- OPH, Obex-Pfeifer-Haas, ZT Ges.m.b.H. für Vermessungswesen, Zams.
- POISEL, R., PREH, A. & HOFMANN, R., 2011: Slope failure process recognition based on mass-movement induced structures.- 2nd Conference on Slope Tectonics, Geological Survey of Austria, Vienna.
- POSCHER, G., 1993: Neuergebnisse der Quartärforschung in Tirol.- Arbeitstagung 1993 der Geologischen Bundesanstalt „Geologie des Oberinntaler Raumes – Schwerpunkt Blatt 144 Landeck“, S. 7-27, Wien.
- POSCHER, G., 2005: B188 Umgehung Gfäll.- Geologisch-geotechnischer Bericht, Objektbericht Tunnel Gfäll.- Amt der Tiroler Landesregierung, 29 S.
- POSCHER, G., MATTLE, B. & HENZINGER, J., 2006: Hangbewegung Zintlwald.- Geologisch-geotechnischer Bericht – Risikobewertung.- unveröffentlichter Bericht, Bearbeitungsstand 1.6.2006, Amt der Tiroler Landesregierung, 65 S.
- PREUSSER, F., REINTER, J. M. & SCHLÜCHTER, C., 2010: Distribution, geometry, age and origin of overdeepened valleys and basins in the Alps and their foreland.- Swiss Journal of Geoscience, 103, p. 407-426.

- RAMAMURTHY, T., VENKATAPPA RAO, G. & SINGH, J., 1993: Engineering behaviour of phyllites.- *Engineering Geology*, 33, p. 209-225.
- REITNER, J. M. & LINNER, M., 2009: Formation and preservation of large scale toppling related to Alpine tectonic structures – Eastern Alps.- *Austrian Journal of Earth Sciences*, Vol. 102/2, p. 68-80, Vienna.
- SCHMID, S. M., FÜGENSCHUH, B., KISSLING, E. & SCHUSTER, R., 2004: Tectonic map and overall architecture of the Alpine orogen.- *Eclogae geol. Helv.*, 97 (2004), p. 93-117, Basel.
- SCHUSTER, R., 2004: The Austroalpine crystalline units in the Eastern Alps. In: HUBMANN, B. & PILLER, W. E. (Eds.), 2004: *Pangeo Austria 2004 – Abstracts*.- Karl-Franzens-Universität Graz, 436 p., Graz.
- SPAUN, G. & THURO, K., 1994: Untersuchungen zur Bohrbarkeit und Zähigkeit des Innbrucker Quarzphyllits.- *Felsbau*, 12/2, S. 111-122.
- THURO, K., 1998: Bohrbarkeit im Sprengvortrieb: Geologisch-geotechnische Grundlagen.- *Münchner Geologische Hefte*, Reihe B, Heft 7 (Festschrift Prof. Spaun), S. 103-123.
- TIRIS, 2013: Tiroler Rauminformationssystem – Tiris Kartendienste: *tirisMaps*.- Amt der Tiroler Landesregierung.- www.tirol.gv.at/statistik-budget/tiris/, accessed May 2013.
- TIROL ATLAS, 2013: Klimadiagramme Land Tirol, Themenmodul Wasser, Periode 1980-2000 (Hydrographischer Dienst Tirol).- Institut für Geographie, Universität Innsbruck.- <http://tirolatlas.uibk.ac.at/graphics/lieth/index.html.de>, downloaded on August 13, 2014.
- TOLLMANN, A., 1977: *Geologie von Österreich, Band 1: Die Zentralalpen*.- 766 S., Deuticke, Vienna.
- TRÖGER, W. E., 1982: *Optische Bestimmung der gesteinsbildenden Minerale*, Teil 1 (Bestimmungstabellen) und Teil 2 (Textband).- Schweizbart'sche Verlagsbuchhandlung.
- USGS, 2014: U.S. Geological Survey, <http://pubs.usgs.gov/fs/2004/3072/images/Fig3grouping-2LG.jpg>, downloaded October 2014.

- VARNES, D. J. & IAEG, 1984: Landslide hazard zonation: a review of principles and practice.- International Association of Engineering Geology, Commission on Landslides and other Mass Movements on Slopes.- published by the United Nations Educational, Scientific and Cultural Organization, 63 p.
- WIECZOREK, G. F., 1996: Landslide triggering mechanisms.- In: TURNER, A. K. & SCHUSTER, R. L.: Special Report 247: Landslides: Investigation and mitigation, TRB, National Research Council, Washington, D.C., p. 76-90.
- WIS, 2013: Wasserinformationssystem Tirol: Wasserbuch- und Wasserwirtschaftsauszüge.- Amt der Tiroler Landesregierung, Abteilung Wasser-, Forst- und Energierecht bzw. Wasserwirtschaft.- https://portal.tirol.gv.at/wisSrvPublic/wis/wbo_ww_search.aspx, downloaded on August 5, 2013.
- ZAMG, 2002: Klimadaten von Österreich (Periode 1971-2000).- Daten Tirol: www.zamg.ac.at/fix/klima/oe71-00/klima2000/klimadaten_oesterreich_1971_frame1.htm, downloaded on August 13, 2014.
- ZANGERL, C., EBERHARDT, E., SCHÖNLAUB, H. & ANEGG, J., 2007: Deformation behavior of deep-seated rockslides in crystalline rock.- Rock Mechanics: Meeting Society's Challenges and Demands, Two Volume Set, Proceedings of the 1st Canada-US Rock Mechanics Symposium, May 2007, p. 901–908, Taylor & Francis Group, Vancouver, Canada.
- ZANGERL, C. & PRAGER, C., 2008: Influence of geological structures on failure initiation, internal deformation and kinematics of rock slides.- American Rock Mechanics Association 08-063, Proceedings 42nd U.S. / 2nd U.S.-Canada Rock Mechanics Symposium, 13 p., San Francisco.
- ZANGERL, C., PRAGER, C., BRANDNER, R., BRÜCKL, E., EDER, S., FELLIN, W., TENTSCHEIT, E., POSCHER G. & SCHÖNLAUB, H., 2008: Methodischer Leitfaden zur prozessorientierten Bearbeitung von Massenbewegungen.- Geo.Alp, Vol. 5, p. 1-51.

ZANGERL, C., PRAGER, C., CHWATAL, W., BRÜCKL, E., KIRSCHNER, H. & BRANDNER, R., 2012: Kinematics and internal deformation of a slow deep-seated rock slide in metamorphic rock (Niedergallmigg, Austria).- In: EBERHARDT, E., FROESE, C., TURNER, K. & LEROUEIL, S. (Eds.), 2012: Landslides and engineered slopes – Protecting society through improved understanding.- CRC press, p. 653-658.

ZISCHINSKY, U., 1968: Über Bergzerreiung und Talzuschub.- Geologische Rundschau, Vol. 58, Issue 2, p. 974-983.

ZISCHINSKY, U., 1969: Über Sackungen.- Rock Mechanics, Vol. 1, Issue 1, p. 30-52.

Internet Sources:

<http://earthscience.at/maps/> (downloaded on July 16, 2014): Wrmvergletscherung sterreichs.- abgeleitet von „Die Ostalpen und ihr Vorland in der letzten Eiszeit (Wrm)“ von D. van Husen, Wien 1987.

Software used for the engineering geological analyses:

LIU, Q., 2004: Key block programs B2HPGL and B10HPGL.- modified after the methods and programs by GOODMAN, R. & SHI, G., 1989.

LIU, Q. & KIEFFER, D. S., 2008: Key block program B04HPGL.- modified after the methods and programs by GOODMAN, R. & SHI, G., 1989.

ROCSCIENCE, 2010: Slide 6.0.- Advanced Slope Stability and Groundwater Seepage Analysis.- Rocscience Inc.

ROCSCIENCE, 2012: Dips 6.0.- Graphical and Statistical Analysis of Orientation Data.- Rocscience Inc.

ROCSCIENCE, 2013: RocTopple 1.0.- Toppling Analysis of Rock Slopes.- Rocscience Inc.

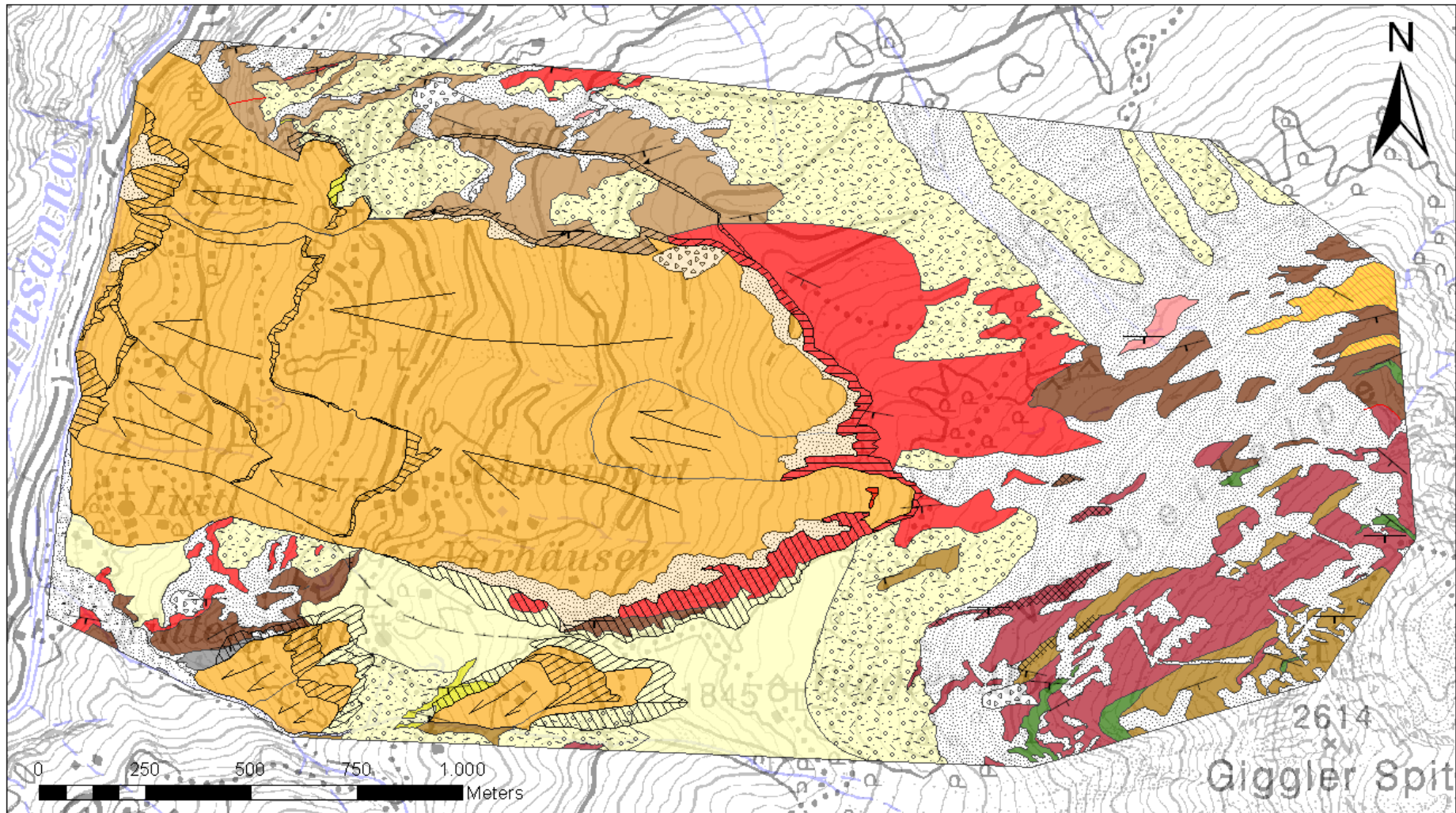
ROCSCIENCE, 2014a: Swedge 6.0.- 3D Surface Wedge Analysis for Slopes.- Rocscience Inc.

ROCSCIENCE, 2014b: Software tools for rock and soil.- Rocscience Inc.

7. Appendix

Appendix 1: Geologic map.....	Appendix page 1
Appendix 2: Geomorphic map.....	Appendix page 2
Appendix 3: Outcrop documentation.....	Appendix page 3
Appendix 4: Structural measurements.....	Appendix page 30
Appendix 5: Thin sections.....	Appendix page 32
Appendix 6: Laboratory testing.....	Appendix page 47
Appendix 7: Block theory analyses.....	Appendix page 60

Appendix 1: Geologic map



Lithologies

Quaternary

-  1 Alluvium
-  2 Talus
-  3 Rockfall blocks
-  4 Landslide Debris
-  5 Moraine Deposits mixed with Talus
-  6 Moraine Deposit

Austroalpine Silvretta Nappe

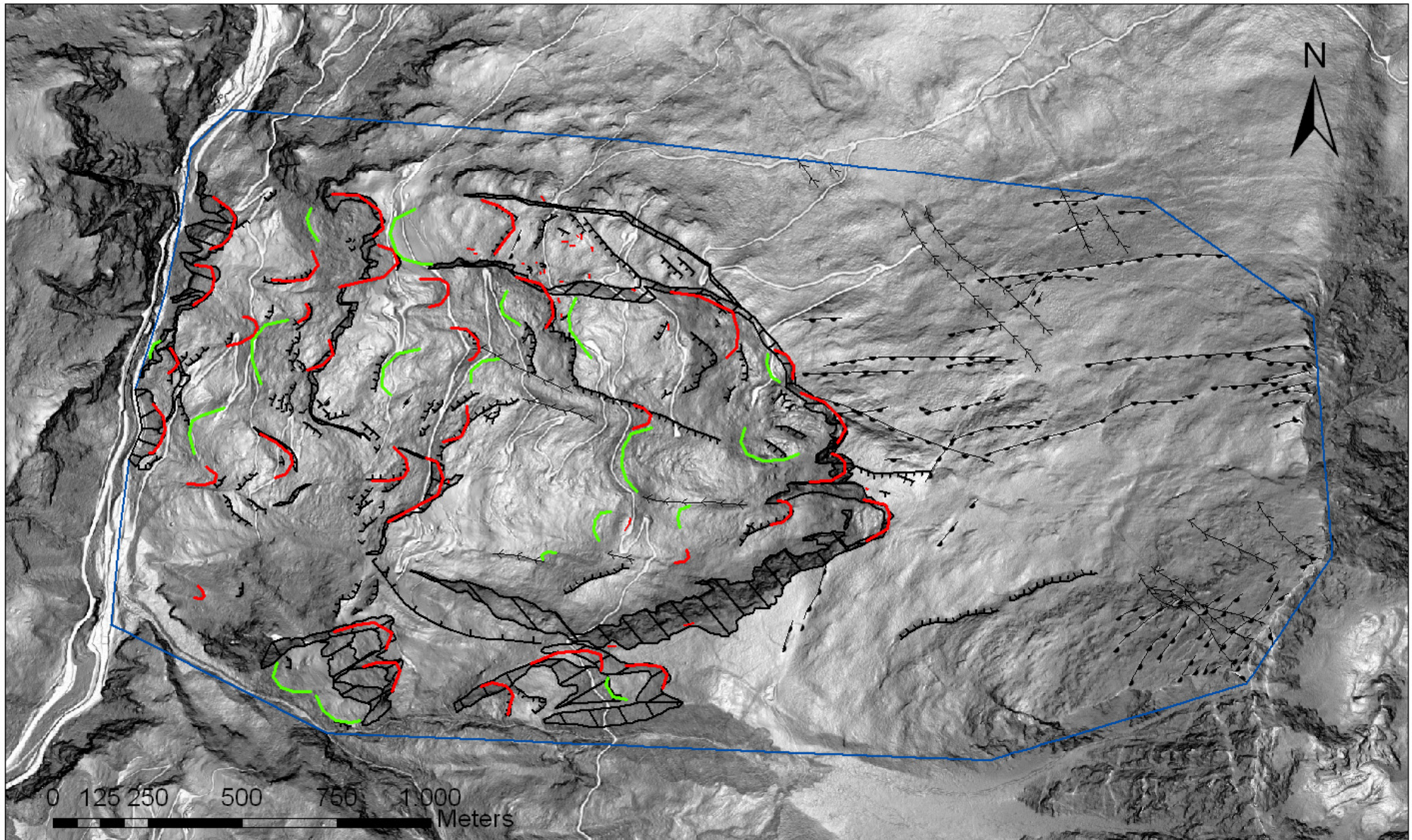
-  7 Quarzite
-  8 Phyllonitic Micaschist
-  9 Paragneiss, dark grey, green
-  10 Micaschist, grey
-  11 Paragneiss, grey, brown
-  12 Biotite-Muscovite Schist
-  13 Amphibolite

-  14 Albite-Blast Schist
-  15 Garnet Micaschist
-  16 Orthogneiss

Symbols

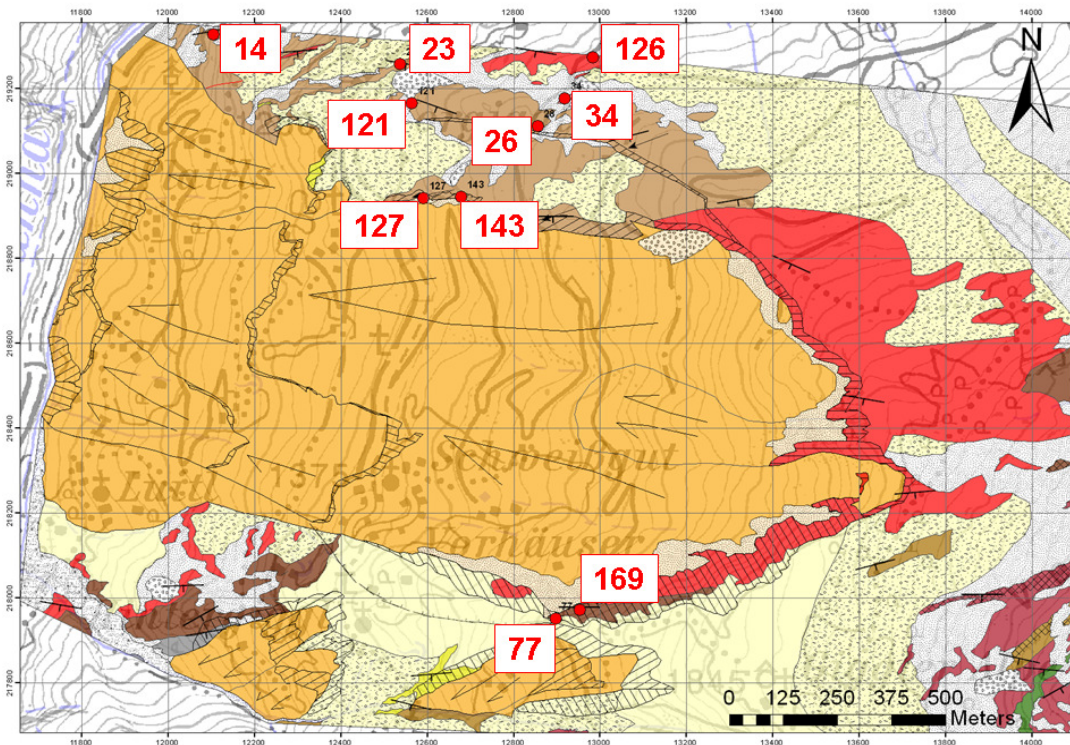
-  Dip and Dip Direction of Fold Axes
-  Dip and Dip Direction of Schistosity
-  Movement Direction of Landslides
-  Fault
-  Scarp
-  Secondary Scarp
-  Cataclasite

Appendix 2: Geomorphic map

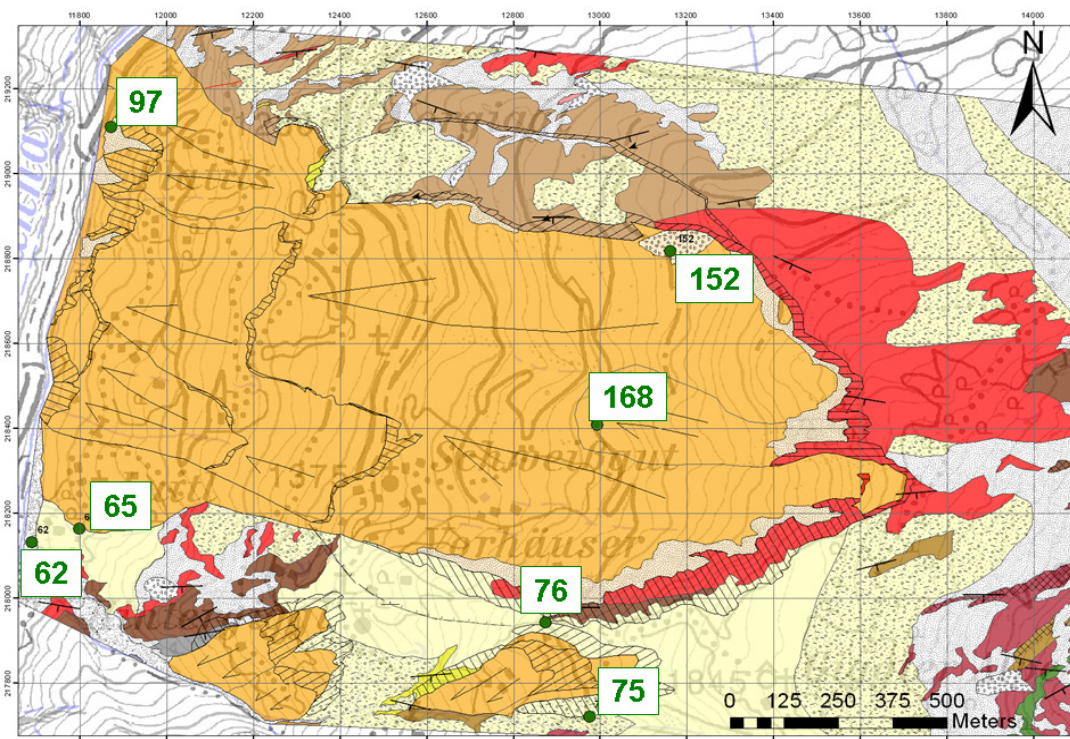


- | | | | | | | | |
|--|---------|--|--------------------------|--|-----------------|--|---------------------|
| | Chute | | Obsequent Break in Slope | | Scarp | | Concave Slope Shape |
| | Crevice | | Normal Break in Slope | | Secondary Scarp | | Convex Slope Shape |

Appendix 3: Outcrop documentation



Geologic map with the locations of the hard rock outcrops (legend see Appendix 1)



Geologic map with the locations of the outcrops in Quaternary deposits (legend see Appendix 1)

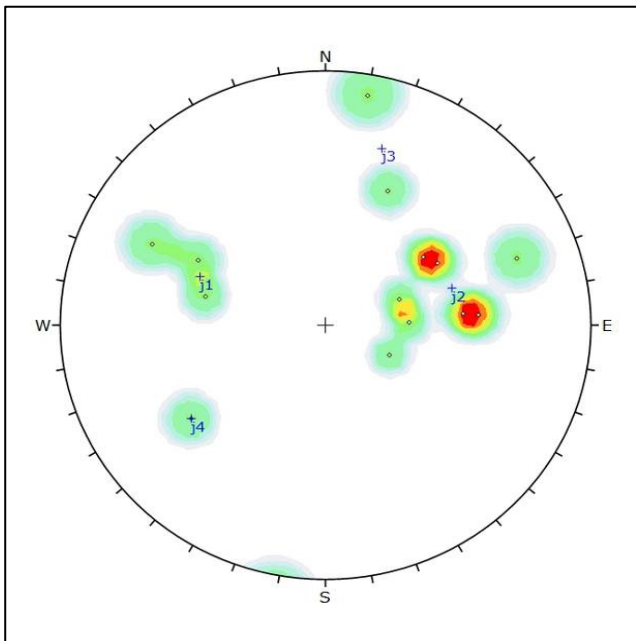
OUTCROP DOCUMENTATION

Outcrop number:	14
Lithology:	Phyllonitic Micaschist (8)
Remarks:	light to dark grey (yellowish to brownish when weathered), partly puckered foliation, quartz lumps and lenses; sometimes garnet bearing

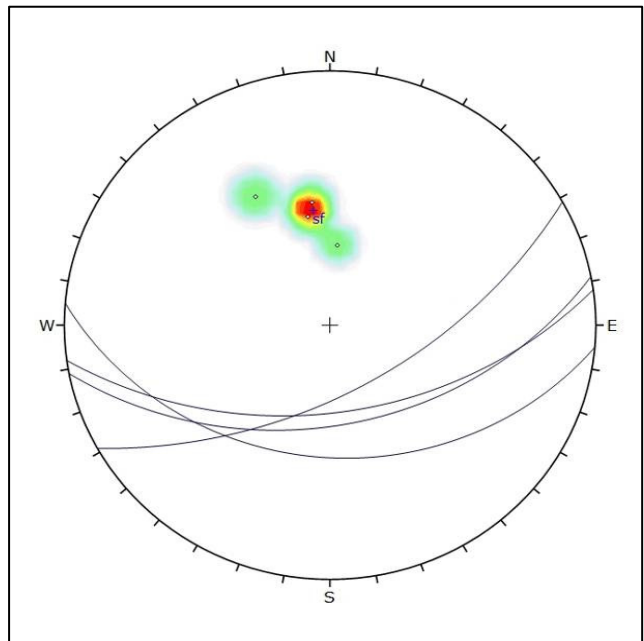
Date:		11.06.2013
Coordinates (GK M28):	x	12105
	y	219327
		± 7 m
Elevation [m]:		1020

Rock material	Weathering	
	<input type="checkbox"/>	fresh
	<input checked="" type="checkbox"/>	slightly weathered
	<input type="checkbox"/>	highly weathered
	<input type="checkbox"/>	completely weathered
	UCS	
	<input type="checkbox"/>	<1 MPa
	<input checked="" type="checkbox"/>	1-5 MPa
	<input type="checkbox"/>	5-25 MPa
	<input type="checkbox"/>	25-50 MPa
	<input type="checkbox"/>	50-100 MPa
	<input type="checkbox"/>	100-250 MPa
	<input type="checkbox"/>	> 250 MPa
	Spacing	
	<input type="checkbox"/>	>2000 mm
	<input type="checkbox"/>	2000-600 mm
	<input type="checkbox"/>	600-200 mm
	<input type="checkbox"/>	200-60 mm
	<input checked="" type="checkbox"/>	60-20 mm
	<input type="checkbox"/>	<20 mm
Block bodies		
<input type="checkbox"/>	polyhedral	
<input checked="" type="checkbox"/>	tabular	
<input type="checkbox"/>	prismatic	
<input type="checkbox"/>	equidimensional	
<input type="checkbox"/>	rhombic	
<input type="checkbox"/>	columnar	

Discontinuities	Type / Set		sf	j1	j2	j3	j4			
	Roughness	cm-m	stepped				X			
			undulating	X	X	X				
	mm	planar						X		
		rough			X	X				
		smooth	X	X					X	
	Spacing [mm]		1	100	50	50	100			
	Aperture [mm]		0 - 1	0	0 - 20	0 - 20	0 - 1			
	Persistence [m]		> 10	> 5	5	> 2	5			
	Water		-	-	-	-	-			
Dip direction / Dip		172 52	118 57	234 49	204 60	54 64				
		185 35	104 50	265 55	190 85					
		169 47	116 72	266 60						
		151 60		240 52						
				250 33						
				250 75						
				268 35						
				296 30						
Remarks		partly plastic fillings								



joint planes



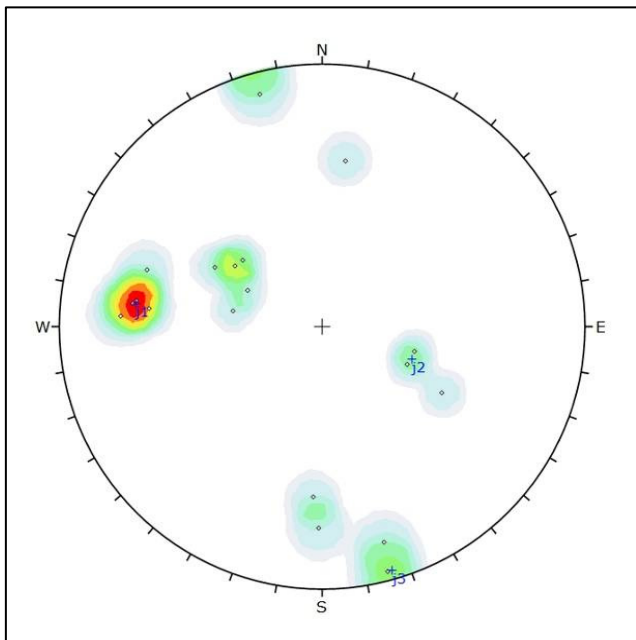
schistosity

OUTCROP DOCUMENTATION

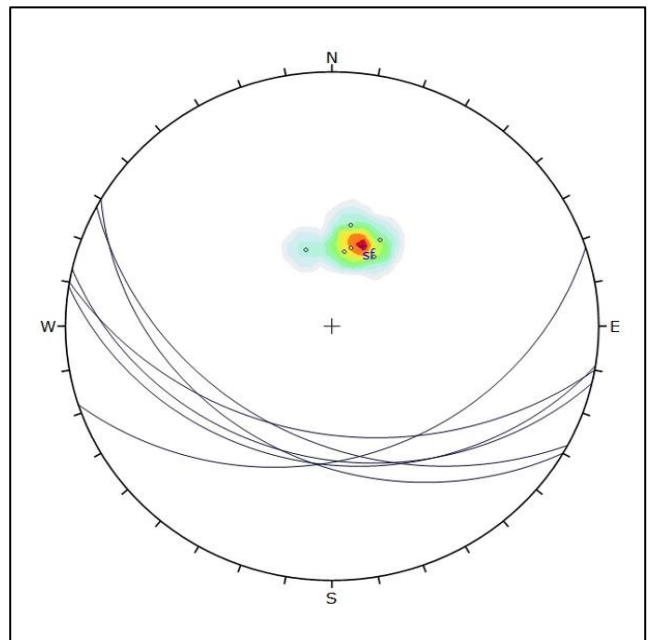
Outcrop number:	23
Lithology:	Phyllonitic Micaschist (8)
Remarks:	light to dark grey, quartz layers up to 5 cm thickness

Date:	24.08.2013		
Coordinates (GK M28):	x	12538	
	y	219257	
		± 6 m	
Elevation [m]:	1292		

Rock material	Weathering		Discontinuities								
		fresh	Type / Set	sf	j1	j2	j3				
	<input checked="" type="checkbox"/>	slightly weathered	Roughness	cm-m	stepped				X		
		highly weathered			undulating	X	X	X			
		completely weathered	mm	planar							
				rough			X	X			
			smooth	X	X						
			Spacing [mm]		0.5 - 2	50	200	100 - 200			
			Aperture [mm]		0	0 - 5	0 - 2	0			
			Persistence [m]		> 10	3 - 5	5	3			
		Water		-	-	-	-				
		UCS		208	42	93	75	294	39	3	66
	<1 MPa			193	35	98	71	299	55	345	88
	1-5 MPa			210	35	108	70	285	40	344	81
<input checked="" type="checkbox"/>	5-25 MPa			189	33	96	67			165	85
	25-50 MPa			190	44	97	72			1	75
	50-100 MPa			162	35	100	38			188	65
	100-250 MPa			Dip direction / Dip		116	35				
	> 250 MPa			FA:		130	43				
				247	25	125	44				
	Spacing			Remarks							
	>2000 mm										
	2000-600 mm										
	600-200 mm										
<input checked="" type="checkbox"/>	200-60 mm										
<input checked="" type="checkbox"/>	60-20 mm										
	<20 mm										
	Block bodies										
	polyhedral										
	tabular										
	prismatic										
	equidimensional										
<input checked="" type="checkbox"/>	rhombic										
	columnar										



joint planes



schistosity



OUTCROP DOCUMENTATION

Outcrop number:	28
Lithology:	Phyllonitic Micaschist (8)
Remarks:	grey to greenish (brownish when weathered), partly partly puckerred foliation

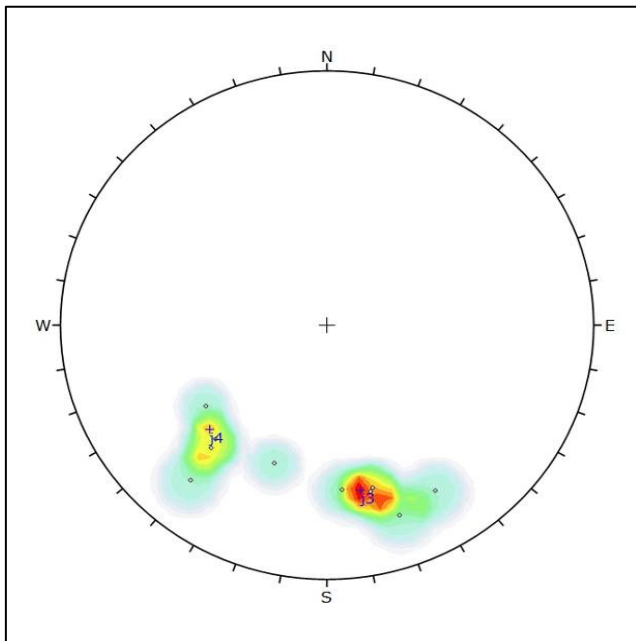
Date:	24.08.2013
--------------	------------

Coordinates (GK M28):	x	12857
	y	219111
		± 7 m

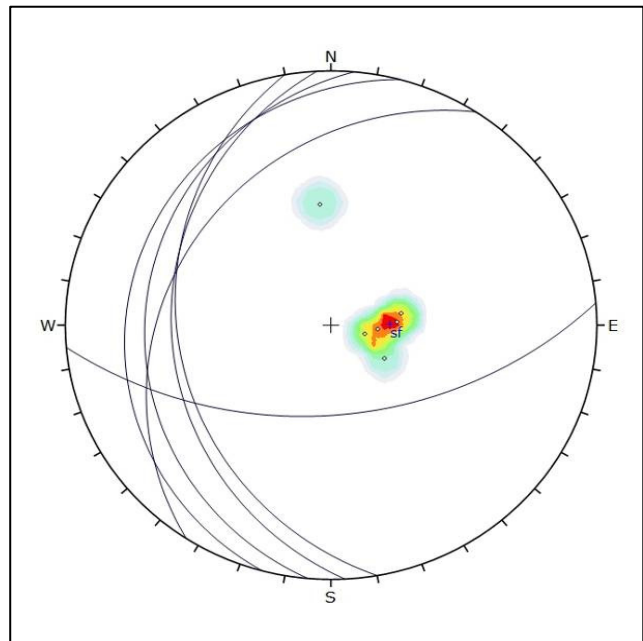
Elevation [m]:	1460
-----------------------	------

Rock material	Weathering	
	<input type="checkbox"/>	fresh
	<input checked="" type="checkbox"/>	slightly weathered
	<input type="checkbox"/>	highly weathered
	<input type="checkbox"/>	completely weathered
	UCS	
	<input type="checkbox"/>	<1 MPa
	<input checked="" type="checkbox"/>	1-5 MPa
	<input type="checkbox"/>	5-25 MPa
	<input type="checkbox"/>	25-50 MPa
	<input type="checkbox"/>	50-100 MPa
	<input type="checkbox"/>	100-250 MPa
	<input type="checkbox"/>	> 250 MPa
	Spacing	
	<input type="checkbox"/>	>2000 mm
	<input type="checkbox"/>	2000-600 mm
	<input type="checkbox"/>	600-200 mm
	<input type="checkbox"/>	200-60 mm
	<input checked="" type="checkbox"/>	60-20 mm
	<input type="checkbox"/>	<20 mm
Block bodies		
<input type="checkbox"/>	polyhedral	
<input checked="" type="checkbox"/>	tabular	
<input type="checkbox"/>	prismatic	
<input type="checkbox"/>	equidimensional	
<input type="checkbox"/>	rhombic	
<input type="checkbox"/>	columnar	

Discontinuities	Type / Set		sf	j3	j4						
	Roughness	cm-m	stepped			X					
			undulating	X	X						
		mm	planar								
			rough		X						
		smooth	X		X						
	Spacing [mm]		1	20 - 50	50 - 100						
	Aperture [mm]		0	0	1 - 10						
	Persistence [m]		> 10	> 2	3						
	Water		-	-	-						
Dip direction / Dip		260 30	355 66	43 63							
		275 20	345 67	20 60							
		267 28	328 75	40 77							
		303 27	340 77	42 66							
		285 15	346 68	55 58							
	175 51										
Remarks		partly plastic fillings									



joint planes



schistosity



OUTCROP DOCUMENTATION

Outcrop number:	34
Lithology:	Orthogneiss (16)
Remarks:	light grey, yellowish, greenish to nearly white; rich in quartz; compact

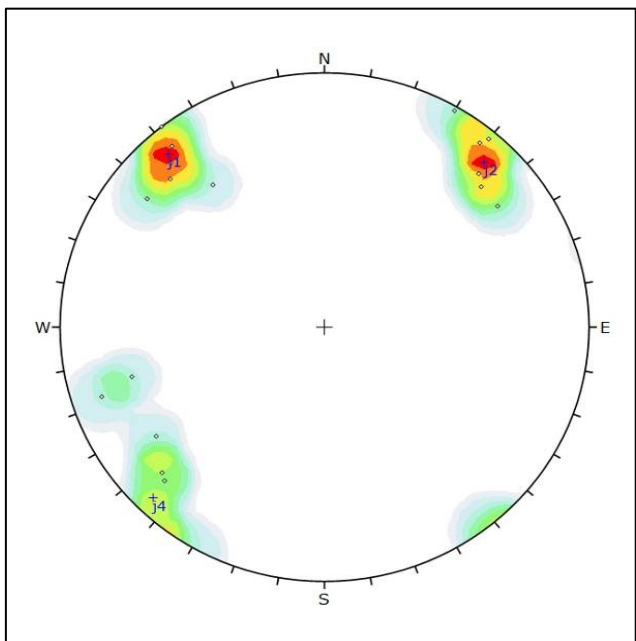
Date:	24.08.2013
--------------	------------

Coordinates (GK M28):	x	12918
	y	219176
		± 10 m

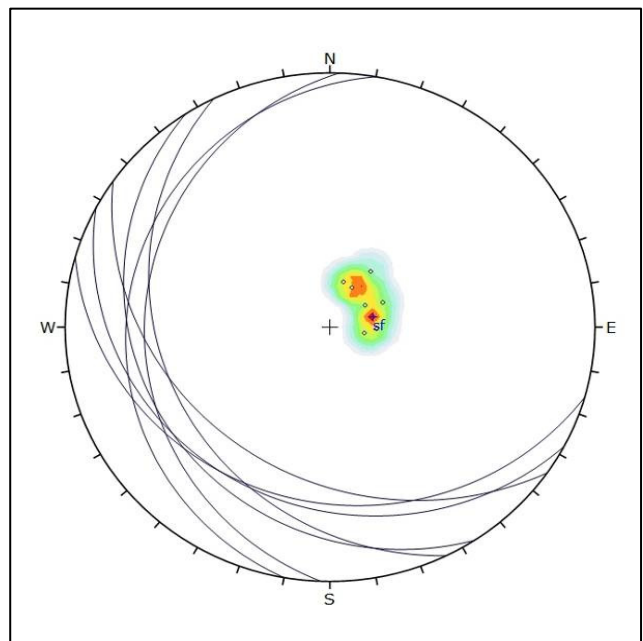
Elevation [m]:	1450
-----------------------	------

Rock material	Weathering	
	<input checked="" type="checkbox"/>	fresh
		slightly weathered
		highly weathered
		completely weathered
	UCS	
		<1 MPa
		1-5 MPa
		5-25 MPa
		25-50 MPa
	<input checked="" type="checkbox"/>	50-100 MPa
		100-250 MPa
		> 250 MPa
	Spacing	
		>2000 mm
		2000-600 mm
		600-200 mm
	<input checked="" type="checkbox"/>	200-60 mm
		60-20 mm
		<20 mm
Block bodies		
	polyhedral	
	tabular	
	prismatic	
<input checked="" type="checkbox"/>	equidimensional	
	rhombic	
	columnar	

Discontinuities	Type / Set		sf	j1	j2	j4				
	Roughness	cm-m	stepped							
			undulating							
			planar	X	X	X	X			
		mm	rough		X	X	X			
			smooth	X						
	Spacing [mm]		> 1	400	500 - 1500	100				
	Aperture [mm]		0 - 10	0 - 1	0 - 2	0 - 1				
	Persistence [m]		> 10	> 4	0.5 - 3	0.2 - 3				
	Water		-	-	-	-				
	Dip direction / Dip		215	30	127	80	220	88	56	75
			244	25	143	70	224	80	47	80
			280	15	138	82	210	89	45	81
			272	20	142	90	234	78	72	83
			237	18	135	79	219	86	75	74
208			20	141	85	227	78			
Remarks										



joint planes



schistosity



OUTCROP DOCUMENTATION

Outcrop number:	77
Lithology:	grey Micaschist (10)
Remarks:	dark grey to greenish, reddish when weathered

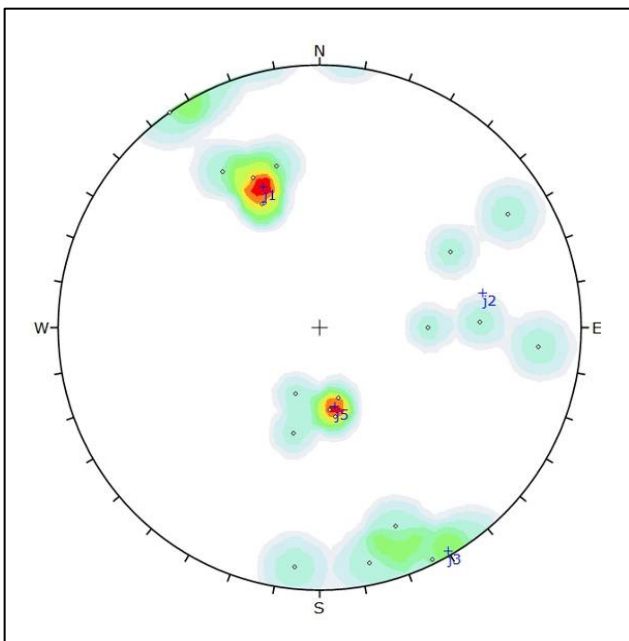
Date:	24.08.2013
--------------	------------

Coordinates (GK M28):	x	12898
	y	217951
		± 7 m

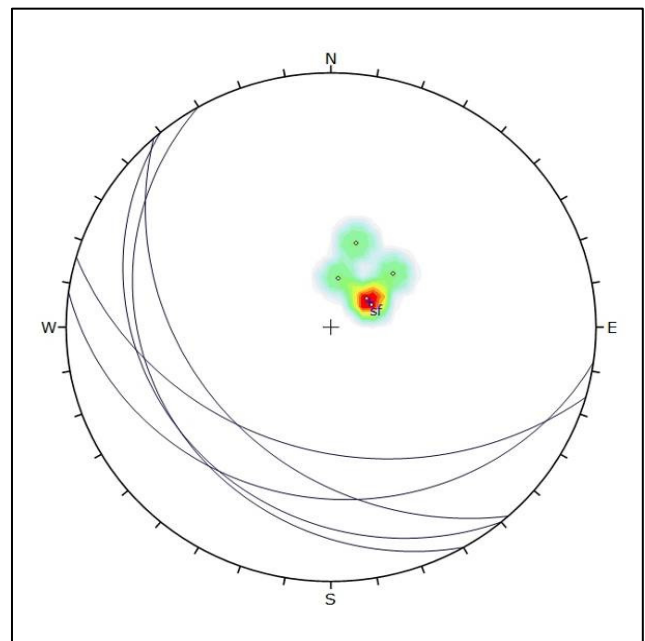
Elevation [m]:	1607
-----------------------	------

Rock material	Weathering	
	<input type="checkbox"/>	fresh
	<input checked="" type="checkbox"/>	slightly weathered
	<input type="checkbox"/>	highly weathered
	<input type="checkbox"/>	completely weathered
	UCS	
	<input type="checkbox"/>	<1 MPa
	<input type="checkbox"/>	1-5 MPa
	<input checked="" type="checkbox"/>	5-25 MPa
	<input type="checkbox"/>	25-50 MPa
	<input type="checkbox"/>	50-100 MPa
	<input type="checkbox"/>	100-250 MPa
	<input type="checkbox"/>	> 250 MPa
	Spacing	
	<input type="checkbox"/>	>2000 mm
	<input type="checkbox"/>	2000-600 mm
	<input type="checkbox"/>	600-200 mm
	<input checked="" type="checkbox"/>	200-60 mm
	<input type="checkbox"/>	60-20 mm
	<input type="checkbox"/>	<20 mm
Block bodies		
<input type="checkbox"/>	polyhedral	
<input type="checkbox"/>	tabular	
<input type="checkbox"/>	prismatic	
<input type="checkbox"/>	equidimensional	
<input checked="" type="checkbox"/>	rhombic	
<input type="checkbox"/>	columnar	

Discontinuities	Type / Set		sf	j1	j2	j3	j5			
	Roughness	cm-m	stepped							
			undulating	X		X	X	X		
			planar		X					
	mm	rough								
		smooth	X	X	X	X	X			
	Spacing [mm]		2 - 50	50 - 200	50 - 1000	50 - 200	20 - 200			
	Aperture [mm]		0	0 - 10	1 - 2	0 - 5	0 - 1			
	Persistence [m]		> 10	> 3	> 2	> 3	0.3 - 2			
	Water		-	-	-	-	-			
Dip direction / Dip		196 38	148 70	270 45	6 85	353 35				
		188 22	156 64	268 63	145 90	20 30				
		230 20	155 55	240 60	348 85	14 45				
		228 35	165 65	239 80	339 78	345 31				
		240 20	156 55	275 80	334 89	350 38				
Remarks										



joint planes



schistosity



OUTCROP DOCUMENTATION

Outcrop number:	121
Lithology:	Phyllonitic Micaschist (8)
Remarks:	strongly foliated, puckered, quartz lenses (1-2 cm thick, rarely up to 10 cm)

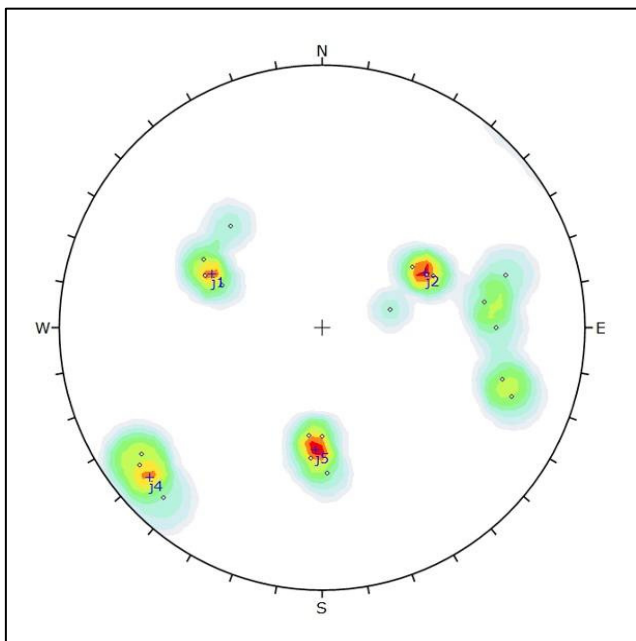
Date:	08.07.2013
--------------	------------

Coordinates (GK M28):	x	12564
	y	219165
		± 8 m

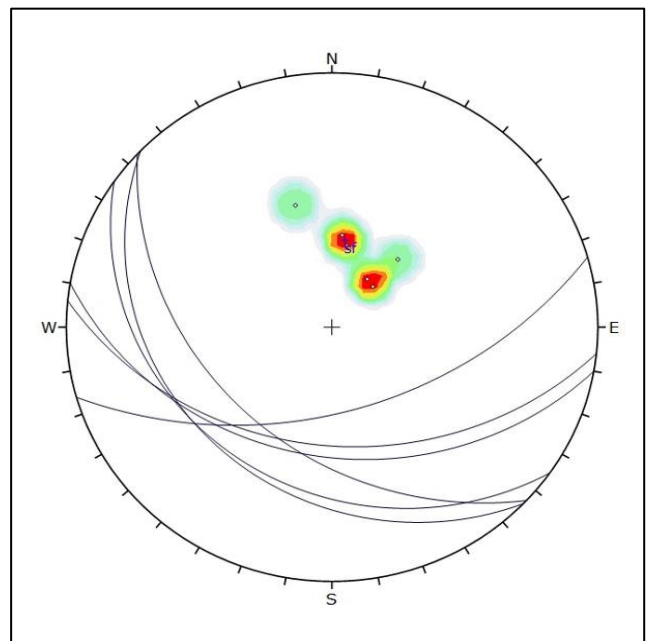
Elevation [m]:	1360
-----------------------	------

Rock material	Weathering	
		fresh
	X	slightly weathered
		highly weathered
		completely weathered
	UCS	
		<1 MPa
		1-5 MPa
	X	5-25 MPa
		25-50 MPa
		50-100 MPa
		100-250 MPa
		> 250 MPa
	Spacing	
		>2000 mm
		2000-600 mm
		600-200 mm
	X	200-60 mm
		60-20 mm
		<20 mm
Block bodies		
	polyhedral	
	tabular	
	prismatic	
	equidimensional	
X	rhombic	
	columnar	

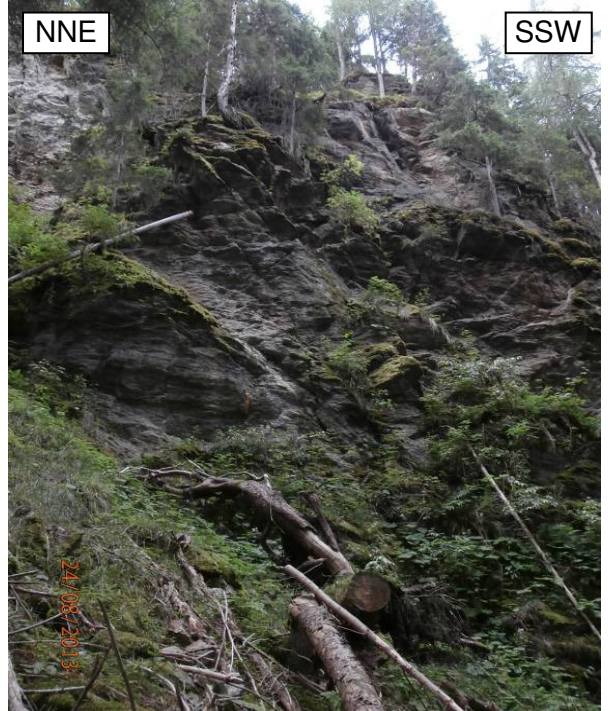
Discontinuities	Type / Set		sf	j1	j2	j4	j5			
	Roughness	cm-m	stepped					X		
			undulating	X	X	X				
			planar				X			
		mm	rough			X		X		
			smooth	X	X		X			
	Spacing [mm]		1	100	200	100 - 500	50 - 100			
	Aperture [mm]		0	0 - 5	0 - 200	0 - 1	0 - 20			
	Persistence [m]		> 10	> 3	> 5	5	>5			
	Water		-	-	-	-	-			
	Dip direction / Dip		190 36	120 55	236 45	55 80	0 45			
			164 53	113 45	245 50	53 82	5 53			
			186 40	114 52	255 30	43 83	358 58			
			215 26	138 55	243 48		7 45			
			223 40		290 75					
		224 25		286 71						
				261 64						
				254 72						
				270 67						
Remarks				plastic fillings		weathered				



joint planes



schistosity



OUTCROP DOCUMENTATION

Outcrop number:	126
Lithology:	dark grey to green Paragneiss (9)
Remarks:	distinctly foliated

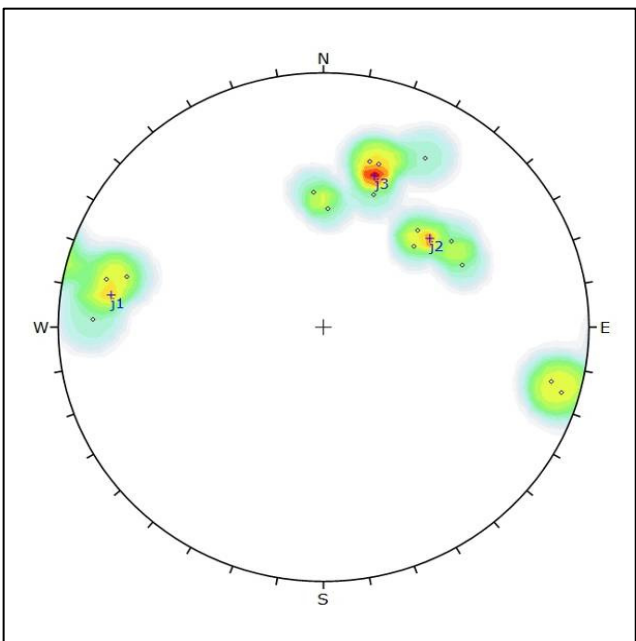
Date:	24.08.2013
--------------	------------

Coordinates (GK M28):	x	12984
	y	219274
		± 12 m

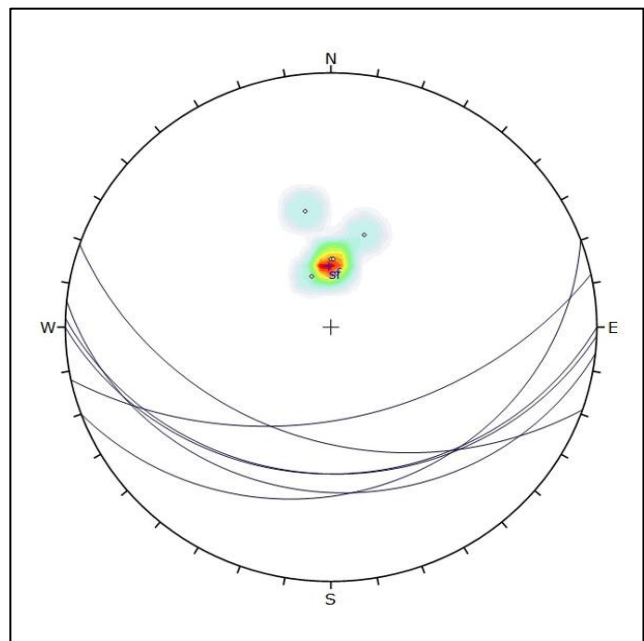
Elevation [m]:	1435
-----------------------	------

Rock material	Weathering	
	<input type="checkbox"/>	fresh
	<input checked="" type="checkbox"/>	slightly weathered
	<input type="checkbox"/>	highly weathered
	<input type="checkbox"/>	completely weathered
	UCS	
	<input type="checkbox"/>	<1 MPa
	<input type="checkbox"/>	1-5 MPa
	<input checked="" type="checkbox"/>	5-25 MPa
	<input type="checkbox"/>	25-50 MPa
	<input type="checkbox"/>	50-100 MPa
	<input type="checkbox"/>	100-250 MPa
	<input type="checkbox"/>	> 250 MPa
	Spacing	
	<input type="checkbox"/>	>2000 mm
	<input type="checkbox"/>	2000-600 mm
	<input type="checkbox"/>	600-200 mm
	<input checked="" type="checkbox"/>	200-60 mm
	<input checked="" type="checkbox"/>	60-20 mm
	<input type="checkbox"/>	<20 mm
Block bodies		
<input type="checkbox"/>	polyhedral	
<input type="checkbox"/>	tabular	
<input type="checkbox"/>	prismatic	
<input type="checkbox"/>	equidimensional	
<input checked="" type="checkbox"/>	rhombic	
<input type="checkbox"/>	columnar	

Discontinuities	Type / Set		sf	j1	j2	j3				
	Roughness	cm-m	stepped							
			undulating	X	X					
		mm	planar			X	X			
			rough			X				
		smooth	X	X		X				
	Spacing [mm]		1	40 - 400	100 - 200	50 - 100				
	Aperture [mm]		0	0	0 - 1	0 - 1				
	Persistence [m]		> 10	> 3	> 5	> 2				
	Water		-	-	-	-				
Dip direction / Dip		199	42	105	75	210	75	176	56	
		186	24	92	82	223	55	182	50	
		180	30	103	80	227	50	195	68	
		168	50	286	86	235	61	198	68	
		182	30	284	83	245	60	200	58	
		160	24							
Remarks			partly slickensides							



joint planes



schistosity





OUTCROP DOCUMENTATION

Outcrop number:	143
Lithology:	Phyllonitic Micaschist (8)
Remarks:	quartz lenses and veins (1-3 cm thick), schistosity at the range of mm and folded

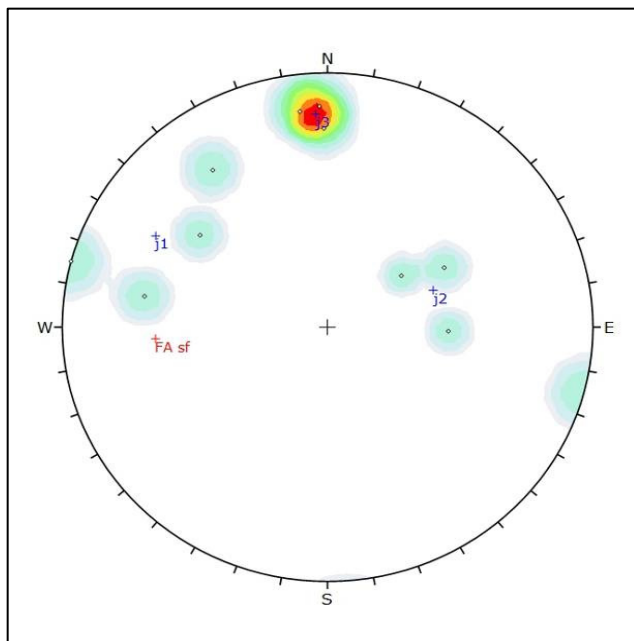
Date:	10.07.2013
--------------	------------

Coordinates (GK M28):	x	12679
	y	218945
		± 9 m

Elevation [m]:	1390
-----------------------	------

Rock material	Weathering	
		fresh
	<input checked="" type="checkbox"/>	slightly weathered
		highly weathered
		completely weathered
	UCS	
		<1 MPa
		1-5 MPa
	<input checked="" type="checkbox"/>	5-25 MPa
		25-50 MPa
		50-100 MPa
		100-250 MPa
		> 250 MPa
	Spacing	
		>2000 mm
		2000-600 mm
	<input checked="" type="checkbox"/>	600-200 mm
	<input checked="" type="checkbox"/>	200-60 mm
		60-20 mm
		<20 mm
Block bodies		
<input checked="" type="checkbox"/>	polyhedral	
<input checked="" type="checkbox"/>	tabular	
	prismatic	
	equidimensional	
	rhombic	
	columnar	

Discontinuities	Type / Set		sf	j1	j2	j3				
	Roughness	cm-m	stepped							
			undulating	X	X	X	X			
			planar							
		mm	rough			X				
			smooth	X	X		X			
	Spacing [mm]		1	50 - 500	500	300 - 600				
	Aperture [mm]		0	0 - 250	20	< 15				
	Persistence [m]		> 10	> 5	> 5	> 10				
	Water		-	-	-	-				
	Dip direction / Dip		FA:	100	70	234	38	173	81	
			266	23	105	90	242	53	179	76
			265	25	127	62	272	49	178	82
					145	74				
	Remarks			partly slickensides		parallel to outcrop surface				



joint planes and fold axis of the schistosity (FA sf)



outcrop surface parallel to j3 (view ~ towards N)



open fractures parallel to j3



open fracture parallel to j1

OUTCROP DOCUMENTATION

Outcrop number:	169
Lithology:	grey Micaschist (10)
Remarks:	dark grey to green, light brown when weathered, strongly foliated and puckered, rich in quartz, quartz lenses up to ~10 cm thickness

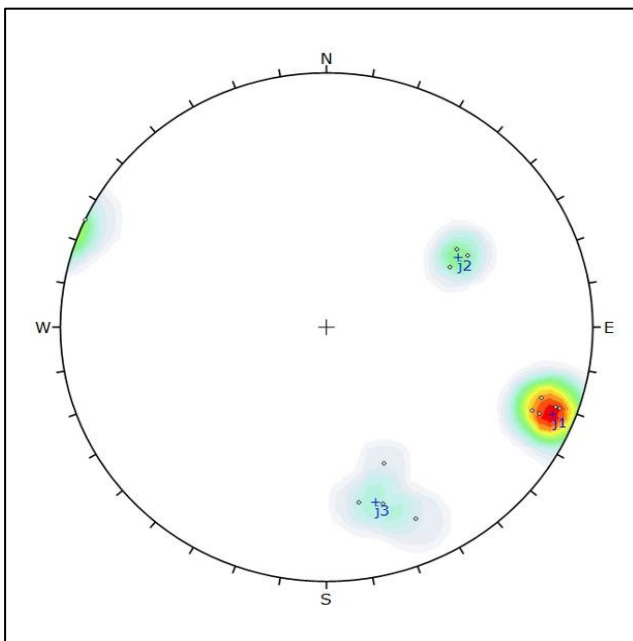
Date:	24.08.2013
--------------	------------

Coordinates (GK M28):	x	12953
	y	217971
		± 17 m

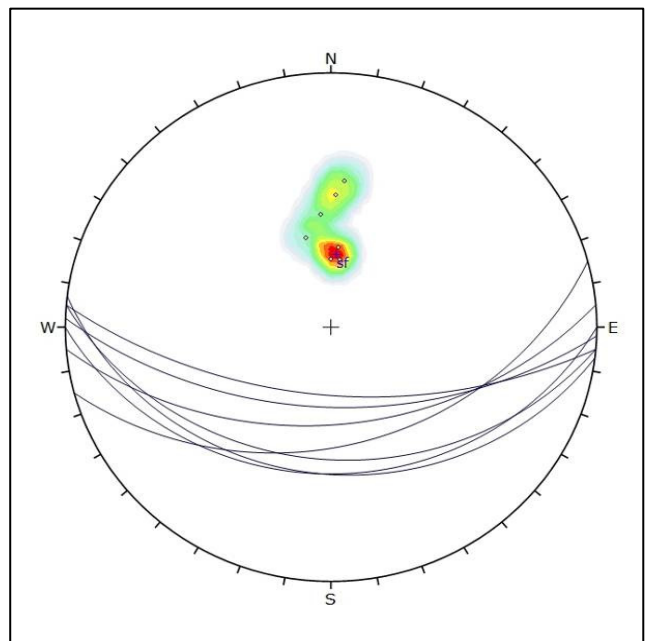
Elevation [m]:	1600
-----------------------	------

Rock material	Weathering	
	<input type="checkbox"/>	fresh
	<input checked="" type="checkbox"/>	slightly weathered
	<input type="checkbox"/>	highly weathered
	<input type="checkbox"/>	completely weathered
	UCS	
	<input type="checkbox"/>	<1 MPa
	<input type="checkbox"/>	1-5 MPa
	<input checked="" type="checkbox"/>	5-25 MPa
	<input type="checkbox"/>	25-50 MPa
	<input type="checkbox"/>	50-100 MPa
	<input type="checkbox"/>	100-250 MPa
	<input type="checkbox"/>	> 250 MPa
	Spacing	
	<input type="checkbox"/>	>2000 mm
	<input type="checkbox"/>	2000-600 mm
	<input checked="" type="checkbox"/>	600-200 mm
	<input checked="" type="checkbox"/>	200-60 mm
	<input type="checkbox"/>	60-20 mm
	<input type="checkbox"/>	<20 mm
Block bodies		
<input type="checkbox"/>	polyhedral	
<input type="checkbox"/>	tabular	
<input type="checkbox"/>	prismatic	
<input type="checkbox"/>	equidimensional	
<input checked="" type="checkbox"/>	rhombic	
<input type="checkbox"/>	columnar	

Discontinuities	Type / Set		sf	j1	j2	j3				
	Roughness	cm-m	stepped		X	X				
			undulating	X			X			
			planar							
		mm	rough			X				
			smooth	X	X			X		
	Spacing [mm]		1 - 5	300 - 1000	100 - 500	150 - 500				
	Aperture [mm]		0 - 2	1 - 10	1 - 2	0 - 10				
	Persistence [m]		> 10	> 5	3 - 4	> 2				
	Water		-	-	-	-				
	Dip direction / Dip		165 40	293 80	242 62	338 60				
			175 48	290 86	243 55	336 79				
			185 35	289 81	238 60	343 72				
			187 30	293 82		350 70				
			182 55	290 85						
180 30			115 90							
FA:		278	27							
Remarks			partly slickensides		partly slickensides					



joint planes



schistosity



OUTCROP DOCUMENTATION

Outcrop number:	62
Lithology:	Alluvium (1)
Remarks:	

Date:	14.06.2013
--------------	------------

Coordinates (GK M28):	x	11689
	y	218132
		± 9 m

Elevation [m]:	960
-----------------------	-----

Material description
sandy gravel (*sa Gr*) featuring subrounded grains, containing also cobbles, boulders and large boulders with diameters of up to ~80 cm which are rounded;
loose state;
components consist of micaschists, paragneisses, orthogneisses and amphibolites;

OUTCROP DOCUMENTATION

Outcrop number:	65
Lithology:	Moraine Deposit (6)
Remarks:	probably no accumulation in terms of ground or side moraines, but sediments that were deposited at the margin of dead ice bodies

Date:	14.06.2013
--------------	------------

Coordinates (GK M28):	x	11798
	y	218163
		± 7 m

Elevation [m]:	1010
-----------------------	------

Material description

silty, sandy gravel (*si sa Gr*) containing also cobbles and boulders with maximum diameters of 20-30 cm; only rarely large boulders (up to 2 m in diameter) were observed;
 components are subrounded to rounded and are not sorted;
 deposit is not compacted but packed in a natural to dense state; glacial striation can only be seen very rarely
 the observed rock types of the components are: different micaschists, paragneisses, orthogneisses, amphibolites, diabases;
 colour is light brown if the deposits are dry and middle brown in a moist state;



OUTCROP DOCUMENTATION

Outcrop number:	75
Lithology:	Moraine Deposit mixed with Talus (5)
Remarks:	

Date:	14.06.2013
--------------	------------

Coordinates (GK M28):	x	12975
	y	217721
		± 8 m

Elevation [m]:	1645
-----------------------	------

Material description

silty, sandy gravel (*si sa Gr*) containing minor cobbles and boulders up to a maximum diameter of ~30 cm;
 components are angular to subrounded or rounded;
 deposit generally is unsorted and ungraded, but can feature layers without cobbles; it is packed in a natural state;
 the observed rock types of the components are: different micaschists, paragneisses, orthogneisses and amphibolites;
 colour is light brown to grey in dry state and middle brown to ochre in moist state;



OUTCROP DOCUMENTATION

Outcrop number:	76
Lithology:	Moraine Deposit (6)
Remarks:	

Date:	14.06.2013
--------------	------------

Coordinates (GK M28):	x	12874
	y	217943
		± 5 m

Elevation [m]:	1615
-----------------------	------

Material description

silty, sandy gravel (*si sa Gr*) containing also cobbles and boulders up to a maximum diameter of 50 cm;
 components are subrounded to rounded and are not sorted;
 deposit is not compacted but packed in a natural to dense state; glacial striation can only be seen very rarely
 the observed rock types of the components are: micaschists, garnet micaschists, paragneisses, amphibolites and garnet
 amphibolites, orthogneisses (augengneisses), diabases and carbonates;
 colour is light brown to greyish in dry state and middle brown to ochre in moist state;



OUTCROP DOCUMENTATION

Outcrop number:	97
Lithology:	Talus (2)
Remarks:	talus fan originating from secondary scarp to the river Trisanna

Date:	18.06.2013
--------------	------------

Coordinates (GK M28):	x	11872
	y	219111
		± 8 m

Elevation [m]:	915
-----------------------	-----

Material description

sandy gravel with cobbles (*sa co Gr*) containing also boulders up to ~50 cm in diameter;
components are angular to subangular and show increasing grainsize with the distance from the rock wall;
loose state;
components only consist of the phyllonitic micaschists (8)



OUTCROP DOCUMENTATION

Outcrop number:	152
Lithology:	Rockfall blocks (3)
Remarks:	

Date:	10.07.2013
--------------	------------

Coordinates (GK M28):	x	13162
	y	218818
		± 10 m

Elevation [m]:	1585
-----------------------	------

Material description

boulders (*Bo*) and large boulders (*LBo*) with diameters up to ~3 m, generally showing increasing grainsize with the distance from the rock wall;
 components are angular and consist of the dark grey to green paragneisses (9)



OUTCROP DOCUMENTATION

Outcrop number:	168
Lithology:	Landslide Debris (4)
Remarks:	

Date:	24.08.2013	
Coordinates (GK M28):	x	12993
	y	218409
		± 6 m
Elevation [m]:	1535	

Material description

large boulders with boulders and cobbles (*bo co LBo*) with maximum diameters of ~5 m;
 components are angular and consist of the phyllonitic micaschists (8);
 deposit is disintegrated and unsorted featuring crevices and fractures;
 hummocky morphology;



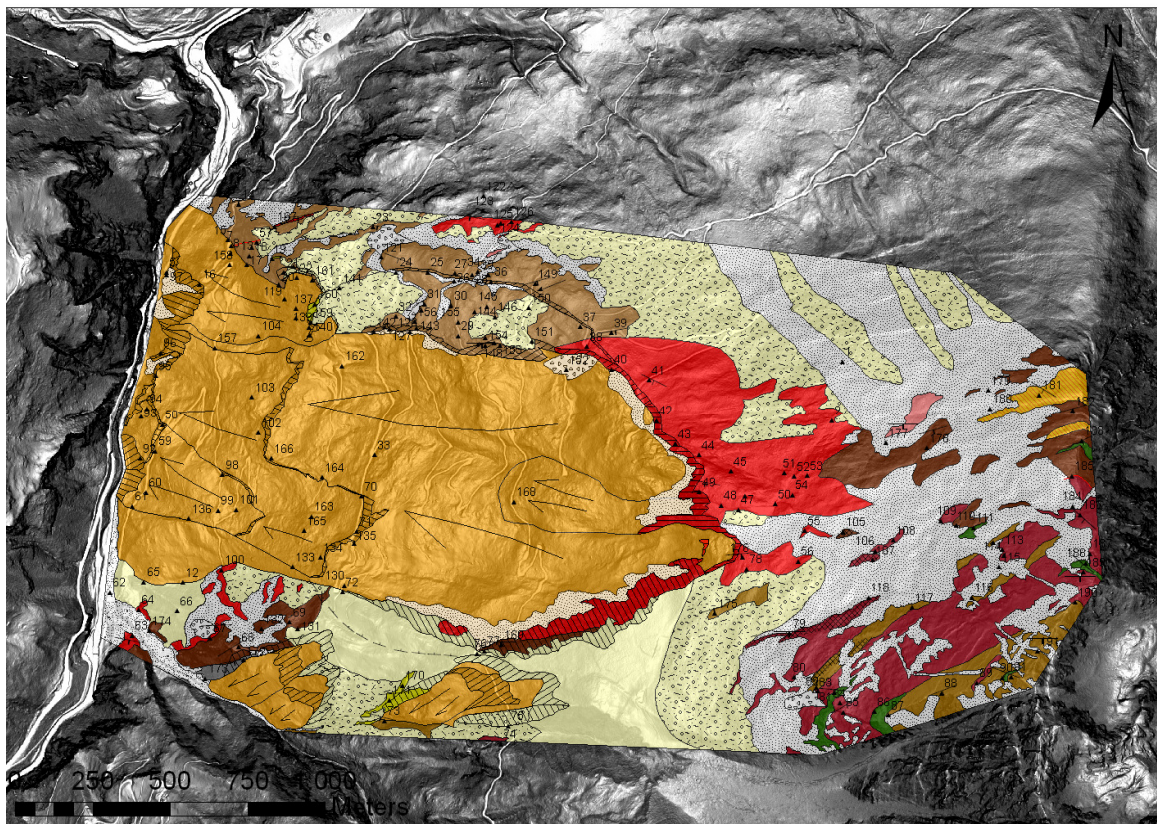
Appendix 4: Structural measurements

Schistosity										
Point number	Dip Direction	Dip		Point number	Dip Direction	Dip		Point number	Dip Direction	Dip
6	169	57		79	162	35		131	180	55
14	172	52		80	270	41		131	173	50
14	185	35		81	193	43		131	178	40
14	169	47		82	305	67		132	163	75
14	151	60		83	185	37		147	320	75
15	153	60		85	150	43		147	340	83
15	166	67		86	147	38		147	165	70
23	208	42		87	160	65		149	165	25
23	193	35		88	170	54		153	255	10
23	210	35		89	168	30		154	193	60
23	189	33		90	200	30		154	161	70
23	190	44		91	167	45		159	192	18
23	162	35		105	160	35		159	187	38
25	257	25		107	220	32		159	210	16
28	260	30		108	236	35		160	108	30
28	275	20		109	238	42		160	100	26
28	267	28		110	203	60		167	178	55
28	303	27		110	175	75		167	181	56
28	285	15		111	210	38		167	171	50
28	175	51		112	175	45		167	55	49
34	215	30		113	260	23		167	35	36
34	244	25		114	200	23		169	165	40
34	280	15		115	247	15		169	175	48
34	272	20		116	153	23		169	185	35
34	237	18		117	260	30		169	187	30
34	208	20		118	192	48		169	182	55
34	196	21		120	193	37		169	180	30
38	187	43		120	195	46		169	185	60
39	170	40		120	170	25		170	180	67
41	205	38		120	183	45		171	170	75
42	208	43		120	215	36		172	170	64
45	155	57		121	190	36		175	165	50
45	150	65		121	164	53		176	171	55
47	200	50		121	186	40		177	180	39
48	175	63		121	215	26		178	158	30
49	187	43		121	223	40		178	175	40
50	210	50		121	224	25		180	193	30
52	175	57		122	190	60		180	210	40
53	170	60		123	207	43		181	220	31
54	175	45		123	215	15		181	213	20
55	172	55		124	180	45		182	166	41
56	173	48		124	183	45		183	156	25
63	190	25		124	177	35		184	216	28
64	145	75		125	212	40		184	240	25
67	178	60		125	182	37		186	174	10
68	145	40		125	173	45		186	240	15
73	194	53		125	208	32		187	150	28
77	196	38		126	199	42		188	223	80
77	188	22		126	186	24		188	210	13
77	230	20		126	180	30		188	220	23
77	228	35		126	168	50		189	184	30
77	240	20		126	182	30		189	176	27
78	182	60		126	160	24		190	177	44
79	205	20		129	274	53		191	180	65

Fold axes		
Point number	Dip direction	Dip
23	247	25
127	260	20
127	280	15
128	260	20
129	272	30
129	252	28
129	243	34
129	202	39
143	266	23
143	265	25
147	255	10
147	247	14
149	249	30
160	84	15
161	65	25
169	278	27

Faults		
Point number	Dip direction	Dip
7	160	75
18	200	35
185	190	40

Slickensides		
Point number	Dip direction	Dip
15	115	67
15	238	65
15	163	52
15	260	67
17	243	65
18	110	90
20	207	57
142	87	45



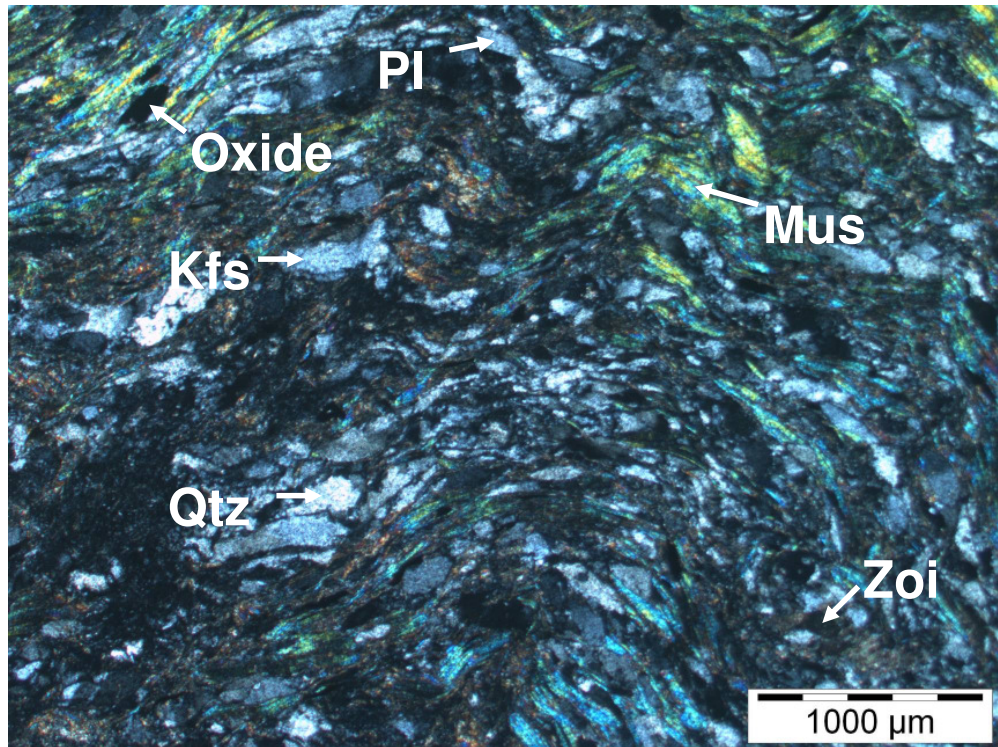
Geologic map with the positions of all documented field points (map legend see Appendix 1)

Appendix 5: Thin sections

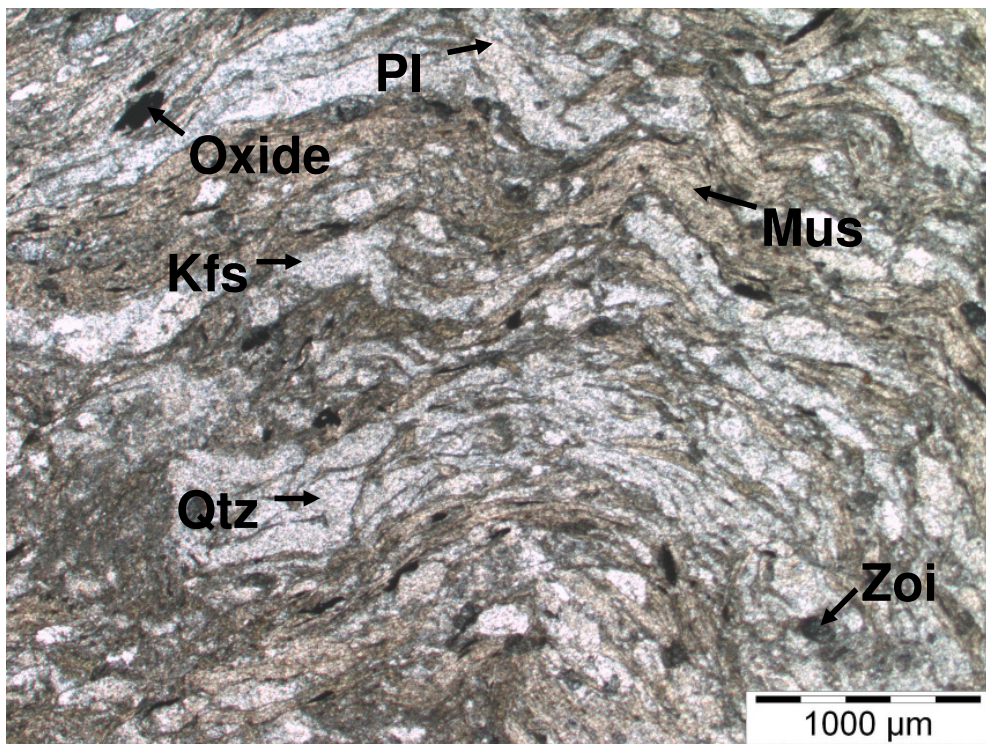
Mineral abbreviations:

Qtz ... Quartz
Pl ... Plagioclase
Kfs ... Kalifeldspar
Mus ... Muscovite
Bt ... Biotite
Ser ... Sericite
Chl ... Chlorite
Grt ... Garnet
Zoi ... Zoisite
CZoi ... Clinozoisite
Hbl ... Hornblende
Cc ... Calcite
Ap ... Apatite
Pyr ... Pyrite

1: Phyllonitic micaschist (8)

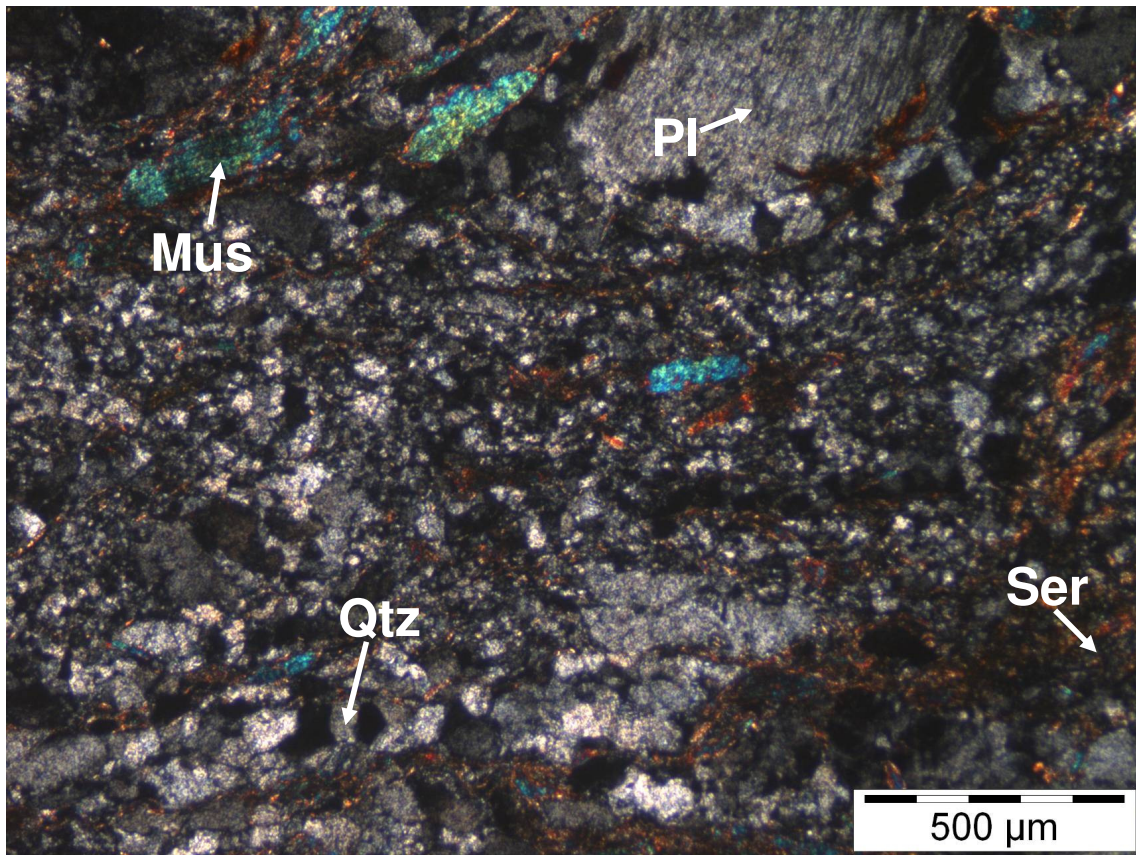


Transmitting light with analysator

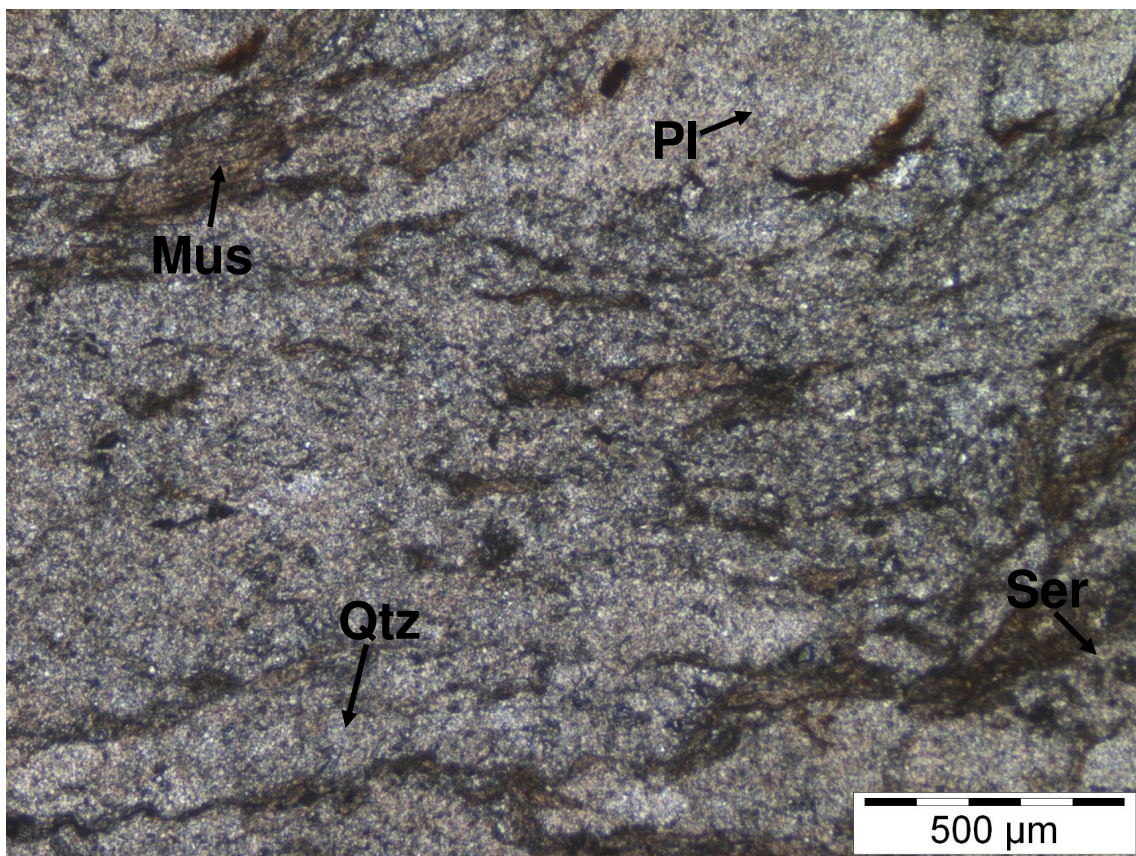


Transmitting light without analysator

2: Orthogneiss (16)

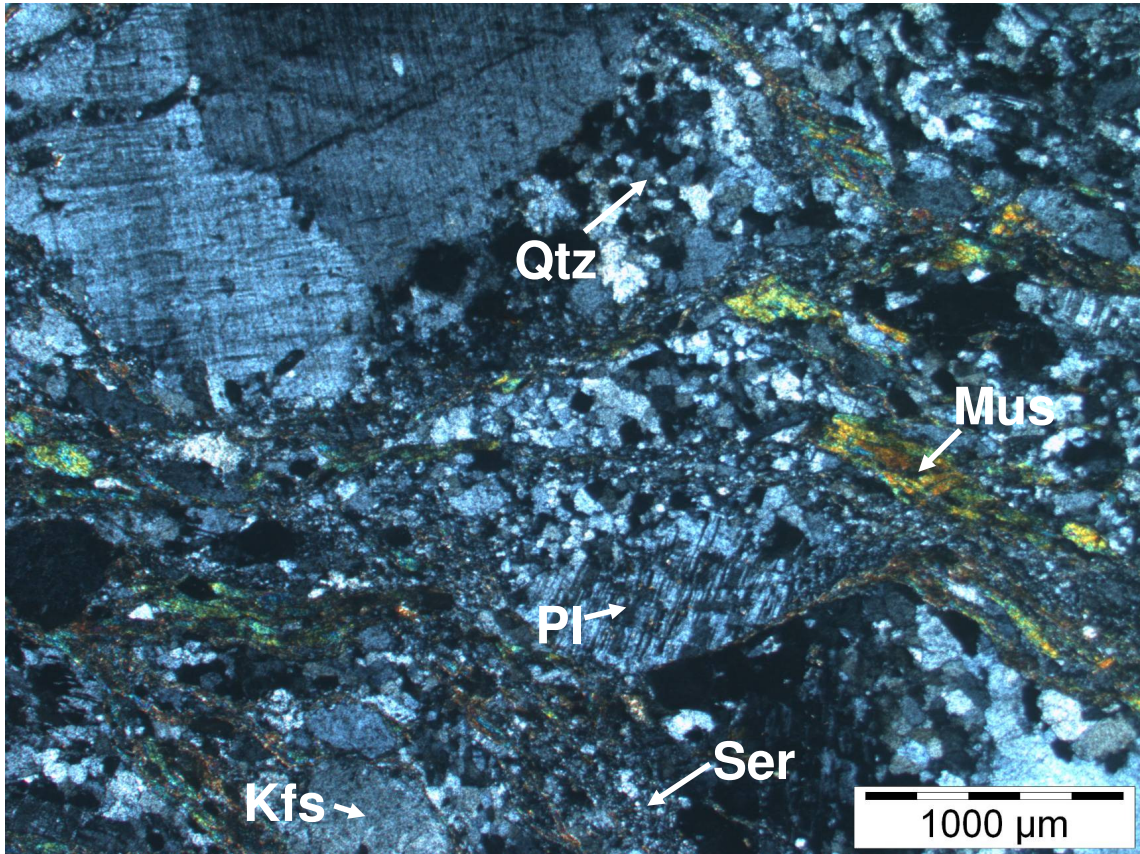


Transmitting light with analysator

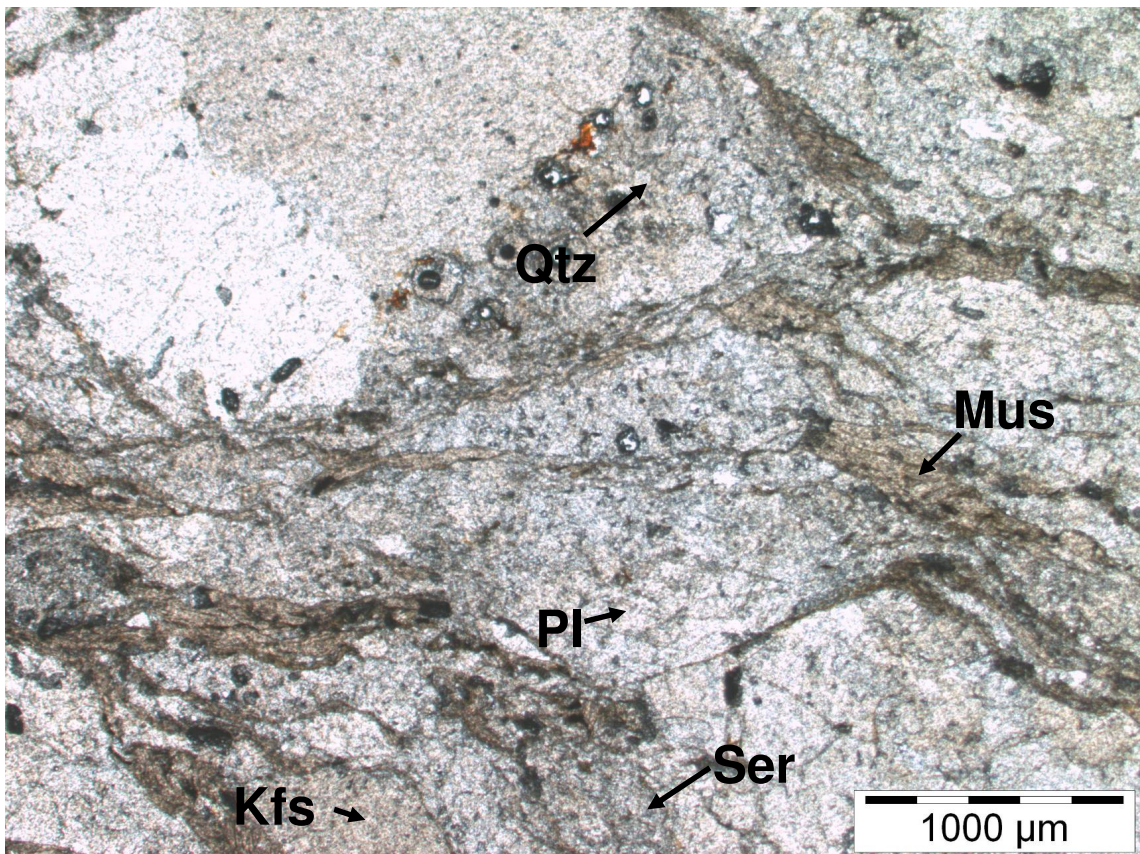


Transmitting light without analysator

3: Orthogneiss (16)

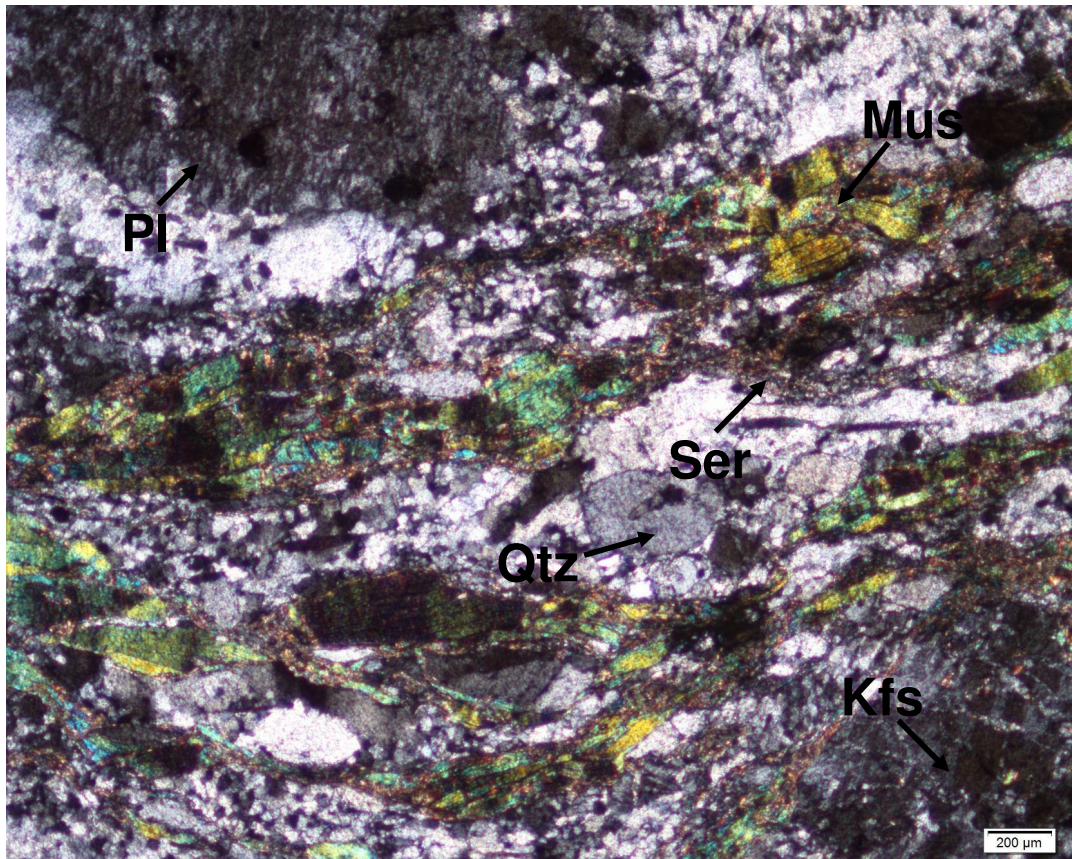


Transmitting light with analysator

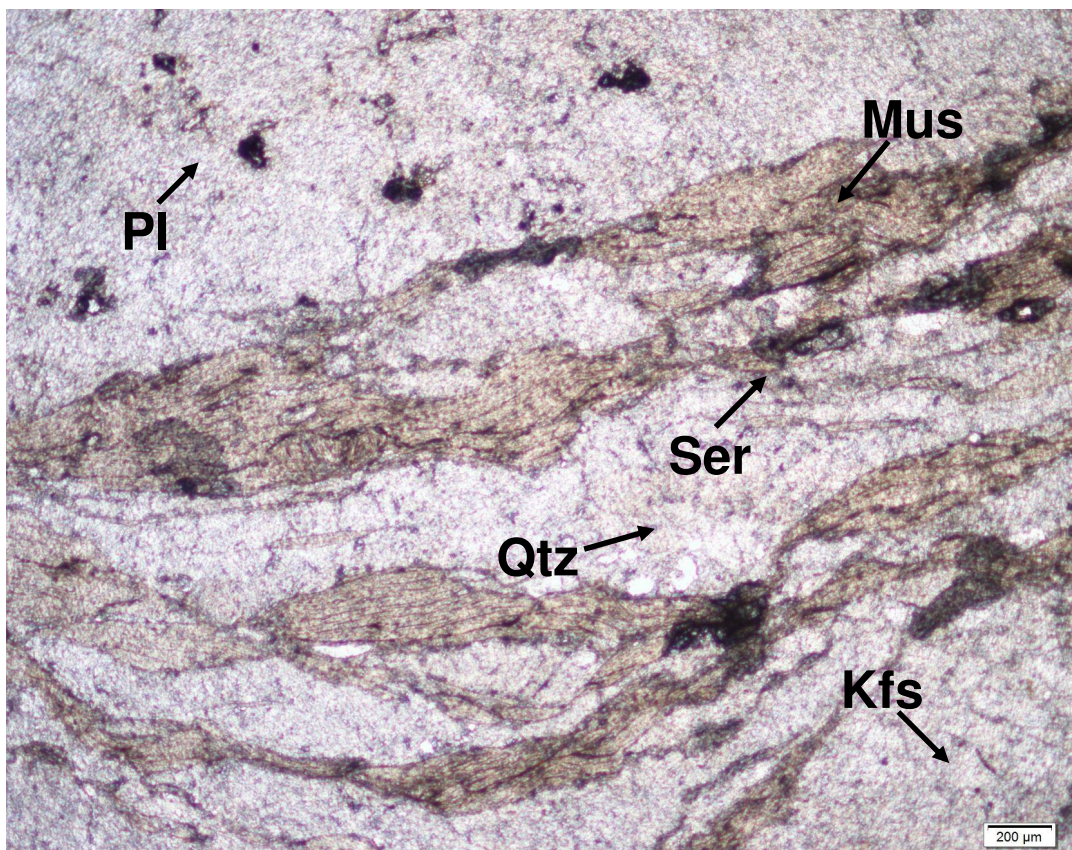


Transmitting light without analysator

4: Orthogneiss (16)

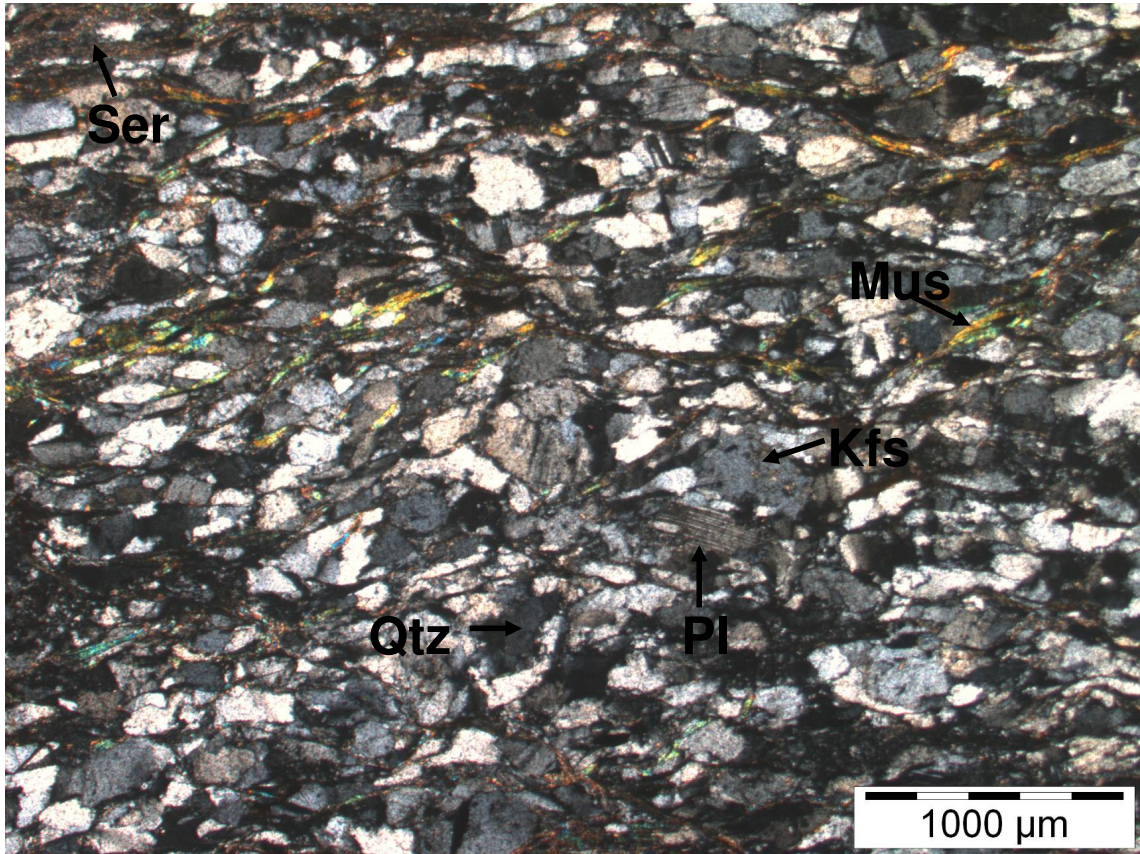


Transmitting light with analysator

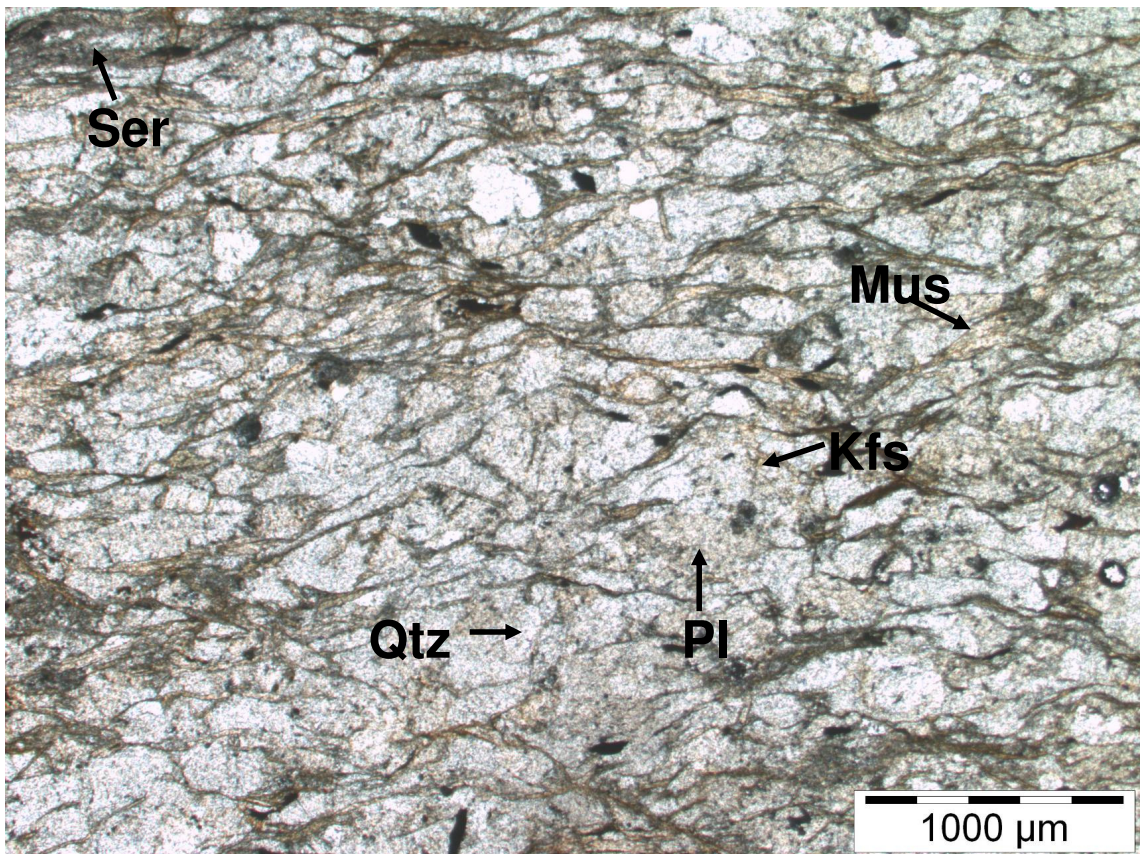


Transmitting light without analysator

5: Paragneiss, dark grey, green (9)

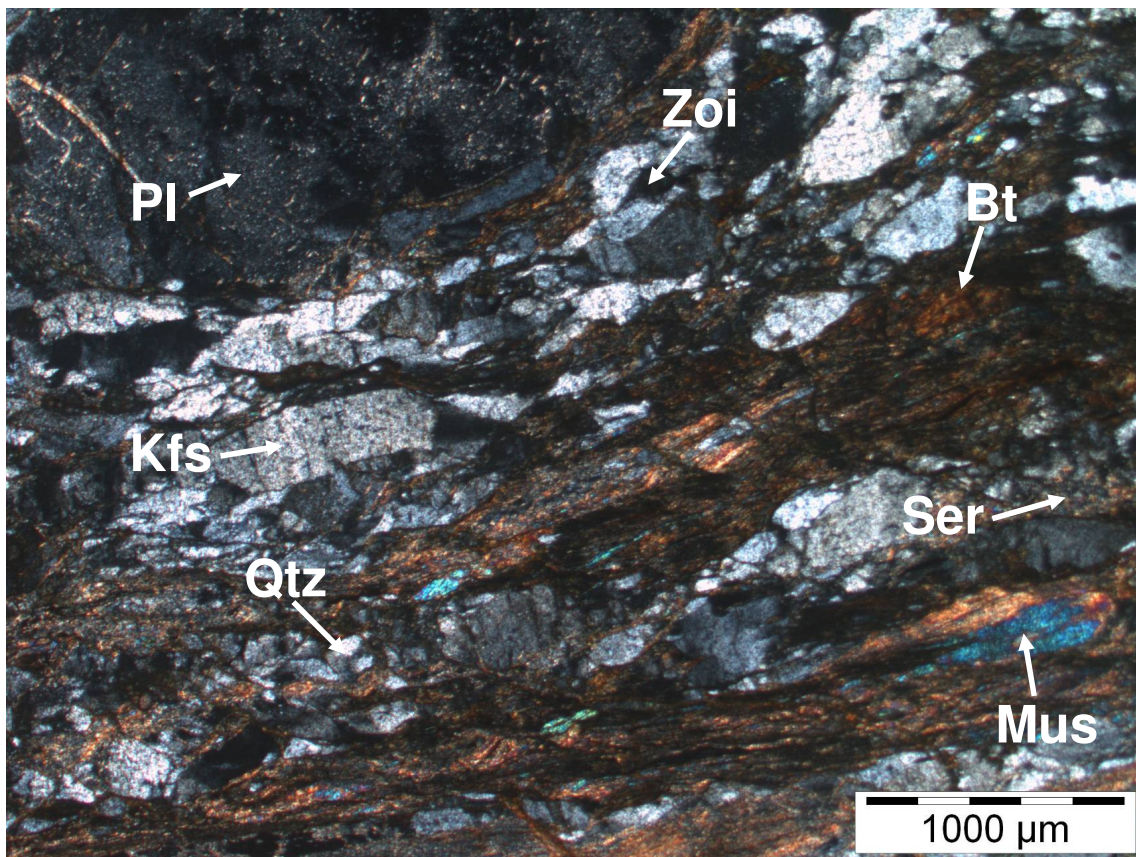


Transmitting light with analyser

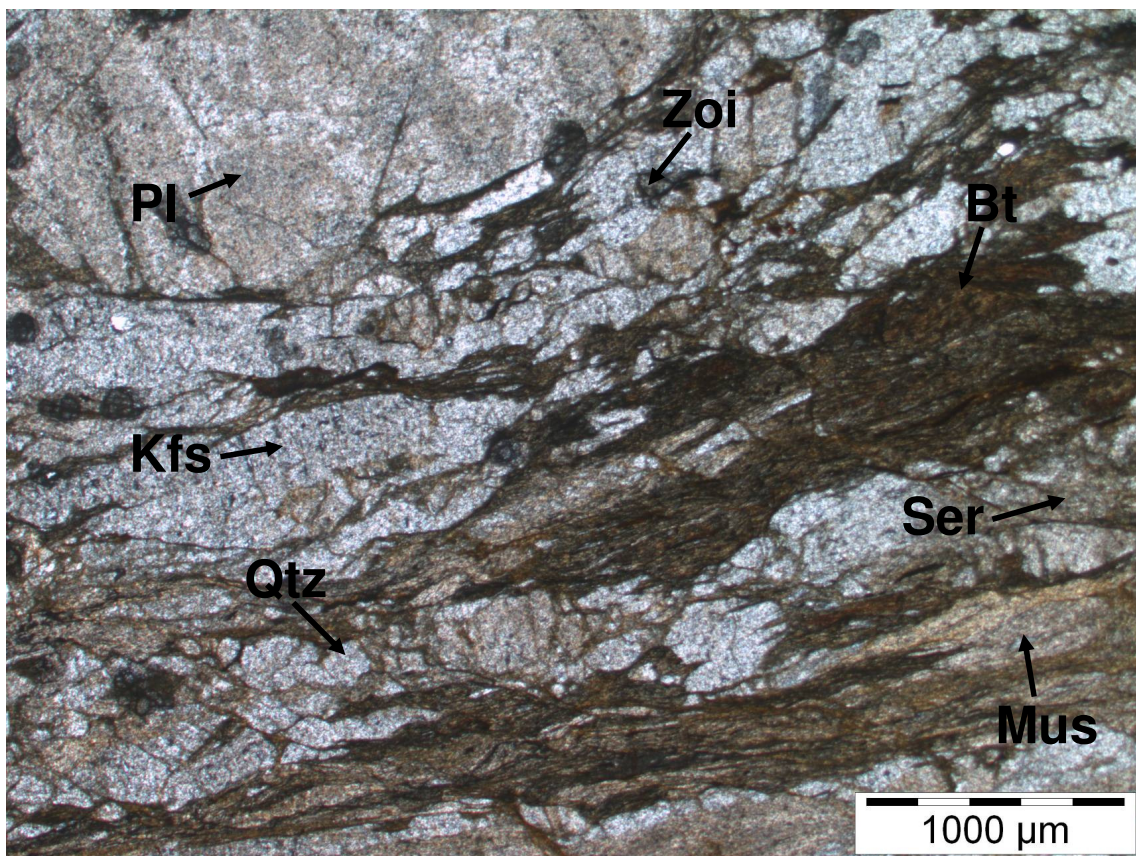


Transmitting light without analyser

6: Cataclasite

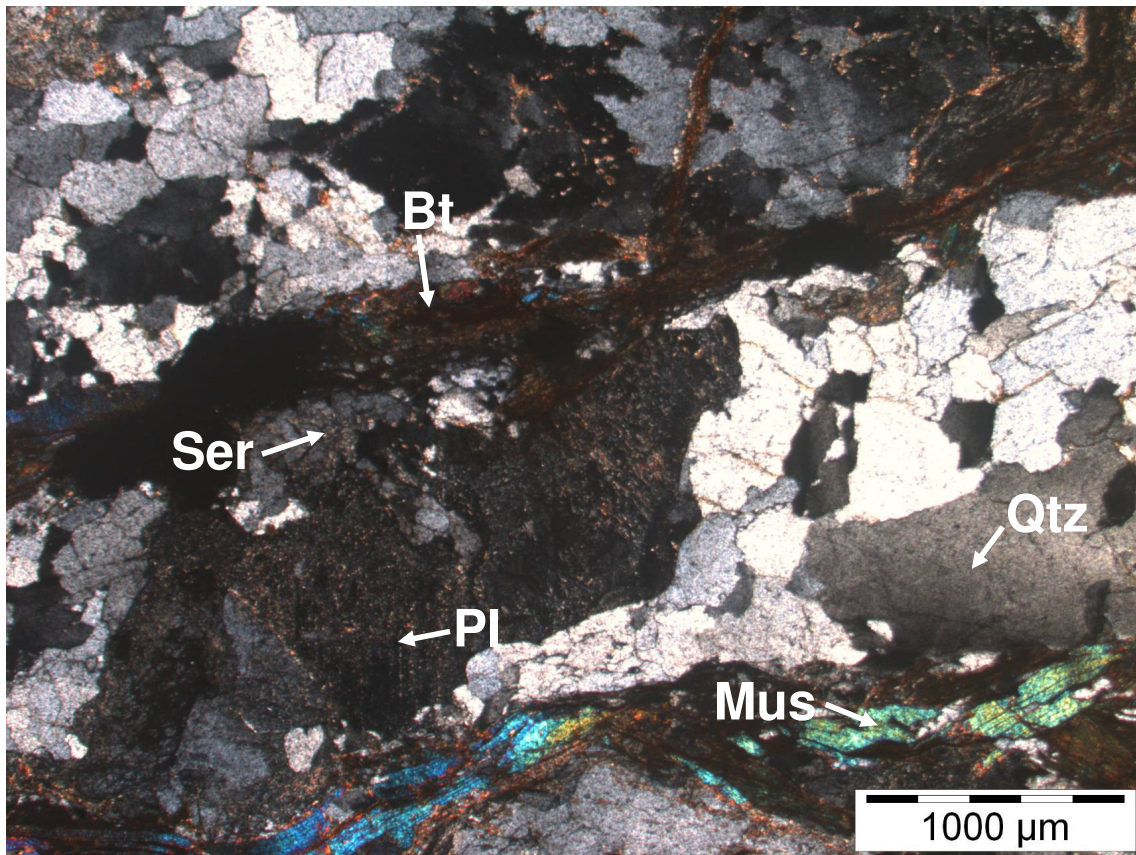


Transmitting light with analysator

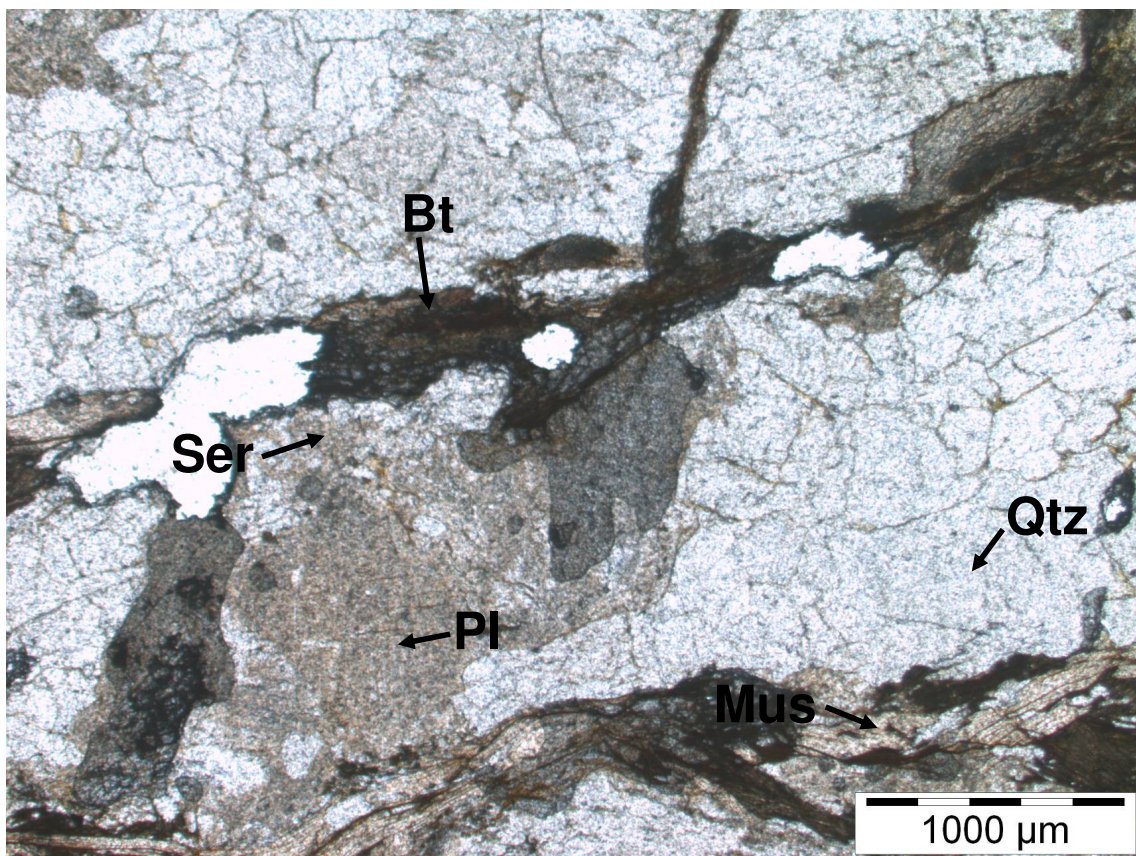


Transmitting light without analysator

7: Paragneiss, grey, brown (11)

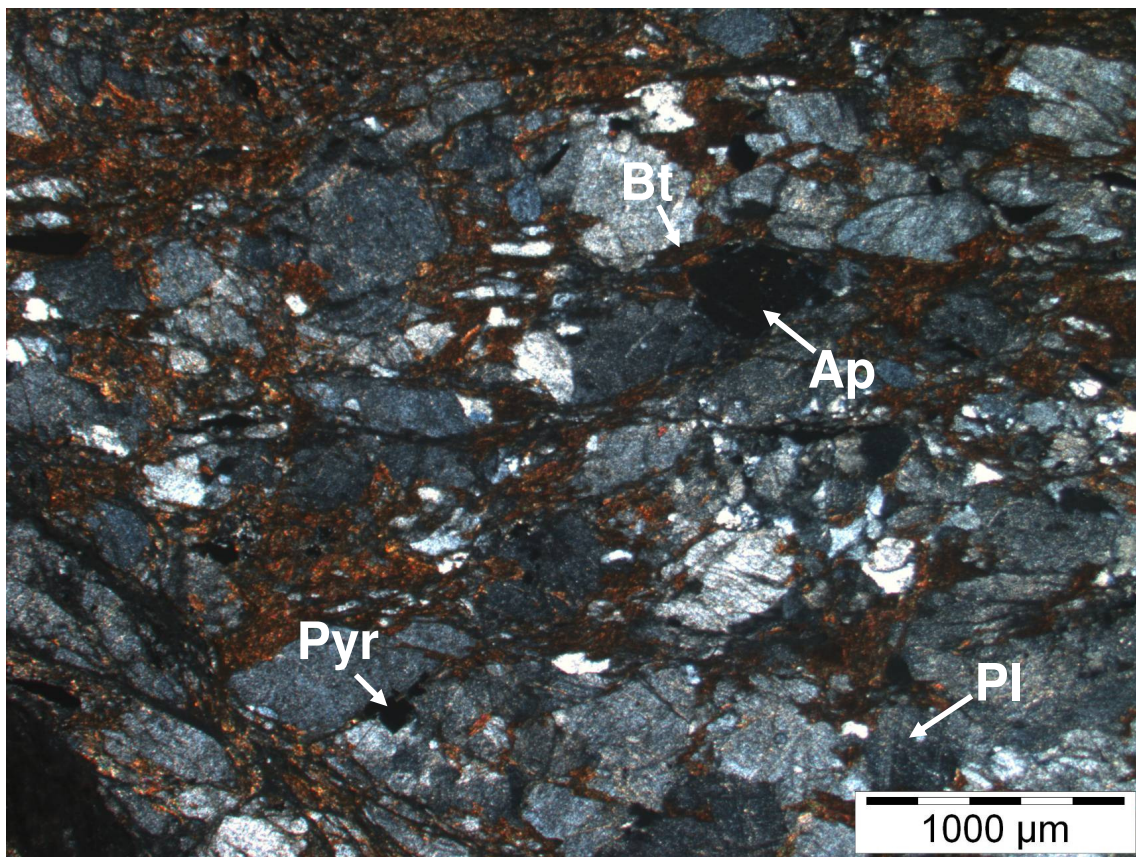


Transmitting light with analyser

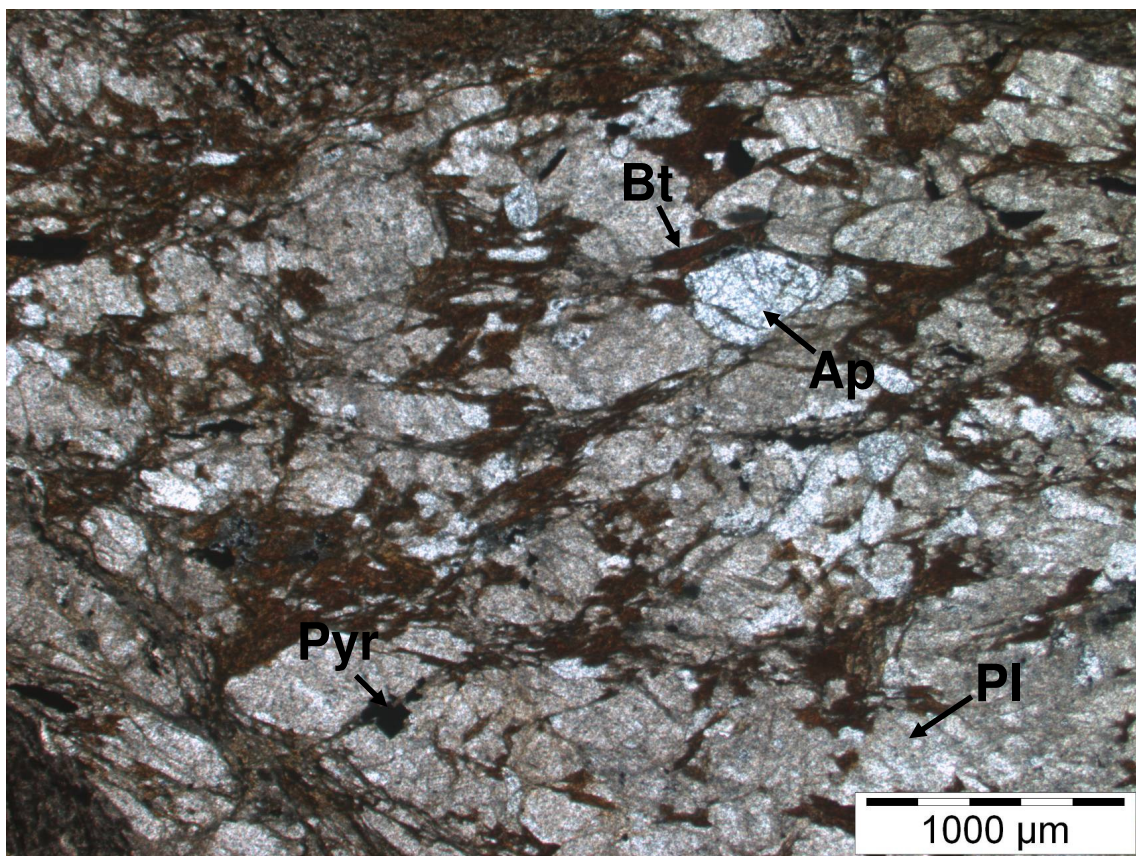


Transmitting light without analyser

8: Cataclasite

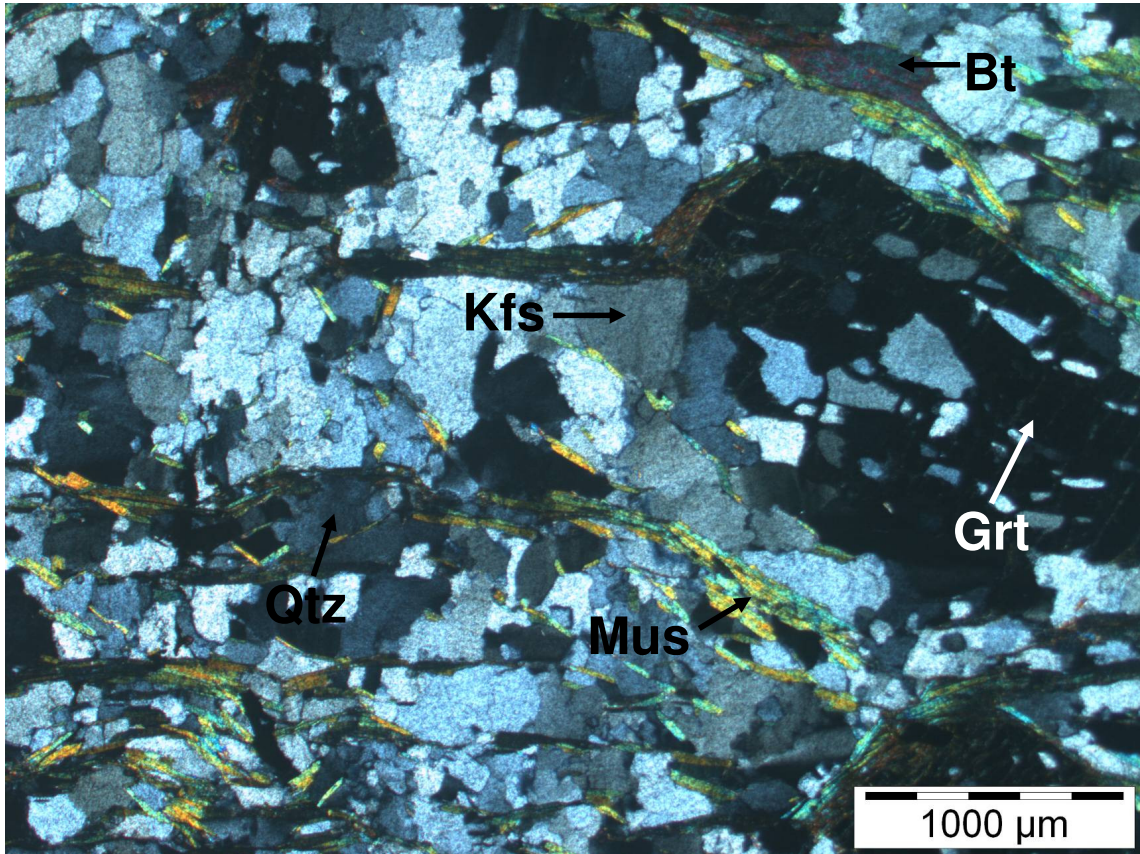


Transmitting light with analyser

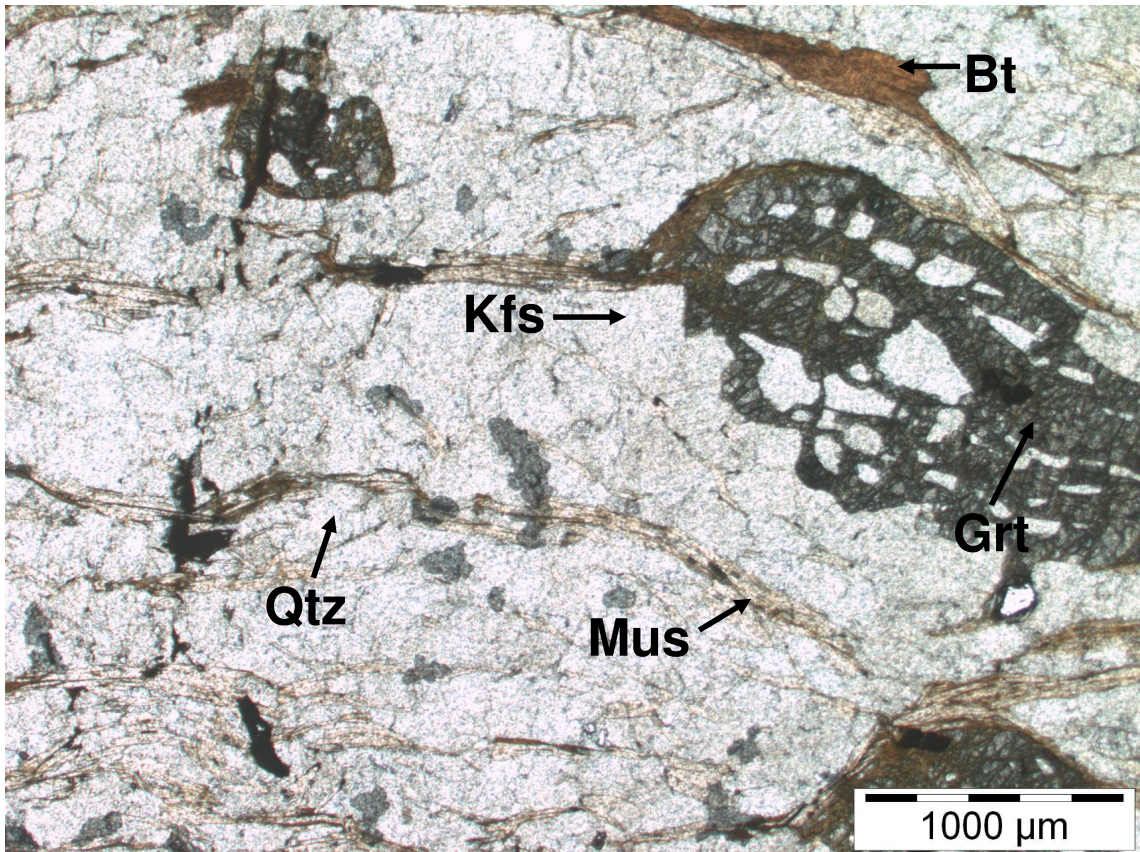


Transmitting light without analyser

9: Garnet micaschist (15)

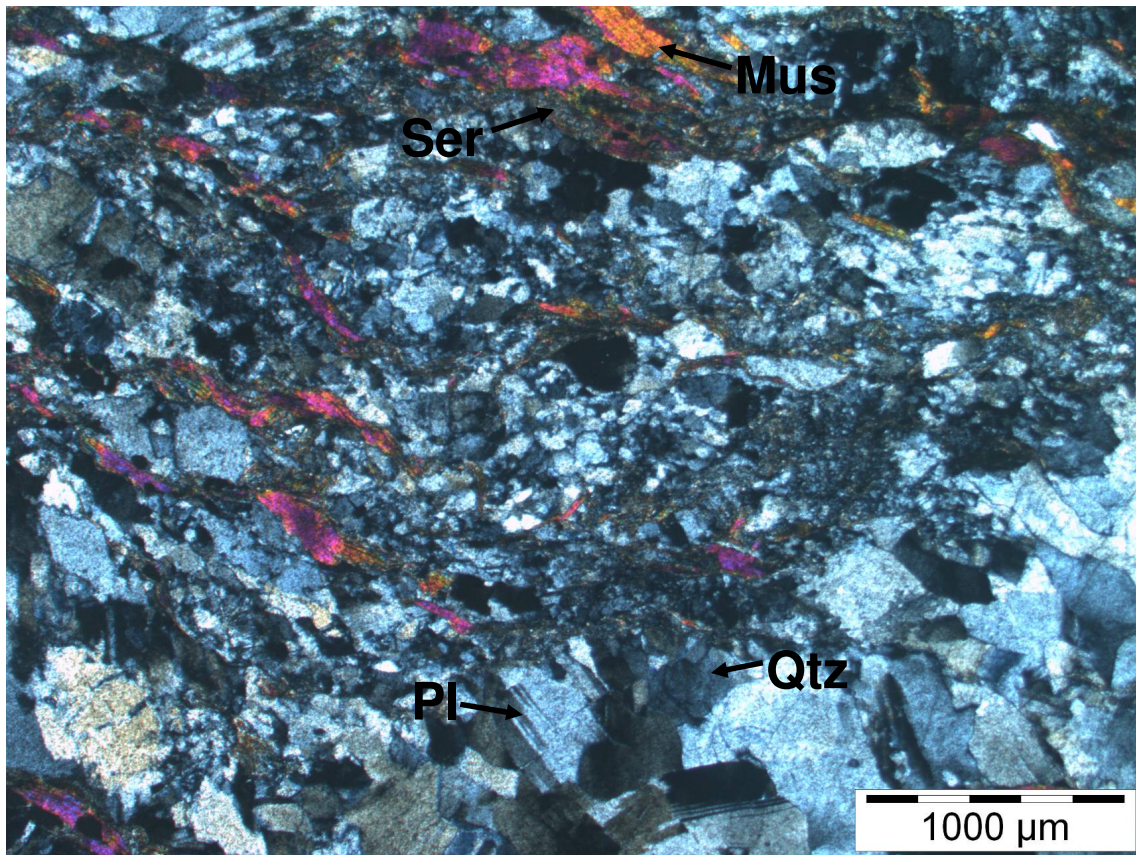


Transmitting light with analyser

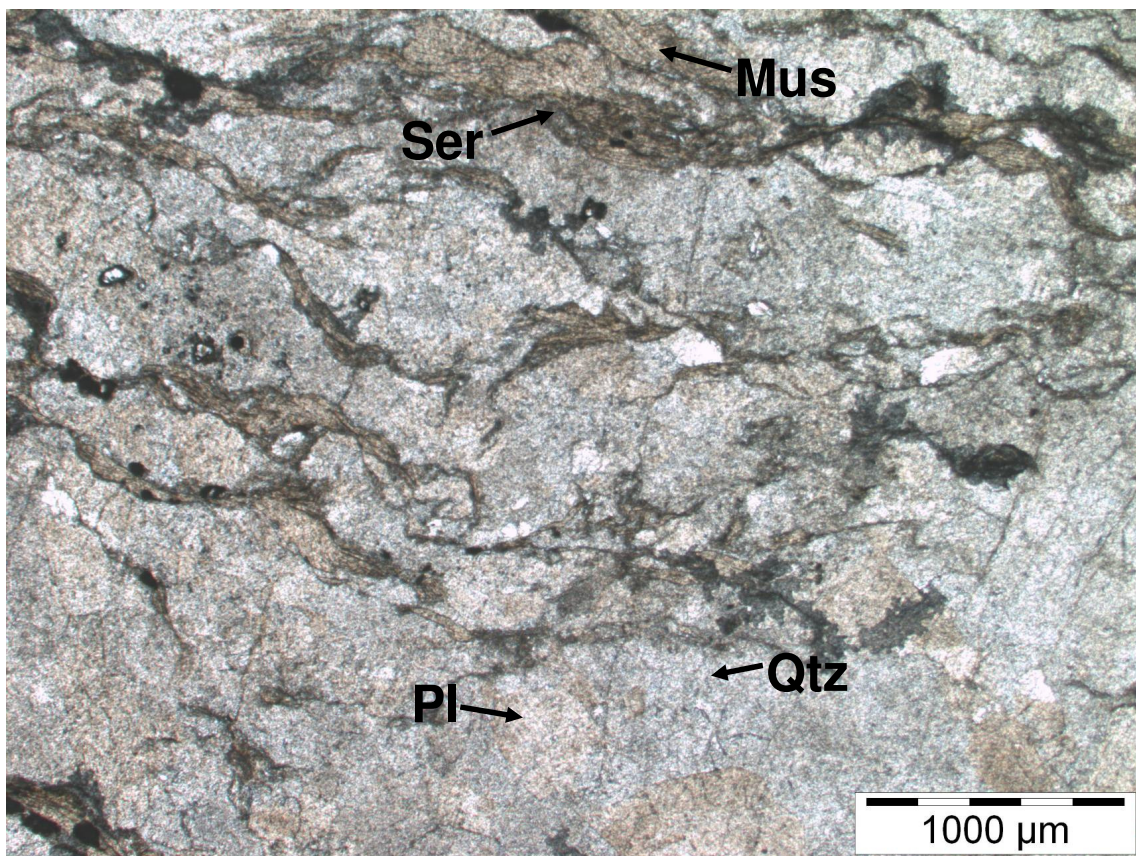


Transmitting light without analyser

10: Orthogneiss (16)

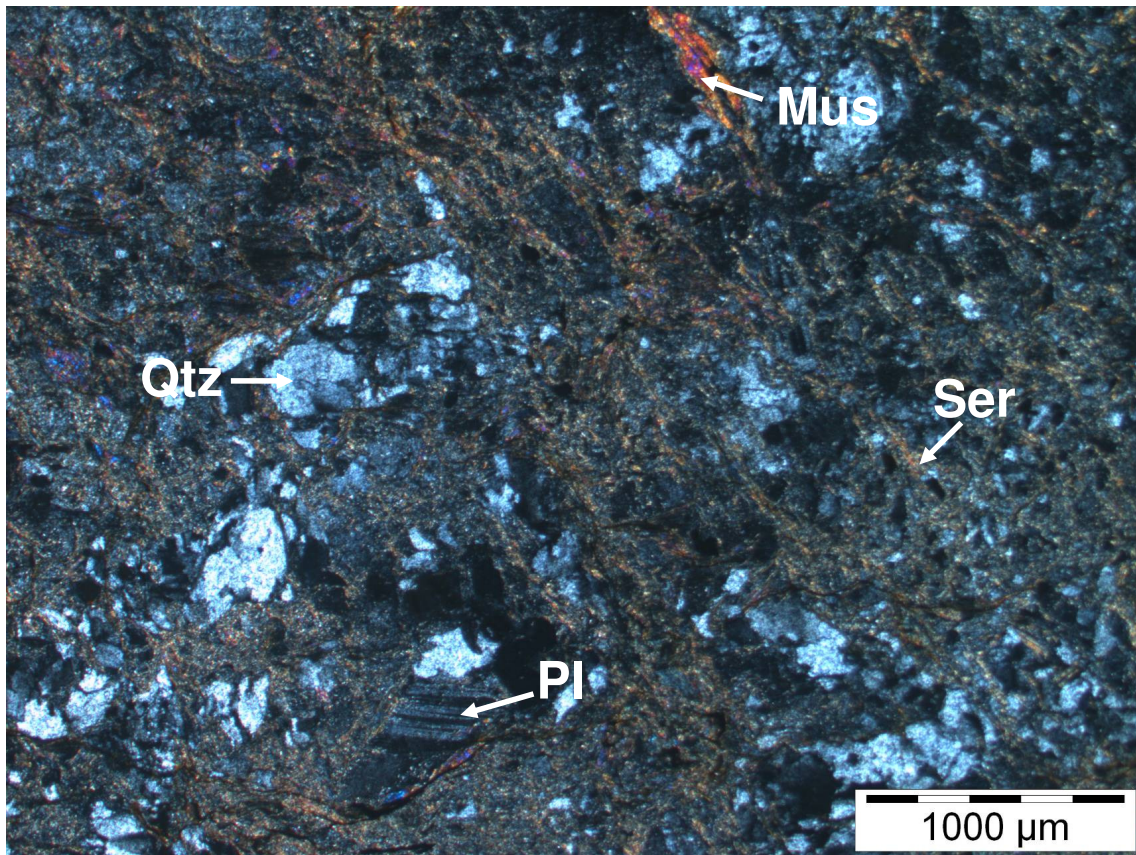


Transmitting light with analysator

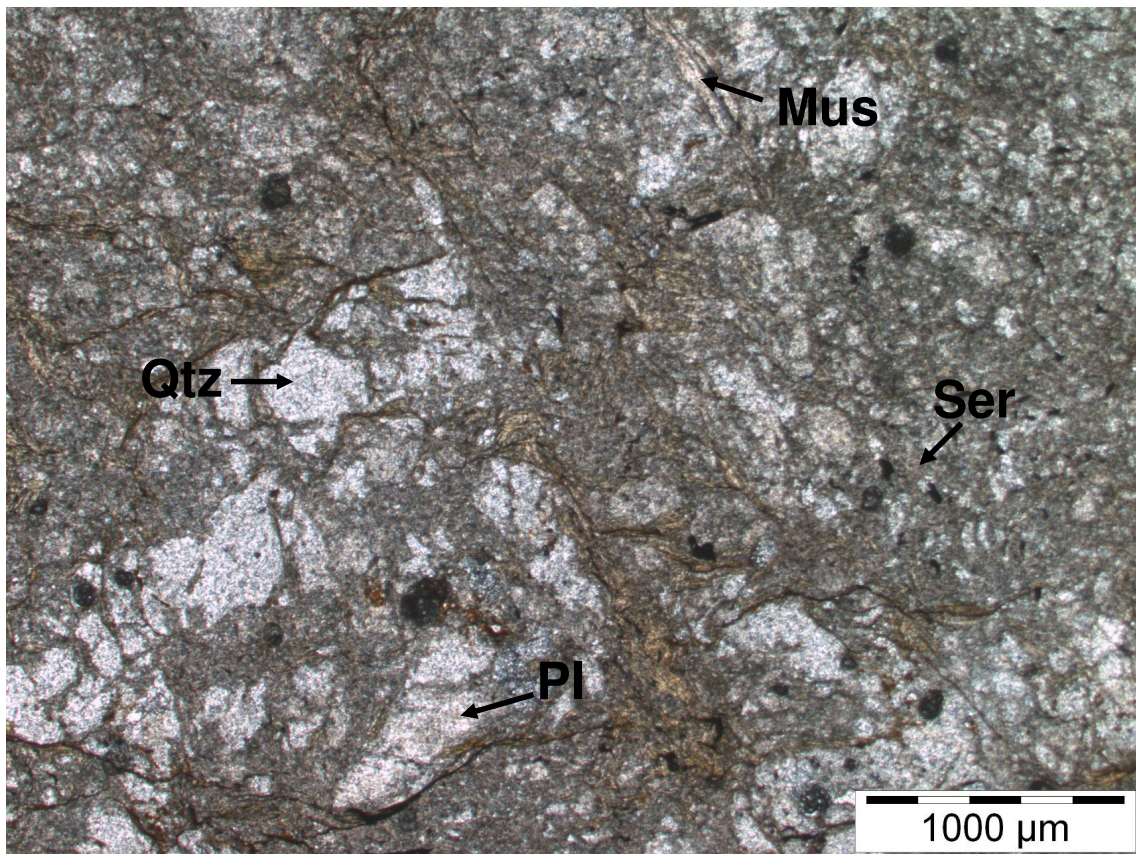


Transmitting light without analysator

11: Cataclasite

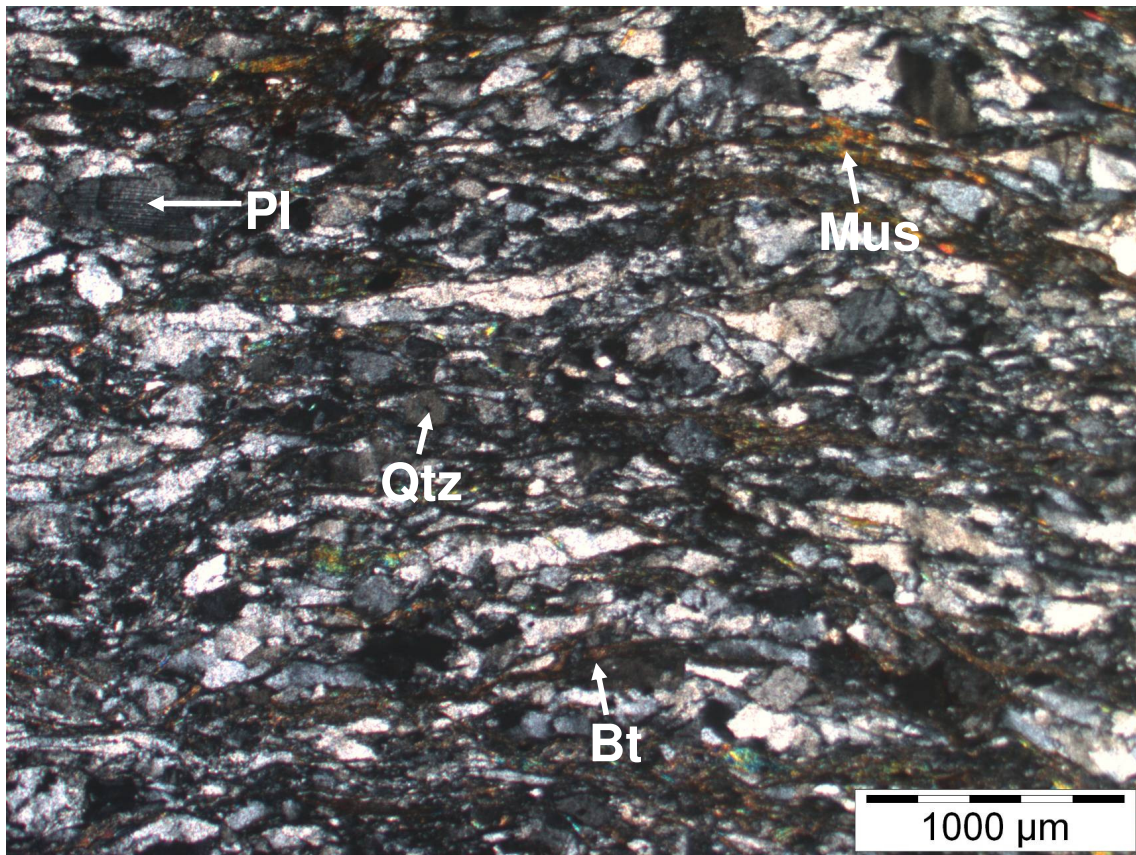


Transmitting light with analyser

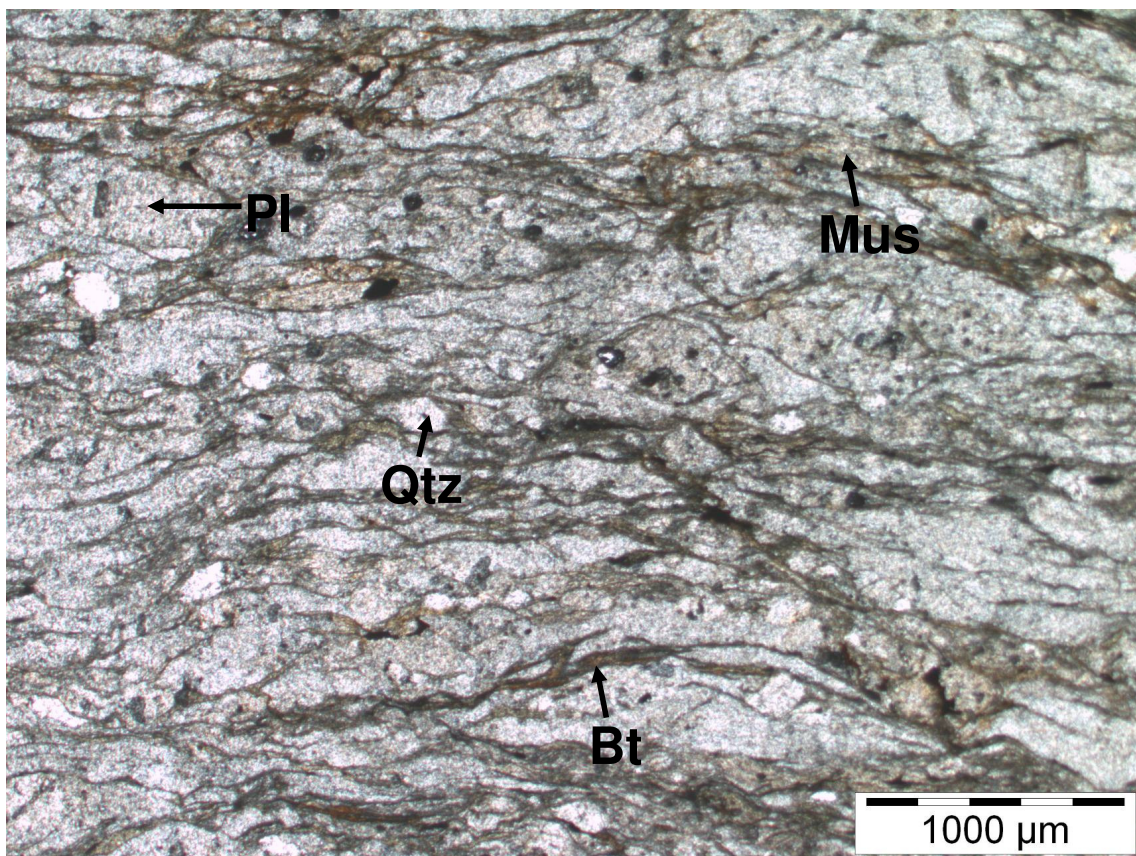


Transmitting light without analyser

12: Paragneiss, dark grey, green (9)

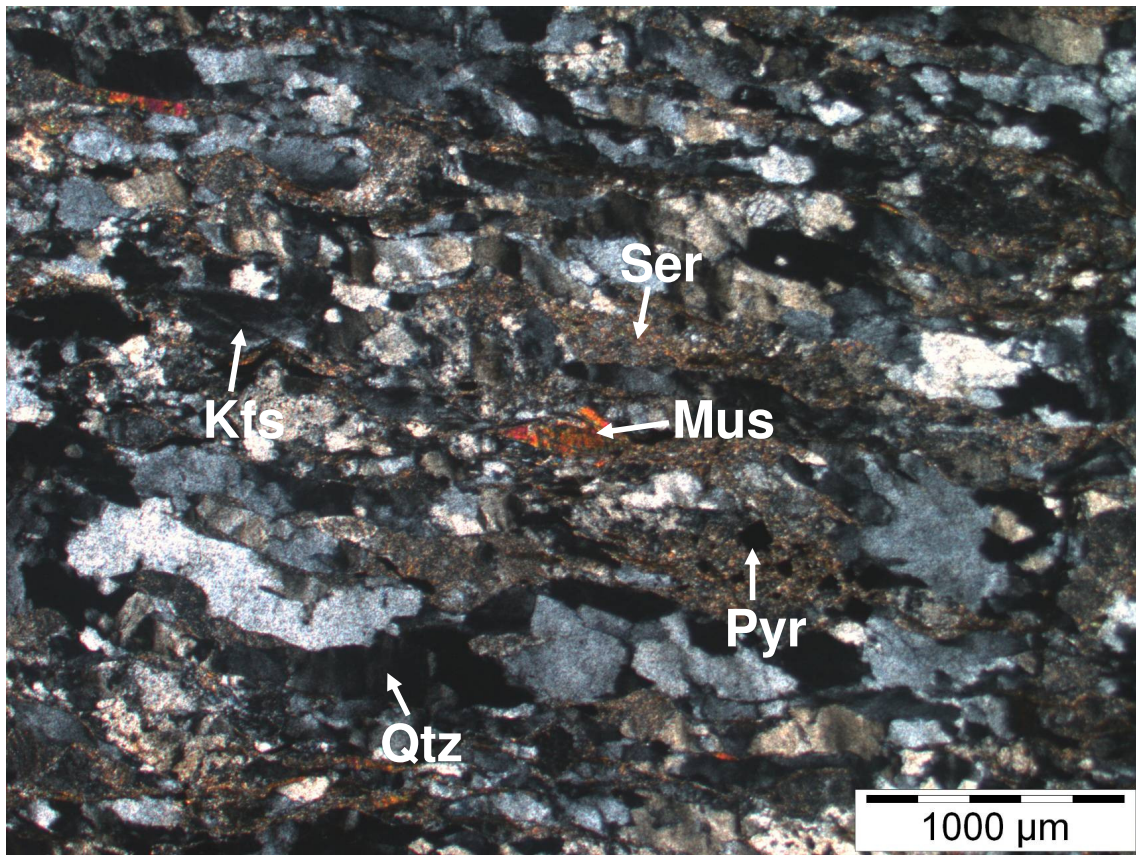


Transmitting light with analyser

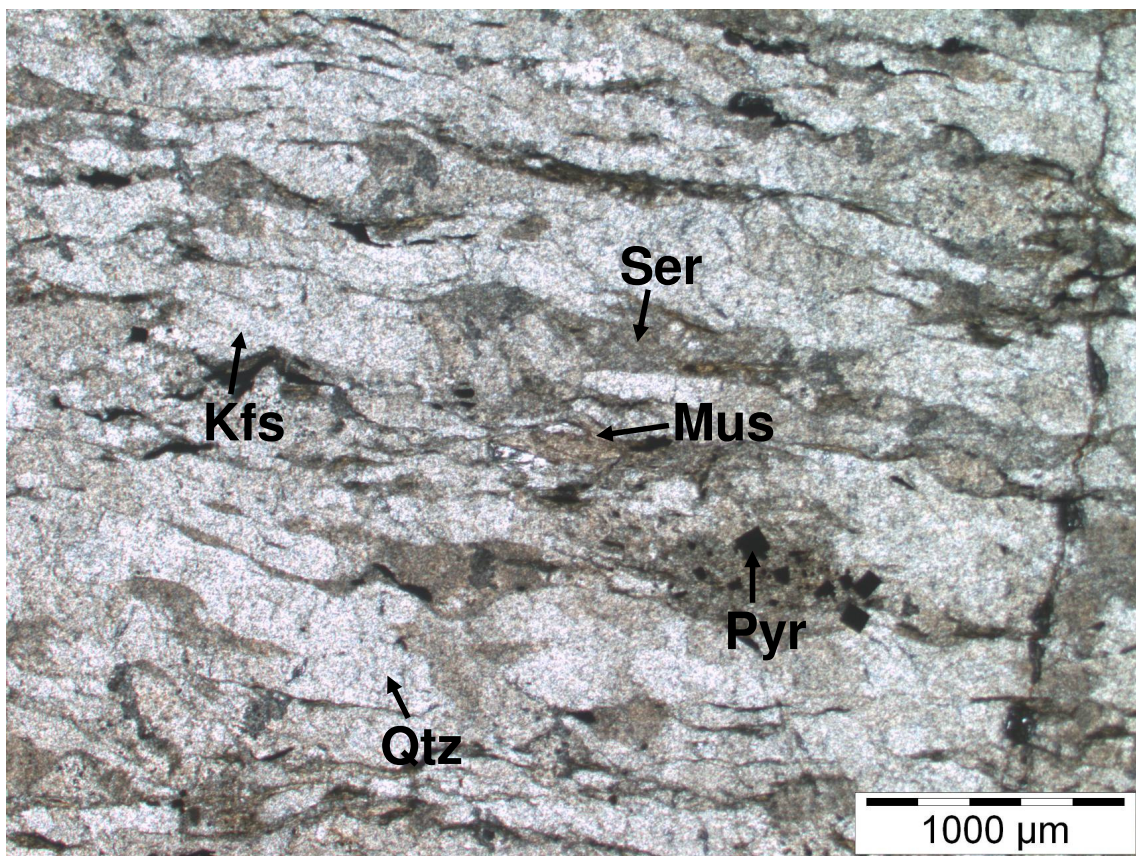


Transmitting light without analyser

13: Paragneiss, grey, brown (11)

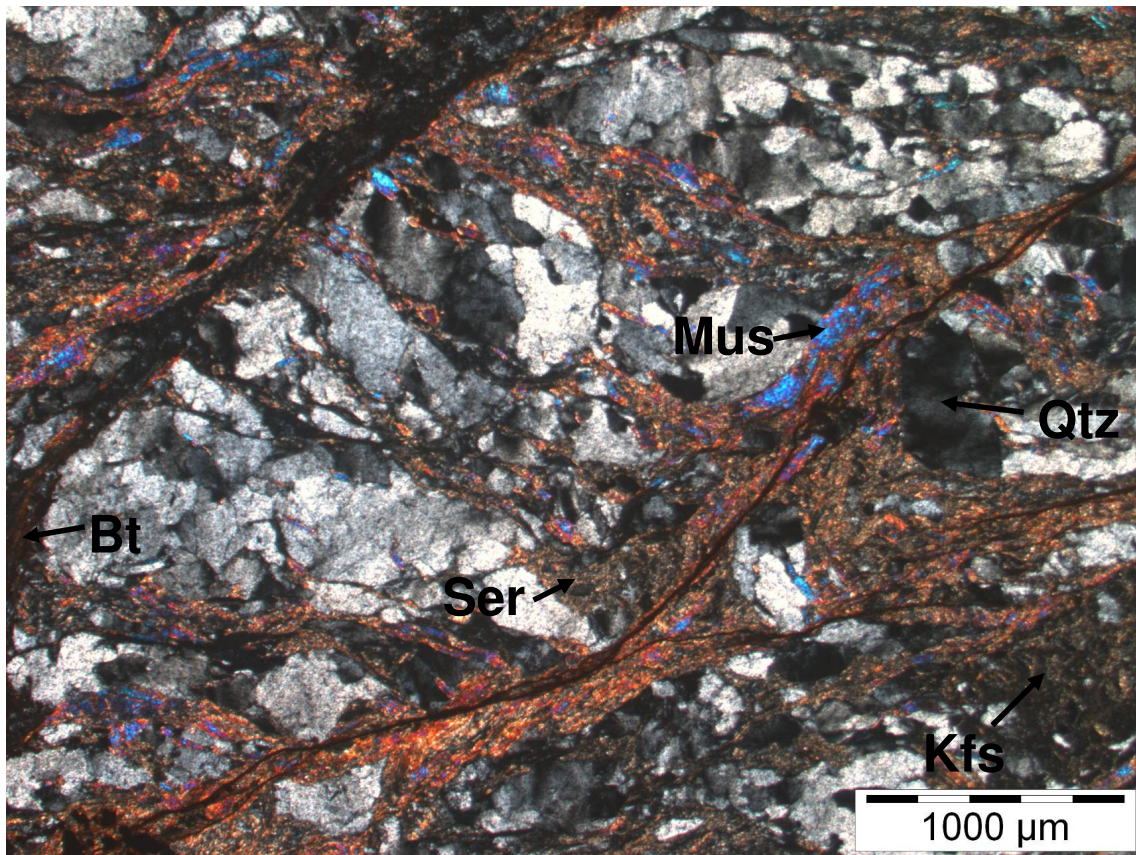


Transmitting light with analyser

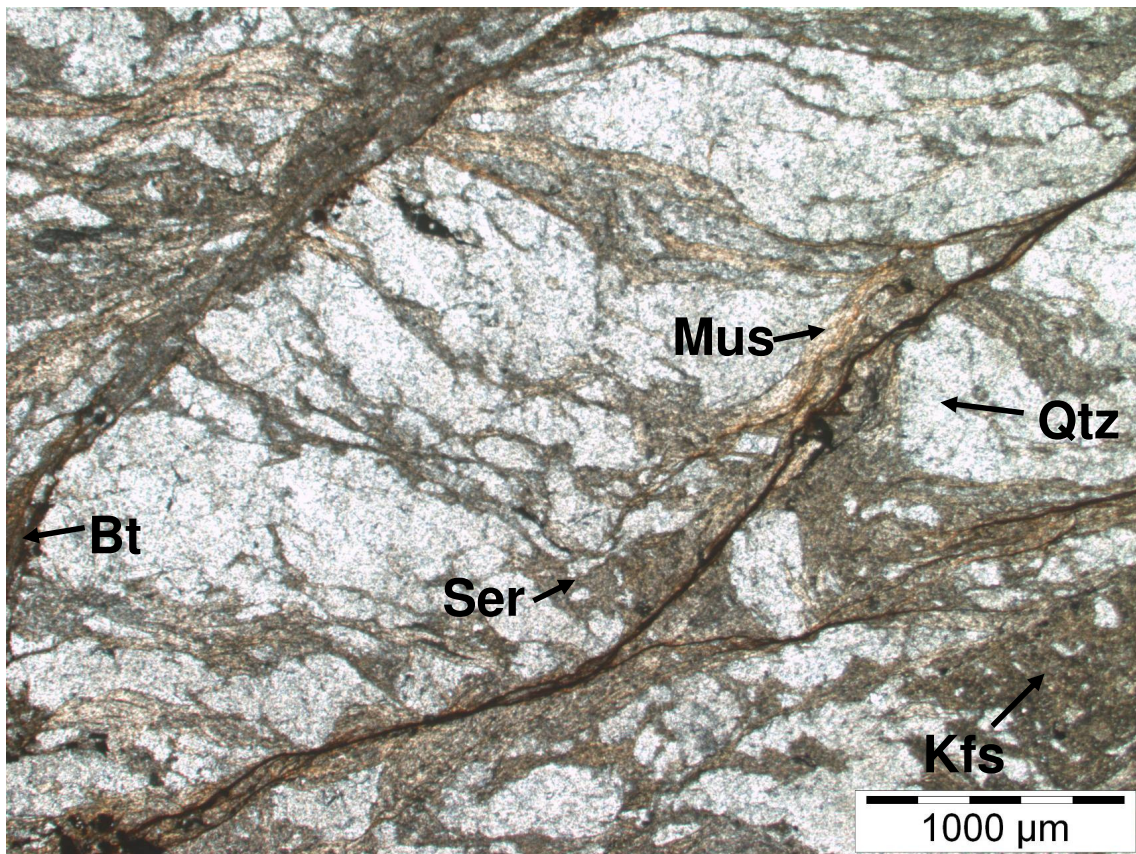


Transmitting light without analyser

14: Paragneiss, dark grey, green (9)

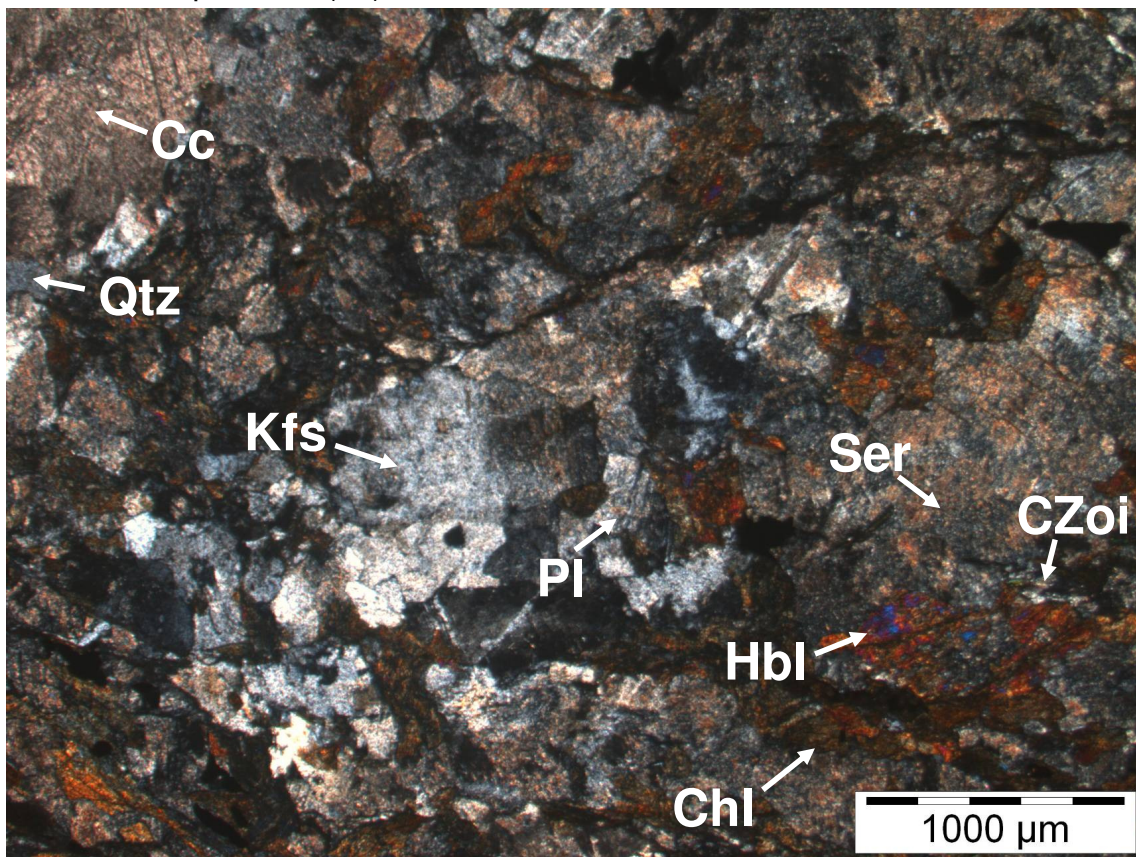


Transmitting light with analysator

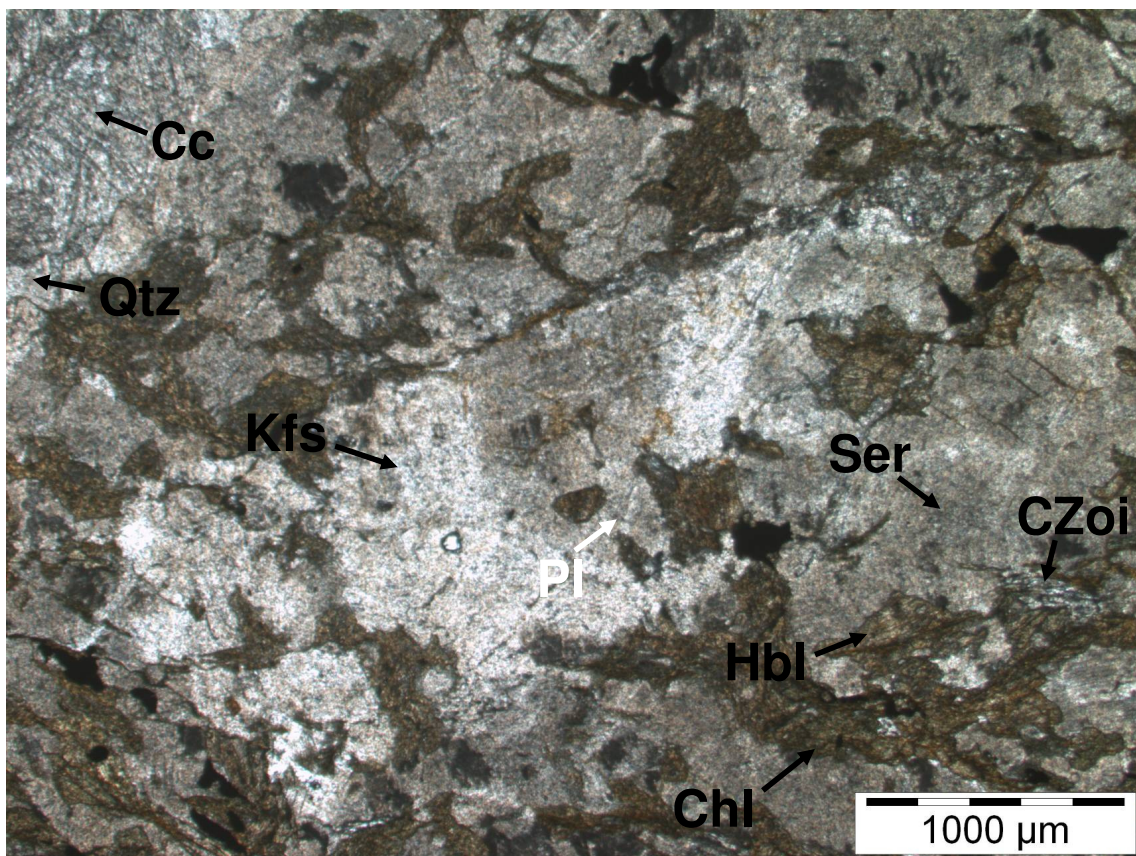


Transmitting light without analysator

15: Amphibolite (13)



Transmitting light with analysator



Transmitting light without analysator

Appendix 6: Laboratory testing

Direct shear tests:

Sample 12/13



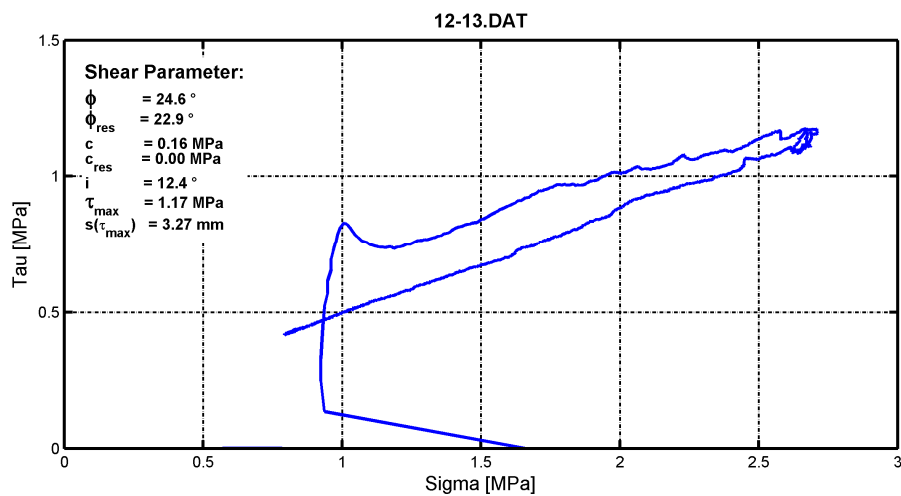
Sample half of the lower shear box after shearing (arrow marks the shear direction)



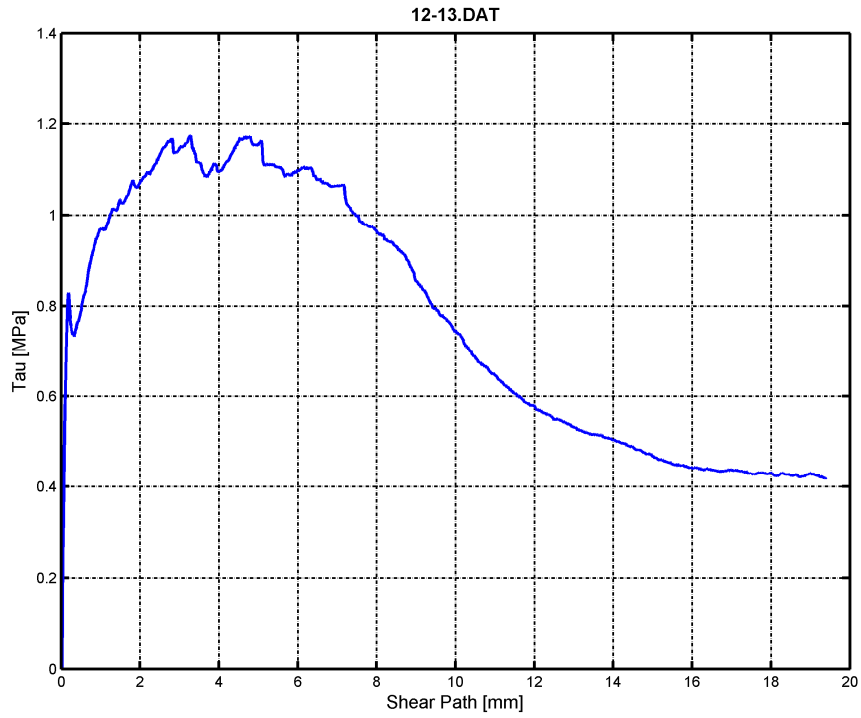
Core sample before setting in grout



Upper and lower sample halves after shearing

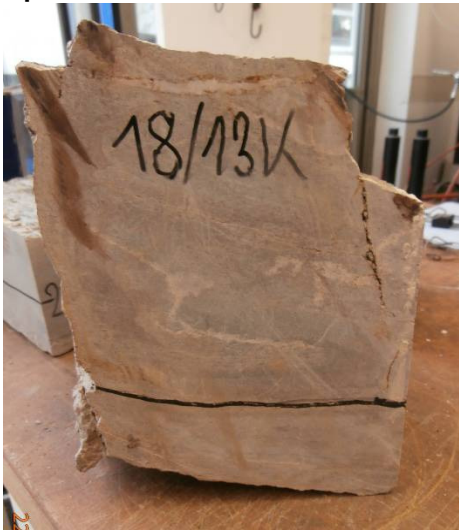


Stress diagram of the direct shear test on sample 12/13 with the obtained shear parameters



Shear stress against shear path of sample 12/13

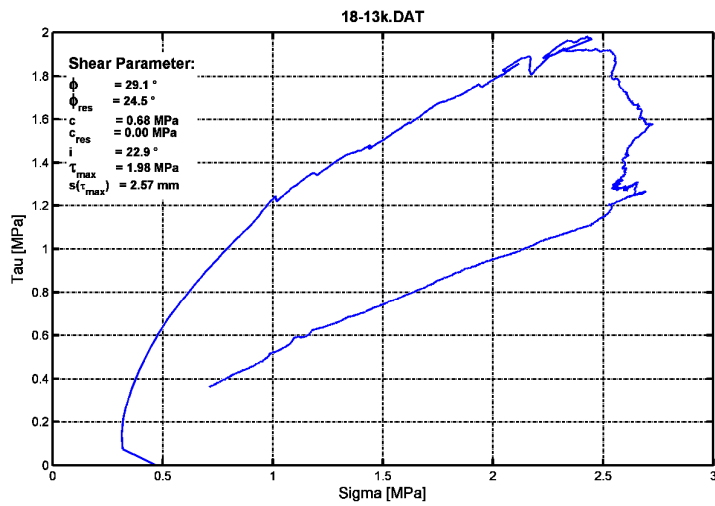
Sample 18/13k



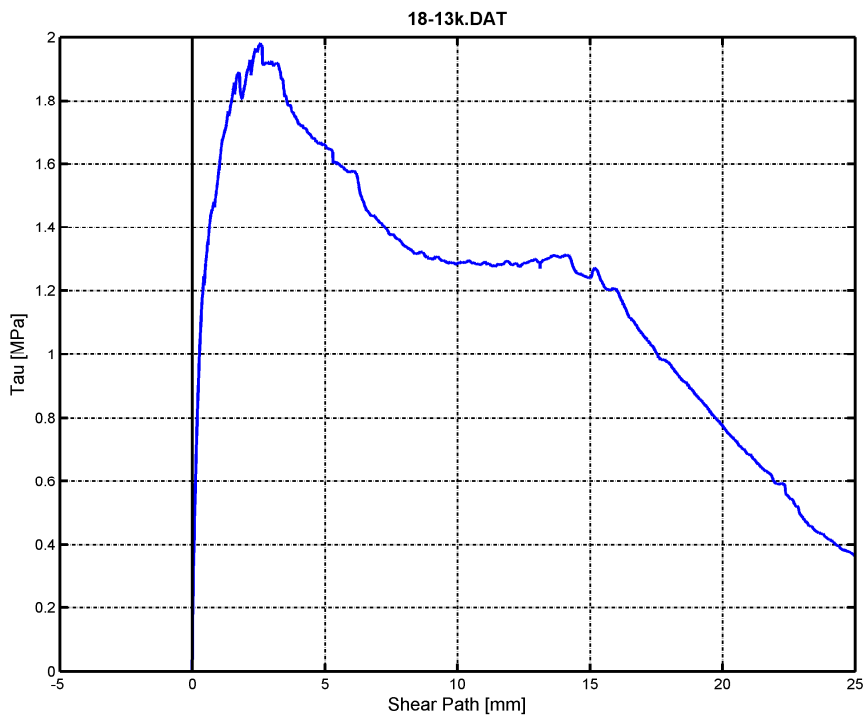
Sample before setting in grout (black line represents the estimated failure surface)



Sample half of the lower shear box after shearing (arrow marks the shear direction)



Stress diagram of the direct shear test on sample 18/13k with the obtained shear parameters



Shear stress against shear path of sample 18/13k

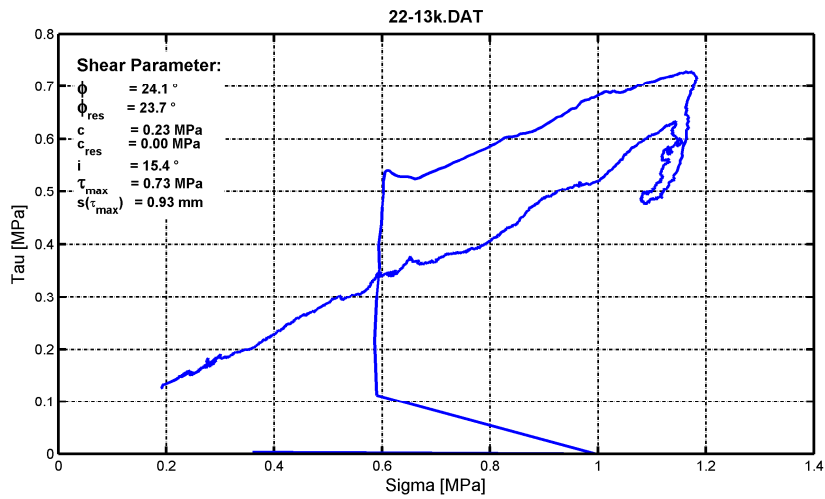
Sample 22/13k



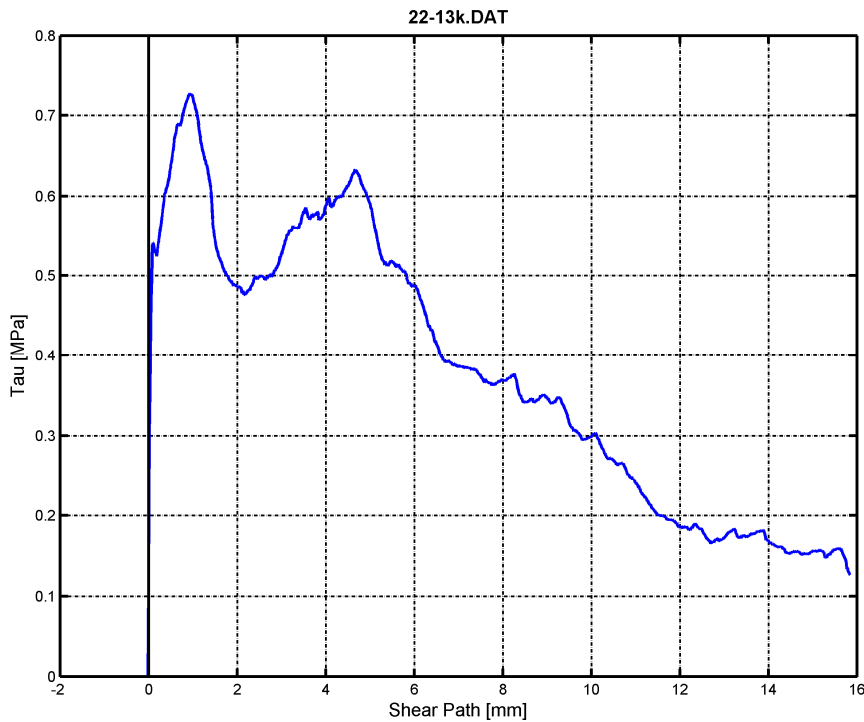
Sample before setting in grout (black line represents the estimated failure surface)



Sample half of the lower shear box after shearing (arrow marks the shear direction)

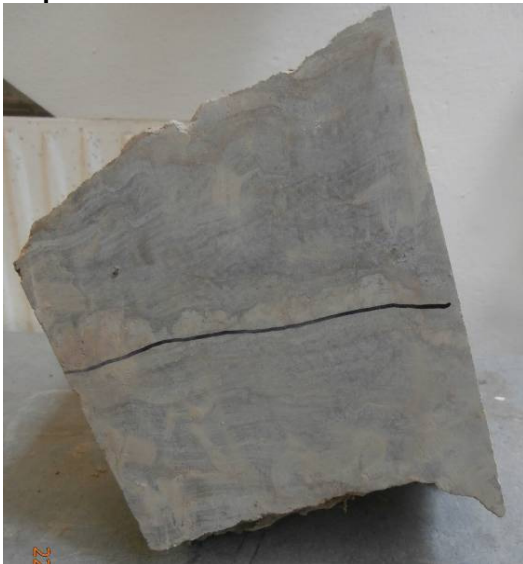


Stress diagram of the direct shear test on sample 22/13k with the obtained shear parameters



Shear stress against shear path of sample 22/13k

Sample 25/13s



Sample before setting in grout (black line represents the estimated failure surface)



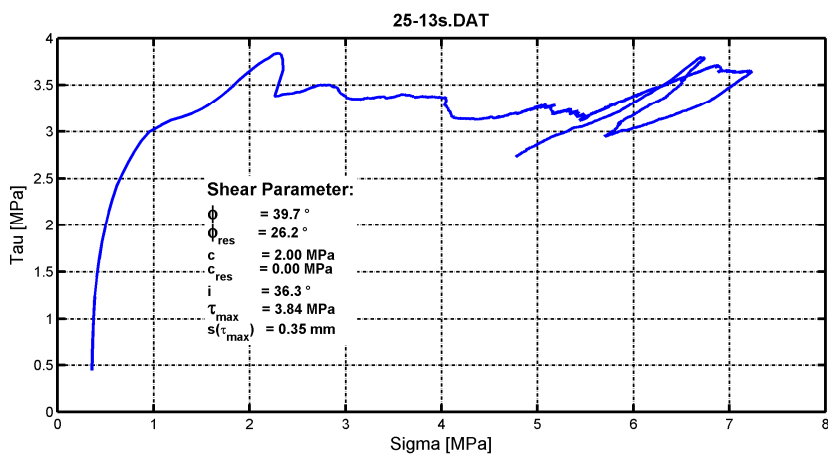
Sample 25/13s during shearing



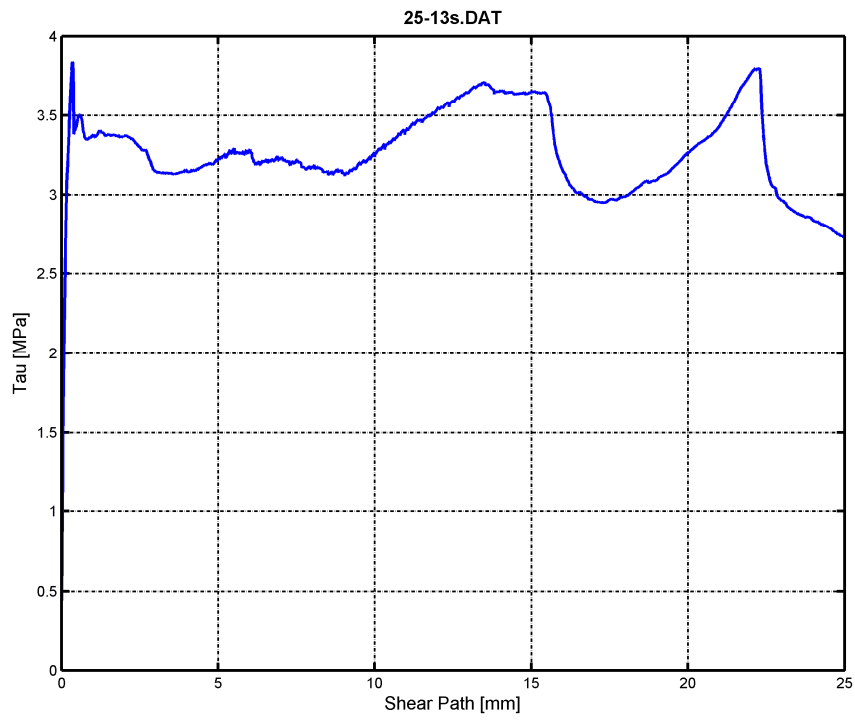
Sample 25/13s during shearing: The failure surface is not entirely located within the 2 cm gap between the shear boxes.



Sample half of the lower shear box after shearing (arrow marks the shear direction)



Stress diagram of the direct shear test on sample 25/13s with the obtained shear parameters



Shear stress against shear path of sample 25/13s

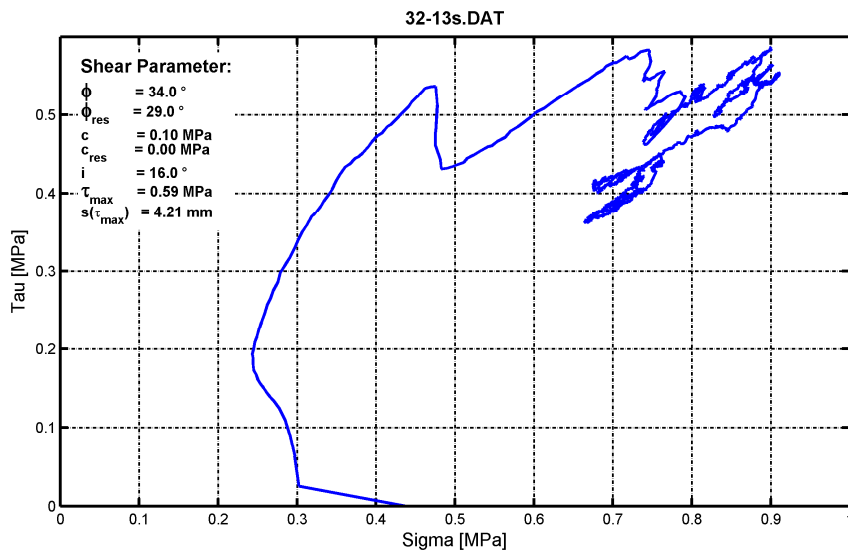
Sample 32/13s



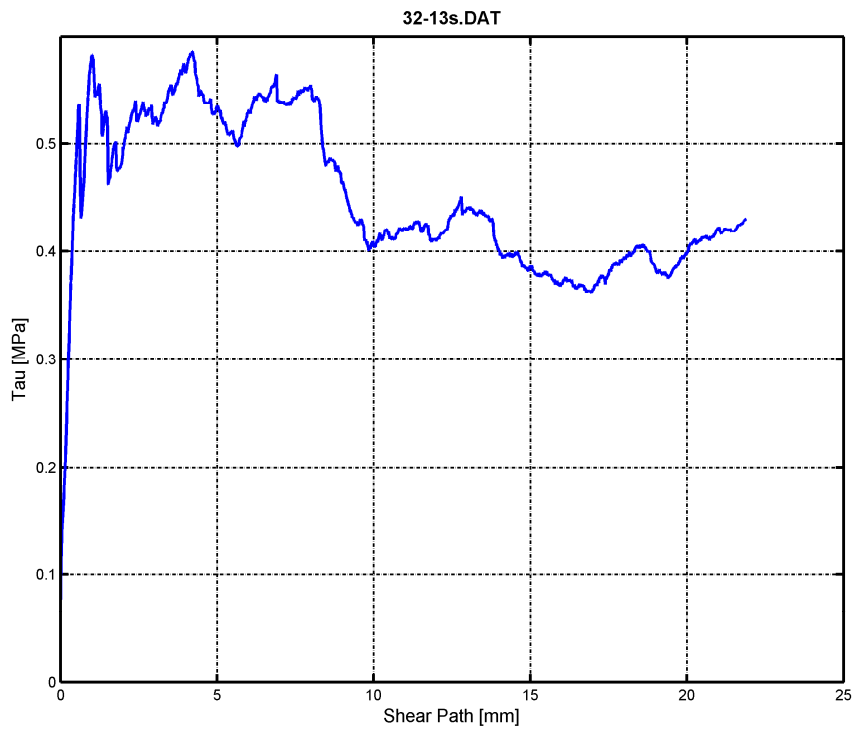
Sample before setting in grout (black line represents the estimated failure surface)



Sample half of the lower shear box after shearing (arrow marks the shear direction)



Stress diagram of the direct shear test on sample 32/13s with the obtained shear parameters



Shear stress against shear path of sample 32/13s

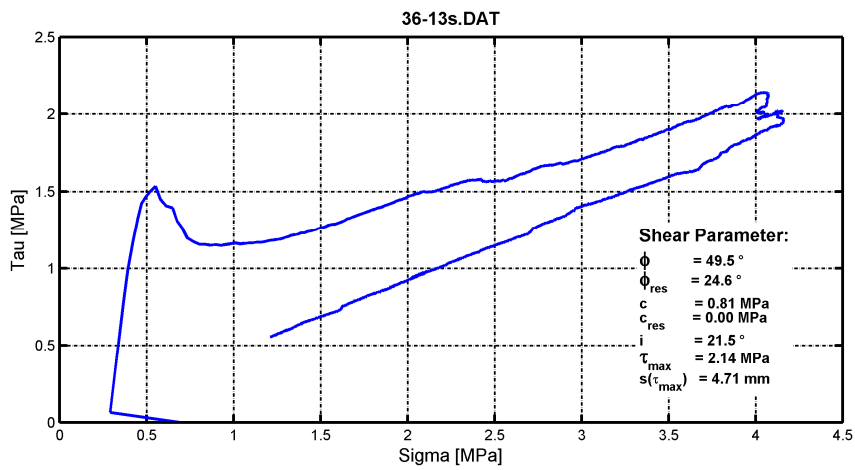
Sample 36/13s



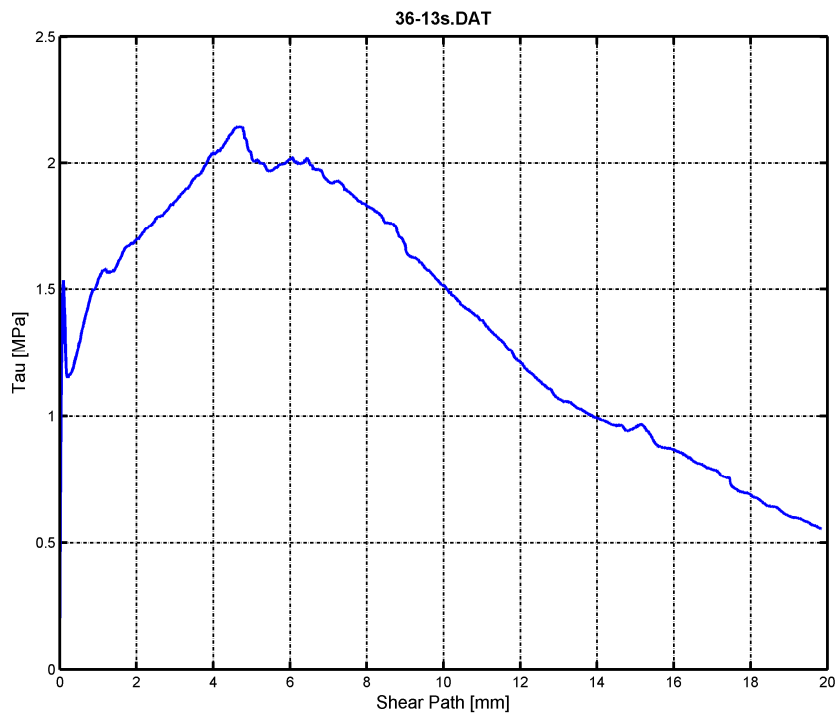
Sample 36/13s was split along a foliation plane before setting in grout



Sample half of the lower shear box after shearing (arrow marks the shear direction)



Stress diagram of the direct shear test on sample 36/13s with the obtained shear parameters



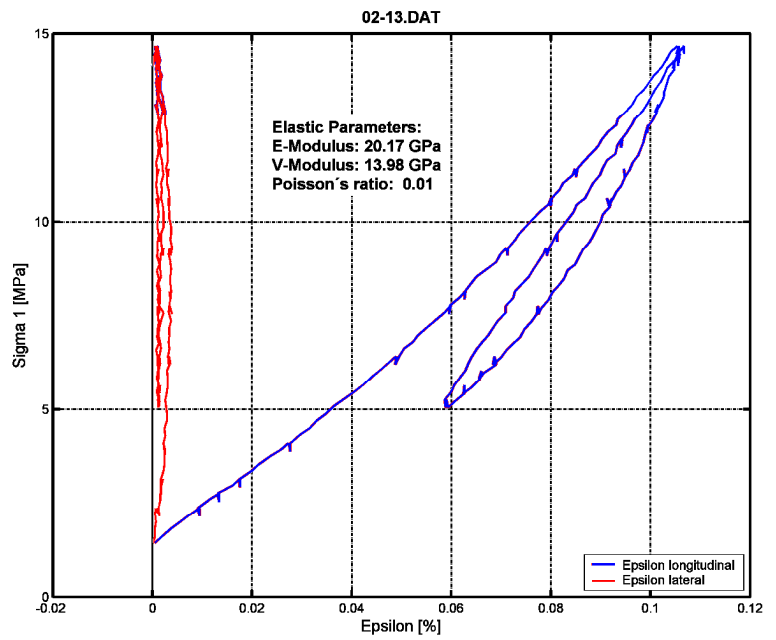
Shear stress against shear path of sample 32/13s

Triaxial compression tests:

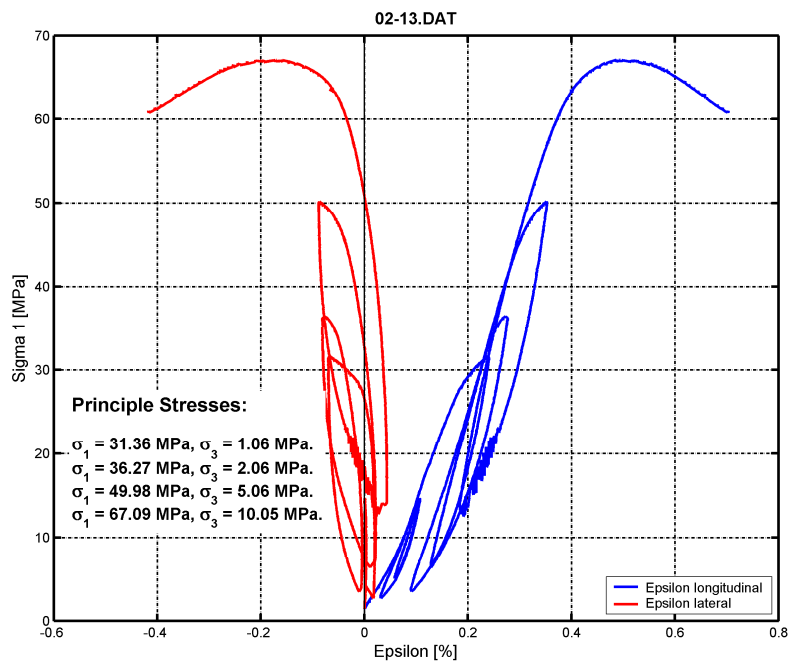
Sample 02/13



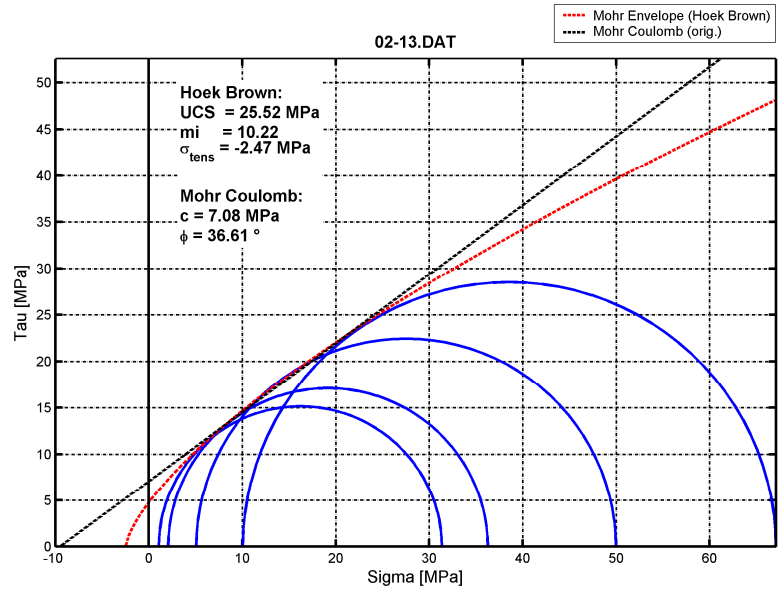
Core sample before testing



Stress versus strain with the obtained elastic parameters

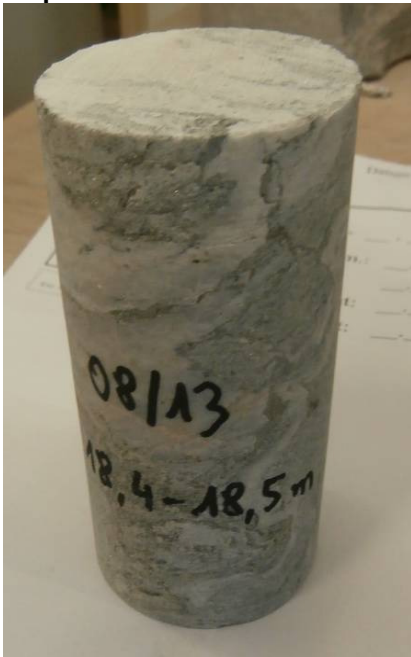


Stress versus strain with the applied principal stresses

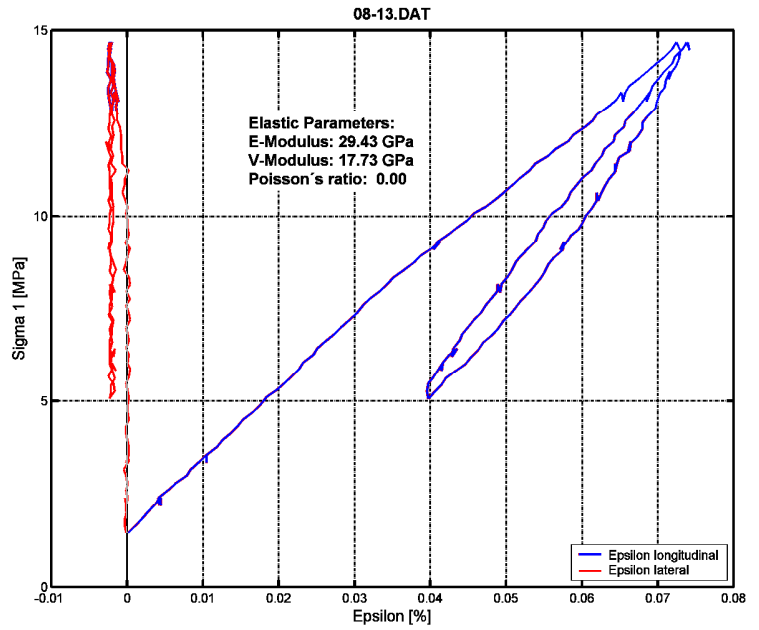


Hoek-Brown and Mohr-Coulomb failure criteria

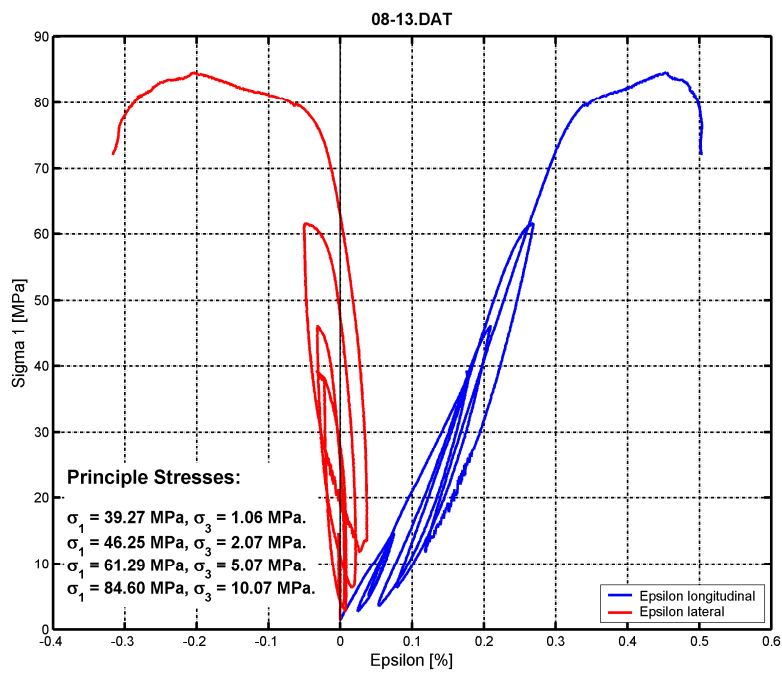
Sample 08/13



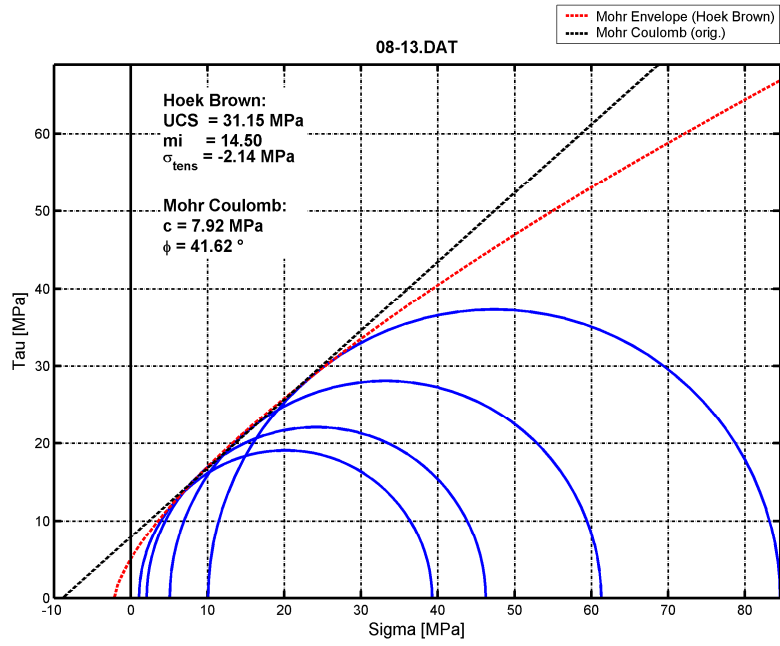
Core sample before testing



Stress versus strain with the obtained elastic parameters



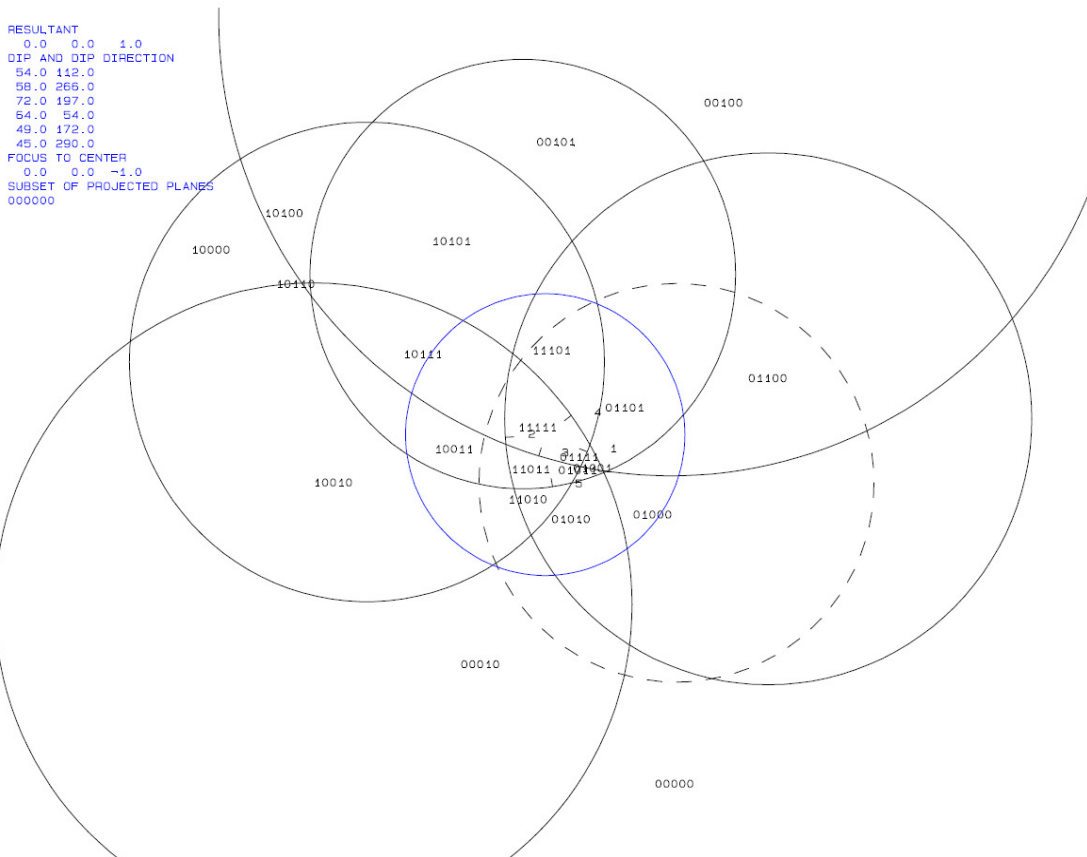
Stress versus strain with the applied principal stresses



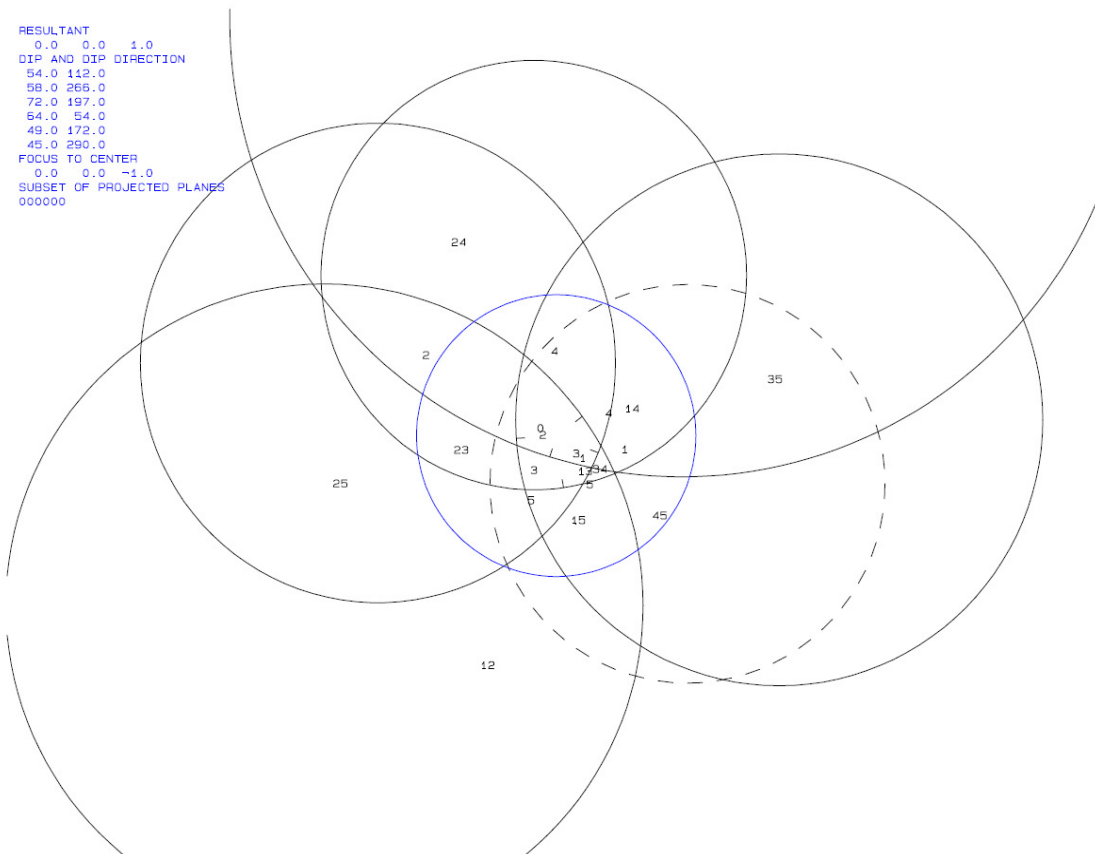
Hoek-Brown and Mohr-Coulomb failure criteria

Appendix 7: Block theory analyses

Outcrop 14:



Whole sphere projection of the joint sets and the schistosity at outcrop 14 showing the joint pyramids (JPs) and their codes. The blue circle is the reference circle; the black dotted circle represents the slope assumed with 290/45.



Whole sphere projection giving the joint plane(s) along which the potential key blocks or key blocks would fail: along the intersection line of j2 and j4 (24).

TABLE 1: Sets and Free Planes

No.	Dip	Dip Direction	Friction Angle
1	54	112	30
2	58	266	30
3	72	197	30
4	64	54	30
5	49	172	30
1	45	290	
2		0	

Resultant force:
0.00D+00 0.00D+00 -1.00D+00

Free plane code for the block:
1

Bearing and rise of tunnel:
0 0

Table 2: Sign of dot product of edge and normal

	0	1	2	3	4	5	6	7	8	9	10
+0	-1	-1	-1	-1	-1	-1	+0	+0	+0	+0	+0
+1	+0	-1	-1	-1	-1	-1	+0	+0	+0	+0	+0
+2	-1	+0	-1	-1	-1	-1	+0	+0	+0	+0	+0
+3	-1	-1	+0	-1	-1	-1	+0	+0	+0	+0	+0
+4	-1	-1	-1	+0	-1	-1	+0	+0	+0	+0	+0
+5	-1	-1	+1	-1	+0	+0	+0	+0	+0	+0	+0
+12	+0	+0	+1	-1	+1	+0	+0	+0	+0	+0	+0
+13	+0	-1	+0	-1	-1	+0	+0	+0	+0	+0	+0
+14	+0	-1	-1	+0	-1	+0	+0	+0	+0	+0	+0
+15	+0	-1	+1	-1	+0	+0	+0	+0	+0	+0	+0
+23	-1	+0	+0	-1	-1	+0	+0	+0	+0	+0	+0
+24	-1	+0	-1	+0	-1	+0	+0	+0	+0	+0	+0
+25	-1	+0	+1	-1	+0	+0	+0	+0	+0	+0	+0
+34	+1	-1	+0	+0	-1	+0	+0	+0	+0	+0	+0
+35	+1	-1	+0	+1	+0	+0	+0	+0	+0	+0	+0
+45	+1	-1	+1	+0	+0	+0	+0	+0	+0	+0	+0

Table 3: Half spaces intersecting cutting pyramid

	0	1	2	3	4	5	6	7	8	9	10
+0	-1	-1	-1	-1	-1	-1	+0	+0	+0	+0	+0
+1	+1	-1	-1	-1	-1	-1	+0	+0	+0	+0	+0
+2	-1	+1	-1	-1	-1	-1	+0	+0	+0	+0	+0
+3	-1	-1	+1	-1	-1	-1	+0	+0	+0	+0	+0
+4	-1	-1	-1	+1	-1	-1	+0	+0	+0	+0	+0
+5	-1	-1	+1	-1	+1	+0	+0	+0	+0	+0	+0
+12	+1	+1	+1	-1	-1	+0	+0	+0	+0	+0	+0
+13	+1	-1	+1	-1	-1	+0	+0	+0	+0	+0	+0
+14	+1	-1	-1	+1	-1	+0	+0	+0	+0	+0	+0
+15	+1	-1	+1	-1	+1	+0	+0	+0	+0	+0	+0
+23	-1	+1	+1	-1	-1	+0	+0	+0	+0	+0	+0
+24	-1	+1	-1	+1	-1	+0	+0	+0	+0	+0	+0
+25	-1	+1	+1	-1	-1	+0	+0	+0	+0	+0	+0
+34	+1	-1	+1	+1	-1	+0	+0	+0	+0	+0	+0
+35	+1	-1	-1	+1	+1	+0	+0	+0	+0	+0	+0
+45	+1	-1	+1	+1	+1	+0	+0	+0	+0	+0	+0

Table 4: Edges of cutting pyramids

+0	+13	+14	+23	+24	+0	+0	+0	+0	+0	+0	+0
+1	+13	+14	+34	+0	+0	+0	+0	+0	+0	+0	+0
+2	+23	+24	-35	-45	+0	+0	+0	+0	+0	+0	+0
+3	+13	+15	+23	+25	+0	+0	+0	+0	+0	+0	+0
+4	-12	+14	+24	+0	+0	+0	+0	+0	+0	+0	+0
+5	+12	+15	+25	+0	+0	+0	+0	+0	+0	+0	+0
+12	+12	-14	-24	+0	+0	+0	+0	+0	+0	+0	+0
+13	+13	+15	+34	+45	+0	+0	+0	+0	+0	+0	+0
+14	-12	+14	-25	+34	+35	+0	+0	+0	+0	+0	+0
+15	+12	+15	-24	+45	+0	+0	+0	+0	+0	+0	+0
+23	+23	+25	-35	+0	+0	+0	+0	+0	+0	+0	+0
+24	-12	-15	+24	-45	+0	+0	+0	+0	+0	+0	+0
+25	+12	-14	+25	-34	-35	+0	+0	+0	+0	+0	+0
+34	+34	+35	+45	+0	+0	+0	+0	+0	+0	+0	+0
+35	-23	-25	+35	+0	+0	+0	+0	+0	+0	+0	+0
+45	-23	-24	+35	+45	+0	+0	+0	+0	+0	+0	+0

Table 5: Key blocks of free plane and concave slope

PYRAMID	PLANE 1	PLANE 2	CONCAVE SLOPE
0	0	1	0
1	0	1	0
2	0	0	0
3	0	1	0
4	0	0	0
5	0	1	0
12	0	0	0
13	0	1	0
14	0	0	0
15	0	0	0
23	0	0	0
24	1	0	0
25	0	0	0
34	0	1	0
35	0	0	0
45	0	0	0

Table 6

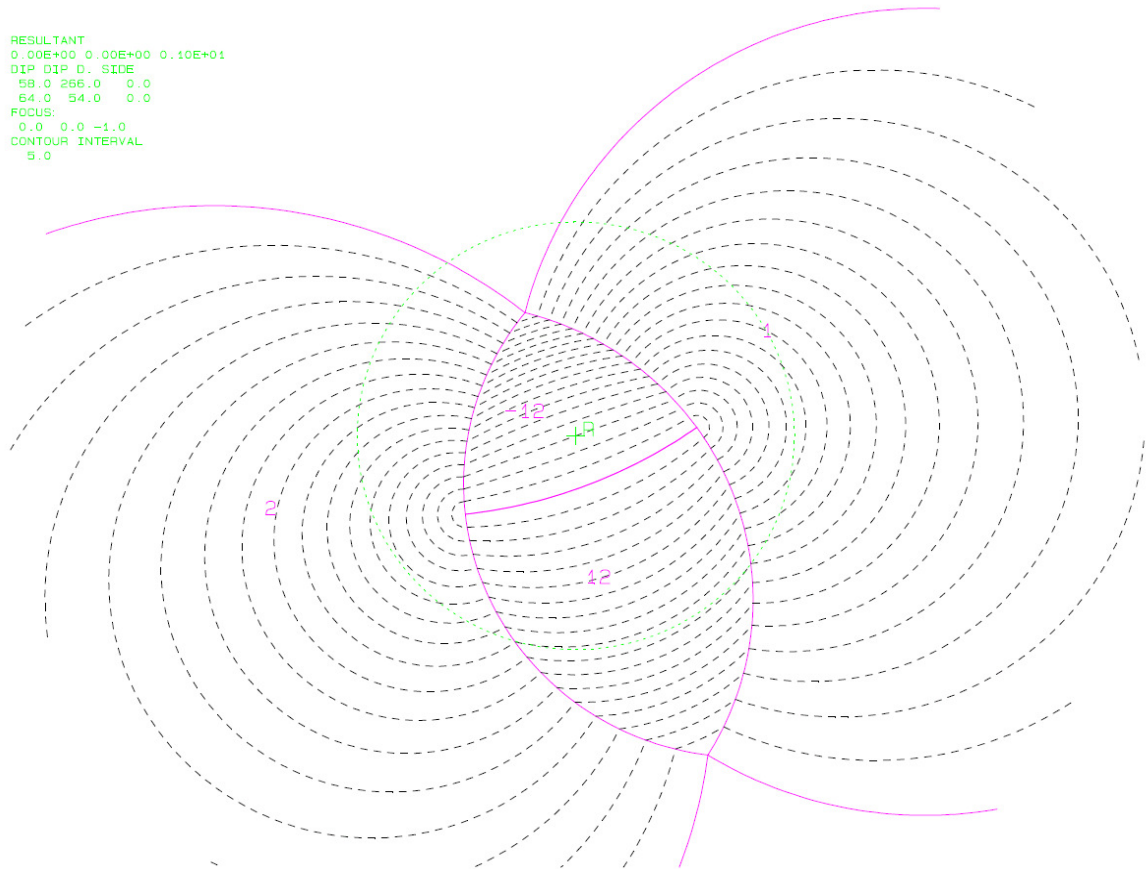
SLIDING PLANE	SLIDING FORCE	SLIDING INTERVAL OF TUNNEL
+0.00	+1.00	+305.72
+1.00	+0.47	+317.53
+2.00	+0.54	+238.38
+3.00	+0.77	+299.91
+4.00	+0.65	+0.00
+5.00	+0.38	+294.45
+12.00	-0.61	+0.00
+13.00	+0.38	+318.38
+14.00	+0.44	+67.30
+15.00	+0.31	+52.86
+23.00	+0.51	+240.77
+24.00	-0.51	+232.86
+25.00	+0.14	+247.30
+34.00	-0.34	+320.33
+35.00	-0.78	+60.77
+45.00	-0.05	+58.38

RESULTANT FORCE
0 -1

AXIS OF TUNNEL
0 1

Tables resulting from the mode analysis

```
RESULTANT
0.00E+00 0.00E+00 0.10E+01
DIP DIP D. SIDE
59.0 266.0 0.0
54.0 54.0 0.0
FOCUS:
0.0 0.0 -1.0
CONTOUR INTERVAL
5.0
```

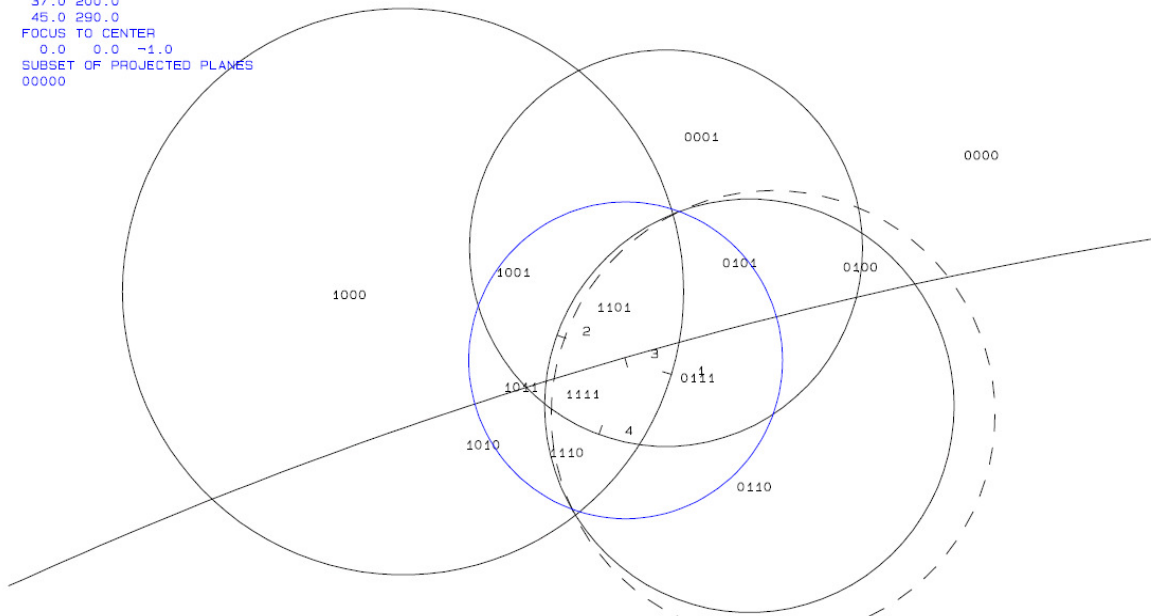


Contour plot of the friction angles for joint set j_2 (= 1) and j_4 (= 2) at outcrop 14. The green circle is the reference circle; R marks the resultant force vector.

Outcrop 23:

```

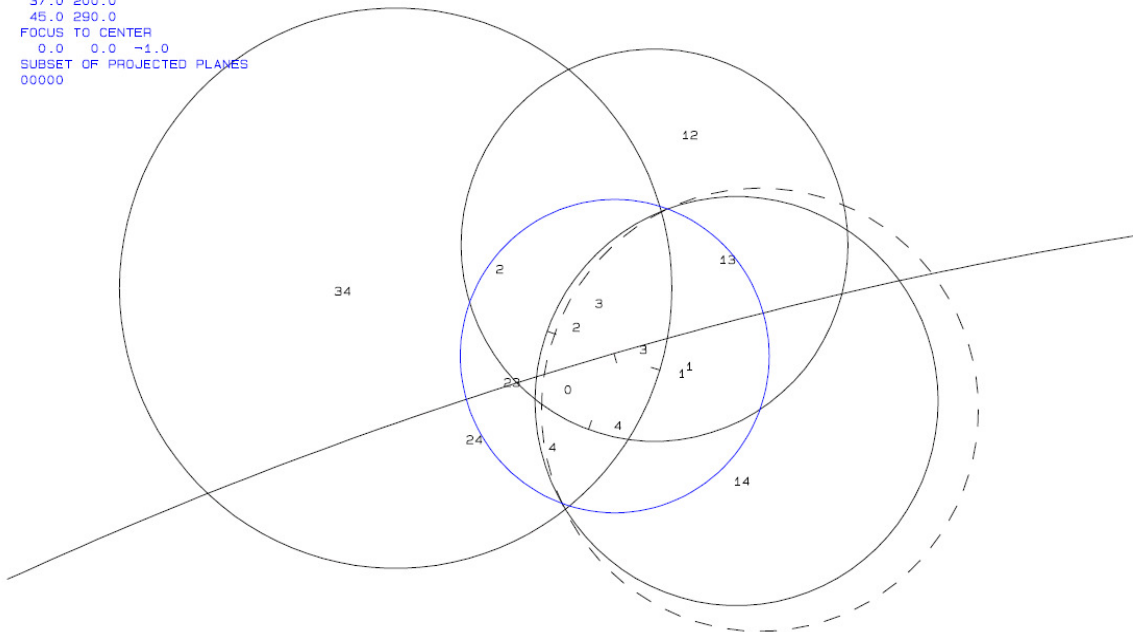
RESULTANT
0.0 0.0 1.0
DIP AND DIP DIRECTION
56.0 107.0
40.0 290.0
88.0 344.0
37.0 200.0
45.0 290.0
FOCUS TO CENTER
0.0 0.0 -1.0
SUBSET OF PROJECTED PLANES
00000
    
```



Whole sphere projection of the joint sets and the schistosity at outcrop 23 showing the joint pyramids (JPs) and their codes. The blue circle is the reference circle; the black dotted circle represents the slope assumed with 290/45.

```

RESULTANT
0.0 0.0 1.0
DIP AND DIP DIRECTION
56.0 107.0
40.0 290.0
88.0 344.0
37.0 200.0
45.0 290.0
FOCUS TO CENTER
0.0 0.0 -1.0
SUBSET OF PROJECTED PLANES
00000
    
```



Whole sphere projection giving the joint plane(s) along which the potential key blocks or key blocks would fail: along the intersection line of j2 and j3 (23), of j3 with the schistosity (34) and along j2 alone (2)

TABLE 1: Sets and Free Planes

No.	Dip	Dip Direction	Friction Angle
1	56	107	30
2	40	290	30
3	88	344	30
4	37	200	30
1	45	290	
2	0	0	

Resultant force:
 0.00D+00 0.00D+00 -1.00D+00

Free plane code for the block:

1

Bearing and rise of tunnel:

0 0

Table 2: Sign of dot product of edge and normal

0	1	2	3	4	5	6	7	8	9	10
+0	-1	-1	-1	-1	+0	+0	+0	+0	+0	+0
+1	+0	-1	-1	-1	+0	+0	+0	+0	+0	+0
+2	-1	+0	+1	-1	+0	+0	+0	+0	+0	+0
+3	-1	-1	+0	-1	+0	+0	+0	+0	+0	+0
+4	-1	-1	-1	+0	+0	+0	+0	+0	+0	+0
+12	+0	+0	+1	-1	+0	+0	+0	+0	+0	+0
+13	+0	-1	+0	-1	+0	+0	+0	+0	+0	+0
+14	+0	-1	-1	+0	+0	+0	+0	+0	+0	+0
+23	-1	+0	+0	-1	+0	+0	+0	+0	+0	+0
+24	-1	+0	-1	+0	+0	+0	+0	+0	+0	+0
+34	-1	+1	+0	+0	+0	+0	+0	+0	+0	+0

Table 3: Half spaces intersecting cutting pyramid

0	1	2	3	4	5	6	7	8	9	10
+0	-1	-1	-1	-1	+0	+0	+0	+0	+0	+0
+1	+1	-1	-1	-1	+0	+0	+0	+0	+0	+0
+2	-1	+1	+1	-1	+0	+0	+0	+0	+0	+0
+3	-1	-1	+1	-1	+0	+0	+0	+0	+0	+0
+4	-1	-1	-1	+1	+0	+0	+0	+0	+0	+0
+12	+1	+1	+1	-1	+0	+0	+0	+0	+0	+0
+13	+1	-1	+1	-1	+0	+0	+0	+0	+0	+0
+14	+1	-1	-1	+1	+0	+0	+0	+0	+0	+0
+23	-1	+1	-1	-1	+0	+0	+0	+0	+0	+0
+24	-1	+1	-1	+1	+0	+0	+0	+0	+0	+0
+34	-1	+1	+1	+1	+0	+0	+0	+0	+0	+0

Table 4: Edges of cutting pyramids

+0	+13	+14	+23	+24	+0	+0	+0	+0	+0	+0
+1	+13	+14	-34	+0	+0	+0	+0	+0	+0	+0
+2	+12	-14	+23	+34	+0	+0	+0	+0	+0	+0
+3	+12	+13	+23	+0	+0	+0	+0	+0	+0	+0
+4	-12	+14	+24	+0	+0	+0	+0	+0	+0	+0
+12	+12	-14	-24	+0	+0	+0	+0	+0	+0	+0
+13	+12	+13	-24	-34	+0	+0	+0	+0	+0	+0
+14	-12	+14	-23	-34	+0	+0	+0	+0	+0	+0
+23	+23	+24	+34	+0	+0	+0	+0	+0	+0	+0
+24	-12	-13	+24	+34	+0	+0	+0	+0	+0	+0
+34	-13	-14	+34	+0	+0	+0	+0	+0	+0	+0

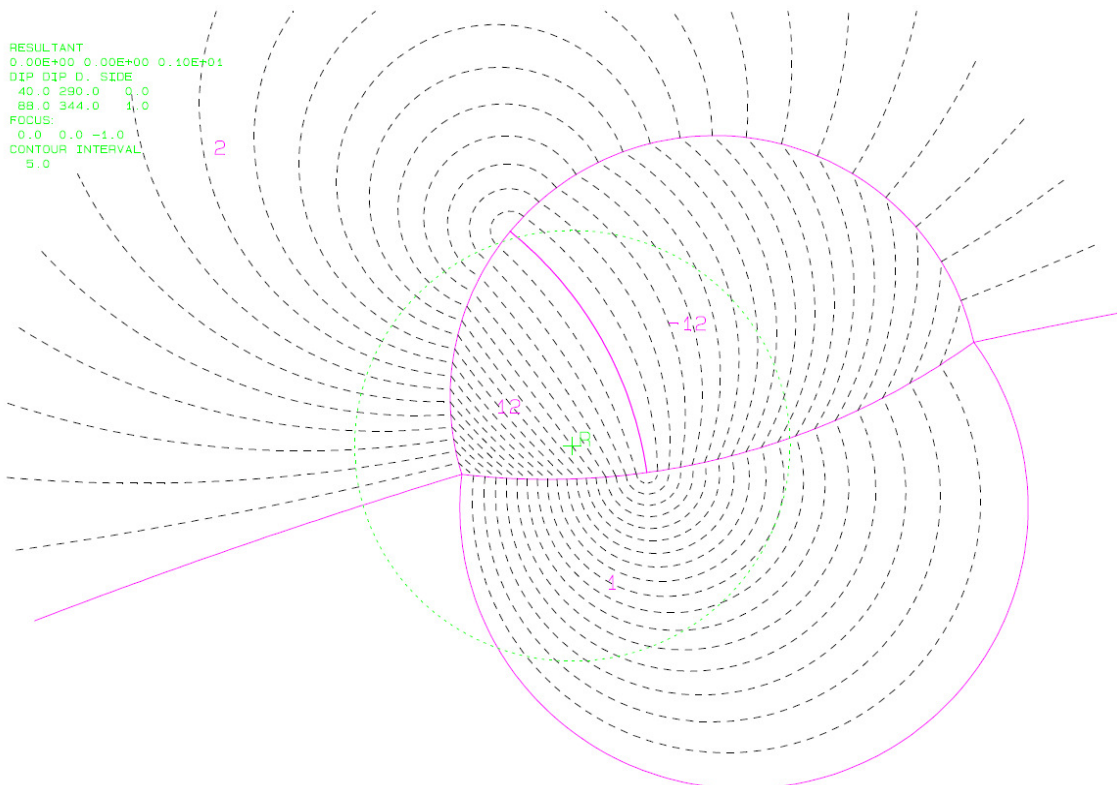
Table 5: Key blocks of free plane and concave slope

PYRAMID	PLANE 1	PLANE 2	CONCAVE SLOPE
0	0	1	0
1	0	0	0
2	1	0	0
3	0	1	0
4	0	0	0
12	0	0	0
13	0	0	0
14	0	0	0
23	1	1	1
24	0	0	0
34	1	0	0

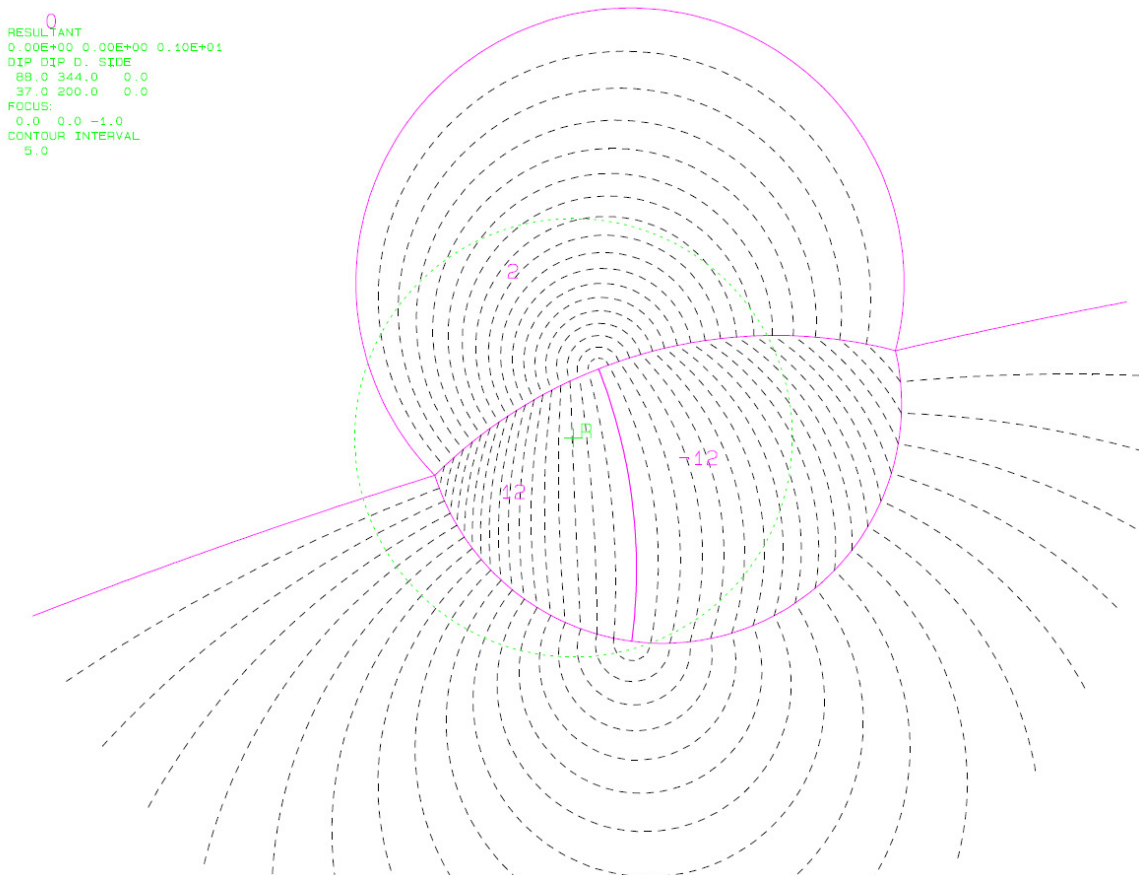
Table 6

SLIDING PLANE	SLIDING FORCE	SLIDING INTERVAL OF TUNNEL
+0.00	+1.00	+308.14
+1.00	+0.51	+24.19
+2.00	+0.20	+0.00
+3.00	+0.98	+354.84
+4.00	+0.14	+283.83
+12.00	-0.83	+103.83
+13.00	+0.17	+32.43
+14.00	-0.00	+0.00
+23.00	-0.14	+215.51
+24.00	-0.07	+212.43
+34.00	-0.49	+204.19
RESULTANT FORCE		
0	0	-1
AXIS OF TUNNEL		
0	1	0

Tables resulting from the mode analysis

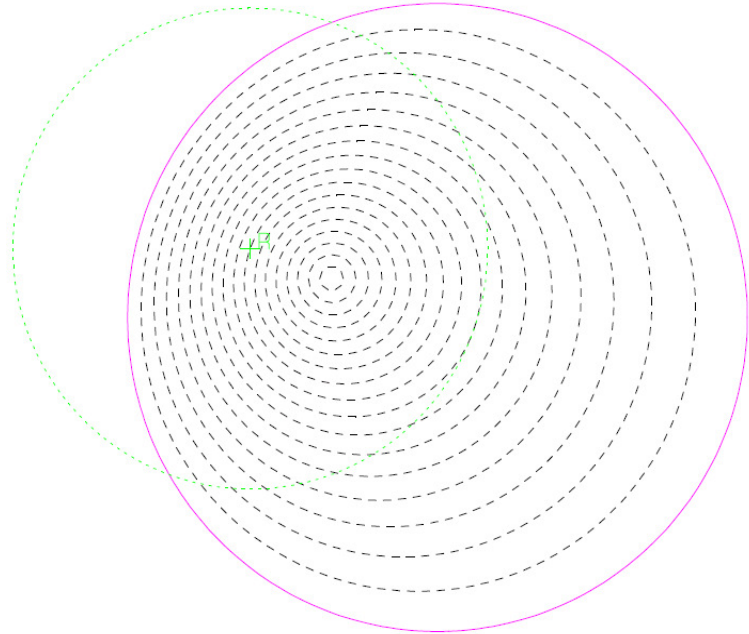


Contour plot of the friction angles for joint set j_2 (= 1) and j_3 (= 2) at outcrop 23. The green circle is the reference circle; R marks the resultant force vector.



Contour plot of the friction angles for joint set j_3 (= 1) and the schistosity (= 2) at outcrop 23. The green circle is the reference circle; R marks the resultant force vector.

```
RESULTANT  
0.00E+00 0.00E+00 0.10E+01  
DIP DIP D. SIDE  
40.0 290.0 0.0  
FOCUS:  
0.0 0.0 -1.0  
CONTOUR INTERVAL  
5.0
```



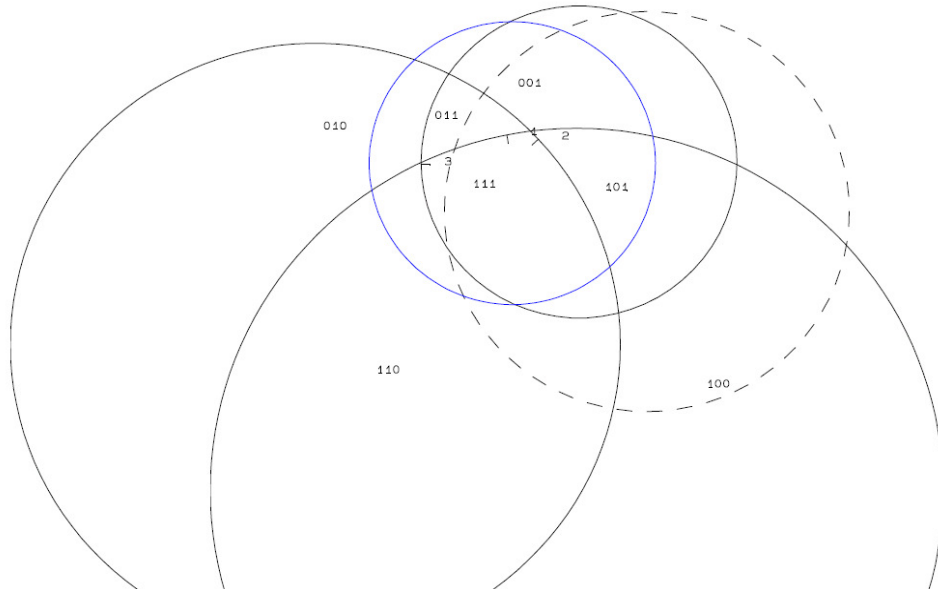
Contour plot of the friction angles for the schistosity alone at outcrop 23. The green circle is the reference circle; R marks the resultant force vector.

Outcrop 28:

```

RESULTANT
0.0 0.0 1.0
DIP AND DIP DIRECTION
67.0 349.0
62.0 47.0
25.0 269.0
45.0 290.0
FOCUS TO CENTER
0.0 0.0 -1.0
SUBSET OF PROJECTED PLANES
0000
    
```

000

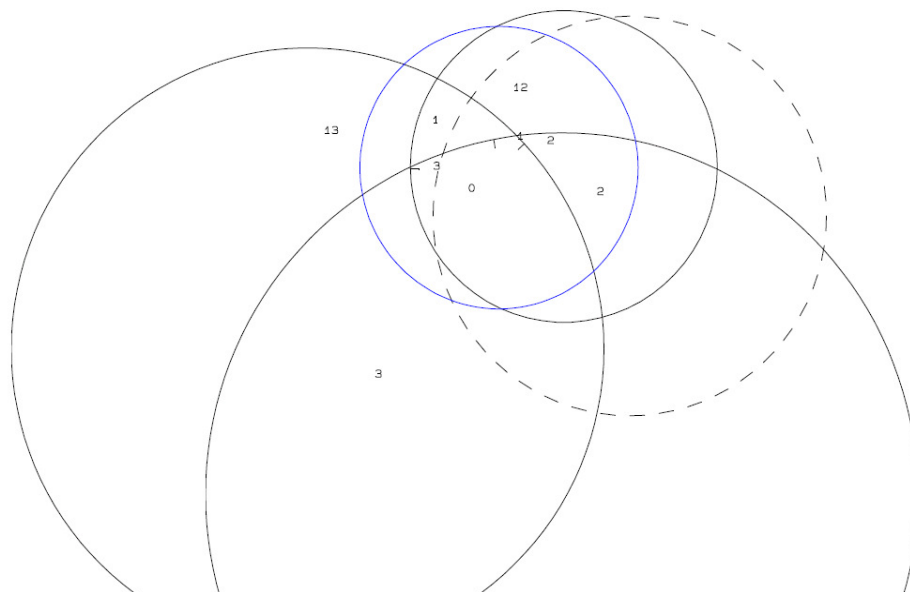


Whole sphere projection of the joint sets and the schistosity at outcrop 28 showing the joint pyramids (JPs) and their codes. The blue circle is the reference circle; the black dotted circle represents the slope assumed with 290/45.

```

RESULTANT
0.0 0.0 1.0
DIP AND DIP DIRECTION
67.0 349.0
62.0 47.0
25.0 269.0
45.0 290.0
FOCUS TO CENTER
0.0 0.0 -1.0
SUBSET OF PROJECTED PLANES
0000
    
```

23



Whole sphere projection giving the joint plane(s) along which the potential key blocks or key blocks would fail: along the intersection line of j3 with the schistosity (13).

TABLE 1: Sets and Free Planes

No.	Dip	Dip Direction	Friction Angle
1	67	349	30
2	62	47	30
3	25	269	30
1	45	290	
2	0	0	

Resultant force:
0.00D+00 0.00D+00 -1.00D+00
Free plane code for the block:
1
Bearing and rise of tunnel:
0 0

Table 2: Sign of dot product of edge and normal

	0	1	2	3	4	5	6	7	8	9	10
	+0	-1	-1	-1	+0	+0	+0	+0	+0	+0	+0
	+1	+0	-1	-1	+0	+0	+0	+0	+0	+0	+0
	+2	-1	+0	-1	+0	+0	+0	+0	+0	+0	+0
	+3	-1	-1	+0	+0	+0	+0	+0	+0	+0	+0
	+12	+0	+0	-1	+0	+0	+0	+0	+0	+0	+0
	+13	+0	-1	+0	+0	+0	+0	+0	+0	+0	+0
	+23	+1	+0	+0	+0	+0	+0	+0	+0	+0	+0

Table 3: Half spaces intersecting cutting pyramid

	0	1	2	3	4	5	6	7	8	9	10
	+0	-1	-1	-1	+0	+0	+0	+0	+0	+0	+0
	+1	+1	-1	-1	+0	+0	+0	+0	+0	+0	+0
	+2	-1	+1	-1	+0	+0	+0	+0	+0	+0	+0
	+3	-1	-1	+1	+0	+0	+0	+0	+0	+0	+0
	+12	+1	+1	-1	+0	+0	+0	+0	+0	+0	+0
	+13	+1	-1	+1	+0	+0	+0	+0	+0	+0	+0
	+23	+1	+1	+1	+0	+0	+0	+0	+0	+0	+0

Table 4: Edges of cutting pyramids

+0	+12	+13	-23	+0	+0	+0	+0	+0	+0	+0
+1	+12	+13	+23	+0	+0	+0	+0	+0	+0	+0
+2	+12	-13	-23	+0	+0	+0	+0	+0	+0	+0
+3	-12	+13	-23	+0	+0	+0	+0	+0	+0	+0
+12	+12	-13	+23	+0	+0	+0	+0	+0	+0	+0
+13	-12	+13	+23	+0	+0	+0	+0	+0	+0	+0
+23	-12	-13	+23	+0	+0	+0	+0	+0	+0	+0

Table 5: Key blocks of free plane and concave slope

PYRAMID	PLANE 1	PLANE 2	CONCAVE SLOPE
0	0	0	0
1	0	1	0
2	0	0	0
3	0	0	0
12	0	0	0
13	1	0	0
23	0	0	0

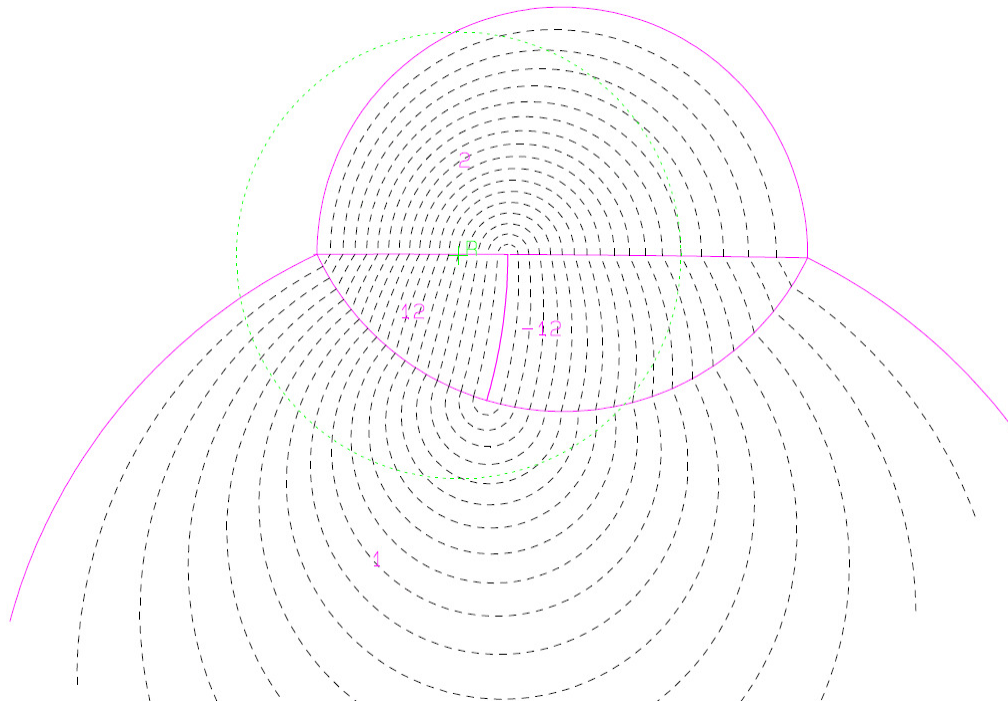
Table 6

SLIDING PLANE	SLIDING FORCE	SLIDING INTERVAL OF TUNNEL
+0.00	+1.00	+24.45
+1.00	+0.69	+285.33
+2.00	+0.61	+24.99
+3.00	-0.10	+0.00
+12.00	+0.57	+0.00
+13.00	-0.10	+204.99
+23.00	-0.44	+204.45

RESULTANT FORCE
0 0 -1
AXIS OF TUNNEL
0 1 0

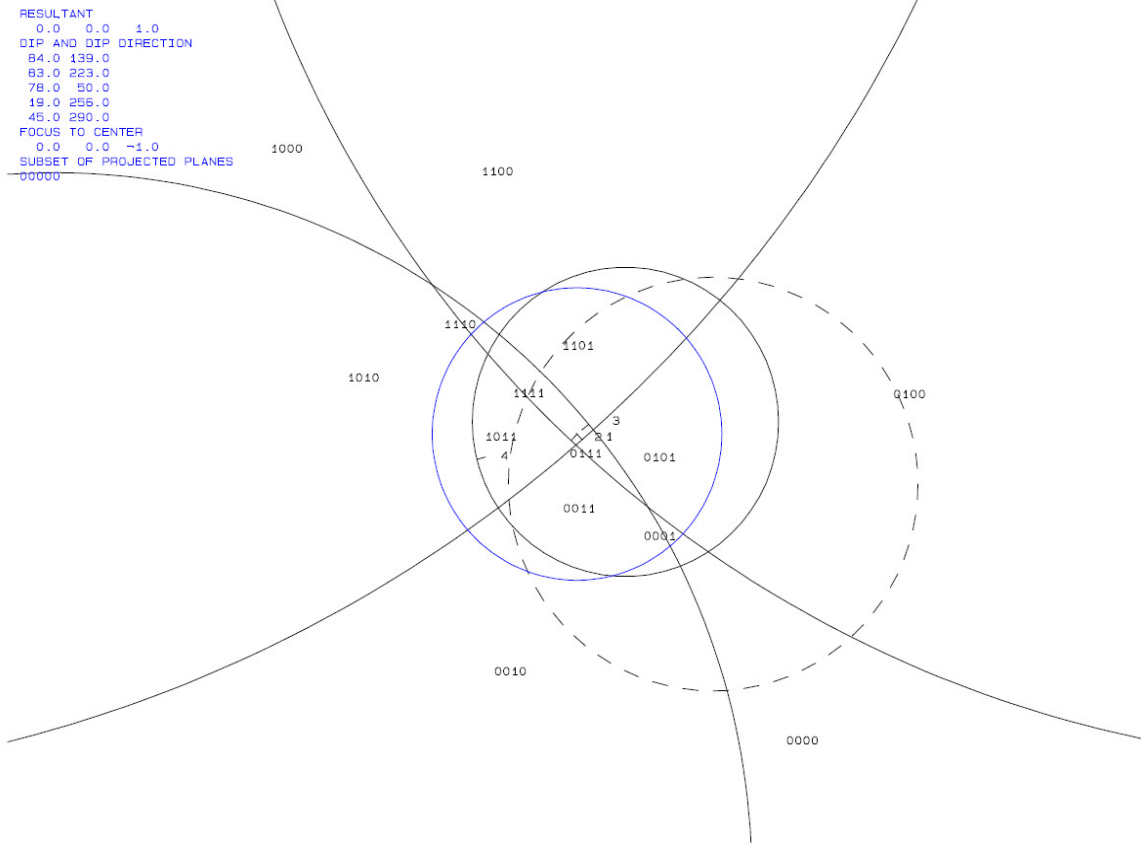
Tables resulting from the mode analysis

```
RESULTANT
0.00E+00 0.00E+00 0.40E+01
DIP DIP D. SIDE
67.0 349.0 0.0
25.0 269.0 0.0
FOCUS:
0.0 0.0 -1.0
CONTOUR INTERVAL
5.0
```

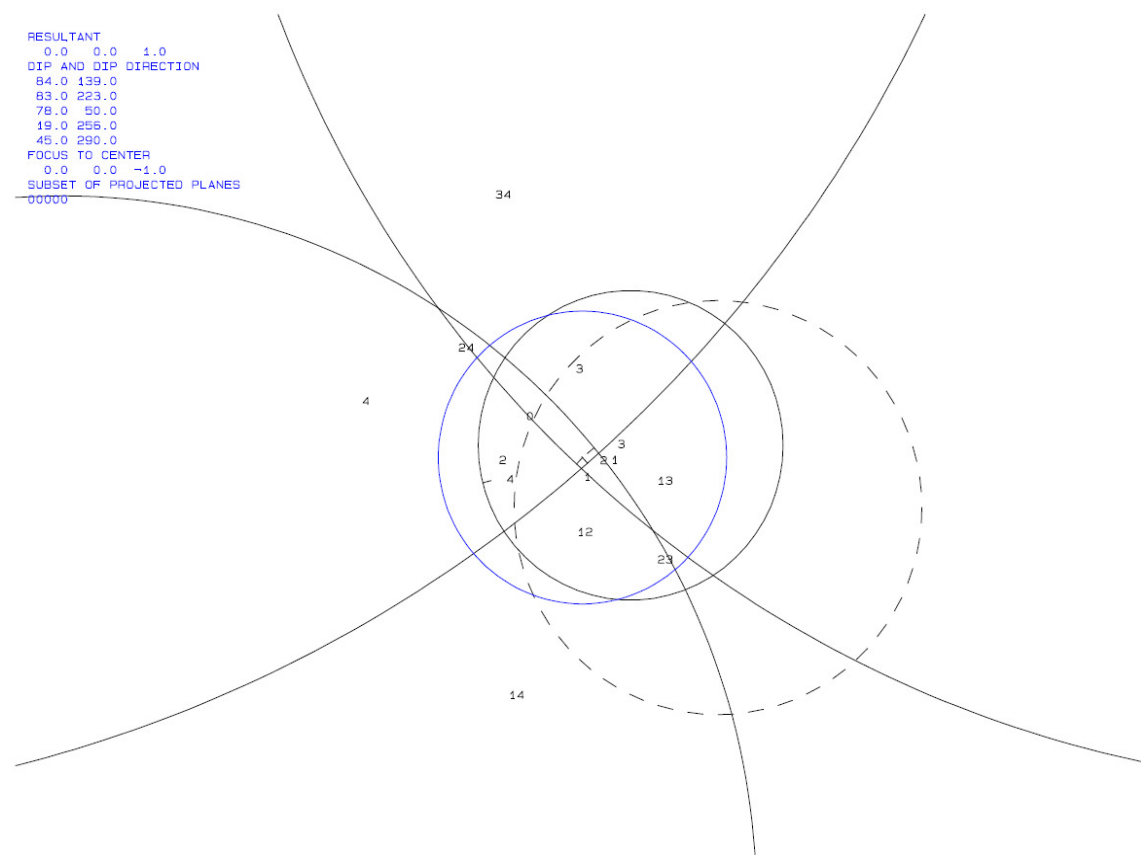


Contour plot of the friction angles for joint set j3 (= 1) and the schistosity (= 2) at outcrop 28. The green circle is the reference circle; R marks the resultant force vector.

Outcrop 34:



Whole sphere projection of the joint sets and the schistosity at outcrop 34 showing the joint pyramids (JPs) and their codes. The blue circle is the reference circle; the black dotted circle represents the slope assumed with 290/45.



Whole sphere projection giving the joint plane(s) along which the potential key blocks or key blocks would fail: along the intersection line of j2 with the schistosity (24) and along the schistosity alone (4).

TABLE 1: Sets and Free Planes

No.	Dip	Dip Direction	Friction Angle
1	84	139	30
2	83	223	30
3	78	50	30
4	19	256	30
1	45	290	
2	0	0	

Resultant force:
 0.00D+00 0.00D+00 -1.00D+00

Free plane code for the block:

1
 Bearing and rise of tunnel:
 0 0

Table 2: Sign of dot product of edge and normal

0	1	2	3	4	5	6	7	8	9	10
+0	-1	-1	-1	-1	+0	+0	+0	+0	+0	+0
+1	+0	-1	-1	-1	+0	+0	+0	+0	+0	+0
+2	-1	+0	-1	-1	+0	+0	+0	+0	+0	+0
+3	-1	-1	+0	-1	+0	+0	+0	+0	+0	+0
+4	-1	+1	-1	+0	+0	+0	+0	+0	+0	+0
+12	+0	+0	-1	-1	+0	+0	+0	+0	+0	+0
+13	+0	-1	+0	-1	+0	+0	+0	+0	+0	+0
+14	+0	+1	-1	+0	+0	+0	+0	+0	+0	+0
+23	+1	+0	+0	-1	+0	+0	+0	+0	+0	+0
+24	-1	+0	-1	+0	+0	+0	+0	+0	+0	+0
+34	-1	-1	+0	+0	+0	+0	+0	+0	+0	+0

Table 3: Half spaces intersecting cutting pyramid

0	1	2	3	4	5	6	7	8	9	10
+0	-1	-1	-1	-1	+0	+0	+0	+0	+0	+0
+1	+1	-1	-1	-1	+0	+0	+0	+0	+0	+0
+2	-1	+1	-1	-1	+0	+0	+0	+0	+0	+0
+3	-1	-1	+1	-1	+0	+0	+0	+0	+0	+0
+4	-1	+1	-1	+1	+0	+0	+0	+0	+0	+0
+12	+1	+1	-1	-1	+0	+0	+0	+0	+0	+0
+13	+1	-1	+1	-1	+0	+0	+0	+0	+0	+0
+14	+1	+1	-1	+1	+0	+0	+0	+0	+0	+0
+23	+1	+1	+1	-1	+0	+0	+0	+0	+0	+0
+24	-1	-1	-1	+1	+0	+0	+0	+0	+0	+0
+34	-1	-1	+1	+1	+0	+0	+0	+0	+0	+0

Table 4: Edges of cutting pyramids

+0	+12	+13	+24	+34	+0	+0	+0	+0	+0	+0
+1	+12	+13	+23	+0	+0	+0	+0	+0	+0	+0
+2	+12	+14	+24	+0	+0	+0	+0	+0	+0	+0
+3	+13	-14	+34	+0	+0	+0	+0	+0	+0	+0
+4	-13	+14	-23	+24	+0	+0	+0	+0	+0	+0
+12	+12	+14	+23	-34	+0	+0	+0	+0	+0	+0
+13	+13	-14	+23	-24	+0	+0	+0	+0	+0	+0
+14	-13	+14	-34	+0	+0	+0	+0	+0	+0	+0
+23	+23	-24	-34	+0	+0	+0	+0	+0	+0	+0
+24	-23	+24	+34	+0	+0	+0	+0	+0	+0	+0
+34	-12	-14	-23	+34	+0	+0	+0	+0	+0	+0

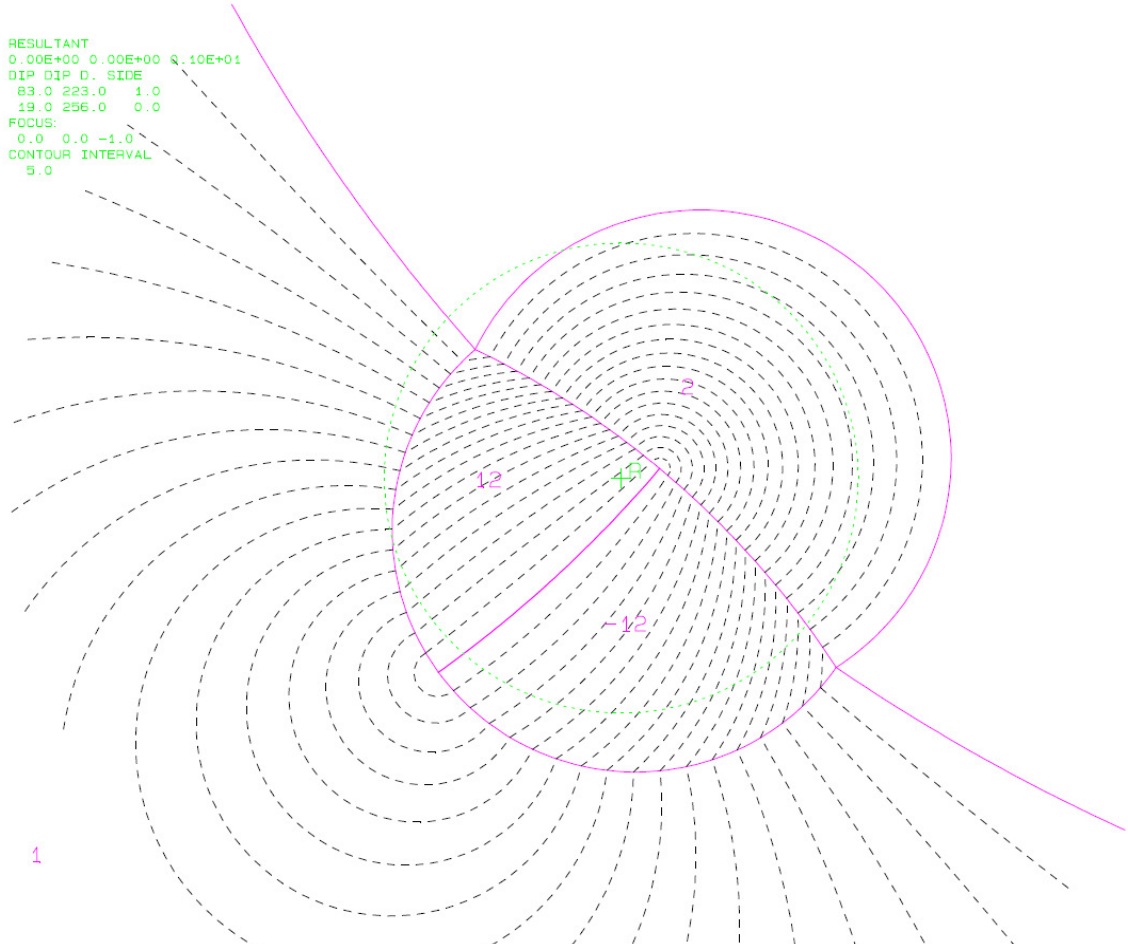
Table 5: Key blocks of free plane and concave slope

PYRAMID	PLANE 1	PLANE 2	CONCAVE SLOPE
0	0	1	0
1	0	1	0
2	0	1	0
3	0	0	0
4	1	0	0
12	0	0	0
13	0	0	0
14	0	0	0
23	0	0	0
24	1	0	0
34	0	0	0

Table 6

SLIDING PLANE	SLIDING FORCE	SLIDING INTERVAL OF TUNNEL
+0.00	+1.00	+282.84
+1.00	+0.93	+332.53
+2.00	+0.92	+269.09
+3.00	+0.86	+0.00
+4.00	-0.22	+202.36
+12.00	+0.87	+12.87
+13.00	+0.80	+22.36
+14.00	-0.35	+0.00
+23.00	-2.74	+14.58
+24.00	-0.58	+194.58
+34.00	-0.59	+192.87
RESULTANT FORCE		
0	0	-1
AXIS OF TUNNEL		
0	1	0

Tables resulting from the mode analysis

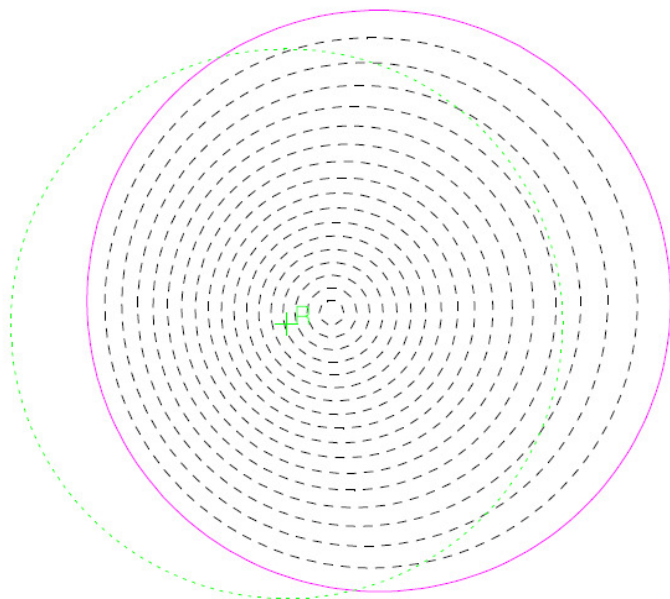


Contour plot of the friction angles for joint set j_2 (= 1) and the schistosity (= 2) at outcrop 34. The green circle is the reference circle; R marks the resultant force vector.

```

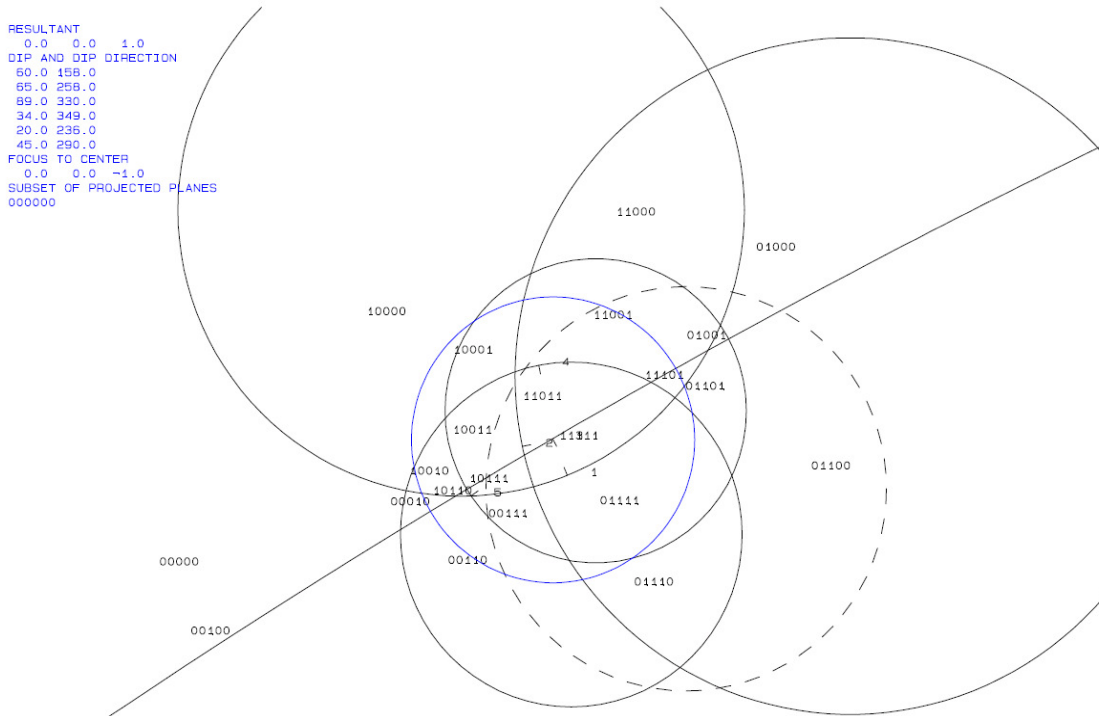
RESULTANT
0.00E+00 0.00E+00 0.10E+01
DIP DIP D. SIDE
19.0 256.0 0.0
FOCUS:
0.0 0.0 -1.0
CONTOUR INTERVAL
5.0

```

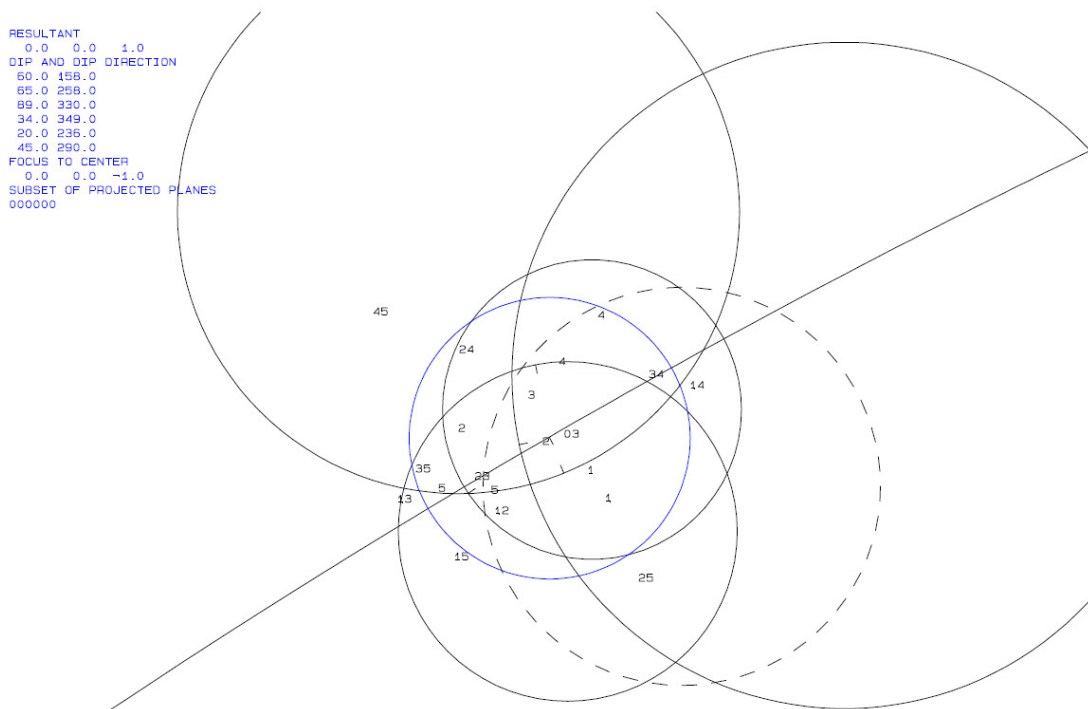


Contour plot of the friction angles for the schistosity alone at outcrop 34. The green circle is the reference circle; R marks the resultant force vector.

Outcrop 77:



Whole sphere projection of the joint sets and the schistosity at outcrop 77 showing the joint pyramids (JPs) and their codes. The blue circle is the reference circle; the black dotted circle represents the slope assumed with 290/45.



Whole sphere projection giving the joint plane(s) along which the potential key blocks or key blocks would fail: along the intersection line of j1 with j3 (13), j2 with j5 (24), j3 with the schistosity (35), j5 with the schistosity (45) and along the schistosity alone (5).

TABLE 1: Sets and Free Planes

No.	Dip	Dip Direction	Friction Angle
1	60	158	30
2	65	258	30
3	89	330	30
4	34	349	30
5	20	236	30
1	45	290	
2	0	0	

Resultant force:
0.00D+00 0.00D+00 -1.00D+00
Free plane code for the block:
1
Bearing and rise of tunnel:
0 0

Table 2: Sign of dot product of edge and normal

	0	1	2	3	4	5	6	7	8	9	10
+0	-1	-1	-1	-1	-1	-1	+0	+0	+0	+0	+0
+1	+0	-1	-1	-1	-1	-1	+0	+0	+0	+0	+0
+2	-1	+0	+1	-1	-1	-1	+0	+0	+0	+0	+0
+3	-1	-1	+0	-1	-1	-1	+0	+0	+0	+0	+0
+4	-1	-1	+1	+0	-1	-1	+0	+0	+0	+0	+0
+5	-1	+1	-1	-1	-1	+0	+0	+0	+0	+0	+0
+12	+0	+0	-1	-1	-1	+0	+0	+0	+0	+0	+0
+13	+0	+1	+0	-1	+1	+0	+0	+0	+0	+0	+0
+14	+0	-1	-1	+0	-1	+0	+0	+0	+0	+0	+0
+15	+0	+1	-1	-1	+0	+0	+0	+0	+0	+0	+0
+23	-1	+0	+0	-1	-1	+0	+0	+0	+0	+0	+0
+24	-1	+0	+1	+0	-1	+0	+0	+0	+0	+0	+0
+25	+1	+0	-1	-1	+0	+0	+0	+0	+0	+0	+0
+34	-1	-1	+0	+0	-1	+0	+0	+0	+0	+0	+0
+35	-1	+1	+0	-1	+0	+0	+0	+0	+0	+0	+0
+45	-1	+1	+1	+0	+0	+0	+0	+0	+0	+0	+0

Table 3: Half spaces intersecting cutting pyramid

	0	1	2	3	4	5	6	7	8	9	10
+0	-1	-1	-1	-1	-1	-1	+0	+0	+0	+0	+0
+1	+1	-1	-1	-1	-1	-1	+0	+0	+0	+0	+0
+2	-1	+1	+1	-1	-1	-1	+0	+0	+0	+0	+0
+3	-1	-1	+1	-1	-1	-1	+0	+0	+0	+0	+0
+4	-1	-1	+1	+1	-1	-1	+0	+0	+0	+0	+0
+5	-1	+1	-1	-1	-1	+1	+0	+0	+0	+0	+0
+12	+1	+1	-1	-1	-1	-1	+0	+0	+0	+0	+0
+13	+1	+1	+1	-1	-1	+1	+0	+0	+0	+0	+0
+14	+1	-1	-1	+1	-1	-1	+0	+0	+0	+0	+0
+15	+1	+1	-1	-1	-1	+1	+0	+0	+0	+0	+0
+23	-1	+1	-1	-1	-1	-1	+0	+0	+0	+0	+0
+24	-1	+1	+1	+1	+1	-1	+0	+0	+0	+0	+0
+25	+1	-1	-1	-1	-1	+1	+0	+0	+0	+0	+0
+34	-1	-1	-1	+1	-1	-1	+0	+0	+0	+0	+0
+35	-1	+1	+1	+1	-1	+1	+0	+0	+0	+0	+0
+45	-1	+1	+1	+1	+1	+1	+0	+0	+0	+0	+0

Table 4: Edges of cutting pyramids

+0	+12	+14	+23	+34	+0	+0	+0	+0	+0	+0
+1	+12	+14	+25	-45	+0	+0	+0	+0	+0	+0
+2	+23	+24	+35	+45	+0	+0	+0	+0	+0	+0
+3	+23	+24	+34	+0	+0	+0	+0	+0	+0	+0
+4	-13	-15	+24	-25	+34	+0	+0	+0	+0	+0
+5	+13	+15	+35	+0	+0	+0	+0	+0	+0	+0
+12	+12	+15	+25	+0	+0	+0	+0	+0	+0	+0
+13	+13	-14	-34	+0	+0	+0	+0	+0	+0	+0
+14	-13	+14	-35	-45	+0	+0	+0	+0	+0	+0
+15	+13	+15	-24	+25	-34	+0	+0	+0	+0	+0
+23	+12	+15	+23	+35	+0	+0	+0	+0	+0	+0
+24	+24	-25	+45	+0	+0	+0	+0	+0	+0	+0
+25	-24	+25	-45	+0	+0	+0	+0	+0	+0	+0
+34	-13	+14	+34	+0	+0	+0	+0	+0	+0	+0
+35	+13	-14	+35	+45	+0	+0	+0	+0	+0	+0
+45	-12	-14	-25	+45	+0	+0	+0	+0	+0	+0

Table 5: Key blocks of free plane and concave slope

PYRAMID	PLANE 1	PLANE 2	CONCAVE SLOPE
0	0	1	0
1	0	0	0
2	0	1	0
3	0	1	0
4	0	0	0
5	1	1	1
12	0	1	0
13	1	0	0
14	0	0	0
15	0	0	0
23	0	1	0
24	1	0	0
25	0	0	0
34	0	0	0
35	1	0	0
45	1	0	0

Table 6

SLIDING PLANE	SLIDING FORCE	SLIDING INTERVAL OF TUNNEL
+0.00	+1.00	+354.39
+1.00	+0.58	+14.63
+2.00	+0.66	+246.81
+3.00	+0.99	+345.59
+4.00	+0.08	+0.00
+5.00	-0.20	+203.74
+12.00	+0.28	+309.65
+13.00	-1.75	+195.09
+14.00	-0.72	+22.66
+15.00	-0.20	+0.00
+23.00	+0.57	+252.40
+24.00	+0.00	+232.54
+25.00	-0.79	+52.54
+34.00	-0.81	+15.09
+35.00	-0.22	+202.66
+45.00	-0.35	+194.63

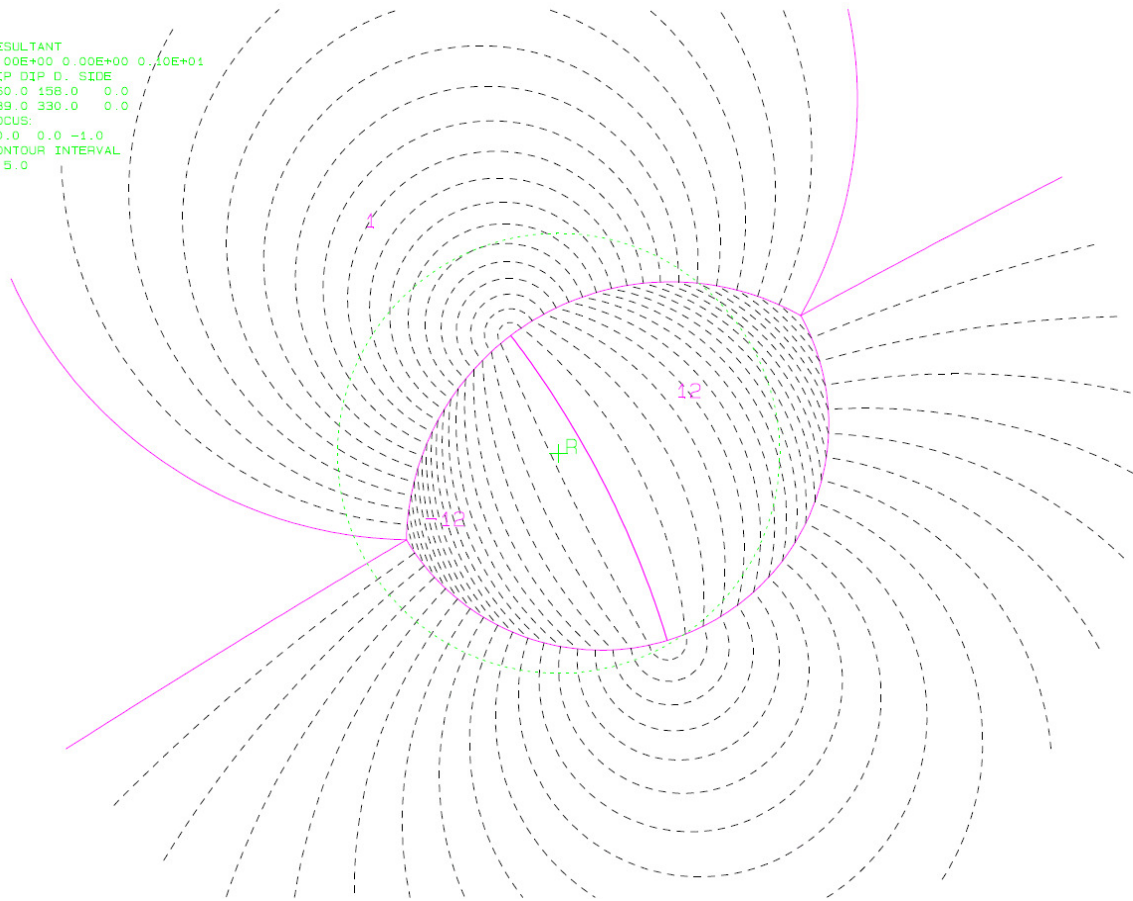
RESULTANT FORCE
0 0 -1
AXIS OF TUNNEL
0 1 0

Tables resulting from the mode analysis

```

RESULTANT
0.00E+00 0.00E+00 0.10E+01
DIP DIP D. SIDE
60.0 158.0 0.0
89.0 330.0 0.0
FOCUS:
0.0 0.0 -1.0
CONTOUR INTERVAL
5.0

```

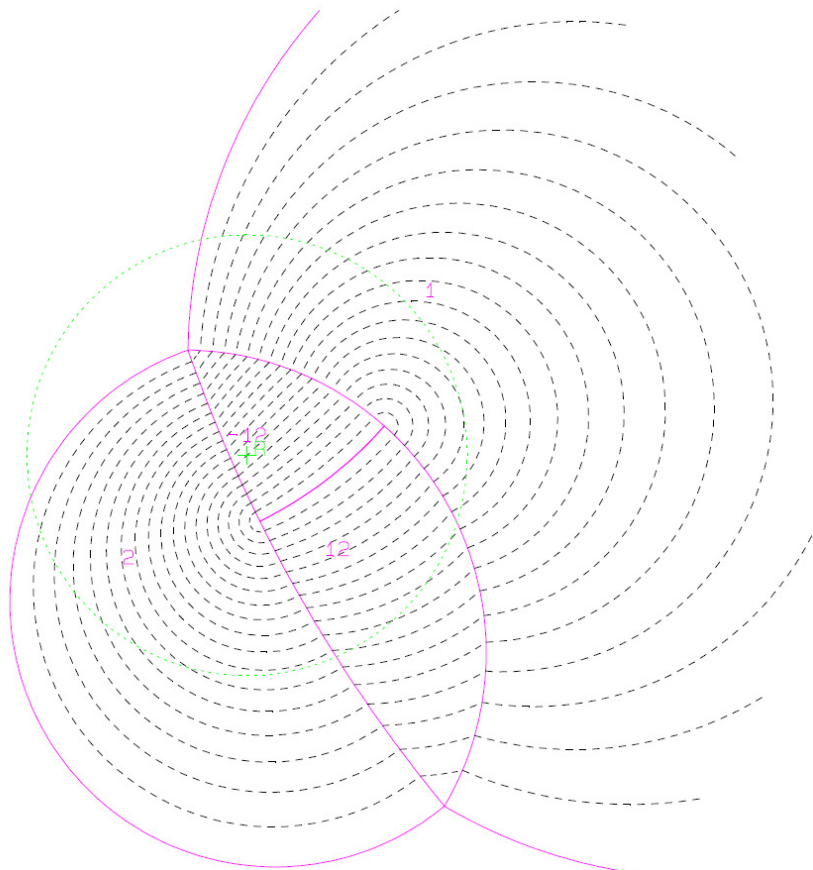


Contour plot of the friction angles for joint set j1 (= 1) and j3 (= 2) at outcrop 77. The green circle is the reference circle; R marks the resultant force vector.

```

RESULTANT
0.00E+00 0.00E+00 0.10E+01
DIP DIP D. SIDE
65.0 258.0 0.0
34.0 349.0 0.0
FOCUS:
0.0 0.0 -1.0
CONTOUR INTERVAL
5.0

```

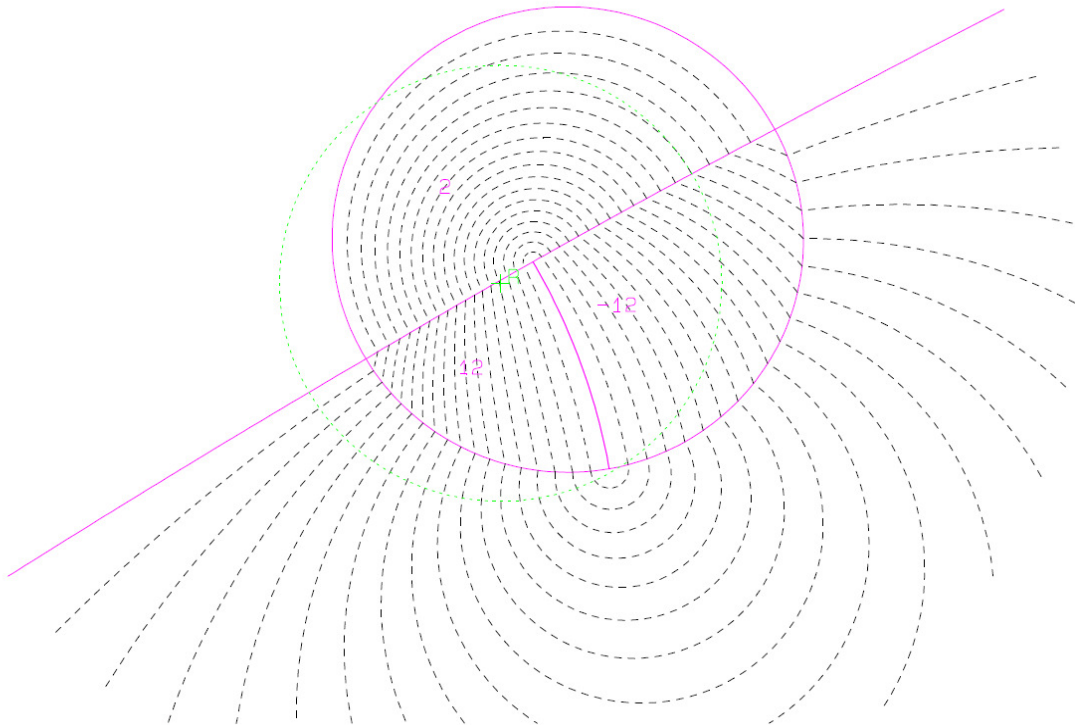


Contour plot of the friction angles for joint set j2 (= 1) and j5 (= 2) at outcrop 77. The green circle is the reference circle; R marks the resultant force vector.

```

RESULTANT
0.00E+00 0.00E+00 0.10E+01
DIP DIP D. SIDE
89.0 330.0 0.0
20.0 236.0 0.0
FOCUS:
0.0 0.0 -1.0
CONTOUR INTERVAL
5.0

```

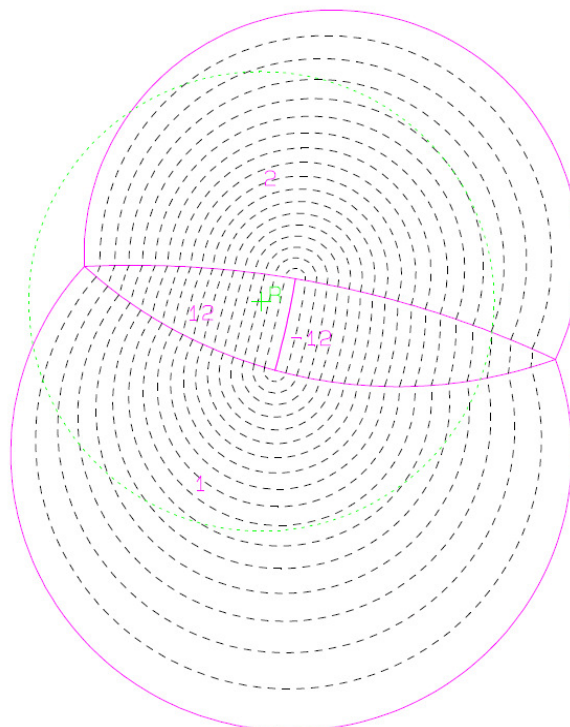


Contour plot of the friction angles for joint set j3 (= 1) and the schistosity (= 2) at outcrop 77. The green circle is the reference circle; R marks the resultant force vector.

```

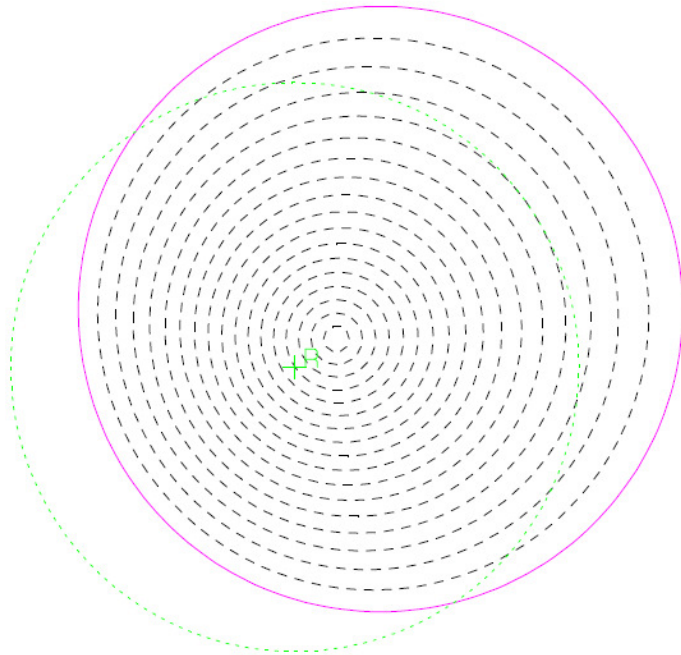
RESULTANT
0.00E+00 0.00E+00 0.10E+01
DIP DIP D. SIDE
34.0 349.0 0.0
20.0 236.0 0.0
FOCUS:
0.0 0.0 -1.0
CONTOUR INTERVAL
5.0

```



Contour plot of the friction angles for joint set j5 (= 1) and the schistosity (= 2) at outcrop 77. The green circle is the reference circle; R marks the resultant force vector.

```
RESULTANT
0.00E+00 0.00E+00 0.10E+01
DIP DIP D. SIDE
20.0 236.0 0.0
FOCUS:
0.0 0.0 -1.0
CONTOUR INTERVAL
5.0
```

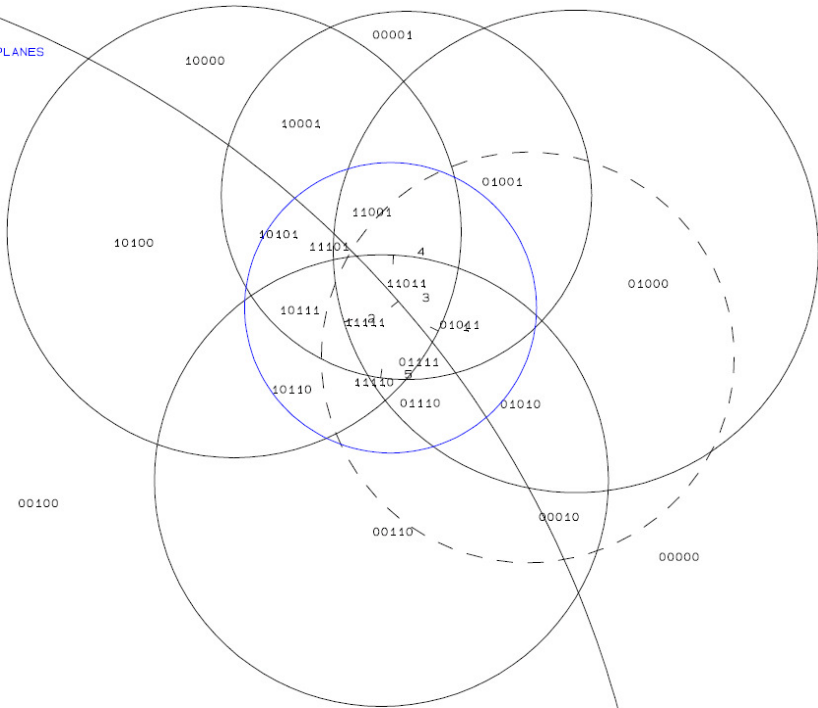


Contour plot of the friction angles for the schistosity alone at outcrop 77. The green circle is the reference circle; R marks the resultant force vector.

Outcrop 121:

```

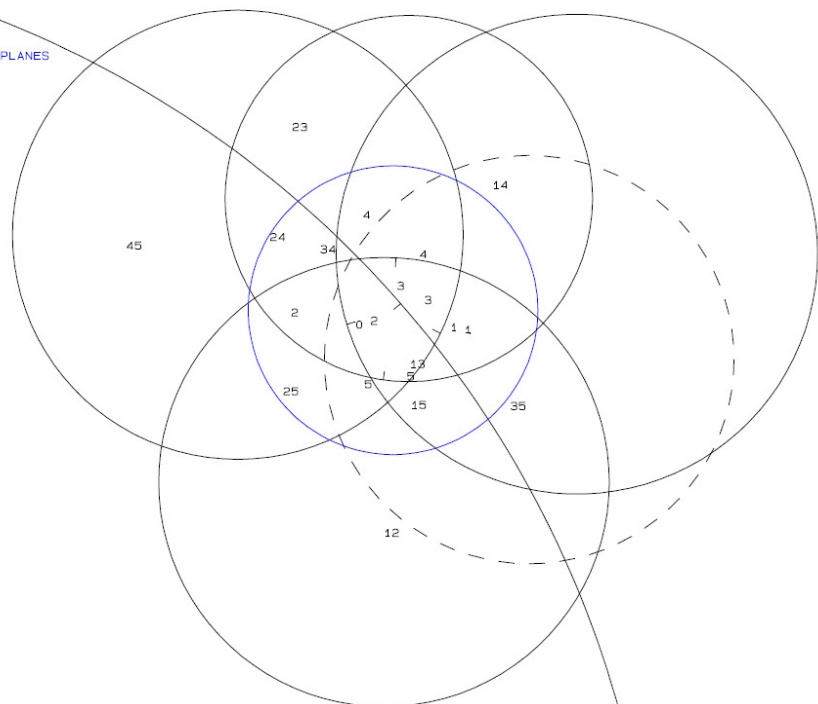
RESULTANT
0.0 0.0 1.0
DIP AND DIP DIRECTION
50.0 115.0
53.0 253.0
52.0 49.0
50.0 3.0
38.0 188.0
45.0 290.0
FOCUS TO CENTER
0.0 0.0 -1.0
SUBSET OF PROJECTED PLANES
000000
    
```



Whole sphere projection of the joint sets and the schistosity at outcrop 121 showing the joint pyramids (JPs) and their codes. The blue circle is the reference circle; the black dotted circle represents the slope assumed with 290/45.

```

RESULTANT
0.0 0.0 1.0
DIP AND DIP DIRECTION
50.0 115.0
53.0 253.0
52.0 49.0
50.0 3.0
38.0 188.0
45.0 290.0
FOCUS TO CENTER
0.0 0.0 -1.0
SUBSET OF PROJECTED PLANES
000000
    
```



Whole sphere projection giving the joint plane(s) along which the potential key blocks or key blocks would fail: along the intersection line of j2 with j4 (23), j2 with j5 (24) and j5 with the schistosity (45).

TABLE 1: Sets and Free Planes

No.	Dip	Dip Direction	Friction Angle
1	50	116	30
2	53	253	30
3	82	49	30
4	50	3	30
5	38	188	30
1	45	290	
2	0	0	

Resultant force:
0.00D+00 0.00D+00 -1.00D+00
Free plane code for the block:
1
Bearing and rise of tunnel:
0 0

Table 2: Sign of dot product of edge and normal

0	1	2	3	4	5	6	7	8	9	10
+0	-1	-1	-1	-1	-1	+0	+0	+0	+0	+0
+1	+0	-1	+1	-1	-1	+0	+0	+0	+0	+0
+2	-1	+0	-1	-1	-1	+0	+0	+0	+0	+0
+3	-1	-1	+0	-1	-1	+0	+0	+0	+0	+0
+4	-1	-1	+1	+0	-1	+0	+0	+0	+0	+0
+5	-1	-1	-1	-1	-1	+0	+0	+0	+0	+0
+12	+0	+0	-1	-1	+1	+0	+0	+0	+0	+0
+13	+0	-1	+0	-1	-1	+0	+0	+0	+0	+0
+14	+0	-1	+1	+0	-1	+0	+0	+0	+0	+0
+15	+0	-1	-1	-1	+0	+0	+0	+0	+0	+0
+23	-1	+0	+0	+1	-1	+0	+0	+0	+0	+0
+24	-1	+0	-1	+0	-1	+0	+0	+0	+0	+0
+25	-1	+0	-1	-1	+0	+0	+0	+0	+0	+0
+34	-1	-1	+0	+0	-1	+0	+0	+0	+0	+0
+35	+1	-1	+0	-1	+0	+0	+0	+0	+0	+0
+45	-1	+1	-1	+0	+0	+0	+0	+0	+0	+0

Table 3: Half spaces intersecting cutting pyramid

0	1	2	3	4	5	6	7	8	9	10
+0	-1	-1	-1	-1	-1	+0	+0	+0	+0	+0
+1	+1	-1	+1	-1	-1	+0	+0	+0	+0	+0
+2	-1	+1	-1	-1	-1	+0	+0	+0	+0	+0
+3	-1	-1	+1	-1	-1	+0	+0	+0	+0	+0
+4	-1	-1	+1	+1	-1	+0	+0	+0	+0	+0
+5	-1	-1	-1	-1	+1	+0	+0	+0	+0	+0
+12	+1	+1	-1	-1	+1	+0	+0	+0	+0	+0
+13	+1	-1	-1	-1	-1	+0	+0	+0	+0	+0
+14	+1	-1	+1	+1	-1	+0	+0	+0	+0	+0
+15	+1	-1	-1	-1	+1	+0	+0	+0	+0	+0
+23	-1	+1	+1	+1	-1	+0	+0	+0	+0	+0
+24	-1	+1	-1	+1	-1	+0	+0	+0	+0	+0
+25	-1	+1	-1	-1	+1	+0	+0	+0	+0	+0
+34	-1	-1	-1	+1	-1	+0	+0	+0	+0	+0
+35	+1	-1	+1	-1	+1	+0	+0	+0	+0	+0
+45	-1	+1	-1	+1	+1	+0	+0	+0	+0	+0

Table 4: Edges of cutting pyramids

+0	+13	+15	+24	+25	+34	+0	+0	+0	+0
+1	+13	+14	+35	-45	+0	+0	+0	+0	+0
+2	+24	+25	+45	+0	+0	+0	+0	+0	+0
+3	+13	+14	+34	+0	+0	+0	+0	+0	+0
+4	-12	+14	+23	+34	+0	+0	+0	+0	+0
+5	+12	+15	+25	+0	+0	+0	+0	+0	+0
+12	+12	-14	-23	-34	+0	+0	+0	+0	+0
+13	+13	+15	+35	+0	+0	+0	+0	+0	+0
+14	-12	+14	-25	-45	+0	+0	+0	+0	+0
+15	+12	+15	-23	+35	+0	+0	+0	+0	+0
+23	-12	-15	+23	-35	+0	+0	+0	+0	+0
+24	+23	+24	-35	+45	+0	+0	+0	+0	+0
+25	+12	-14	+25	+45	+0	+0	+0	+0	+0
+34	+23	+24	+34	+0	+0	+0	+0	+0	+0
+35	-23	-24	+35	-45	+0	+0	+0	+0	+0
+45	-13	-14	-35	+45	+0	+0	+0	+0	+0

Table 5: Key blocks of free plane and concave slope

PYRAMID	PLANE 1	PLANE 2	CONCAVE SLOPE
0	0	1	0
1	0	0	0
2	0	1	0
3	0	1	0
4	0	0	0
5	0	1	0
12	0	0	0
13	0	1	0
14	0	0	0
15	0	0	0
23	1	0	0
24	1	0	0
25	0	0	0
34	0	1	0
35	0	0	0
45	1	0	0

Table 6

SLIDING PLANE	SLIDING FORCE	SLIDING INTERVAL OF TUNNEL
+0.00	+1.00	+303.62
+1.00	+0.39	+2.37
+2.00	+0.45	+247.68
+3.00	+0.91	+322.64
+4.00	+0.39	+0.00
+5.00	+0.16	+285.84
+12.00	-0.35	+0.00
+13.00	+0.28	+326.17
+14.00	-0.08	+82.90
+15.00	+0.09	+37.22
+23.00	-0.77	+217.22
+24.00	-0.03	+223.28
+25.00	+0.13	+262.90
+34.00	-0.07	+240.31
+35.00	-0.40	+43.28
+45.00	-0.76	+182.37

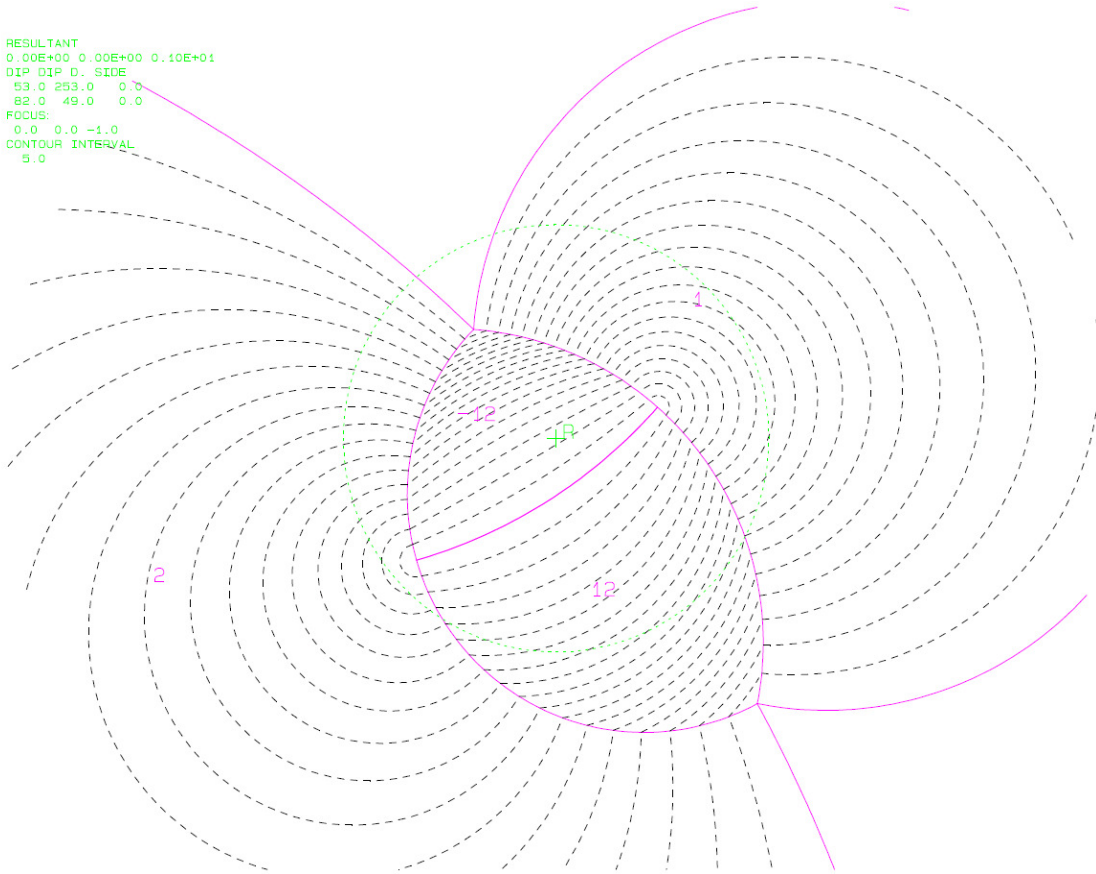
RESULTANT FORCE
0 -1
AXIS OF TUNNEL
0 1

Tables resulting from the mode analysis

```

RESULTANT
0.00E+00 0.00E+00 0.10E+01
DIP DIP D. SIDE
53.0 253.0 0.0
82.0 49.0 0.0
FOCUS:
0.0 0.0 -1.0
CONTOUR INTERVAL
5.0

```

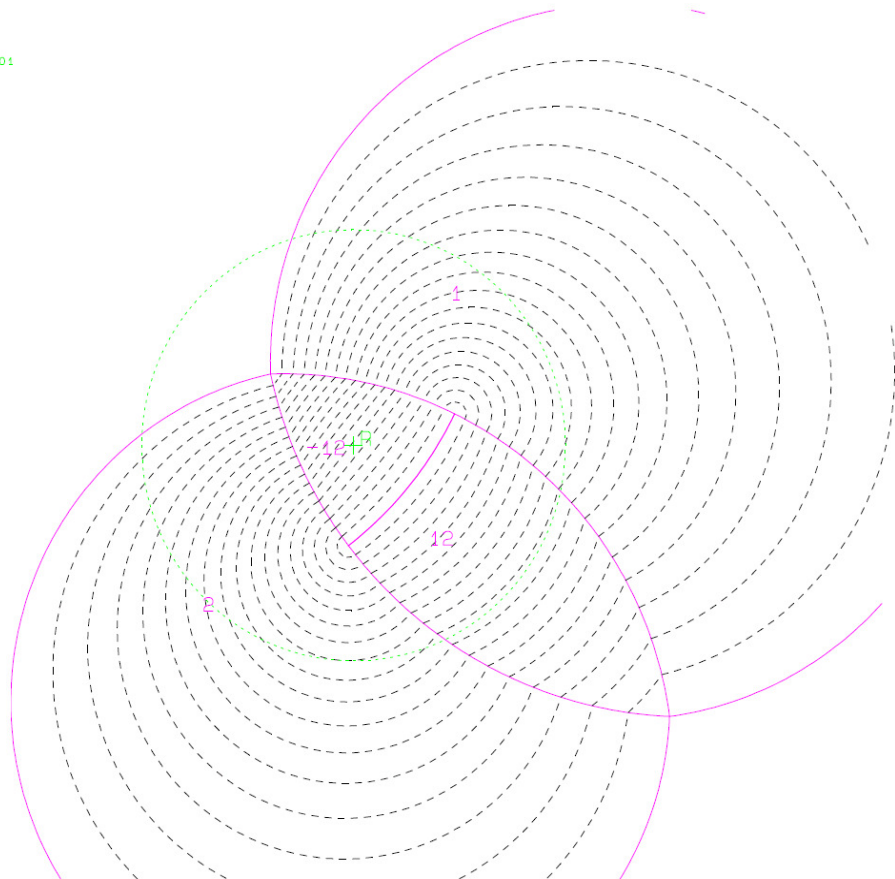


Contour plot of the friction angles for joint set j2 (= 1) and j4 (= 2) at outcrop 121. The green circle is the reference circle; R marks the resultant force vector.

```

RESULTANT
0.00E+00 0.00E+00 0.10E+01
DIP DIP D. SIDE
53.0 253.0 0.0
50.0 3.0 0.0
FOCUS:
0.0 0.0 -1.0
CONTOUR INTERVAL
5.0

```

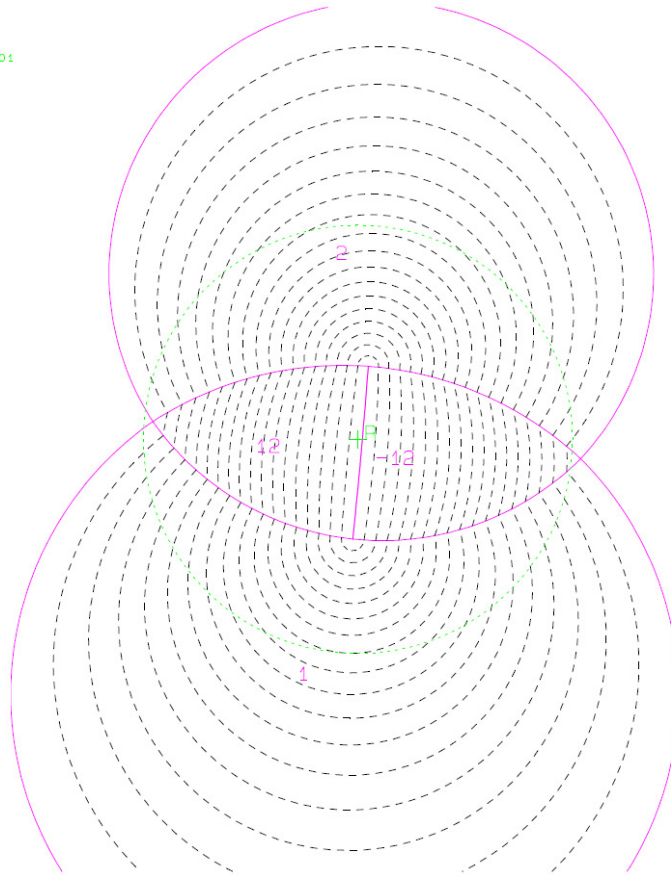


Contour plot of the friction angles for joint set j2 (= 1) and j5 (= 2) at outcrop 121. The green circle is the reference circle; R marks the resultant force vector.

```

RESULTANT
0.00E+00 0.00E+00 0.10E+01
DIP DIP D. SIDE
50.0 3.0 0.0
38.0 188.0 0.0
FOCUS:
0.0 0.0 -1.0
CONTOUR INTERVAL
5.0

```

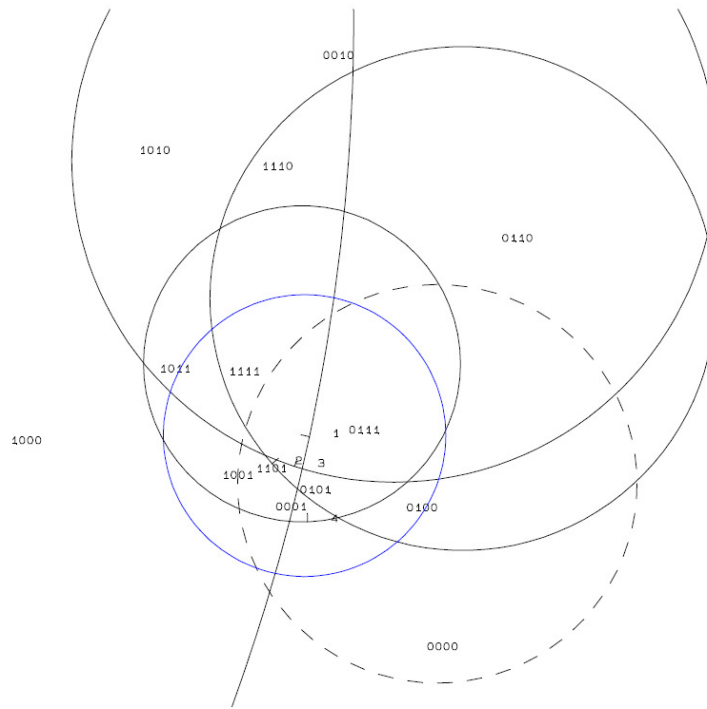


Contour plot of the friction angles for joint set j5 (= 1) and the schistosity (= 2) at outcrop 121. The green circle is the reference circle; R marks the resultant force vector.

Outcrop 126:

```

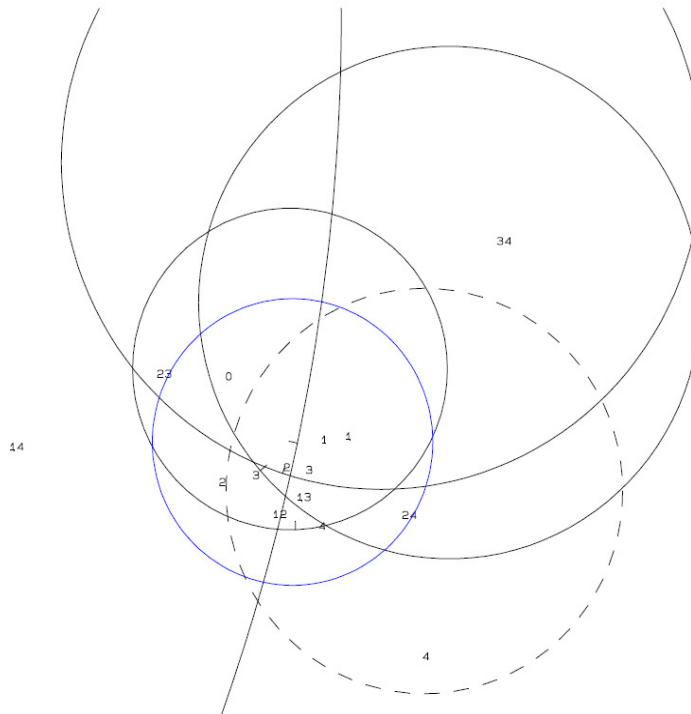
RESULTANT
0.0 0.0 1.0
DIP AND DIP DIRECTION
86.0 102.0
56.0 229.0
54.0 198.0
27.0 178.0
45.0 290.0
FOCUS TO CENTER
0.0 0.0 -1.0
SUBSET OF PROJECTED PLANES
00000
    
```



Whole sphere projection of the joint sets and the schistosity at outcrop 126 showing the joint pyramids (JPs) and their codes. The blue circle is the reference circle; the black dotted circle represents the slope assumed with 290/45.

```

RESULTANT
0.0 0.0 1.0
DIP AND DIP DIRECTION
86.0 102.0
56.0 229.0
54.0 198.0
27.0 178.0
45.0 290.0
FOCUS TO CENTER
0.0 0.0 -1.0
SUBSET OF PROJECTED PLANES
00000
    
```



Whole sphere projection giving the joint plane(s) along which the potential key blocks or key blocks would fail. In this case the removable blocks are all safe (type III blocks).

TABLE 1: Sets and Free Planes

No.	Dip	Dip Direction	Friction Angle
1	86	102	30
2	56	229	30
3	64	198	30
4	27	178	30
1	45	290	
2	0	0	

Resultant force:
 0.00D+00 0.00D+00 -1.00D+00

Free plane code for the block:

1
 Bearing and rise of tunnel:
 0 0

Table 2: Sign of dot product of edge and normal

0	1	2	3	4	5	6	7	8	9	10
+0	-1	-1	-1	-1	+0	+0	+0	+0	+0	+0
+1	+0	-1	-1	-1	+0	+0	+0	+0	+0	+0
+2	-1	+0	+1	-1	+0	+0	+0	+0	+0	+0
+3	-1	-1	+0	-1	+0	+0	+0	+0	+0	+0
+4	+1	+1	+1	+0	+0	+0	+0	+0	+0	+0
+12	+0	+0	+1	-1	+0	+0	+0	+0	+0	+0
+13	+0	-1	+0	-1	+0	+0	+0	+0	+0	+0
+14	+0	+1	+1	+0	+0	+0	+0	+0	+0	+0
+23	-1	+0	+0	-1	+0	+0	+0	+0	+0	+0
+24	+1	+0	+1	+0	+0	+0	+0	+0	+0	+0
+34	+1	-1	+0	+0	+0	+0	+0	+0	+0	+0

Table 3: Half spaces intersecting cutting pyramid

0	1	2	3	4	5	6	7	8	9	10
+0	-1	-1	-1	-1	+0	+0	+0	+0	+0	+0
+1	+1	-1	-1	-1	+0	+0	+0	+0	+0	+0
+2	-1	+1	+1	-1	+0	+0	+0	+0	+0	+0
+3	-1	-1	+1	-1	+0	+0	+0	+0	+0	+0
+4	+1	+1	+1	+1	+0	+0	+0	+0	+0	+0
+12	+1	+1	+1	-1	+0	+0	+0	+0	+0	+0
+13	+1	-1	+1	-1	+0	+0	+0	+0	+0	+0
+14	-1	+1	+1	+1	+0	+0	+0	+0	+0	+0
+23	-1	+1	-1	-1	+0	+0	+0	+0	+0	+0
+24	+1	-1	+1	+1	+0	+0	+0	+0	+0	+0
+34	+1	-1	-1	+1	+0	+0	+0	+0	+0	+0

Table 4: Edges of cutting pyramids

+0	+13	-14	+23	-24	+0	+0	+0	+0	+0	+0
+1	+13	-14	+34	+0	+0	+0	+0	+0	+0	+0
+2	+12	+14	+23	-34	+0	+0	+0	+0	+0	+0
+3	+12	+13	+23	+0	+0	+0	+0	+0	+0	+0
+4	-13	+14	-23	+24	+0	+0	+0	+0	+0	+0
+12	+12	+14	+24	+0	+0	+0	+0	+0	+0	+0
+13	+12	+13	+24	+34	+0	+0	+0	+0	+0	+0
+14	-13	+14	-34	+0	+0	+0	+0	+0	+0	+0
+23	+23	-24	-34	+0	+0	+0	+0	+0	+0	+0
+24	-23	+24	+34	+0	+0	+0	+0	+0	+0	+0
+34	-12	-14	-23	+34	+0	+0	+0	+0	+0	+0

Table 5: Key blocks of free plane and concave slope

PYRAMID	PLANE 1	PLANE 2	CONCAVE SLOPE
0	0	0	0
1	0	0	0
2	0	0	0
3	0	1	0
4	0	0	0
12	0	1	0
13	0	1	0
14	0	0	0
23	0	0	0
24	0	0	0
34	0	0	0

Table 6

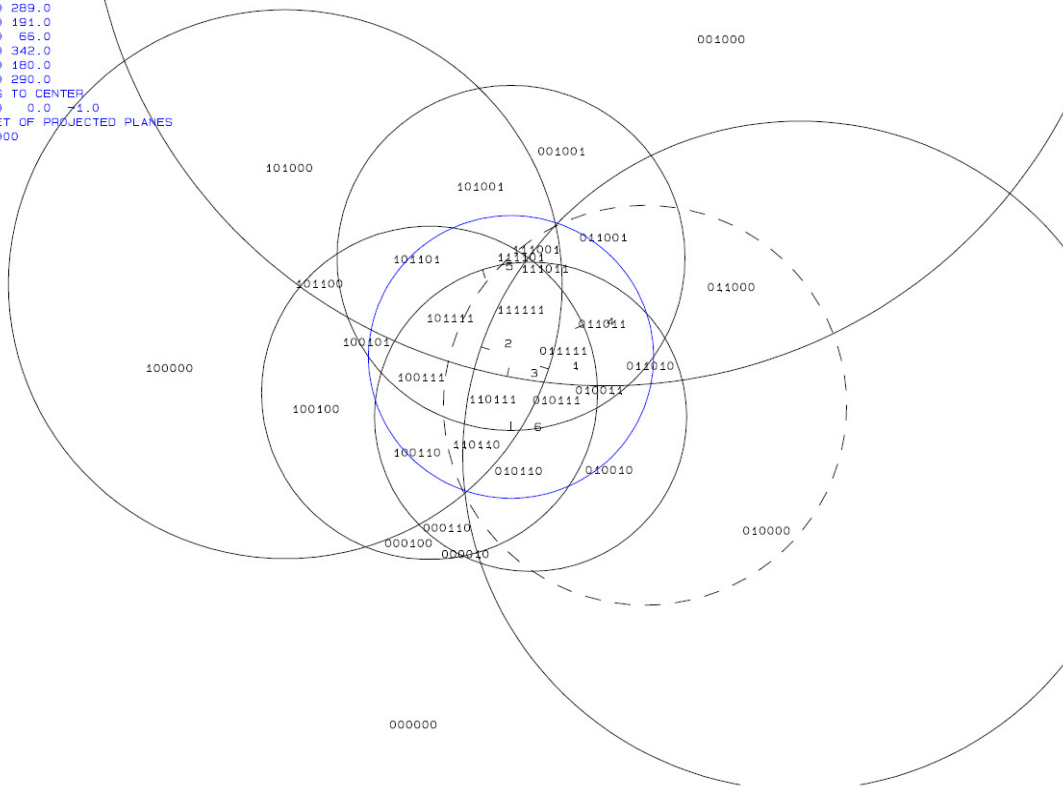
SLIDING PLANE	SLIDING FORCE	SLIDING INTERVAL OF TUNNEL
+0.00	+1.00	+0.00
+1.00	+0.96	+70.79
+2.00	+0.51	+263.26
+3.00	+0.65	+267.99
+4.00	-0.06	+0.00
+12.00	+0.07	+308.29
+13.00	+0.58	+346.07
+14.00	-0.13	+250.79
+23.00	+0.22	+238.03
+24.00	-0.29	+58.03
+34.00	-0.94	+83.26
RESULTANT FORCE		
0	0	-1
AXIS OF TUNNEL		
0	1	0

Tables resulting from the mode analysis

Outcrop 127:

```

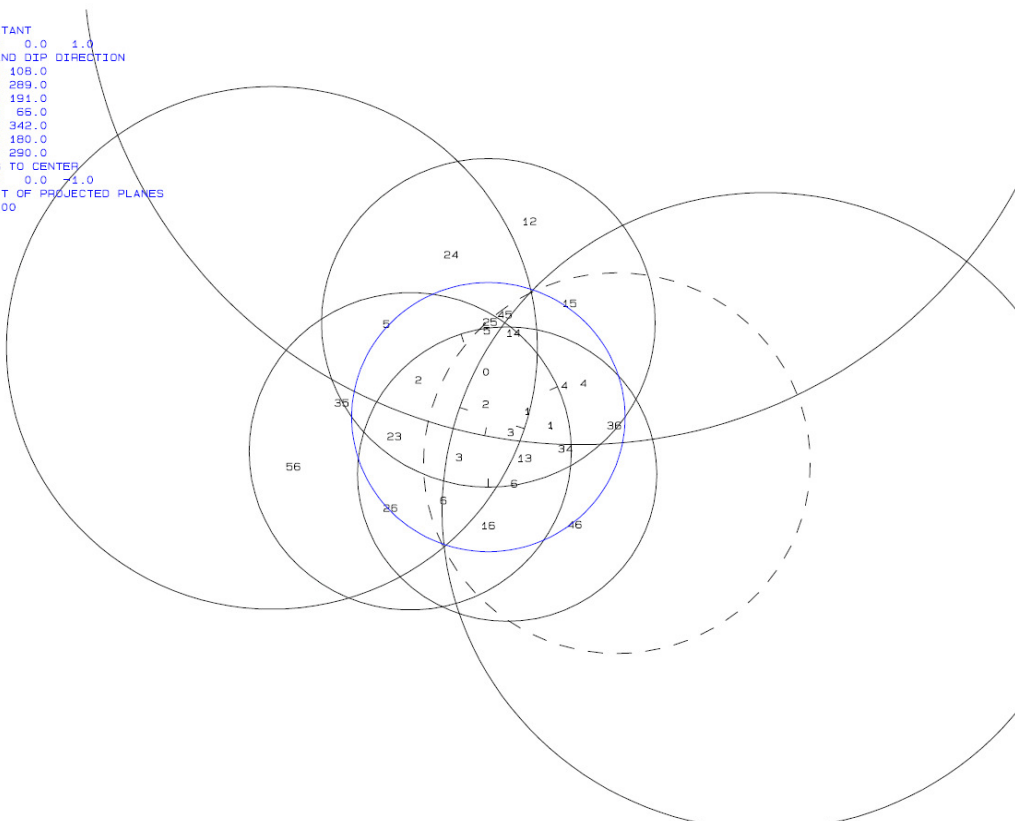
RESULTANT
0.0 0.0 1.0
DIP AND DIP DIRECTION
59.0 108.0
65.0 289.0
74.0 191.0
32.0 65.0
24.0 342.0
35.0 180.0
45.0 290.0
FOCUS TO CENTER
0.0 0.0 1.0
SUBSET OF PROJECTED PLANES
0000000
    
```



Whole sphere projection of the joint sets and the schistosity at outcrop 127 showing the joint pyramids (JPs) and their codes. The blue circle is the reference circle; the black dotted circle represents the slope assumed with 290/45.

```

RESULTANT
0.0 0.0 1.0
DIP AND DIP DIRECTION
59.0 108.0
65.0 289.0
74.0 191.0
32.0 65.0
24.0 342.0
35.0 180.0
45.0 290.0
FOCUS TO CENTER
0.0 0.0 1.0
SUBSET OF PROJECTED PLANES
0000000
    
```



Whole sphere projection giving the joint plane(s) along which the potential key blocks or key blocks would fail: along the intersection line of j1 with j2 (12), j3 with j5 (35) and j5 with the schistosity (56).

TABLE 1: Sets and Free Planes

No.	Dip	Dip Direction	Friction Angle
1	59	108	30
2	65	289	30
3	74	191	30
4	32	66	30
5	24	342	30
6	35	180	30
1	45	290	
2	0	0	

Resultant force:
0.00D+00 0.00D+00 -1.00D+00

Free plane code for the block:

1

Bearing and rise of tunnel:

0 0

Table 2: Sign of dot product of edge and normal

0	1	2	3	4	5	6	7	8	9	10
+0	-1	-1	-1	-1	-1	-1	+0	+0	+0	+0
+1	+0	-1	-1	-1	-1	-1	+0	+0	+0	+0
+2	-1	+0	-1	-1	-1	-1	+0	+0	+0	+0
+3	-1	-1	+0	-1	-1	-1	+0	+0	+0	+0
+4	+1	-1	-1	+0	-1	-1	+0	+0	+0	+0
+5	-1	+1	-1	-1	+0	-1	+0	+0	+0	+0
+6	-1	-1	+1	-1	-1	+0	+0	+0	+0	+0
+12	+0	+0	-1	+1	+1	-1	+0	+0	+0	+0
+13	+0	-1	+0	-1	-1	-1	+0	+0	+0	+0
+14	+0	-1	-1	+0	-1	-1	+0	+0	+0	+0
+15	+0	-1	-1	+1	+0	-1	+0	+0	+0	+0
+16	+0	-1	+1	-1	-1	+0	+0	+0	+0	+0
+23	-1	+0	+0	-1	-1	-1	+0	+0	+0	+0
+24	-1	+0	-1	+0	+1	-1	+0	+0	+0	+0
+25	-1	+0	-1	-1	+0	-1	+0	+0	+0	+0
+26	-1	+0	+1	-1	-1	+0	+0	+0	+0	+0
+34	+1	-1	+0	+0	-1	-1	+0	+0	+0	+0
+35	-1	+1	+0	-1	+0	-1	+0	+0	+0	+0
+36	+1	-1	+0	+1	-1	+0	+0	+0	+0	+0
+45	-1	-1	-1	+0	+0	-1	+0	+0	+0	+0
+46	+1	-1	+1	+0	-1	+0	+0	+0	+0	+0
+56	-1	+1	+1	-1	+0	+0	+0	+0	+0	+0

Table 3: Half spaces intersecting cutting pyramid

0	1	2	3	4	5	6	7	8	9	10
+0	-1	-1	-1	-1	-1	-1	+0	+0	+0	+0
+1	+1	-1	-1	-1	-1	-1	+0	+0	+0	+0
+2	-1	+1	-1	-1	-1	-1	+0	+0	+0	+0
+3	-1	-1	+1	-1	-1	-1	+0	+0	+0	+0
+4	+1	-1	-1	+1	-1	-1	+0	+0	+0	+0
+5	-1	+1	-1	-1	+1	-1	+0	+0	+0	+0
+6	-1	-1	+1	-1	-1	+1	+0	+0	+0	+0
+12	+1	+1	-1	+1	+1	-1	+0	+0	+0	+0
+13	+1	-1	+1	-1	-1	-1	+0	+0	+0	+0
+14	-1	-1	-1	+1	-1	-1	+0	+0	+0	+0
+15	+1	-1	-1	+1	+1	-1	+0	+0	+0	+0
+16	+1	-1	+1	-1	-1	+1	+0	+0	+0	+0
+23	-1	+1	+1	-1	-1	-1	+0	+0	+0	+0
+24	-1	+1	-1	+1	+1	-1	+0	+0	+0	+0
+25	-1	-1	-1	-1	+1	-1	+0	+0	+0	+0
+26	-1	+1	+1	-1	-1	+1	+0	+0	+0	+0
+34	+1	-1	+1	+1	-1	-1	+0	+0	+0	+0
+35	-1	+1	+1	-1	-1	-1	+0	+0	+0	+0
+36	+1	-1	-1	+1	-1	+1	+0	+0	+0	+0
+45	-1	-1	-1	+1	+1	-1	+0	+0	+0	+0
+46	+1	-1	+1	+1	-1	+1	+0	+0	+0	+0
+56	-1	+1	+1	-1	+1	+1	+0	+0	+0	+0

Table 4: Edges of cutting pyramids

+0	+13	+14	+23	+25	+45	+0	+0	+0	+0	+0
+1	+13	+14	+34	+0	+0	+0	+0	+0	+0	+0
+2	+23	+25	+35	+0	+0	+0	+0	+0	+0	+0
+3	+13	+16	+23	+26	+0	+0	+0	+0	+0	+0
+4	+14	+15	+34	+36	-56	+0	+0	+0	+0	+0
+5	+24	+25	+35	-36	-46	+0	+0	+0	+0	+0
+6	-12	+16	+26	+0	+0	+0	+0	+0	+0	+0
+12	+12	-16	-26	+0	+0	+0	+0	+0	+0	+0
+13	+13	+16	+34	+46	+0	+0	+0	+0	+0	+0
+14	+14	+15	+45	+0	+0	+0	+0	+0	+0	+0
+15	+12	+15	-26	-56	+0	+0	+0	+0	+0	+0
+16	-12	+16	-24	+46	+0	+0	+0	+0	+0	+0
+23	+23	+26	+35	+56	+0	+0	+0	+0	+0	+0
+24	+12	-16	+24	-46	+0	+0	+0	+0	+0	+0
+25	+24	+25	+45	+0	+0	+0	+0	+0	+0	+0
+26	-12	-15	+26	+56	+0	+0	+0	+0	+0	+0
+34	+34	+36	+46	+0	+0	+0	+0	+0	+0	+0
+35	+35	-36	+56	+0	+0	+0	+0	+0	+0	+0
+36	-35	+36	-56	+0	+0	+0	+0	+0	+0	+0
+45	+12	+15	+24	+45	+0	+0	+0	+0	+0	+0
+46	-24	-25	-35	+36	+46	+0	+0	+0	+0	+0
+56	-14	-15	-34	-36	+56	+0	+0	+0	+0	+0

Tables resulting from the mode analysis

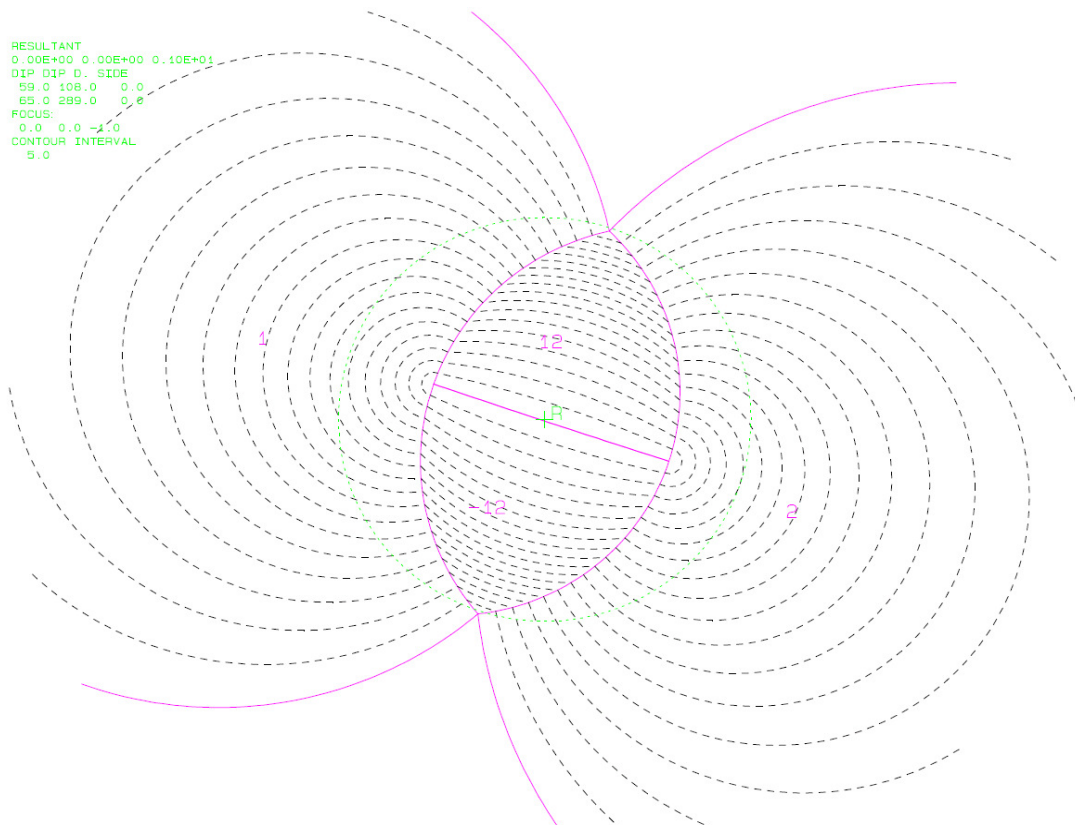
Table 5: Key blocks of free plane and concave slope

PYRAMID	PLANE 1	PLANE 2	CONCAVE SLOPE
0	0	1	0
1	0	1	0
2	0	1	0
3	0	1	0
4	0	0	0
5	0	0	0
6	0	0	0
12	1	0	0
13	0	1	0
14	0	1	0
15	0	0	0
16	0	0	0
23	0	1	0
24	0	0	0
25	0	1	0
26	0	0	0
34	0	1	0
35	1	0	0
36	0	0	0
45	0	1	0
46	0	0	0
56	1	0	0

Table 6

SLIDING PLANE	SLIDING FORCE	SLIDING INTERVAL	OF TUNNEL
+0.00	+1.00	+317.84	+60.90
+1.00	+0.56	+334.11	+116.79
+2.00	+0.66	+289.81	+11.07
+3.00	+0.80	+296.79	+45.44
+4.00	+0.04	+4.90	+137.84
+5.00	-0.12	+295.91	+337.27
+6.00	+0.10	+279.52	+357.06
+12.00	-1.21	+99.52	+177.06
+13.00	+0.48	+337.27	+99.52
+14.00	-0.37	+327.41	+121.46
+15.00	-0.36	+45.44	+147.41
+16.00	+0.08	+0.00	+0.00
+23.00	+0.46	+240.90	+4.90
+24.00	-0.40	+0.00	+0.00
+25.00	-0.35	+301.46	+109.81
+26.00	-0.11	+225.44	+327.41
+34.00	-0.27	+350.29	+154.11
+35.00	-0.56	+191.07	+350.29
+36.00	-1.18	+11.07	+170.29
+45.00	-0.21	+357.06	+115.91
+46.00	-0.27	+115.91	+157.27
+56.00	-0.57	+184.90	+317.84
RESULTANT FORCE			
0	0	-1	
AXIS OF TUNNEL			
0	1	0	

Tables resulting from the mode analysis

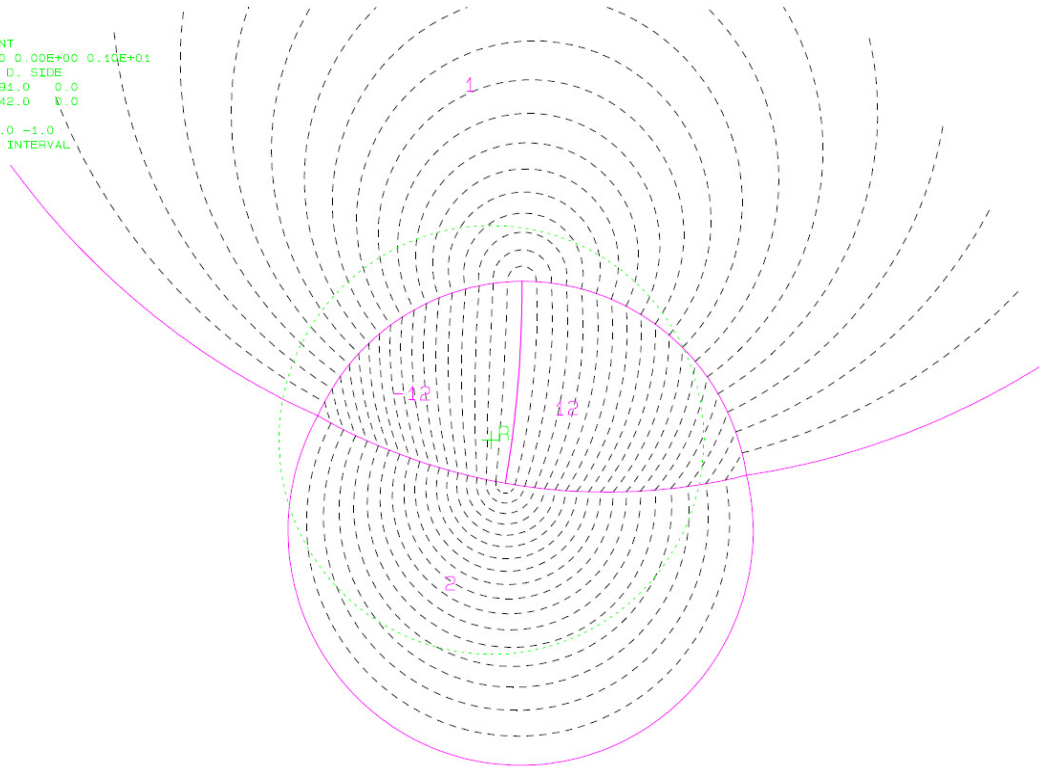


Contour plot of the friction angles for joint set j1 (= 1) and j2 (= 2) at outcrop 127. The green circle is the reference circle; R marks the resultant force vector.

```

RESULTANT
0.00E+00 0.00E+00 0.10E+01
DIP DIP D. SIDE
74.0 191.0 0.0
24.0 342.0 0.0
FOCUS:
0.0 0.0 -1.0
CONTOUR INTERVAL
5.0

```

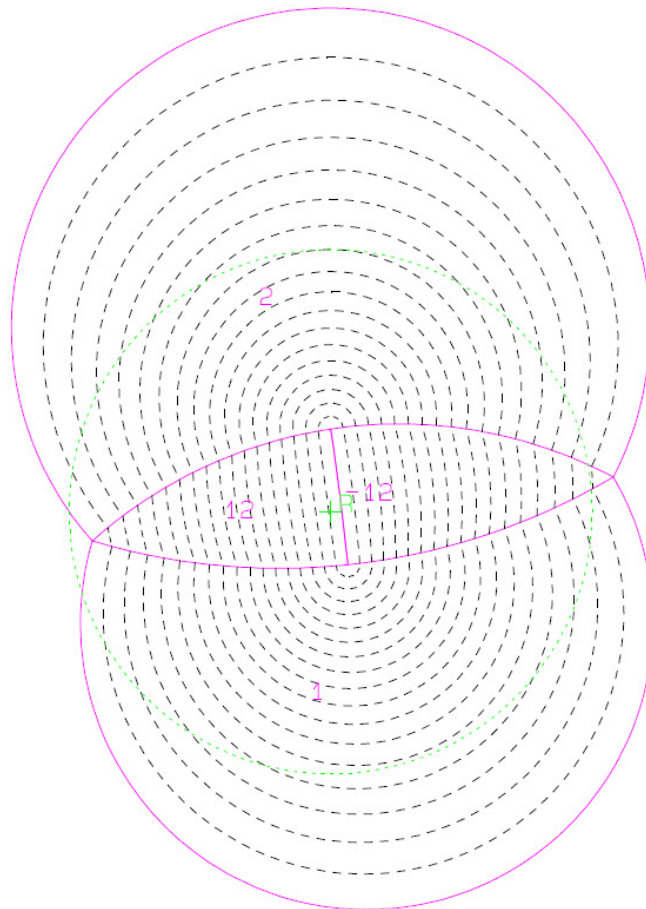


Contour plot of the friction angles for joint set j3 (= 1) and j5 (= 2) at outcrop 127. The green circle is the reference circle; R marks the resultant force vector.

```

RESULTANT
0.00E+00 0.00E+00 0.10E+01
DIP DIP D. SIDE
24.0 342.0 0.0
35.0 180.0 0.0
FOCUS:
0.0 0.0 -1.0
CONTOUR INTERVAL
5.0

```

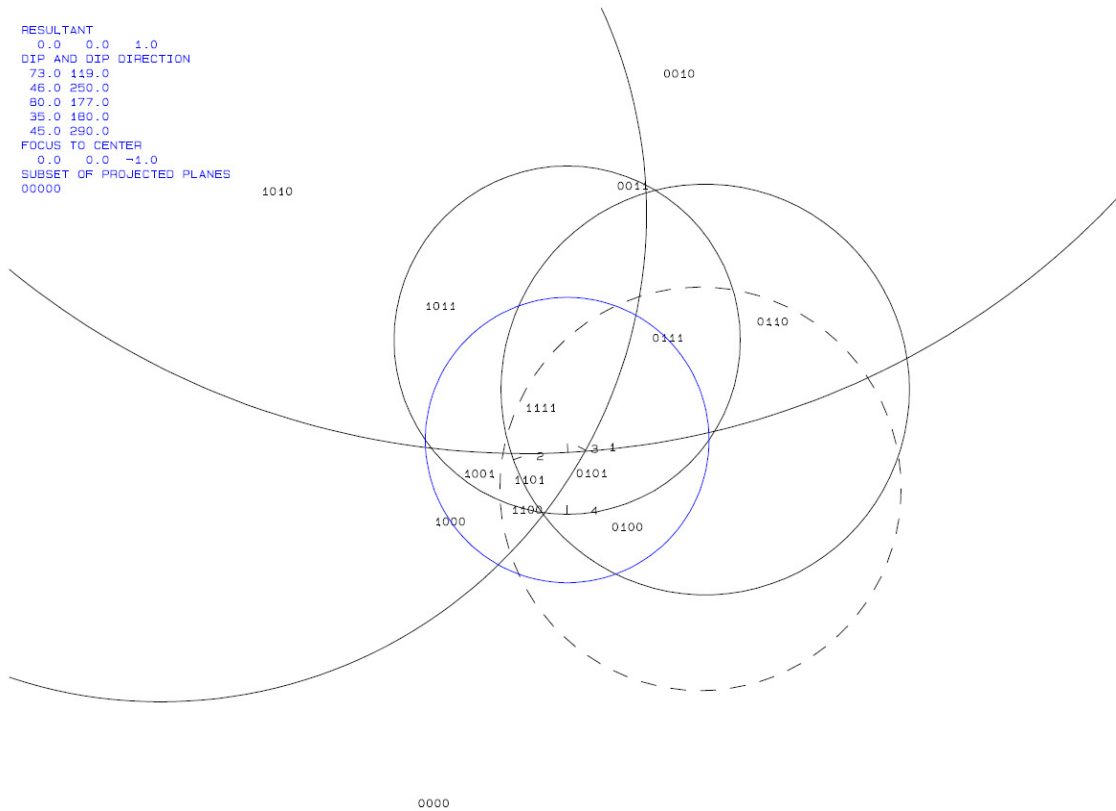


Contour plot of the friction angles for joint set j5 (= 1) and the schistosity (= 2) at outcrop 127. The green circle is the reference circle; R marks the resultant force vector.

Outcrop 143:

```

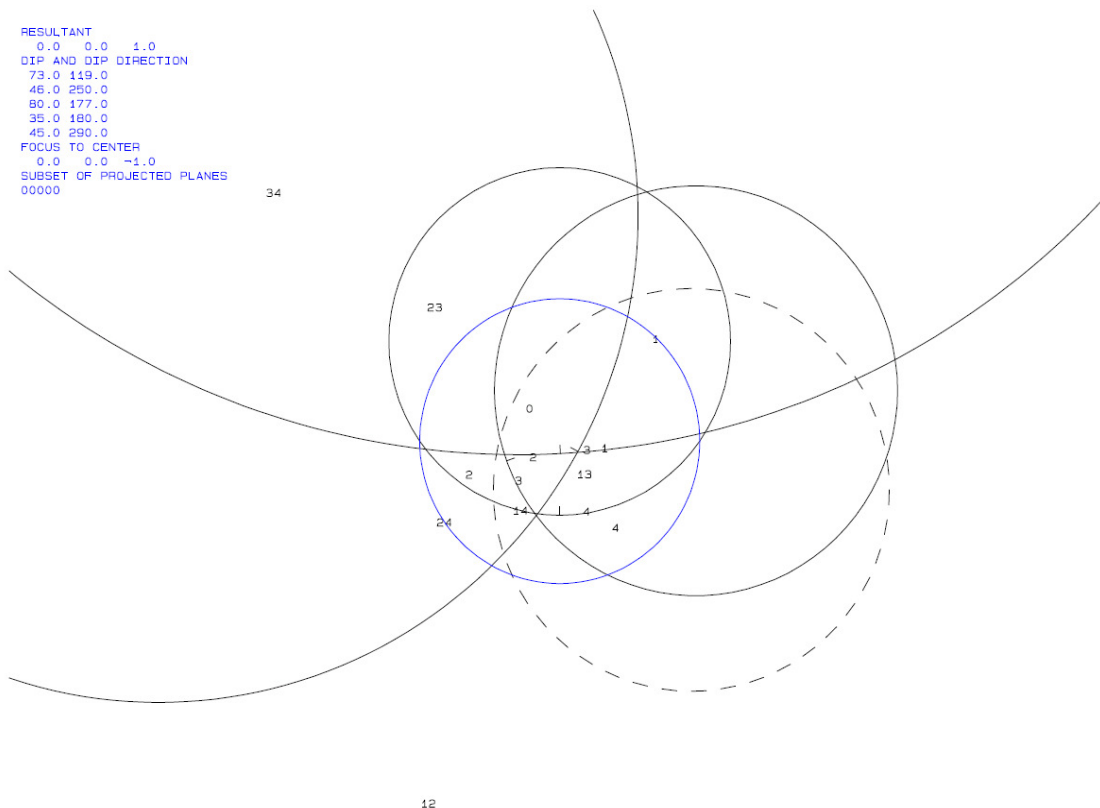
RESULTANT
0.0 0.0 1.0
DIP AND DIP DIRECTION
73.0 119.0
46.0 250.0
80.0 177.0
35.0 180.0
45.0 290.0
FOCUS TO CENTER
0.0 0.0 -1.0
SUBSET OF PROJECTED PLANES
00000
    
```



Whole sphere projection of the joint sets and the schistosity at outcrop 143 showing the joint pyramids (JPs) and their codes. The blue circle is the reference circle; the black dotted circle represents the slope assumed with 290/45.

```

RESULTANT
0.0 0.0 1.0
DIP AND DIP DIRECTION
73.0 119.0
46.0 250.0
80.0 177.0
35.0 180.0
45.0 290.0
FOCUS TO CENTER
0.0 0.0 -1.0
SUBSET OF PROJECTED PLANES
00000
    
```



Whole sphere projection giving the joint plane(s) along which the potential key blocks or key blocks would fail: along the intersection line of j3 with the schistosity (34).

TABLE 1: Sets and Free Planes

No.	Dip	Dip Direction	Friction Angle
1	73	119	30
2	46	250	30
3	80	177	30
4	35	180	30
1	45	290	
2	0	0	

Resultant force:
 0.00D+00 0.00D+00 -1.00D+00

Free plane code for the block:

1
 Bearing and rise of tunnel:
 0 0

Table 2: Sign of dot product of edge and normal

	0	1	2	3	4	5	6	7	8	9	10
+0	-1	-1	-1	-1	-1	+0	+0	+0	+0	+0	+0
+1	+0	-1	-1	-1	-1	+0	+0	+0	+0	+0	+0
+2	-1	+0	+0	+1	-1	+0	+0	+0	+0	+0	+0
+3	-1	-1	+0	-1	+0	+0	+0	+0	+0	+0	+0
+4	+1	-1	+1	+0	+0	+0	+0	+0	+0	+0	+0
+12	+0	+0	+1	+1	+0	+0	+0	+0	+0	+0	+0
+13	+0	-1	+0	-1	+0	+0	+0	+0	+0	+0	+0
+14	+0	-1	+1	+0	+0	+0	+0	+0	+0	+0	+0
+23	-1	+0	+0	-1	+0	+0	+0	+0	+0	+0	+0
+24	-1	+0	+1	+0	+0	+0	+0	+0	+0	+0	+0
+34	-1	+1	+0	+0	+0	+0	+0	+0	+0	+0	+0

Table 3: Half spaces intersecting cutting pyramid

	0	1	2	3	4	5	6	7	8	9	10
+0	-1	-1	-1	-1	-1	+0	+0	+0	+0	+0	+0
+1	+1	-1	-1	-1	-1	+0	+0	+0	+0	+0	+0
+2	-1	+1	+1	+1	-1	+0	+0	+0	+0	+0	+0
+3	-1	-1	+1	+1	-1	+0	+0	+0	+0	+0	+0
+4	+1	-1	+1	+1	+1	+0	+0	+0	+0	+0	+0
+12	+1	+1	+1	+1	+1	+0	+0	+0	+0	+0	+0
+13	+1	-1	+1	+1	-1	+0	+0	+0	+0	+0	+0
+14	-1	-1	+1	+1	+0	+0	+0	+0	+0	+0	+0
+23	-1	+1	-1	-1	+0	+0	+0	+0	+0	+0	+0
+24	-1	+1	+1	+1	+0	+0	+0	+0	+0	+0	+0
+34	-1	+1	-1	+1	+0	+0	+0	+0	+0	+0	+0

Table 4: Edges of cutting pyramids

+0	-12	+13	+23	+0	+0	+0	+0	+0	+0	+0
+1	-12	+13	-24	-34	+0	+0	+0	+0	+0	+0
+2	+23	+24	+34	+0	+0	+0	+0	+0	+0	+0
+3	+13	+14	+23	+24	+0	+0	+0	+0	+0	+0
+4	+12	+14	-23	-34	+0	+0	+0	+0	+0	+0
+12	+12	-13	-23	+0	+0	+0	+0	+0	+0	+0
+13	+13	+14	-34	+0	+0	+0	+0	+0	+0	+0
+14	+12	+14	+24	+0	+0	+0	+0	+0	+0	+0
+23	-12	-14	+23	+34	+0	+0	+0	+0	+0	+0
+24	+12	-13	+24	+34	+0	+0	+0	+0	+0	+0
+34	-13	-14	+34	+0	+0	+0	+0	+0	+0	+0

Table 5: Key blocks of free plane and concave slope

PYRAMID	PLANE 1	PLANE 2	CONCAVE SLOPE
0	0	0	0
1	0	0	0
2	0	1	0
3	0	1	0
4	0	0	0
12	0	0	0
13	0	0	0
14	0	1	0
23	0	0	0
24	0	0	0
34	1	0	0

Table 6

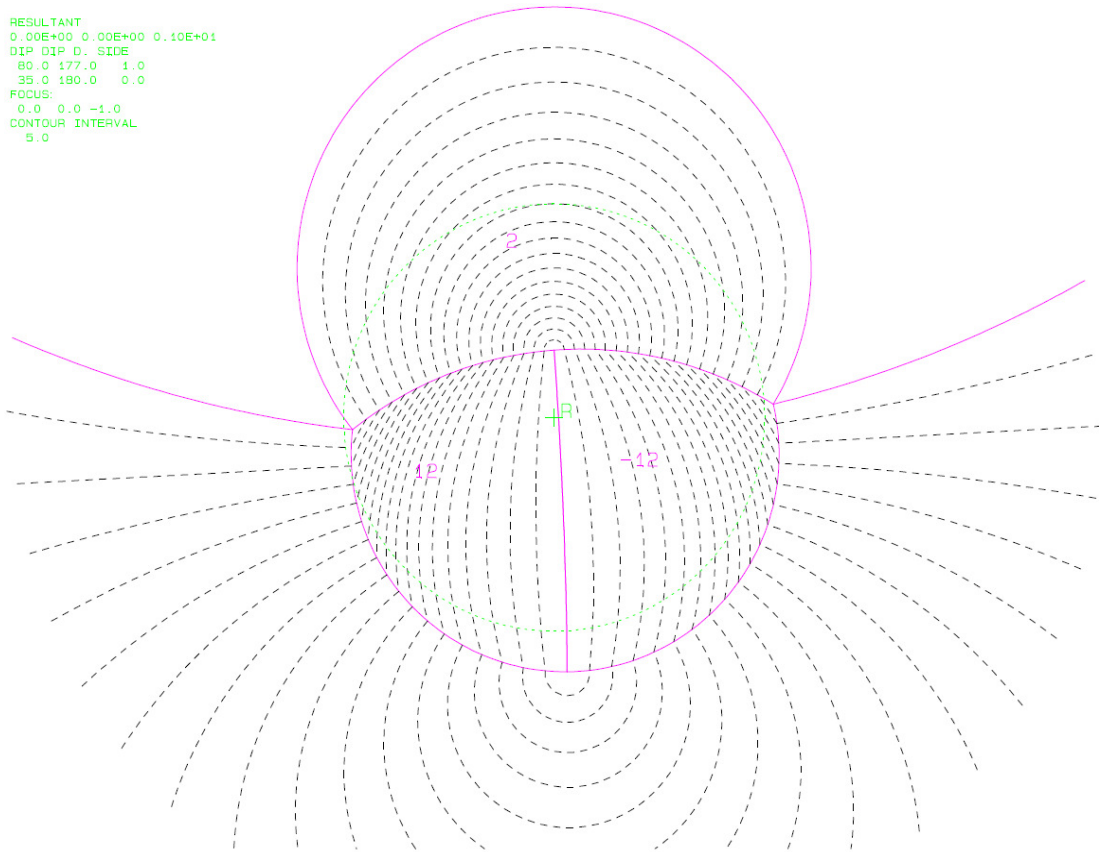
SLIDING PLANE	SLIDING FORCE	SLIDING INTERVAL OF TUNNEL
+0.00	+1.00	+0.00
+1.00	+0.79	+64.28
+2.00	+0.32	+243.08
+3.00	+0.88	+284.53
+4.00	+0.10	+46.61
+12.00	-0.22	+64.28
+13.00	+0.78	+0.00
+14.00	-0.06	+2.40
+23.00	+0.27	+66.15
+24.00	+0.04	+63.08
+34.00	-1.23	+244.28
		+284.53
		+246.15

RESULTANT FORCE
 0 -1

AXIS OF TUNNEL
 0 1 0

Tables resulting from the mode analysis

```
RESULTANT
0.00E+00 0.00E+00 0.10E+01
DIP DIP D. SIDE
80.0 177.0 1.0
35.0 180.0 0.0
FOCUS:
0.0 0.0 -1.0
CONTOUR INTERVAL
5.0
```

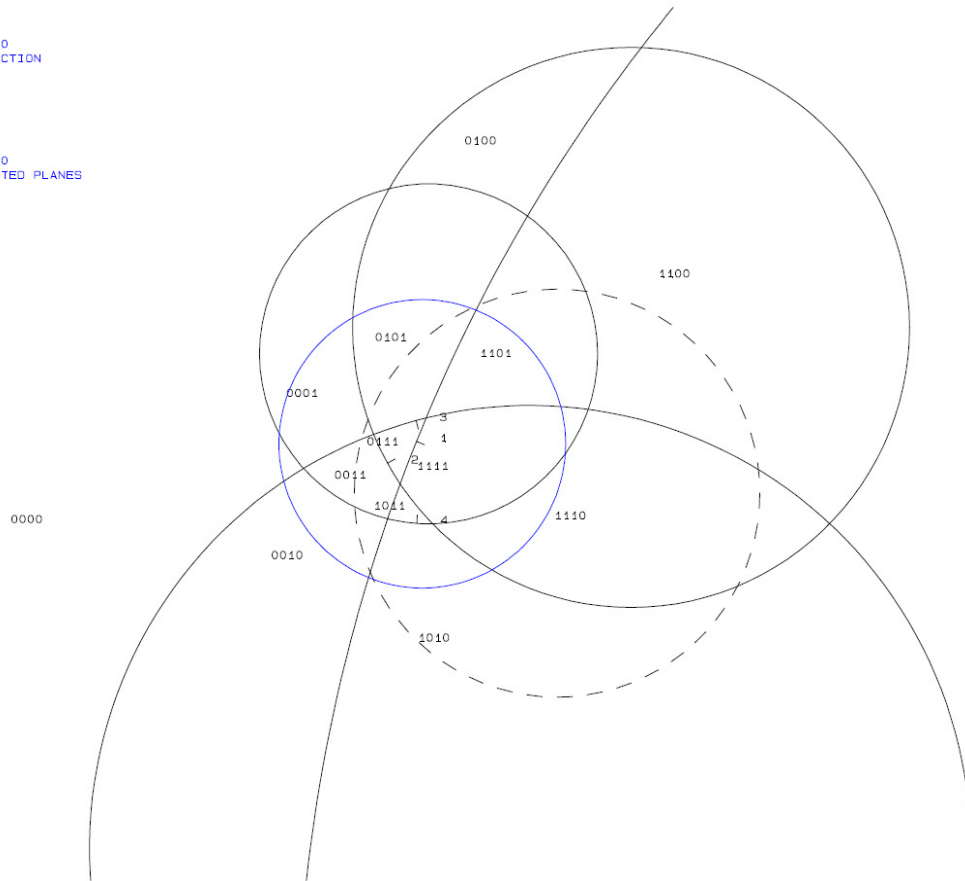


Contour plot of the friction angles for joint set j3 (= 1) and the schistosity (= 2) at outcrop 143. The green circle is the reference circle; R marks the resultant force vector.

Outcrop 169:

```

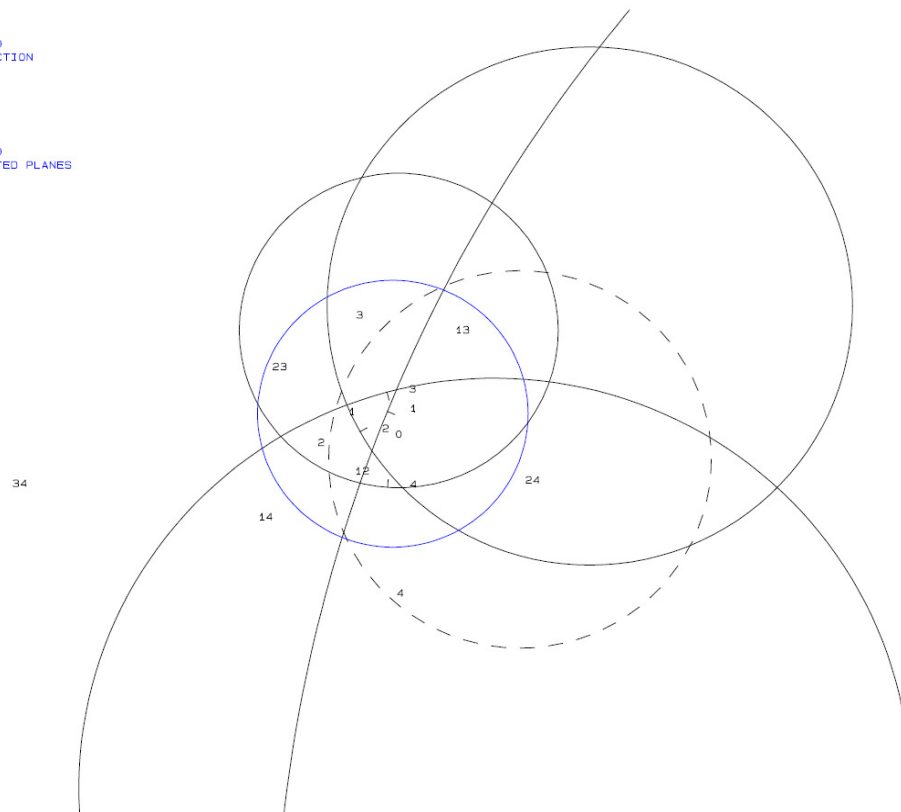
RESULTANT
0.0 0.0 1.0
DIP AND DIP DIRECTION
85.0 292.0
59.0 241.0
71.0 345.0
32.0 184.0
45.0 290.0
FOCUS TO CENTER
0.0 0.0 -1.0
SUBSET OF PROJECTED PLANES
00000
    
```



Whole sphere projection of the joint sets and the schistosity at outcrop 169 showing the joint pyramids (JPs) and their codes. The blue circle is the reference circle; the black dotted circle represents the slope assumed with 290/45.

```

RESULTANT
0.0 0.0 1.0
DIP AND DIP DIRECTION
85.0 292.0
59.0 241.0
71.0 345.0
32.0 184.0
45.0 290.0
FOCUS TO CENTER
0.0 0.0 -1.0
SUBSET OF PROJECTED PLANES
00000
    
```



Whole sphere projection giving the joint plane(s) along which the potential key blocks or key blocks would fail: along the intersection line of j3 with the schistosity (34).

TABLE 1: Sets and Free Planes

No.	Dip	Dip Direction	Friction Angle
1	85	292	30
2	59	241	30
3	71	345	30
4	32	184	30
1	45	290	
2	0	0	

Resultant force:
 0.00D+00 0.00D+00 -1.00D+00
 Free plane code for the block:
 1
 Bearing and rise of tunnel:
 0 0

Table 2: Sign of dot product of edge and normal

	0	1	2	3	4	5	6	7	8	9	10
+0	-1	-1	-1	-1	-1	+0	+0	+0	+0	+0	+0
+1	+0	-1	-1	-1	-1	+0	+0	+0	+0	+0	+0
+2	+1	+0	-1	-1	-1	+0	+0	+0	+0	+0	+0
+3	+1	-1	+0	-1	-1	+0	+0	+0	+0	+0	+0
+4	-1	+1	-1	+0	+0	+0	+0	+0	+0	+0	+0
+12	+0	+0	-1	-1	-1	+0	+0	+0	+0	+0	+0
+13	+0	-1	+0	-1	-1	+0	+0	+0	+0	+0	+0
+14	+0	+1	-1	+0	+0	+0	+0	+0	+0	+0	+0
+23	+1	+0	+0	-1	-1	+0	+0	+0	+0	+0	+0
+24	-1	+0	-1	+0	+0	+0	+0	+0	+0	+0	+0
+34	+1	+1	+0	+0	+0	+0	+0	+0	+0	+0	+0

Table 3: Half spaces intersecting cutting pyramid

	0	1	2	3	4	5	6	7	8	9	10
+0	-1	-1	-1	-1	-1	+0	+0	+0	+0	+0	+0
+1	+1	-1	-1	-1	-1	+0	+0	+0	+0	+0	+0
+2	+1	+1	-1	-1	-1	+0	+0	+0	+0	+0	+0
+3	+1	-1	+1	-1	-1	+0	+0	+0	+0	+0	+0
+4	-1	+1	-1	+1	+1	+0	+0	+0	+0	+0	+0
+12	-1	+1	-1	-1	-1	+0	+0	+0	+0	+0	+0
+13	-1	-1	+1	-1	-1	+0	+0	+0	+0	+0	+0
+14	+1	+1	-1	+1	+1	+0	+0	+0	+0	+0	+0
+23	+1	+1	+1	-1	-1	+0	+0	+0	+0	+0	+0
+24	-1	-1	-1	-1	+1	+0	+0	+0	+0	+0	+0
+34	+1	+1	+1	+1	+1	+0	+0	+0	+0	+0	+0

Table 4: Edges of cutting pyramids

+0	+12	+13	+24	-34	+0	+0	+0	+0	+0	+0	+0
+1	+12	+13	+23	+0	+0	+0	+0	+0	+0	+0	+0
+2	+12	+14	+23	+34	+0	+0	+0	+0	+0	+0	+0
+3	+13	-14	+23	-24	+0	+0	+0	+0	+0	+0	+0
+4	-13	+14	-23	+24	+0	+0	+0	+0	+0	+0	+0
+12	+12	+14	+24	+0	+0	+0	+0	+0	+0	+0	+0
+13	+13	-14	-34	+0	+0	+0	+0	+0	+0	+0	+0
+14	-13	+14	+34	+0	+0	+0	+0	+0	+0	+0	+0
+23	+23	-24	+34	+0	+0	+0	+0	+0	+0	+0	+0
+24	-23	+24	-34	+0	+0	+0	+0	+0	+0	+0	+0
+34	-12	-13	-24	+34	+0	+0	+0	+0	+0	+0	+0

Table 5: Key blocks of free plane and concave slope

PYRAMID	PLANE 1	PLANE 2	CONCAVE SLOPE
0	0	0	0
1	0	1	0
2	0	1	0
3	0	0	0
4	0	0	0
12	0	1	0
13	0	0	0
14	0	0	0
23	0	0	0
24	0	0	0
34	1	0	0

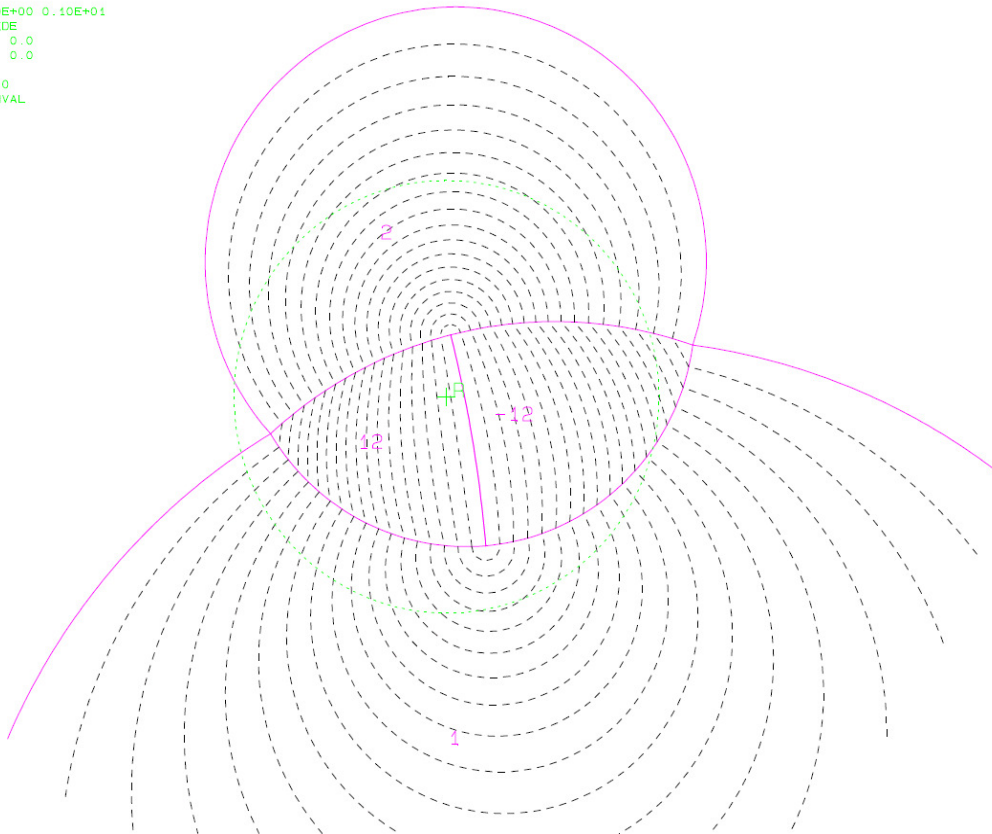
Table 6

SLIDING PLANE	SLIDING FORCE	SLIDING INTERVAL OF TUNNEL
+0.00	+1.00	+9.78
+1.00	+0.95	+273.19
+2.00	+0.56	+251.01
+3.00	+0.76	+0.00
+4.00	+0.04	+0.00
+12.00	+0.22	+281.88
+13.00	+0.60	+54.17
+14.00	-0.09	+234.17
+23.00	+0.29	+232.40
+24.00	-0.09	+52.40
+34.00	-0.68	+189.78

RESULTANT FORCE
 0 0 -1
 AXIS OF TUNNEL
 0 1 0

Tables resulting from the mode analysis

```
RESULTANT
0.00E+00 0.00E+00 0.10E+01
DIP DIP D. SIDE
71.0 345.0 0.0
32.0 184.0 0.0
FOCUS:
0.0 0.0 -1.0
CONTOUR INTERVAL
5.0
```



Contour plot of the friction angles for joint set j3 (= 1) and the schistosity (= 2) at outcrop 169. The green circle is the reference circle; R marks the resultant force vector.